

## Copyright Undertaking

This thesis is protected by copyright, with all rights reserved.

**By reading and using the thesis, the reader understands and agrees to the following terms:**

1. The reader will abide by the rules and legal ordinances governing copyright regarding the use of the thesis.
2. The reader will use the thesis for the purpose of research or private study only and not for distribution or further reproduction or any other purpose.
3. The reader agrees to indemnify and hold the University harmless from and against any loss, damage, cost, liability or expenses arising from copyright infringement or unauthorized usage.

### IMPORTANT

If you have reasons to believe that any materials in this thesis are deemed not suitable to be distributed in this form, or a copyright owner having difficulty with the material being included in our database, please contact [lbsys@polyu.edu.hk](mailto:lbsys@polyu.edu.hk) providing details. The Library will look into your claim and consider taking remedial action upon receipt of the written requests.

**ADVANCING LINK CRITICALITY ANALYSIS FOR LARGE-  
SCALE ROAD NETWORKS AND BRIDGE-CENTRIC  
TRANSPORT NETWORKS: A NETWORK EQUILIBRIUM  
APPROACH**

**DANIYAR KURMANKHOJAYEV**

**PhD**

**The Hong Kong Polytechnic University**

**2025**

The Hong Kong Polytechnic University

Department of Civil and Environmental Engineering

**ADVANCING LINK CRITICALITY ANALYSIS FOR LARGE-  
SCALE ROAD NETWORKS AND BRIDGE-CENTRIC TRANSPORT  
NETWORKS: A NETWORK EQUILIBRIUM APPROACH**

Daniyar KURMANKHOJAYEV

A thesis submitted in partial fulfilment of the requirement for the degree of  
Doctor of Philosophy

December 2024

## **CERTIFICATE OF ORIGINALITY**

I hereby declare that this thesis is my own work and that, to the best of my knowledge and belief, it reproduces no material previously published or written, nor material that has been accepted for the award of any other degree or diploma except where due acknowledgement has been made in the text.

\_\_\_\_\_ (Signed)

Daniyar KURMANKHOJAYEV (Name of student)



## **DEDICATION**

I dedicate this entire doctoral journey to my beautiful and devoted wife, Mrs. Laura MAUKENOVA, whose immense sacrifice, remarkable resilience, and unwavering patience have been invaluable throughout this journey. I also dedicate this journey to my children, Ms. Aiganym KURMANKHOJAYEVA and Mr. Rolan KURMANKHOJAYEV, whose presence and pure love have been a constant source of motivation, inspiration, and joy, giving my life profound purpose and meaning. I dedicate this journey to my mother, Mrs. Sholpan KURMANKHOJAYEVA, whose unconditional love, trust, and support have been indispensable during this journey. Lastly, I dedicate this to my entire extended family for their enduring support.

# ABSTRACT

Link criticality analysis for road networks is essential for mitigating and withstanding disruptive events. Frontier methods for link criticality analysis rely heavily on equilibrium traffic assignment (TA) models, which provide consistent network traffic flows and travel costs. These methods can account for network connectivity, redundancy, travel demand, individual travel choices, and congestion effects induced by traveler interactions. Conceptually, these methods define link criticalities in terms of their functional importance for normal network operations, as indicated by equilibrium TA model. Conventional methods assess link criticalities using a full-scan approach, which entails sequentially deactivating each link, solving a TA problem for each network modification, and subsequently reactivating the link before proceeding to the next one. While feasible for small networks, this approach is impractical for large-scale networks. Most studies have focused on the computational aspects of the problem, aiming either to approximate or bypass the full-scan process. In doing so, these studies often neglected the need for behaviorally plausible TA models for effective link criticality analysis. This oversight highlights the motivation for this thesis.

It is well known that travelers often have incomplete knowledge of network conditions, which affects their individual route choices, and that they may switch modes of travel, change their departure times, or forego trips altogether in response to congestion. Ignoring these factors in TA models can lead to traffic flow patterns and network efficiency measures that do not adequately represent reality. Consequently, link criticality analysis methods based on TA models without these considerations may provide a poor representation of actual link criticalities. Nonetheless, most studies have assessed network link criticalities using user equilibrium TA models with fixed demand (UE-FD or UE), which is known to assume that

travelers have perfect knowledge of network conditions, always use the least-cost routes, and never change their intention to travel, departure time, and mode of travel. To bridge this gap, this thesis advances an efficient link criticality analysis method by adopting stochastic user equilibrium (SUE) TA model with elastic demand (ED). In contrast to UE, SUE relaxes the assumption of perfect knowledge of network state and assigns traffic flows across all considered routes rather than just the least-cost routes, while ED adjusts travel demand based on congestion levels. The experiments show that the advanced method can prevent overestimating the criticality of links on least-cost routes, which is common for UE-based methods. Using real-world networks, it demonstrates that this method is applicable to large-scale road networks and consistent with the full-scan methods.

Route similarity issues, stemming from route overlaps, are common in road networks. These issues not only substantially distort route choice probabilities, making similar routes less attractive from a travel cost perspective, but also impact origin-destination (O-D) travel demands. This can dramatically change total travel demand, O-D demand patterns, network flow patterns, travel costs, and, hence, link criticalities. Although the concept of route similarity has been well-explored within the context of SUE TA, its application in link criticality analysis remains limited. To address this research gap, this thesis adopts the cross-nested logit (CNL) SUE model with ED, which can flexibly capture the effects of route similarity on both disaggregate (or individuals') route choices and aggregate travel demand. It then incorporates this model into the selected link criticality analysis method. The results of the experiments demonstrate that the criticalities of links belonging to similar routes can be considerably overestimated if route similarity is not considered.

Bridges play a vital role in road networks that are divided by obstacles like rivers and valleys. They connect different parts of the network and are essential for reaching certain

destinations. Due to their limited number, they often become traffic bottlenecks, disproportionately affecting travel costs, and overall network performance. It has been recognized that bridges greatly influence route choice behavior, with travelers typically selecting bridges first and then deciding on the connecting routes. Despite this recognition, the functional importance of bridges has not been sufficiently emphasized in network equilibrium and link criticality analysis contexts. To address this research gap, this thesis introduces the concept of bridge-centric transport networks and develops a joint bridge-route choice model to better reflect how travelers first select bridges and then decide on the connecting routes. Then, it develops a network equilibrium model that encapsulates the joint bridge-route choice model along with a customized route-based solution algorithm, which consists of a bridge-centric choice set generation method and a route equilibration method. Finally, it applies the developed methodology to link criticality analysis. The results of the experiments demonstrate that network equilibrium models can produce substantially different traffic flow patterns and link criticality values, depending on whether they account for the importance of bridges in route choice. They also suggest that link criticality analysis methods based on traditional models may greatly underestimate the criticality of bridges.

In summary, this thesis advances link criticality analysis by integrating nuanced equilibrium TA models that account for travelers' imperfect perception of network conditions, their responses to congestion, and route similarity issues. Emphasizing the crucial role of bridges in the route choice process, it also develops a bridge-centric framework, which includes a joint bridge-route choice model, a network equilibrium model, and a customized route-based algorithm, and integrates it into the selected link criticality analysis method. The properties of the resulting methods are thoroughly investigated, and their validity and applicability to large-scale networks are demonstrated using real-world networks.

# LIST OF PUBLICATIONS

## JOURNAL PAPERS

- Kurmankhojayev, D.**, Li, G., and Chen, A. (2024). Link criticality index: Refinement, framework extension, and a case study. *Reliability Engineering & System Safety*, 243, 109889. (Published)
- Kurmankhojayev, D.**, Tan, H., and Chen, A. (2024). A methodological foundation for proactive disruption mitigation in transport networks: Integrating route similarity and elastic demand in stochastic user equilibrium-based link criticality analysis. *Reliability Engineering & System Safety*, 111084. (Published)
- Kurmankhojayev, D.**, Gu, Y., and Chen, A. (2024). Bridges matter: Modeling joint bridge and route choice equilibrium with bridge-centric choice set generation. (Under revision with *Transportation Research Part A*)
- Kurmankhojayev, D.**, Gu, Y., Tan, H., and Chen, A. (2024). Proactive disruption mitigation: Bridge criticality analysis with a bridge-centric traffic assignment framework. (Under review with *Reliability Engineering & System Safety*)

## CONFERENCE PAPERS

- Kurmankhojayev, D.**, Li, G., and Chen, A. (2022). A computationally efficient link criticality ranking with perception error and route overlapping for road transport networks. In *2022 13th International Conference on Reliability, Maintainability, and Safety (ICRMS)*, 154-158, IEEE. (Received Best Conference Paper Award)
- Kurmankhojayev, D.**, Li, G., and Chen, A. (2022). Adaptive Barzilai-Borwein projection method with application to mixed-flow multiclass traffic assignment. *The 26th International Conference of Hong Kong Society for Transportation Studies*.
- Li, G., Gu, Y., Chen, A., and **Kurmankhojayev, D.** (2022). A trip-chain-based path flow estimator framework for connected and autonomous vehicles. *The 26th International Conference of Hong Kong Society for Transportation Studies*.

**Kurmankhojayev, D.,** Hu, Z., Chen, A., and Ma, W. (2022). Simultaneous calibration of traffic demand and transport network using real-world multisource data. *Journal of the Eastern Asia Society for Transportation Studies*, 14, 601-615.

## ACKNOWLEDGEMENTS

Never in my life have I felt as miserable and insecure as I did during my PhD journey. Never have I felt as confident as I do now, having completed it. Reflecting on my experience, I realize that the biggest challenges I faced were recognizing cultural differences, working on my emotional maturity, and developing efficient communication skills to understand and fulfill my roles as a PhD candidate, husband, father, son, colleague, and friend. Now, I am confident that I have learned invaluable lessons and dramatically increased my resilience, all thanks to the unwavering support and collective efforts of everyone involved. This journey has shaped me into a more resilient person, and for that, I am deeply grateful.

My special appreciation goes to the Research Institute for Sustainable Urban Development (RISUD) for giving me a PhD full scholarship, to the Department of Civil and Environmental Engineering (CEE) for providing with all the necessary resources to carry out my research, and to The Hong Kong Polytechnic University (PolyU) for providing a plethora of opportunities for personal and professional growth.

I am highly indebted to my chief supervisor, Prof. Anthony Chen, for his invaluable advice, continuous support, and endless patience throughout my study. Prof. Chen taught me that mastering one tool professionally is far more valuable than having a superficial knowledge of many. True mastery, he argued, is demonstrated by a deep understanding of the tool's properties, the ability to clearly explain these properties to others, and the skill to apply the tool to real-life problems. The lessons I learned from him taught me to think critically and systematically and shaped me as a researcher. Prof. Chen's professionalism and kindness were truly inspiring.

My gratitude extends to my co-supervisors, Ir Prof. William H. K. Lam and Prof. Edward Chung. It was a great honour to receive constructive comments of two highly esteemed professors on my research.

I would like to extend my heartfelt thanks to all my research team members for their unwavering support and invaluable advice. In particular, I wish to acknowledge my colleagues and friends, Dr. Gu Yu, Mr. Heqing Tan, Mr. Umer Mansoor, and Mr. Zhengyang Li for their open-mindedness, hard work, and remarkable resilience, which I had the privilege

to witness. Special thanks to Dr. Yingying Xu and Ms. Zhuowei Wang, whose support during the final stages of my PhD was indispensable.

I am profoundly grateful to all my office mates and friends for accompanying me on this journey. The moments shared with you are highly valued and will be fondly remembered. It was my honor to meet Dr. Mohammed Abdul-Rahman, Dr. Mark Kyeredey Ansah, Dr. Elvis Wu, and Dr. Nikolay Lyapunov. Our countless discussions helped me overcome many challenges. Special thanks to Mr. Jay Bidal and Prof. Alessandro Stocchino for sharing their passion for squash with me.

As a hall tutor, I would like to extend my appreciation to the Student Affairs Office for granting me the opportunity to serve at Student Hall. I am particularly grateful to Dr. Andrew Chu, Mr. Ivan Chung, and Ms. Grace Tang for imparting the essence of empathy and servant leadership, and for equipping us, the hall tutors, with effective techniques for recognizing biases and thriving in multi- and inter-cultural environments. My gratitude also extends to my Wuxian Hall warden-tutor team. It was an honor to be a part of such a talented and multifaceted team. I am especially thankful to my warden, Professor Thomas Lee, whose exemplary leadership and management skills significantly contributed to my professional growth and development. Lastly, I would like to acknowledge my fellow tutors from other halls: Dr. Partha P. Debnath, Ms. Caroline Du, Mr. Chandra S. Das, Ms. Mohana Das, Ms. Qinyu Jia, and Ms. Mehrnaz Alizadeh. Sharing the bittersweet moments of PhD life in vibrant Hong Kong with you all was invaluable. Your support has been truly appreciated.

Last but not the least, I thank the Chair of Board of Examiners Prof. Jinxia Liu (CEE PolyU) and my two external examiners: Prof. Mustafa Anil Yazici of Stony Brook University and Prof. Shauhrat S. Chopra of the City University of Hong Kong, for their great critic and suggestions.



# TABLE OF CONTENTS

<b>DEDICATION.....</b>	<b>ii</b>
<b>ABSTRACT .....</b>	<b>iii</b>
<b>LIST OF PUBLICATIONS.....</b>	<b>vi</b>
<b>ACKNOWLEDGEMENTS .....</b>	<b>viii</b>
<b>TABLE OF CONTENTS .....</b>	<b>x</b>
<b>LIST OF FIGURES.....</b>	<b>xiv</b>
<b>LIST OF TABLES.....</b>	<b>xix</b>
<b>LIST OF ABBREVIATIONS.....</b>	<b>xxii</b>
<b>CHAPTER 1 Introduction.....</b>	<b>1</b>
1.1 Research background.....	1
1.2 Motivation and research gaps.....	5
1.3 Research objectives and contributions .....	7
1.4 Thesis organization.....	9
<b>CHAPTER 2 Literature review .....</b>	<b>12</b>
2.1 Network equilibrium models .....	12
2.1.1 Network equilibrium models for road networks .....	13
2.1.1.1 Behavioral route choice assumptions .....	14
2.1.1.2 Equilibrium traffic assignment problem formulations .....	15
2.1.1.3 Logit-based route choice equilibrium models .....	16
2.1.1.4 Logit-based route choice equilibrium models with elastic demand .....	17
2.1.2 Network equilibrium models for bridge-centric transport networks .....	18
2.1.2.1 Modeling joint bridge-route choice .....	18
2.1.2.2 Bridge-route choice set generation.....	19
2.1.2.3 Modeling joint bridge-route choice network equilibrium .....	21
2.2 Link criticality analysis methods.....	22
2.3 Link criticality analysis applications .....	25
2.4 Chapter summary.....	26
<b>PART I Advancing link criticality analysis: Road networks .....</b>	<b>28</b>
<b>CHAPTER 3 Link criticality index: Stochastic user equilibrium model with elastic demand .....</b>	<b>29</b>
3.1 Motivation .....	29
3.2 Equilibrium traffic assignment model .....	32
3.2.1 Notation .....	32
3.2.2 Route choice models .....	32
3.2.3 Equivalent MP formulation .....	33

3.2.4	Travel demand model .....	34
3.2.5	Solution algorithm .....	35
3.3	Link criticality index .....	36
3.3.1	Original UE-based LCI .....	36
3.3.2	Refined UE-based LCI .....	41
3.3.3	SUE-based LCI.....	42
3.3.4	SUE-ED-based LCI.....	42
3.4	Numerical experiments.....	43
3.4.1	Experiment 1: Two O-D pair network .....	44
3.4.2	Experiment 2: Loophole network.....	46
3.4.2.1	UE-based LCI vs. SUE-based LCI.....	46
3.4.2.2	SUE-based LCI vs. SUE-ED-based LCI.....	50
3.4.2.3	Discussion on demand elasticity .....	53
3.4.3	Experiment 3: Real-size networks.....	56
3.4.3.1	Setting model parameters for real-size networks .....	56
3.4.3.2	Computational complexity analysis .....	59
3.4.3.3	Criticality of bridges in the city of Winnipeg.....	60
3.5	Chapter summary.....	64

## **CHAPTER 4 Incorporating route similarity and demand elasticity into link criticality analysis .....**

4.1	Motivation .....	66
4.2	Route similarity and link criticality analysis .....	67
4.2.1	Sources of route similarity .....	68
4.2.2	Impact of route similarity on travel demand .....	69
4.2.3	Impact of route similarity on link criticality .....	70
4.3	Addressing route similarity in SUE.....	71
4.3.1	Probabilistic route choice model .....	71
4.3.2	Travel demand model.....	77
4.3.3	Equivalent MP formulation .....	77
4.3.4	Solution algorithm.....	79
4.4	Route similarity in LCI.....	80
4.4.1	Link criticality index .....	80
4.4.2	Illustrative example .....	83
4.5	Numerical experiments.....	84
4.5.1	Experiment 1: A toy network .....	84
4.5.1.1	Computation of LCI .....	85
4.5.1.2	Impact of route similarity on LCI.....	87
4.5.2	Experiment 2: Large-scale networks .....	91
4.5.2.1	Setting model parameters for real-size networks .....	91
4.5.2.2	Computational complexity analysis .....	93
4.5.2.3	Ranking bridge criticality for Winnipeg network .....	95
4.6	Chapter summary.....	99

## **PART II Advancing link criticality analysis: Bridge-centric transport networks..... 100**

### **CHAPTER 5 Bridges matter: Modeling joint bridge and route choice equilibrium with bridge-centric choice set generation .....**

5.1	Motivation .....	101
5.2	Modeling joint bridge-route choice equilibrium with bridge-centric choice set generation .....	105
5.2.1	Modeling bridge choice alternatives .....	107
5.2.1.1	Bridge choice alternatives and their viability .....	107
5.2.1.2	Availability perception attribute.....	110
5.2.1.3	Availability perception value .....	111
5.2.1.4	Illustrative example for calculating availability perception .....	113
5.2.2	Bridge-route choice model with availability perception of bridges .....	115
5.2.2.1	Specification of utility function with availability perception of bridges 116	
5.2.2.2	Joint probabilistic bridge-route choice model .....	117
5.2.2.3	Illustration of model's features .....	118
5.2.3	Equivalent MP formulation .....	121
5.2.3.1	Proof of equivalence.....	124
5.2.3.2	Proof of uniqueness .....	126
5.2.4	Solution algorithm.....	127
5.2.4.1	Automatic identification of bridge O-D pairs .....	128
5.2.4.2	Bridge-centric choice set generation .....	129
5.2.4.3	Network flow update .....	133
5.3	Numerical experiments.....	135
5.3.1	Experiment 1: A toy network .....	135
5.3.1.1	Equilibrium solution.....	135
5.3.1.2	Impact of demand level on route choice probabilities .....	137
5.3.2	Experiment 2: A large-scale network.....	138
5.3.2.1	Bridge choice set generation .....	138
5.3.2.2	Setting model parameters .....	141
5.3.2.3	Computational complexity analysis .....	142
5.3.2.4	Flow allocation comparison .....	144
5.3.3	Discussion on practical implications .....	146
5.4	Chapter summary.....	147

## **CHAPTER 6 Proactive disruption mitigation: Bridge criticality analysis with a bridge-centric traffic assignment framework ..... 148**

6.1	Motivation .....	148
6.2	Bridge-centric link criticality analysis methodology .....	150
6.2.1	Bridge-centric network equilibrium framework.....	150
	<i>Bridge-centric transport network model</i> .....	151
	<i>Joint bridge-route choice model</i> .....	151
	<i>Equivalent mathematical programming (MP) formulation</i> .....	153
6.2.2	Bridge-centric link criticality index .....	154
6.3	Numerical experiments.....	157
6.3.1	Experiment 1: A toy bridge-centric transport network .....	158
6.3.1.1	Impact of TA model on bridge criticality .....	160
6.3.1.2	Sensitivity analysis .....	163
6.3.2	Experiment 2: The Nguyen-Dupuis network .....	164
6.3.2.1	Impact of network structure on bridge criticality .....	165

6.3.2.2	Impact of choice set on bridge criticality .....	167
6.3.2.3	Impact of non-uniform O-D travel demands on bridge criticality .....	168
6.3.3	Experiment 3: Large-scale bridge-centric transport network.....	170
6.3.3.1	Descriptive analysis of the Winnipeg network.....	171
6.3.3.2	Model parameter settings .....	174
6.3.3.3	Bridge criticality analysis for the Winnipeg network .....	174
6.3.3.4	Impact of maximum bridge sequence length on bridge criticality .....	175
6.3.3.5	Computational complexity analysis .....	177
6.3.3.6	Impact of structural vulnerability coefficients on bridge criticality ....	177
6.3.3.7	Reliability implications .....	179
6.3.4	Supplementary material.....	180
6.4	Chapter summary.....	183
<b>CHAPTER 7 Conclusions.....</b>		<b>184</b>
7.1	Summary of research contributions.....	184
7.2	Limitations and future research directions .....	186
<b>REFERENCES .....</b>		<b>188</b>

## LIST OF FIGURES

Figure 1.1. Flowchart for analyzing losses from disruptive events.....	2
Figure 1.2. Alternative interpretations of criticality of network links.....	4
Figure 1.3. Research objectives.....	9
Figure 2.1. Summary of network equilibrium TA models with MP formulation. ....	14
Figure 2.2. Flowcharts of route- and bridge-centric choice set generation approaches. ....	20
Figure 2.3. Classification of link criticality analysis methods. ....	23
Figure 3.1. Flowchart for the link criticality index (LCI) method. ....	30
Figure 3.2. Equivalent MP formulation for the MNL-SUE-ED model.....	34
Figure 3.3. Partial linearization algorithm with the SRA step size. ....	35
Figure 3.4. Properties of weights for LCI. ....	38
Figure 3.5. A potential limitation of the original UE-based LCI. ....	39
Figure 3.6. A three-link network with two identical parallel links. ....	40
Figure 3.7. Loophole network. ....	46
Figure 3.8. Analysis of SUE-based LCI fluctuations at each iteration. ....	48
Figure 3.9. Discrepancy of LCI values of two identical links.....	49
Figure 3.10. Impact of dispersion parameter on SUE-based LCI. ....	50
Figure 3.11. Demand changes during the equilibration. ....	51
Figure 3.12. Flow fluctuations on Link 2 during the equilibration process. ....	52
Figure 3.13. Link flow changes during the equilibration process. ....	52
Figure 3.14. Impact of demand function parameters on LCI. ....	53

Figure 3.15. Three-link network.....	53
Figure 3.16. Two large-scale test networks and their characteristics.....	56
Figure 3.17. Effect of route choice model parameters on the total coefficient of variation for the Winnipeg and Chicago Sketch networks. ....	58
Figure 3.18. Impact of demand function parameters on total travel demand for two real-size networks.....	58
Figure 3.19. The Winnipeg network and selected bridges. ....	61
Figure 3.20. Spearman’s rank correlation coefficients.....	64
Figure 4.1 Route similarity issue in the Winnipeg network.....	68
Figure 4.2. Impact of route similarity on travel demand.....	70
Figure 4.3. Concept of link criticality analysis: Emphasis on route similarity. ....	71
Figure 4.4. MNL and CNL route choice model structures.....	72
Figure 4.5. Loophole network: Emphasis on shared link.....	75
Figure 4.6. Studying effects of route similarity on link criticality analysis. ....	75
Figure 4.7. Impact of route similarity on route choice.....	76
Figure 4.8. Sensitivity analysis for CNL.....	77
Figure 4.9. MP formulations for MNL-SUE-ED and CNL-SUE-ED models. ....	78
Figure 4.10. Partial linearization algorithm with the SRA step size. ....	80
Figure 4.11. Explanation of the link criticality index (LCI) method. ....	81
Figure 4.12. Intermediate values of components for two CNL-SUE-based LCI methods. ..	86
Figure 4.13. Impact of FFTT of shared link on four LCI methods. ....	88
Figure 4.14. Impact of choice set size on four LCI methods. ....	89

Figure 4.15. Impact of FFTT of non-overlapping route on four LCI methods. ....	90
Figure 4.16. Two large-scale test networks and their characteristics.....	91
Figure 4.17. Effect of route choice model parameters on the total coefficient of variation for the Winnipeg and Chicago Sketch networks. ....	92
Figure 4.18. Computational time for assessing criticality of all links in the Winnipeg and Chicago Sketch networks.....	94
Figure 4.19. The Winnipeg network and selected bridges. ....	95
Figure 4.20. Correlation of bridge LCI values and ranks.....	97
Figure 5.1. Bridge choice alternatives for the Winnipeg network. ....	103
Figure 5.2. Wuhan, China and some most frequent bridge choice alternatives. ....	108
Figure 5.3. Bridge choice alternatives in Winnipeg, Canada, and New York, US. ....	108
Figure 5.4. Bridge choice alternatives grouped based on the route length. ....	114
Figure 5.5. Impact of $\beta$ on availability perception value of bridge choice alternatives. ....	115
Figure 5.6. Toy network and its bridge-route choice model. ....	119
Figure 5.7. Impact of Link 1's FFTT on availability perception of bridge choice alternatives. .....	120
Figure 5.8. Impacts of FFTT and parameter $\eta$ on choice probability for Route 1.....	121
Figure 5.9. Flowchart for solution algorithm. ....	127
Figure 5.10. Method for automatically identifying bridge O-D pairs. ....	128
Figure 5.11. Three scenarios of routes with bridges for the Winnipeg network. ....	130
Figure 5.12. Flowchart for the bridge choice set generation. ....	131
Figure 5.13. Illustration of two-step shortest route algorithm.....	133

Figure 5.14. Impact of demand level on route choice probabilities. ....	137
Figure 5.15. Availability perception values for bridge choice alternatives at $M = 2$ . ....	140
Figure 5.16. Number of bridge choice alternatives before and after truncation. ....	140
Figure 5.17. Sensitivity analysis on the parameters of the availability perception value. ..	141
Figure 5.18. Effect of the selected choice model parameters on the total coefficient of variation for the Winnipeg network. ....	142
Figure 5.19. Convergence characteristics of the solution algorithm. ....	143
Figure 5.20. The Winnipeg network: Link flow difference visualized on GIS map. ....	145
Figure 5.21. Equilibrium link flow differences for IAPL-MNL and MNL-SUE models. ..	146
Figure 6.1. Network models: Road network vs. bridge-centric transport network. ....	151
Figure 6.2. Rationale for incorporating structural vulnerability weights into LCI. ....	155
Figure 6.3. Bridge-centric link criticality index. ....	156
Figure 6.4. A toy network and structure of the corresponding joint bridge-route choice model. .....	159
Figure 6.5. Sorted criticality values for MNL-SUE LCI and bridge-centric LCI methods.	161
Figure 6.6. Decomposition of two LCI methods by components and iteration. ....	162
Figure 6.7. Sensitivity analysis for parameter beta of the IAPL-MNL-SUE model. ....	163
Figure 6.8. Impact of the parameter eta of the bridge-centric TA model on LCI values. ...	164
Figure 6.9. Impact of demand level on criticality of bridges. ....	164
Figure 6.10. The Nguyen-Dupius bridge-centric transport network. ....	165
Figure 6.11. Bridge criticality scores and weights for the Nguyen-Dupius network. ....	166
Figure 6.12. Weights for bridges: Enumerated choice set vs. generated choice set. ....	168



Figure 6.13. LCI values for non-uniform demand: Enumerated vs. generated choice sets.	170
Figure 6.14. The Winnipeg network: Emphasis on bridges. ....	171
Figure 6.15. Schematic representation of land use in the Winnipeg network. ....	172
Figure 6.16. O-D pairs with the highest travel demands. ....	173
Figure 6.17. Spearman correlation of bridge criticality ranks across four LCI methods. ...	176
Figure 6.18. Top 100 critical links according to IAPL-MNL-SUE-based LCI.....	179

## LIST OF TABLES

Table 2.1. Lifecycle of disruptive events. ....	25
Table 2.2. Summary of TA-based link criticality methods. ....	27
Table 3.1. Notation. ....	32
Table 3.2. Equilibration process and LCI computation. ....	40
Table 3.3. An arbitrary iteration of original and refined UE-based LCI methods. ....	45
Table 3.4. Link criticality values and rankings for the loophole network. ....	47
Table 3.5. SUE-based LCI and SUE-ED-based LCI values for the loophole network. ....	51
Table 3.6. Link criticality values for SUE (max demand = 40). ....	54
Table 3.7. Link criticality values for SUE-ED (max demand = 20). ....	55
Table 3.8. Link criticality values for SUE-ED. ....	56
Table 3.9. Convergence characteristics: SUE-based LCI vs. UE-based LCI. ....	59
Table 3.10. List of considered bridges. ....	61
Table 3.11. Top-10 LCI critical rank bridges of the Winnipeg network. ....	62
Table 3.12. LCI values and ranking of bridges in the Winnipeg network. ....	63
Table 4.1. Computing route-based weights for LCI. ....	83
Table 4.2. LCI values with and without considering route similarity. ....	85
Table 4.3. Parameter settings for the Winnipeg and Chicago Sketch networks. ....	93
Table 4.4. Computational characteristics of four SUE models for two real-sized networks. ....	94
Table 4.5. Top 5 critical bridges according to LCI method. ....	96
Table 4.6. Bridge LCI based on two SUE models with FD for the Winnipeg network. ....	98

Table 4.7. Bridge LCI based on two SUE models with ED for the Winnipeg network. ....	98
Table 5.1. Notation.....	106
Table 5.2. Average availability perception values of bridge choice alternatives.....	114
Table 5.3. Route flows for three SUE models.....	136
Table 5.4. Objective function values for three SUE models. ....	136
Table 5.5. Equilibrium probabilities for different demand levels. ....	138
Table 5.6. Region-based distribution of O-D pairs and corresponding bridge sequences. .	139
Table 5.7. Number of region-based bridge sequences and O-D specific bridge choice alternatives. ....	139
Table 5.8. Convergence characteristics: MNL-SUE vs. IAPL-MNL-SUE. ....	144
Table 6.1. Analyzing feature impacts on bridge criticality across experiments.....	157
Table 6.2. Criticality values for MNL-SUE and bridge-centric LCI. ....	160
Table 6.3. Characteristics of bridges in the Nguyen-Dupius network. ....	166
Table 6.4. Bridge criticalities: Enumerated vs. implicit choice sets. ....	168
Table 6.5. Bridge criticalities: Non-uniform travel demand. ....	169
Table 6.6. Top 5 critical bridges for the Winnipeg network ( $M=I$ ). ....	174
Table 6.7. Top 5 critical bridges for three $M$ settings. ....	175
Table 6.8. Computation efforts of the LCI methods (CPU time in sec.).....	177
Table 6.9. Impact of structural vulnerability coefficients on bridge criticality rankings. ...	178
Table 6.10. Specification of the bridge and route choice sets (the Nguyen-Dupuis network). .....	180

Table 6.11. Link attributes for the Nguyen-Dupuis network with uniform O-D travel demands.	
.....	181
Table 6.12. Link attributes for the Nguyen-Dupuis network with non-uniform O-D travel demands..	
.....	181
Table 6.13. Criticality values and ranks for bridge-centric LCI with different parameter settings (the Winnipeg network).	
.....	182

## LIST OF ABBREVIATIONS

AON	All-or-noting traffic assignment
CBD	Central business district
CNL	Cross-nested logit
ED	Elastic demand
FD	Fixed demand
FFTT	Free flow travel time
IAPL	Implicit/availability perception logit
IID	Independent and identical distribution
LCI	Link criticality index
LOS	Level of service
MC	Marginal cost
MNL	Multinomial logit
MP	Mathematical programming
O-D	Origin-destination
RGAP	Relative gap
RMSE	Root mean square error
SRA	Self-regulated averaging
SUE	Stochastic user equilibrium
TA	Traffic assignment
UE	User equilibrium

# CHAPTER 1

## Introduction

---

### 1.1 Research background

Transportation networks are essential for the movement of people and goods, playing a vital role in the economic and social development of cities. However, they are vulnerable to various hazards, which pose potential threats that can damage infrastructure and disrupt network operations ([Xu and Chopra, 2023](#)). Hazards vary in type, frequency, and intensity. When a hazard occurs and severely disrupts the network, it becomes a disaster, leading to significant direct and indirect socio-economic losses ([Adam et al., 2024](#)). For example, in 2009, floods in Cumbria destroyed or damaged 20 bridges, resulting £34 million in repair and replacement costs, along with significant societal impacts ([Council, 2011](#)). Similarly, the 2013 floods in the Danube and Elbe River regions of Central Europe caused road and rail closures, erosion of embankments and streets, damage to bridges, and landslides blocking railways, with total economic damage estimated at over €12 billion ([MunichRe, 2013](#)). In 2018, a section of the Polcevera viaduct in Genoa, Italy, tragically collapsed during a rainstorm, resulting in the deaths of 43 people ([Rymsza, 2021](#)). These examples highlight the importance of effective disaster management to mitigate risks and minimize the impact of such events on transportation infrastructure and society.

Disaster management focuses on prioritization and optimization of pre- and post-disaster investment strategies to enhance a transportation system's resilience and minimize disaster-related losses ([Zhang et al., 2023](#)). One of the initial steps for disaster management is the assessment of the consequences of disruptive events. This includes evaluating potential or

actual structural damage, direct and indirect economic losses, and social impacts expressed in terms of travel delays or casualties ([Faturechi and Miller-Hooks, 2015](#)). Figure 1.1 shows a simplified flowchart for analyzing losses from disruptive events. In this context, a disruptive event encompasses both hazards and disasters.

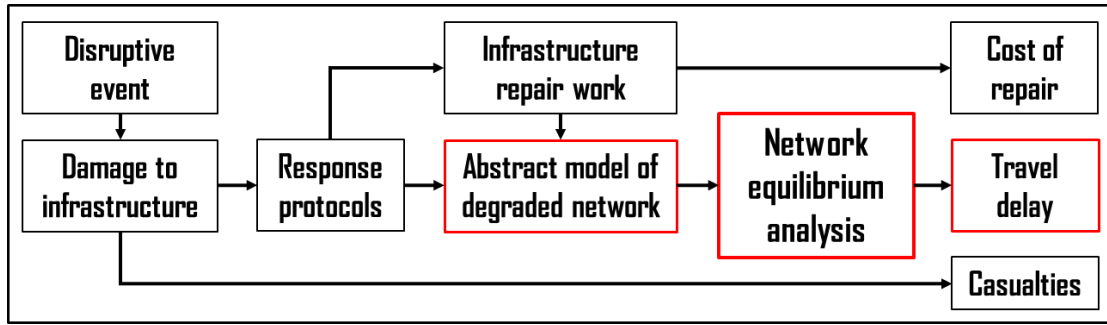


Figure 1.1. Flowchart for analyzing losses from disruptive events.

As illustrated in Figure 1.1, a disruptive event can damage transportation infrastructure, necessitating immediate safety measures and emergency response actions. To ensure travelers' safety, infrastructure managers may impose traffic restrictions, which reduce the traffic capacity of the affected infrastructure elements. Direct economic losses arise from the repair work required for the damaged infrastructure repair, while indirect economic losses result from travel delays caused by the reduced capacity ([Argyroudis et al., 2019](#)). Network travel delays are often evaluated through network equilibrium traffic assignment (TA) models. These models evaluate travel costs and traffic flows based on abstract representation of physical road network, origin-destination (O-D) travel demands, travelers' route choice behavior, and their interactions. Equilibrium TA models provide a robust, objective, and reproducible basis for decision-making and are used frequently in transport planning applications ([Capacci et al., 2022](#)). In summary, losses can be measured using various efficiency measures such as direct monetary costs, travel delay, or number of casualties, with TA models being often used for their estimation.

To mitigate the impact of disruptive events, disaster management may need to prioritize critical network facilities due to limited resources. This often requires network component criticality analysis, which generally evaluates the importance of individual network components (Du et al., 2022). This analysis might consider both structural characteristics (such as age and repair cost) and functional characteristics (such as capacity, travel time, impact on travelers' route choices). Unlike loss estimation (Figure 1.1), which typically focuses on realistically reproducing the consequences of disruptive events and may need to assess the impact of multiple network facility failures simultaneously, network component criticality analysis aims to objectively assess criticality of individual components (Zhou et al., 2019). It may seem that assessing criticality of individual components is an easier task than loss estimation, given that simultaneous failures are not considered. However, assessing the criticality of a network component can be seen as performing loss estimation for a disruptive event that causes the failure of the specified component. In its most intuitive form, assessing criticality of all network components might require multiple loss estimation procedures (Jansuwan and Chen, 2015). Therefore, network component criticality analysis tends to be independent of actual disruptive events and can be more computationally intensive than loss estimation.

This thesis specifically confines its scope to link criticality. Links are abstract representations of roadways and can be characterized by their free flow travel time (FFTT), capacity, and flow-dependent cost functions. There are multiple ways to define the criticality of these links. Figure 1.2 schematically outlines several interpretations of the criticality of network links.



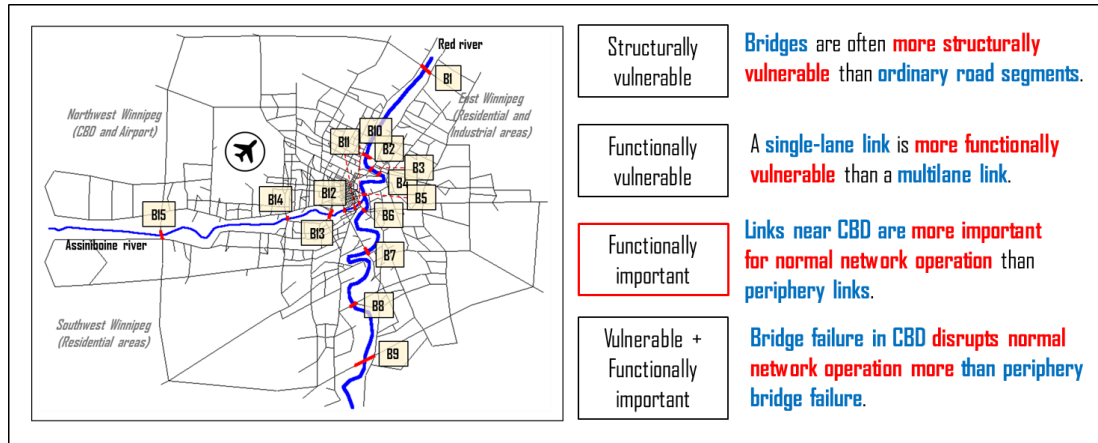


Figure 1.2. Alternative interpretations of criticality of network links.

As shown in Figure 1.2, links may exhibit structural vulnerability, functional vulnerability, functional importance, or a combination of these factors. Bridges, for instance, often demonstrate greater structural vulnerability compared to standard road segments due to elevated structural components. Similarly, single-lane links are more prone to functional vulnerability, as accidents or disruptions can completely block traffic flow, unlike multi-lane alternatives. Conversely, links located near central business districts (CBDs) tend to hold higher functional importance for network efficiency than peripheral links, given their role in high-traffic zones. A CBD bridge exemplifies overlapping risks, combining structural vulnerability (e.g., elevated design) with heightened functional importance due to its critical location. This framework highlights how distinct attributes shape a link's role and resilience within transportation networks.

This thesis addresses the problem of link criticality analysis in terms of functional importance. Link criticality analysis methods based on functional importance measures can be roughly divided into two groups: topology-based methods and network equilibrium TA-based methods. Topology-based methods focus on network connectivity aspects (Corley and Sha, 1982, Fulkerson and Harding, 1977, Holme et al., 2002, Latora and Marchiori, 2001) and are applicable in scenarios where common travel demand and congestion effects can be

neglected, such as evacuation or emergency planning ([Sugiura and Kurauchi, 2023](#)). In contrast, TA-based approaches provide a more comprehensive evaluation by considering individual traveler behavior and interactions ([Jansuwan and Chen, 2015](#), [Jenelius, 2009](#), [Jenelius et al., 2006](#), [Nagurney and Qiang, 2007](#), [Sullivan et al., 2010](#)), making them suitable for applications where travel demand and congestion effects cannot be neglected, such as in the development of mitigation strategies at the pre-disruption stage ([Gu et al., 2020](#)). Therefore, this thesis focuses on TA-based link criticality analysis methods, which are crucial for developing effective mitigation strategies in scenarios where these factors effects cannot be ignored.

## 1.2 Motivation and research gaps

Link criticality analysis for road networks is essential for mitigating and withstanding disruptive events. Frontier methods for link criticality analysis rely heavily on network equilibrium TA models, which provide consistent network traffic flows and travel costs ([Faturechi and Miller-Hooks, 2015](#)). These methods can account for network connectivity, redundancy, travel demand, individual travel choices, and congestion effects induced by traveler interactions. Conceptually, these methods define link criticalities in terms of their functional importance for normal network operations, as indicated by equilibrium TA model. Conventional methods assess link criticalities using a full-scan approach, which entails sequentially deactivating each link, solving a TA problem for each network modification, and subsequently reactivating the link before proceeding to the next one. While feasible for small networks, this approach is impractical for large-scale networks ([Almotahari and Yazici, 2019](#)). Most studies have focused on the computational aspects of the problem, aiming either to approximate ([Chen et al., 2012b](#), [Knoop et al., 2012](#)) or bypass the full-scan process ([Almotahari and Yazici, 2019](#), [Gauthier et al., 2018](#)). In doing so, these studies often neglected

the need for behaviorally plausible TA models for effective link criticality analysis. TA models mimic travelers' route choice behavior and the congestion effects induced by their interactions. These models generate traffic flows and travel costs, which are used for evaluating link criticalities. As a result, equilibrium TA models are fundamental to TA-based link criticality analysis methods. If these models inaccurately represent travelers' behavior and congestion, the evaluations can be considerably imprecise. This possibility for inaccuracies underscores the critical need to address the following research gaps identified in this thesis.

**Research gap 1:** Numerous studies have assessed network link criticalities using user equilibrium (UE) ([Beckmann et al., 1956](#)) models with fixed demand (FD), which assume that travelers try to minimize their travel costs, having perfect knowledge of network conditions and travel demand insensitive to network congestion (i.e., travel demand is inelastic to level of service of the network). However, it is well known that travelers often have incomplete knowledge of network conditions, which affects their individual route choices ([Daganzo and Sheffi, 1977](#)), and that they may switch modes of travel, change their departure times, or forego trips altogether in response to network congestion ([Kitthamkesorn et al., 2016](#)). Ignoring these factors in TA models can lead to traffic flow patterns and network performance that do not adequately represent reality ([Prashker and Bekhor, 2004](#)). As a result, link criticality analysis based on such restricted TA models may also provide a poor representation of actual link criticalities.

**Research gap 2:** Route similarity issues, stemming from route overlaps, are common in road networks ([Chen et al., 2012a](#)). These issues not only substantially distort route choice probabilities, making similar routes less attractive from a travel cost perspective, but also impact O-D travel demands ([Xu and Chen, 2013](#)). This can dramatically change total travel demand, O-D demand patterns, network flow patterns, travel costs, and, hence, link

criticalities. Although the concept of route similarity has been well-explored within the context of stochastic user equilibrium (SUE) TA (Bekhor et al., 2008, Chen et al., 2012a, Prashker and Bekhor, 2004), its application in link criticality analysis remains limited.

**Research gaps 3 and 4:** Bridges play a vital role in road networks that are divided by obstacles like rivers and valleys (Habib et al., 2013). They connect different parts of the network and are essential for reaching certain destinations. Due to their functional importance, they often become traffic bottlenecks, disproportionately affecting travel costs, and overall network performance (Alizadeh et al., 2018). It has been recognized that bridges greatly influence route choice behavior (Manley et al., 2015), with travelers typically selecting bridges first and then deciding on the connecting routes (Kazagli et al., 2016). Despite this recognition, the functional importance of bridges has not been sufficiently emphasized in network equilibrium and link criticality analysis contexts. Existing models treat all links as ordinary road segments, which may not fully capture the behavioral impact of bridges as critical infrastructure components.

### 1.3 Research objectives and contributions

Motivated by the above research gaps, this thesis aims to enhance link criticality analysis, with specific research objectives as follows:

1. **To incorporate perception error and travel demand elasticity into link criticality analysis.** This objective focuses on the first research gap. It aims at advancing a selected link criticality analysis method by relaxing the assumptions of perfect travel cost perception and FD adopting SUE TA model with elastic demand (ED).
2. **To incorporate the effects of route similarity and elastic demand into link criticality analysis.** This objective addresses the second research gap. It aims at incorporating the cross-nested logit (CNL) SUE model with ED (CNL-SUE-ED), which can flexibly

capture the effects of route similarity on both disaggregate (or individuals') route choices and aggregate elastic travel demand, into the selected link criticality analysis method.

3. **To emphasize the crucial role of bridges in network equilibrium analysis.** This objective investigates the third research gap. It introduces the concept of bridge-centric transport networks and develops a new joint bridge and route choice model to better reflect how travelers first select bridges and then decide on the connecting routes. Then, it develops a network equilibrium model that encapsulates the joint bridge and route choice model along with a customized route-based solution algorithm, which consists of a bridge-centric choice set generation method and a route equilibration method.
4. **To apply the developed bridge-centric network equilibrium framework to the criticality analysis of bridges.** This objective addresses the fourth research gap. Acknowledging the unique functional importance of bridges in route choice, it investigates how emphasizing the role of bridges in route choice models and network equilibrium models influences bridge criticalities. By integrating a bridge-centric network equilibrium framework into a selected link criticality analysis method, this study conducts experiments to demonstrate the method's effectiveness and feasibility.

The research objectives of this thesis are schematically summarized in Figure 1.3. As illustrated, the thesis encompasses four research objectives, grouped into two parts. The first part aims to advance link criticality analysis by examining various behavioral issues such as user perception error and the ED issue in the first objective, and route similarity and the ED issue in the second objective. These issues have been thoroughly investigated in the context of equilibrium TA but have been overlooked in link criticality analysis. The second part investigates user behavior, including joint bridge-route choice. Empirical studies indicate that bridges can considerably impact route choice compared to ordinary links. A bridge-centric framework is developed, which includes a bridge-route choice model, a bridge-route choice

equilibrium model, and a customized solution algorithm. This framework is also incorporated into the link criticality analysis.

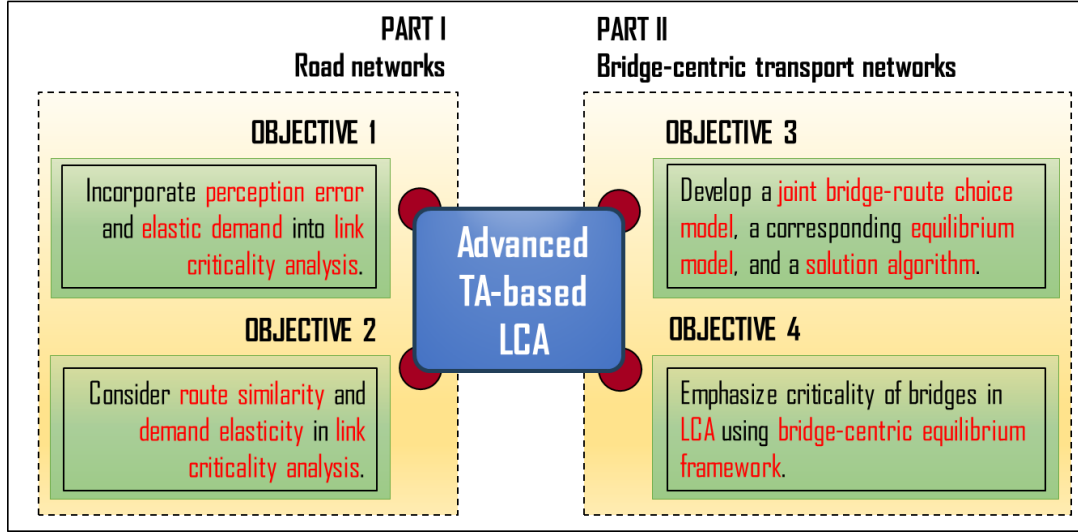


Figure 1.3. Research objectives.

## 1.4 Thesis organization

This thesis consists of seven chapters. Chapter 1 introduces the research problem, while Chapter 2 reviews relevant literature. Chapters 3 to 6 are divided into two parts: Part 1 (Chapters 3 and 4) advances link criticality analysis for road networks, and Part 2 (Chapters 5 and 6) focuses on advancing link criticality analysis for more general bridge-centric transport networks. Chapter 7 provides the concluding remarks. The detailed content of each chapter is explained below.

**Chapter 1: Introduction** establishes the foundation for the thesis. It begins with an overview of the research background, providing context for the study. This is followed by the motivation for the research, explaining why the study is important. The chapter then clearly outlines the research objectives and contributions, detailing what the study aims to achieve. Finally, it concludes with a description of the thesis structure, giving an outline of the subsequent chapters.

**Chapter 2: Literature review** conducts an in-depth analysis of existing studies pertinent to this research. It examines route choice models, network equilibrium TA models, and link criticality analysis methods, forming the foundation for the methodologies employed in this study.

**Chapter 3: Link criticality index: Stochastic user equilibrium model with elastic demand** addresses the first research objective by employing a TA-based link criticality analysis method. It thoroughly examines the method's properties, identifies and resolves deficiencies of the original method, and demonstrates the applicability of the advanced method to large-scale networks.

**Chapter 4: Incorporating route similarity and demand elasticity into link criticality analysis** addresses the second research objective. Building on the foundation established in Chapter 3, it integrates the CNL-SUE-ED model into the link criticality analysis method, effectively capturing the influence of route similarity on both individual route choices and aggregate travel demand. Similar to Chapter 3, it provides a comprehensive analysis of the method's properties, emphasizing the critical role of route similarity in link criticality analysis for large-scale networks.

**Chapter 5: Bridges matter: Modeling joint bridge and route choice equilibrium with bridge-centric choice set generation** addresses the third research objective by developing a bridge-centric framework. This framework includes a joint bridge-route choice model, a new bridge-centric network equilibrium model, and a customized route-based algorithm, highlighting the critical role of bridges in travelers' route choice. It also analyzes and discusses the model's impact on traffic flow patterns compared to traditional models that do not emphasize bridges as important components of transport networks.

**Chapter 6: Advancing bridge criticality analysis: Joint bridge-route choice equilibrium approach** addresses the fourth research objective. It integrates the developed

bridge-centric network equilibrium model and customized route-based algorithm into the selected link criticality analysis method and applies it to bridge criticality analysis in a large-scale network. It demonstrates that link criticality analysis methods based on traditional models can substantially underestimate the criticality of bridges and overestimate the criticality of links representing ordinary road segments.

**Chapter 7: Conclusions** finalize the thesis by providing a summary of the research findings, contributions, and potential future work. This chapter emphasizes the study's impacts and suggests further research to expand the proposed methods' scope and applicability.



# CHAPTER 2

## Literature review

---

The primary objective of this thesis is to advance methodology for link criticality analysis utilizing network equilibrium traffic assignment (TA) models. This chapter provides a review of the existing literature on network equilibrium TA models and link criticality analysis methods.

### 2.1 Network equilibrium models

Network equilibrium TA models are essential for TA-based link criticality analysis methods. These models simulate travelers' route choice behavior and the congestion effects resulting from their interactions. They generate traffic flows and travel costs, which are used to evaluate link criticalities. If these models implausibly represent travelers' behavior and congestion, the evaluations can be misleading.

This section reviews some prominent network equilibrium models. It is organized according to the mathematical network models. The mathematical network models abstract the physical roadway infrastructure and serve as one of the inputs to the network equilibrium analysis. This section distinguishes between two types of transport networks: road networks and bridge-centric transport networks. In road networks, no distinction is made between ordinary road segments and bridges, whereas in bridge-centric transport networks, this distinction is explicitly considered. A road network can be considered as a special case of bridge-centric transport networks. When there are no or limited number of bridges, a bridge-centric transport network can be viewed as an ordinary road network.

### **2.1.1 Network equilibrium models for road networks**

In congested networks, travelers make trips from their origins to destinations using routes they believe minimize their travel costs. When aggregated, individual travelers' route choices create traffic flow, which leads to congestion. Congestion forces travelers to seek alternative routes and keep changing routes until they believe they cannot further minimize their travel costs. Any disruption to the network may influence or force travelers to seek alternative travel options. Equilibrium TA models simulate this behavior. They integrate individual travel choices and their aggregated impact on transportation systems. The fundamental aim of equilibrium TA is to obtain traffic flow patterns given a mathematical network model, origin-destination (O-D) demand matrix, travelers' route choice behavioral assumptions, and flow-dependent link cost functions ([Sheffi, 1985](#)).

This section reviews behavioral route choice assumptions, logit-based route choice models, and network equilibrium models, both with fixed demand and elastic demand. Figure 2.1 summarizes the contents of the section.

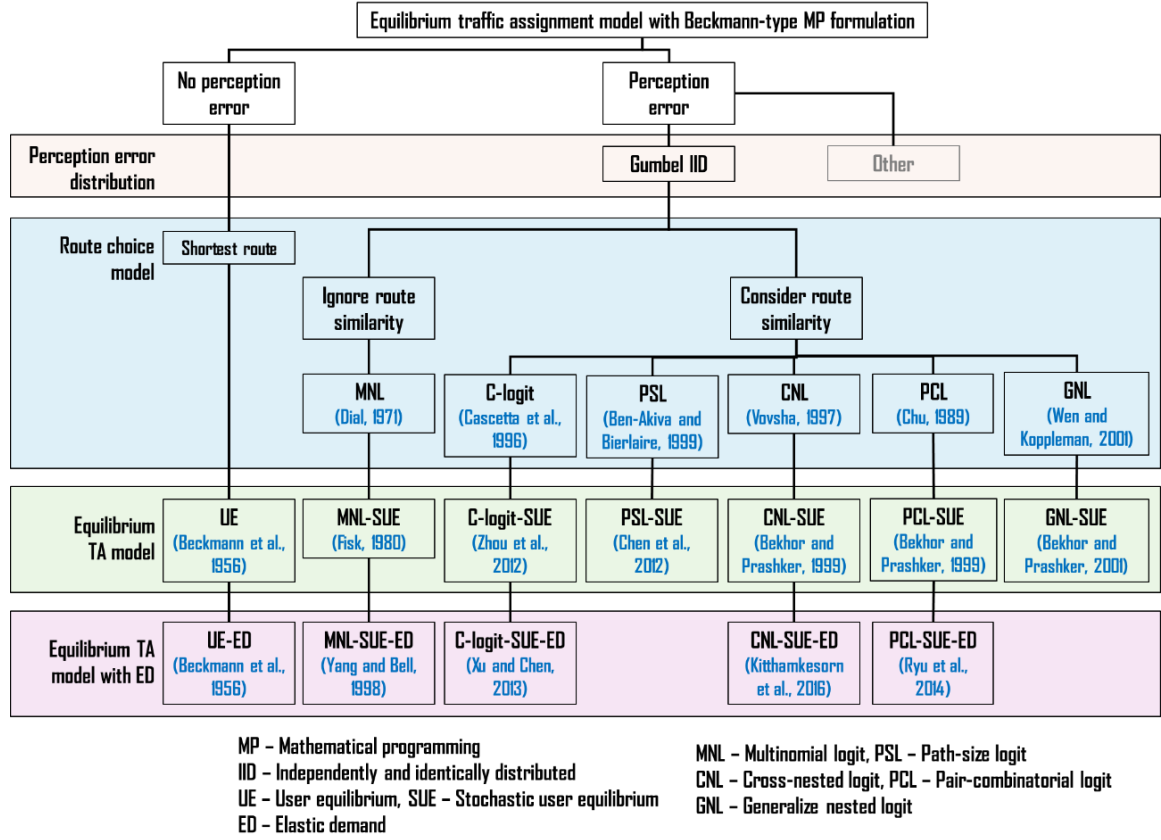


Figure 2.1. Summary of network equilibrium TA models with MP formulation.

### 2.1.1.1 Behavioral route choice assumptions

Two prominent behavioral route choice principles are well-known in the literature: deterministic user equilibrium (UE) and stochastic user equilibrium (SUE). UE follows Wardrop's first principle (Wardrop, 1952). It assumes that all travelers are rational (i.e., choose the least-cost routes) and they possess perfect knowledge of network state (i.e., have no perception errors). At equilibrium, no traveler can experience a lower travel time by unilaterally changing routes (Sheffi, 1985). The UE principle has long been criticized for assuming perfect knowledge of travel costs of all available routes in the network, as travelers typically make decisions based on their perceived travel costs, which contain perception errors, rather than actual costs.

[Daganzo and Sheffi \(1977\)](#) extended the UE principle to the SUE principle by adopting random utility models (RUMs) for adding stochasticity to travel choice behavior at the individual level. RUMs incorporate perception errors into travel disutility function and relax the unrealistic assumption of perfect knowledge of travel costs. Therefore, in SUE, travelers are assumed to choose routes with the minimum perceived (rather than the actual) travel disutility. The perceived error, as well as perceived travel cost, is assumed to follow a certain distribution.

Different distributional assumptions for the random error term lead to the development of various route choice models. Some of these models have closed-form probability expressions, while others do not (i.e., open-form probability expressions). The formulation of a network equilibrium TA model depends on whether it adopts a closed-form model, as discussed in the next subsection.

#### ***2.1.1.2 Equilibrium traffic assignment problem formulations***

There are various ways to formulate an equilibrium TA problem. For example, it can be formulated as an equivalent mathematical programming (MP) problem, nonlinear complementarity problem, variational inequality, or fixed point ([Cantarella et al., 2015](#)). The latter three formulations are considered more general than the MP formulation. For example, equivalent MP formulations are not necessarily available for network equilibrium TA problems with asymmetric transportation costs ([Liu et al., 2021](#)). However, these formulations lack some important theoretical features that MP formulation approach can provide. Specifically, a MP formulation is beneficial because it (i) explicitly defines the objective function, constraints, decision variables, and optimality conditions, making it highly interpretable ([Beckmann et al., 1956](#), [Fisk, 1980](#), [Prashker and Bekhor, 2004](#), [Yang and Bell, 1998](#)), and (ii) aids in developing efficient algorithms that can effectively determine the

direction, step sizes, and stopping criteria in the search process (Chen et al., 2013, Damberg et al., 1996, Du et al., 2021, Frank and Wolfe, 1956, Larsson and Patriksson, 1992, Leblanc, 1975).

### ***2.1.1.3 Logit-based route choice equilibrium models***

A probabilistic route choice model is a core component of SUE TA models. Among all, the closed-form route choice models are valued for their analytical tractability. Consequently, SUE models that incorporate these route choice models can be formulated as MP problems. This subsection reviews well-known logit-based route choice models, which exemplify closed-form route choice models and are used throughout the entire thesis.

The multinomial logit (MNL) model, a discrete choice model frequently used in route choice, is based on RUM. It assumes that the random components of each utility function are independently and identically distributed (IID) Gumbel variables. The probability of choosing a route is determined by the difference in measured utilities between that route and all others (Dial, 1971). The MNL model has a closed-form probability solution, which makes it analytically convenient. However, its structure cannot capture similarities among routes due to the independence assumption of random terms (Bekhor and Prashker, 1999, Vovsha, 1997).

Many efforts have been made to develop various extended logit choice models to address this issue. The developed models can be categorized into three types based on how they handle route similarity. The first type incorporates modification terms into the utility function's systematic component to adjust route choice probabilities: the C-logit model (Cascetta et al., 1996, Zhou et al., 2012) and the path-size logit (PSL) model (Ben-Akiva and Bierlaire, 1999, Chen et al., 2012a). The second group modifies the error term of the utility function, allowing a more flexible nested model structure: the paired combinatorial logit (PCL) model (Bekhor and Prashker, 1999, Chen et al., 2014, Chu, 1989, Pravinongvuth and Chen, 2005), the cross-

nested logit (CNL) model (Bekhor and Prashker, 1999, Vovsha, 1997), and the generalized nested logit (GNL) model (Bekhor and Prashker, 2001, Wen and Koppelman, 2001). The third group extends the previous models by incorporating route similarities into the error structure of the utility function, using mixed logit models (i.e., open-form probability expressions that cannot be analytically evaluated), which are out of the scope of the current research.

Logit-based route choice models are used in SUE TA. Fisk (1980) provided equivalent MP formulation for MNL-SUE. Zhou et al. (2012) provided equivalent MP formulation for C-logit-SUE. Equivalent MP formulations for CNL-SUE, PCL-SUE, and GNL-SUE were given by (Bekhor and Prashker, 1999, Bekhor and Prashker, 2001).

#### ***2.1.1.4 Logit-based route choice equilibrium models with elastic demand***

Besides route choice, travelers can have other travel choices such as travel choice (whether to travel or not), destination choice (where to travel), and mode choice (which mode to use) (Meyer, 2016). If congestion is too high, travelers may cancel their trips, choose less congested destinations, or use other travel modes. Conversely, low congestion levels may induce previously hidden travel demand. These phenomena can be captured by a variable demand function that accounts for demand elasticity in relation to congestion levels (Beckmann et al., 1956, Kitthamkesorn et al., 2016, Yang and Bell, 1998). Therefore, a TA model with elastic demand (ED) function allows to account for these behavioral features of travelers.

Beckmann et al. (1956) formulated the UE TA problem with ED as a convex optimization problem that assumed perfect knowledge of network state. To account for travelers' imperfect knowledge on network conditions, Yang and Bell (1998) extended the MNL-SUE model with fixed demand proposed by Fisk (1980). The model formulated by Yang and Bell (1998)

overlooks the impact of route similarity on route choice behavior. To account for route similarity, [Xu and Chen \(2013\)](#) extended [Zhou et al. \(2012\)](#) and provided a MP formulation for the C-logit-SUE problem with ED. Similarly, [Ryu et al. \(2014\)](#) extended [Bekhor and Prashker \(1999\)](#) and provided an equivalent MP formulation for the PCL-SUE problem with ED. [Kitthamkesorn et al. \(2016\)](#) developed an equivalent MP for the combined modal split and TA model as a CNL-SUE-ED model to explicitly capture mode and route similarities under congested networks. The mode choice was modelled using the nested logit model ([Ben-Akiva and Lerman, 1985b](#)) and the route choice was modelled through the CNL model ([Bekhor and Prashker, 1999](#)).

## **2.1.2 Network equilibrium models for bridge-centric transport networks**

Existing SUE models treat all links as ordinary road segments, which may not fully capture the behavioral impact of bridges as critical infrastructure components of transportation networks. This section discusses the key elements of a bridge-centric network equilibrium framework.

### ***2.1.2.1 Modeling joint bridge-route choice***

The real-world evidence supporting the hypothesis that bridge choice is distinct from route choice is provided in [Manley et al. \(2015\)](#), [Habib et al. \(2013\)](#), and [Alizadeh et al. \(2018\)](#). [Manley et al. \(2015\)](#) observed that taxi drivers' route choices in London were influenced by anchor points, including bridges. [Habib et al. \(2013\)](#) and [Alizadeh et al. \(2018\)](#) reported that hierarchical bridge-route choice models could better represent the route choice behavior in Montreal, Canada.

Researchers have made great efforts to adopt discrete choice models in the context of route choice ([Chen et al., 2012a](#), [Prashker and Bekhor, 2004](#), [Prato, 2009](#)). These models can

be further adopted to solve the joint bridge-route choice problem. The MNL model provides a closed-form probability expression which can enhance computational efficiency. The implicit availability/perception logit (IAPL) model, an extension of MNL, models the implicit perception/availability of an alternative (Cascetta and Papola, 2001). It inherits all its features and additionally accounts for potential choice set misspecification. This misspecification occurs because analysts may not fully understand travelers' preferences and may inaccurately specify the choice set. Such misspecification can bias traffic flow predictions (Bliemer and Bovy, 2008, Bovy, 2009, Prato, 2009). In the IAPL model, choice set misspecification is addressed using an 'availability perception value', a function based on the availability attributes of the choice alternatives. This value ranges from 0 to 1, providing intermediate degrees of availability for a choice alternative. It can also be interpreted as the probability of a choice alternative being included in the choice set (Cascetta and Papola, 2001). The main benefits of the IAPL model are its operational flexibility and its ability to circumvent the computational burden associated with the explicit availability/perception and choice approaches (Ben-Akiva and Boccara, 1995).

#### ***2.1.2.2 Bridge-route choice set generation***

Consideration of bridge impact on route choices may require modifications not only in choice models but also in choice set generation techniques. Figure 2.2 shows route-centric and bridge-centric choice set generation techniques.



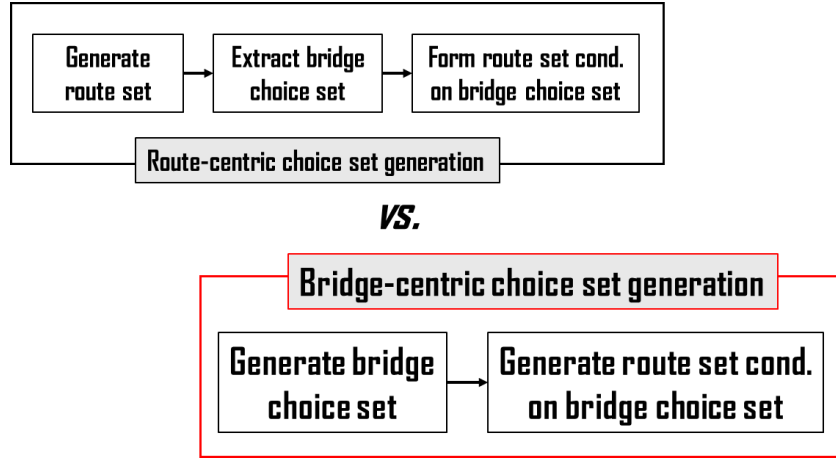


Figure 2.2. Flowcharts of route- and bridge-centric choice set generation approaches.

A review of the literature reveals that in existing studies on the joint bridge-route choice problem, choice sets were mainly generated in a route-centric manner (Alizadeh et al., 2018). As shown in Figure 2.2, for each O-D pair, the process was as follows: first, generate a set of routes; then, from these routes, extract bridge choice sets; and finally, form route choice sets conditioned on the bridge choice sets. However, existing route set generation techniques can produce unrealistic alternatives, such as long-detour routes, overly similar routes, or overly complex routes (Bekhor et al., 2008, Bovy, 2009, Prato, 2009). A bridge set extracted from these routes may contain unreasonably long bridge choice alternatives<sup>1</sup>. Consequently, routes based on these bridge choice alternatives may also be unrealistic. To avoid the issue with the bridge choice set, existing studies (Alizadeh et al., 2018) assumed that O-D pairs utilized identical bridge choice sets consisting of single-bridge choice alternatives (i.e., each bridge choice alternative is associated with a bridge sequence of length one). This assumption permitted the manual enumeration and elimination of unreasonable bridge choice alternatives. However, in general bridge-centric transport networks, this assumption may not hold because it oversimplifies the complexity of real-world bridge-centric transport networks. For example,

<sup>1</sup> A bridge choice alternative is a feasible sequence of bridges connecting O-D pair. It may consist of one or several bridges.

travelers between different O-D pairs may have different sets of feasible or preferable bridges based on factors such as distance, toll, traffic conditions, and personal preferences. Then, the assumption of single-bridge choice alternatives implies that each route only involves crossing one bridge. This may not be the case in complex bridge-centric transport networks where routes may involve crossing multiple bridges. Moreover, there may be multiple destinations that would not necessarily consider the same set of bridges. Travelers going to different destinations may choose different bridges even if they start from the same origin. This issue remains unaddressed in the literature. Further research on generating bridge choice sets and conditioned route choice sets is required.

### ***2.1.2.3 Modeling joint bridge-route choice network equilibrium***

Although the existing empirical results have shown several behavioral issues need to (or can) be incorporated to enhance the modeling of bridge and route choice, these issues are based on discrete choice modeling and cannot endogenously consider the congestion effect, which is a critical factor for modeling traffic bottlenecks like bridges. Congestion effects may influence travelers to choose alternative bridges or routes when the primary ones are congested or not available, which in turn can impact the network-level traffic flow pattern. Consistent prediction of traffic flow patterns in urban networks necessitates modeling the interplay between congestion and travel choices. To the best of our knowledge, the existing studies on modeling joint bridge-route choice did not consider the effects of congestion on the travelers' choices. [Habib et al. \(2013\)](#) developed a choice model that simultaneously addressed bridge choice set formation and bridge choice, enabling the adjustment of analysts' errors in choice set specification. Nevertheless, their study did not consider the congestion effects and the overall route choice connecting the origin to the destination. [Alizadeh et al. \(2018\)](#) extended the scope to include joint bridge-route choice analysis. While the latter

tackled the joint bridge-route choice issue, it did not account for congestion effects and choice set formation. Further research is therefore necessary to consider the impact of joint bridge-route choice and congestion effects on traffic flow patterns as a joint bridge-route network equilibrium model.

## 2.2 Link criticality analysis methods

This section reviews methodologies for link criticality analysis and identifies existing research gaps. Figure 2.3 provides a visual summary of these methods in terms of two important issues: thoroughness of analysis and computational efficiency.

As shown in Figure 2.3, link criticality analysis methods can be represented by two dominant methodologies: topology-based methods, which emphasize the structural characteristics of networks ([Corley and Sha, 1982](#), [Fulkerson and Harding, 1977](#), [Holme et al., 2002](#), [Latora and Marchiori, 2001](#)), and TA-based methods, which integrate considerations of travel behavior, demand, and congestion effects ([Jenelius, 2009](#), [Jenelius et al., 2006](#), [Nagurney and Qiang, 2007](#), [Scott et al., 2006](#), [Sullivan et al., 2010](#)).

Topology-based methods, on the one hand, could be used for planning evacuation or emergency lifesaving strategies after disruptive events when the typical travel demand and congestion effects could be neglected ([Sugiura and Kurauchi, 2023](#)). On the other hand, they were arguably inapplicable for planning transportation infrastructure reinforcement (prior to disruptive events) or reconstruction plans (after disruptive events) when congestion effects and drivers' travel behavior could not be neglected. While topology-based methods have their specific applications, the limitations in addressing congestion and travel behavior necessitated the use of TA-based methods for a more comprehensive evaluation of link criticality.

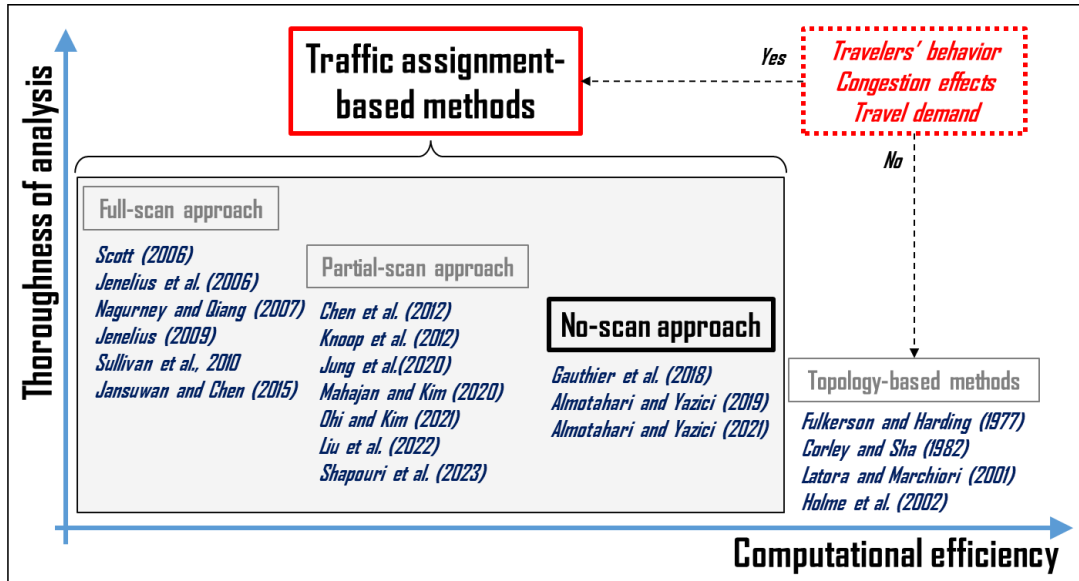


Figure 2.3. Classification of link criticality analysis methods.

Early TA-based methods used a full network scan methodology. This methodology evaluated link criticalities by systematically deactivating links and analyzing the resulting impact on overall network efficiency by solving an equilibrium TA problem for each network change (Nagurney and Qiang, 2007). While thorough, this approach was impractical for large-scale networks due to the need to solve the TA problem for each link deactivation, which entails solving a large number of TAs (Chen et al., 2012b, Jung et al., 2020, Knoop et al., 2012). Subsequent TA-based methods reduced the computational burden by scanning a subset of links (Knoop et al., 2012, Liu et al., 2022, Shapouri et al., 2023), limiting the impact area of link deactivation (Chen et al., 2012b), or using equally sized link grids (Jung et al., 2020, Mahajan and Kim, 2020, Ohi and Kim, 2021). However, these methods overlooked critical links, ignored global effects of link removal, or failed to capture individual link importance, respectively. Additionally, the latter methods still relied on network scan methodology, which might limit their application in large-scale networks. To address this issue, methods that eliminated network scanning altogether were explored. One such method was the link criticality index (LCI) proposed by (Almotahari and Yazici, 2019, Almotahari and Yazici,

2021). This method assessed the criticality of all links based on flow fluctuations during a single equilibrium TA procedure, making it one of the most efficient methods for link criticality analysis.

Besides computational complexities, many TA-based link criticality analysis methods may produce implausible results due to their reliance on oversimplified TA models. Numerous studies assessed network link criticalities using UE TA (Almotahari and Yazici, 2019, Almotahari and Yazici, 2021, Jenelius, 2009, Nagurney and Qiang, 2007, Sullivan et al., 2010). UE assumes that travelers have perfect knowledge of route costs, enabling them to consistently choose the least-cost routes. This assumption was often considered unrealistic, as travelers might not always know the exact least-cost routes (Sheffi, 1985). Complementing this, only a few studies including Jansuwan and Chen (2015) refined link criticality assessment measures by extending them to SUE.

To the best of our knowledge, no studies have addressed the issue of route similarity, demand elasticity, and bridge choice in link criticality analysis context. Route similarity is a common issue in road networks. It affects not only route choice but also travel demand (Prashker and Bekhor, 2004). Physical infrastructure elements may differ in the roles they play in the system. Empirical studies indicate that some elements, such as bridges, may be more critical than others, such as ordinary road links. Therefore, they may impact travelers' route choice behavior in different ways (Alizadeh et al., 2018, Habib et al., 2013, Kazagli et al., 2016, Manley et al., 2015). All these can alter traffic flow pattern, travel costs, and consequently, link criticality values. Conventional network equilibrium models overlook these features, potentially biasing the results of any subsequent analysis.

This section has reviewed link criticality analysis methods, with a particular emphasis on TA-based approaches. The subsequent section discusses application of these methods in network resilience analysis.

## 2.3 Link criticality analysis applications

Link criticality analysis in transport networks is closely related to network resilience analysis (Almotahari and Yazici, 2019, Zhou et al., 2019). Resilience is a complex multi-disciplinary concept that includes a wide range of tasks including assessment, monitoring, evaluation, planning, prioritization, and management of transportation system to prepare for, withstand, and recover from disruptive events (Berdica, 2002, Faturechi and Miller-Hooks, 2015, Gu et al., 2020, Serdar et al., 2022, Zhou et al., 2019). These tasks are summarized in Table 2.1.

Table 2.1. Lifecycle of disruptive events.

Stage	Phase	Tasks	Remarks
Pre-disruption	Mitigation	<ul style="list-style-type: none"> <li>Find critical network elements.</li> <li>Assess the vulnerability of critical elements.</li> <li>Design and execute network enhancement projects.</li> </ul>	To evaluate the potential negative effects of disruptive events and design proactive measures, it is important to consider congestion and travel demand.
	Preparedness	<ul style="list-style-type: none"> <li>Design contingency protocols and awareness campaigns.</li> <li>Train rescue teams.</li> <li>Pre-position equipment.</li> </ul>	
Post-disruption	Response	<ul style="list-style-type: none"> <li>Monitor and assess system's performance.</li> <li>Operate emergency and evacuation services.</li> </ul>	Congestion and travel demand other than emergency can be neglected.
	Recovery	<ul style="list-style-type: none"> <li>Assess consequences of disruptive event.</li> <li>Prioritize reconstruction works.</li> <li>Develop restoration works and travel demand management strategies.</li> </ul>	To select a recovery program that effectively restores the system to its normal operational state, it is important to consider congestion and travel demand.

As shown in Table 2.1, there are four phases in the life cycle of a disruptive event: mitigation, preparedness, response, and recovery (Faturechi and Miller-Hooks, 2015). The mitigation and preparedness phases occur at the pre-disruption stage, focusing on anticipating and reducing potential negative impacts of disruptive events. The response and recovery phases occur at the post-disruption stage, involving actions to restore network efficiency. Mitigation strategies, such as retrofitting components or increasing capacity, aim to prevent or minimize impacts (Twumasi-Boakye and Sobanjo, 2018). Preparedness strategies, including awareness campaigns, training, and pre-positioning equipment, enhance response

efficiency. The response includes emergency rescue and medical services (Sugiura and Kurauchi, 2023). The recovery phase concerns system repairs.

Based on Table 2.1, the proposed method can potentially be utilized during the mitigation and preparedness phases to identify critical network elements and plan network retrofitting works. However, while the current method offers some insights into the recovery phase, it may not be suitable for planning restoration works, as this phase requires more complex analyses to effectively schedule concurrent restoration activities in degraded networks (Peng et al., 2024).

In summary, link criticality analysis is indispensable for designing proactive strategies to mitigate medium- to long-term disruptions, such as infrastructure degradation, climate hazards, and systemic cascades.

## 2.4 Chapter summary

In summary, equilibrium TA integrates individual traveler choices and their aggregated impacts on transportation systems, which results in congestion. It provides traffic flow patterns and quantifies network performance based on assumed travel behavior and demand levels. Numerous studies highlight the importance of explicitly modeling features such as traveler perception errors, route similarity, demand elasticity, and recognizing that links may represent infrastructure elements of different criticalities for a behaviorally plausible simulation of traveler behavior in congested transportation networks.

By considering traveler behavioral characteristics and congestion effects, equilibrium TA provides a means to define a normal operational network state, which serves as a reference for TA-based link criticality analysis. Early TA-based link criticality analysis methods required a full-scan process to assess all link criticalities, limiting their applicability to small-scale networks. In contrast, recent methods have eliminated the need for the full-scan process,

making them suitable for large-scale networks. However, these recent methods have overlooked the importance of nuanced modeling of travelers' behavior and network structure, which may greatly influence the reference state of the networks and, consequently, the criticality of links. This thesis aims to address this issue by incorporating detailed behavioral modeling and network structure into analysis to enhance TA-based link criticality analysis.

Table 2.2 summarizes TA-based methods for link criticality analysis and highlights the research gaps addressed in this thesis.

Table 2.2. Summary of TA-based link criticality methods.

Reference	Method.	Equilibrium TA model	Travelers' perception error	Demand elasticity	Route similarity	Bridge choice
<i>Scott et al. (2006), Jenelius et al., (2006), Nagurney &amp; Qiang (2007), Jenelius (2009), Sullivan et al. (2010)</i>	Full scan	UE	×	×	×	×
<i>Jansuwan &amp; Chen (2015)</i>	Full scan	MNL-SUE	✓	×	×	×
<i>Knoop et al. (2012), Liu et al. (2022), Shapouri et al. (2023), Chen et al. (2012b), Jung et al. (2020), Mahajan &amp; Kim (2020), Ohi and Kim (2021)</i>	Approx. scan	UE	×	×	×	×
<i>Almotahari &amp; Yazici (2019, 2021)</i>	No scan	UE	×	×	×	×
<b>Chapter 3</b>	<b>No scan</b>	MNL-SUE-ED	✓	✓	×	×
<b>Chapter 4</b>	<b>No scan</b>	CNL-SUE-ED	✓	✓	✓	×
<b>Chapter 5 and 6</b>	<b>No scan</b>	IAPL-MNL-SUE	✓	×	×	✓



# PART I

## **Advancing link criticality analysis: Road networks**

---

Real transportation systems are abstracted by mathematical network models, which are essential for network analysis. These models are referred to as road networks. Part I advances link criticality analysis by integrating nuanced network equilibrium traffic assignment (TA) models based on simplified road network representations that consider all links as ordinary road segments.

## CHAPTER 3

# Link criticality index: Stochastic user equilibrium model with elastic demand

---

This chapter adopts an efficient link criticality method, namely link criticality index (LCI), and advances it from user equilibrium TA with fixed demand (UE-FD or UE) to stochastic user equilibrium (SUE) TA with elastic demand (ED). These extensions effectively account for the stochastic nature of travelers' route choice (i.e., the assumption of travelers' perfect knowledge of network travel time is relaxed) and acknowledge the existence of travel choices beyond route choice (i.e., the assumption of fixed demand is relaxed).

### 3.1 Motivation

Link criticality index (LCI), developed by [Almotahari and Yazici \(2019\)](#), is one of the state-of-the-art TA-based method for link criticality analysis. This method circumvents the full-scan process that is prevalent in most TA-based methods, while still producing link criticality evaluations that are consistent with those obtained from full-scan-based approaches. Like all TA-based methods for link criticality analysis, the LCI method effectively captures the impact of network connectivity, travel demand, individual travel choice behavior, congestion effects, and redundancy. Unlike many TA-based methods, the LCI method assesses the criticality of all links in a single equilibrium TA procedure.

Figure 3.1 illustrates the overall methodology of computing LCI.

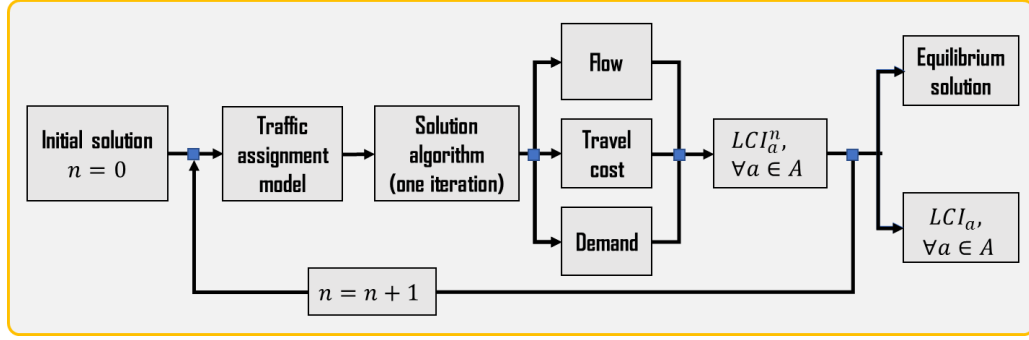


Figure 3.1. Flowchart for the link criticality index (LCI) method.

As shown in Figure 3.1, the LCI method assesses link criticality by examining traffic flow fluctuations during the equilibration procedure within a single TA execution. This method posits that links which consistently experience additional traffic flows, even when saturated, are essential for network operation and are therefore critical.

However, the original LCI method cannot plausibly reflect common travelers' behavior due to the adoption of UE TA model, which is known to assume that travelers have a perfect perception of travel costs, which results in a behaviorally restrictive route choice model (Daganzo and Sheffi, 1977, Jansuwan and Chen, 2015, Prashker and Bekhor, 2004); fixed and known travel demand, which neglects the fact that travelers may change their travel plans in response to congestion (Kitthamkesorn et al., 2016, Ryu et al., 2014, Xu and Chen, 2013, Yang and Bell, 1998). Additionally, the all-or-nothing (AON) network loading approach is typical for UE TA. AON assigns O-D demand exclusively to the shortest route and disregards other routes (Sheffi, 1985). This can result in zero-flow routes when used with a route-based solution algorithm. There are two key issues with this for the UE-based LCI method. First, a route may bear zero flow but still contribute to the criticality of a link serving that route. Although this can be interpreted as LCI accounting for network redundancy (i.e., each route crossing a link enhances the network redundancy provided by that link), it can be inappropriate when there are highly unattractive routes with respect to travel cost (e.g., long

detour routes). Routes like these can mistakenly appear in route choice sets, which is a common issue in practice (Bliemer and Bovy, 2008). This can potentially lead to an overestimation of a link's criticality. Second, it is possible for two shortest routes to exist in an iteration, where the first route may have a link that is identical to a link in the second route. Since the AON loads all travel demand onto a single route in each iteration, the second route can be neglected. This can lead to different rankings for identical links.

Motivated by the above challenges, this chapter aims to refine the functional form of the UE-based LCI to address the zero-flow problem, should an analyst opt to adhere to the UE TA model in the LCI method. Next, it advances the LCI method by integrating SUE and SUE with ED (SUE-ED) models. This advancement relaxes the assumption of perfect travel time perception, effectively addressing all the aforementioned issues associated with the AON network loading approach. Consequently, it offers a more behaviorally realistic framework for analyzing link criticality in a road network. Without loss of generality, this study adopts the SUE and SUE-ED TA models provided by Fisk (1980) and Yang and Bell (1998), respectively. These TA models assume that travelers choose their routes according to the multinomial logit (MNL) model (Dial, 1971), one of the simplest closed-form probabilistic route choice models. Formulated as mathematical programming (MP) problems, these TA models guarantee the existence and uniqueness of equilibrium solutions. To demonstrate the properties of the SUE-based and SUE-ED-based LCI methods, these advanced techniques are applied to several toy networks. To validate the concept, the methods are also tested on a real-size road network.

The remainder of the chapter is organized as follows. Section 3.2 introduces the methodology, including notation, equilibrium TA model formulation, and solution algorithm. Sections 3.3 elaborates on the original and refined LCI methods. Sections 3.4 and 3.5 present the numerical results and concluding remarks, respectively.

## 3.2 Equilibrium traffic assignment model

This section briefly introduces the MNL route choice model and the equivalent MP formulations.

### 3.2.1 Notation

Table 3.1 provides a notation list.

Table 3.1. Notation.

Sets	
$\mathcal{N}$	Set of nodes in the network
$\mathcal{A}$	Set of directed links
$\mathcal{W}$	Set of O–D pairs
$\mathcal{R}^w$	Set of routes connecting O–D pair $w$
Parameters/inputs	
$\delta_{ar}^w$	Element of the route–link incidence matrix corresponding to an O–D pair $w$ , route $r$ , and link $a$
$\theta$	Dispersion parameter of a route choice model
$\xi$	Demand function scaling parameter, which reflects the sensitivity of demand to travel cost
$\bar{q}^w$	Maximum (or potential) demand for O–D pair $w$
Intermediate variables/functions	
$c_r^{w,n}$	Deterministic travel time on route $r$ of O–D pair $w$ at iteration $n$
$C_r^{w,n}$	Perceived travel time on route $r$ of O–D pair $w$ at iteration $n$
$p_r^w$	Probability of choosing route $r$ of O–D pair $w$
$x_a$	Flow on link $a$
$t_a$	Travel time on link $a$
$mc_a$	Marginal cost of traveling on link $a$
$D^w$	Demand function for O–D pair $w$
$Q$	Total network demand
$S_a^n$	Unweighted criticality score for link $a$ at iteration $n$
$\gamma^w$	Demand-specific weight of O–D pairs $w$ used in LCI
$\mu_r^{w,n}$	Route-specific weight for a route $r$ of an O–D $w$ at iteration $n$
$LCI_a$	Link criticality index for link $a$
Decision variables	
$f_r^w$	Flow on route $r$ of O–D pair $w$
$q^w$	Demand of O–D pair $w$ (for ED)

### 3.2.2 Route choice models

The random utility model framework is a well-known framework used in modeling route choice. It incorporates travelers' perception error in the random utility model, i.e.:

$$C_r^w = c_r^w + \varepsilon_r^w, \quad \forall r \in \mathcal{R}^w, \forall w \in \mathcal{W} \quad (3.1)$$

where  $C_r^w$  is the perceived travel time on route  $r$  of O–D pair  $w$ ,  $c_r^w$  is the deterministic travel time on route  $r$  of O–D pair  $w$ , and  $\varepsilon_r^w$  random error term.

It assumes that the perception error term,  $\varepsilon_r^w$ , is represented by the independently and identically distributed (IID) Gumbel random variable with the theoretical expectation  $E[\varepsilon_r^w] = 0$  and variance  $Var[\varepsilon_r^w] = \frac{\pi^2 \theta^2}{6}$ ,  $\forall r \in \mathcal{R}^w$ . The dispersion parameter  $\theta$  measures the sensitivity of route choices with respect to travel cost (Sheffi, 1985). The MNL model provides a closed-form probability expression, i.e.:

$$P_r^w = \frac{e^{-\theta c_r^w}}{\sum_{l \in \mathcal{R}^w} e^{-\theta c_l^w}}, \quad \forall r \in \mathcal{R}^w, \forall w \in \mathcal{W} \quad (3.2)$$

Owing to the IID assumption, this model cannot consider (i) the similarity between travel alternatives and (ii) alternative-specific perception variances with respect to the heterogeneity of travel alternatives. However, it is sufficient for us to analyze the properties of LCI in the context of SUE. For more information on logit-based route choice models, interested readers may refer to (Prashker and Bekhor, 2004).

### 3.2.3 Equivalent MP formulation

This study adopts two models, namely multinomial logit stochastic user equilibrium (MNL-SUE) and multinomial logit stochastic user equilibrium with elastic demand (MNL-SUE-ED). Solutions of both models satisfy the SUE conditions (3.3), and the solution of MNL-SUE-ED additionally satisfies the ED function (3.5).

$$f_r^w = P_r^w q^w, \quad \forall r \in \mathcal{R}^w, \forall w \in \mathcal{W} \quad (3.3)$$

where  $f_r^w$  is flow on route  $r$  of O–D pair  $w$ ,  $P_r^w$  is probability of choosing route  $r$  of O–D pair  $w$ ,  $q^w$  is demand of O–D pair  $w$ .

The equivalent MNL-SUE and MNL-SUE-ED MP formulations are shown in Figure 3.2.

$$\begin{aligned}
& \text{UE (Beckmann et al., 1956)} & \text{MNL-SUE (Fisk, 1980)} & \text{MNL-SUE-ED (Yang and Bell, 1998)} \\
& \min \sum_{\forall a} \int_0^{x_a} t_a(\zeta) d\zeta & + \frac{1}{\theta} \sum_{\forall w} \sum_{\forall r} f_r^w \ln f_r^w & - \sum_{\forall w} \int_0^{q^w} D^{w^{-1}}(\zeta) d\zeta - \frac{1}{\theta} \sum_{\forall w} q^w \ln q^w \\
& \text{Subject to } \sum_r f_r^w = q^w, \forall w & \text{Definitional constraints} & \\
& f_r^w \geq 0, \forall r, \forall w & x_a = \sum_{\forall w} \sum_{\forall r} \delta_{ar}^w f_r^w, \forall a \in A & \\
& \text{(for ED)} \quad q^w \geq 0, \forall w & &
\end{aligned}$$

Figure 3.2. Equivalent MP formulation for the MNL-SUE-ED model.

As shown in Figure 3.2, the MP formulation for the MNL-SUE TA problem was developed by (Fisk, 1980), and it was extended by (Yang and Bell, 1998) to MNL-SUE-ED. The objective function of the MNL-SUE-ED formulation has four terms. The first term is equivalent to the well-known Beckmann transformation objective function. The second term corresponds to the route-flow based entropy term. The third term is an inverse demand function term for the UE with ED problem. The fourth term represents the demand entropy term.

In the proceeding sections, MNL-SUE and MNL-SUE-ED are referred to as SUE and SUE-ED, respectively.

### 3.2.4 Travel demand model

Travel demand may be influenced by the level of service (LOS) on the network. As congestion increases, travelers may decide to change their travel choices (Sheffi, 1985). To address this phenomenon, travel demand between every O-D pair in the network can be assumed to be a function of LOS in (3.4).

$$q^w = D^w(u^w), \quad \forall w \in \mathcal{W} \quad (3.4)$$

where  $u^w$  is the expected perceived cost (EPC) between O-D pair  $w$ . The demand function is monotonically decreasing in the O-D travel cost, bounded from above, and invertible. The inverse of the demand function is given in (3.5):

$$u^w = D^{w^{-1}}(q^w), \quad \forall w \in \mathcal{W} \quad (3.5)$$

The inverse of the demand function can be interpreted as: the network user's travel benefits or the price they are ready to pay for their travel (Sheffi, 1985).

### 3.2.5 Solution algorithm

This section presents a partial linearization method for solving the SUE and SUE-ED problems. Figure 3.3 provides a detailed flowchart of the method.

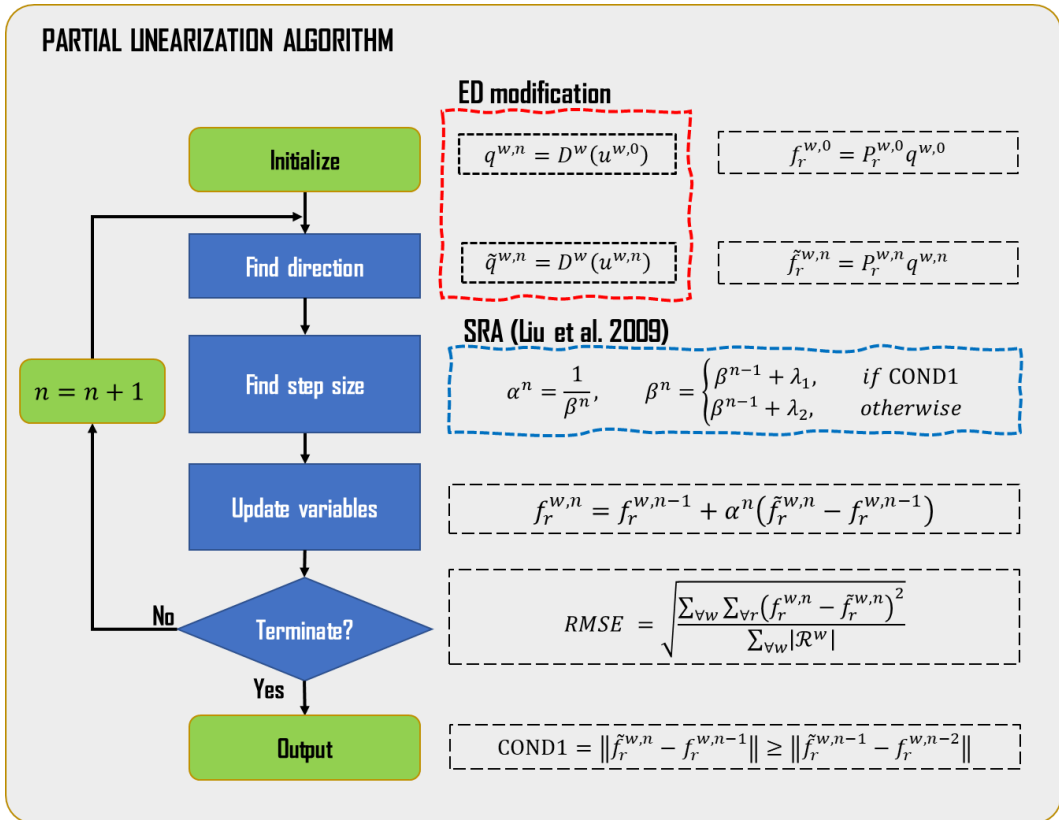


Figure 3.3. Partial linearization algorithm with the SRA step size.

The partial linearization method is a type of descent direction method used for continuous optimization problems (Patriksson, 2015). It iteratively determines a search direction and step



size until convergence is reached. To obtain the search direction, a partially linearized subproblem is solved using a first-order approximation of the first and third terms of the objective function (see Figure 3.2). The algorithm for SUE and SUE-ED is similar, but for SUE-ED, the partial linearized subproblem needs to calculate travel demand based on the current route cost pattern to satisfy the ED function as shown in Figure 3.3.

The SUE-ED's objective function is quite complex (i.e., involving four summations: one over all links, one over all routes, and two over all O-D pairs) and hence computationally expensive to evaluate. To solve this, the self-regulated averaging (SRA) scheme proposed by (Liu et al., 2009) to determine an appropriate step size without the need to evaluate the objective function was used. SRA employs the residual error  $\beta$  and step size in the current iteration to determine the next step size and guarantees convergence with either  $\lambda_1 > 1$  or  $0 < \lambda_2 < 1$  controlling the decreasing speed. Refer to (Patriksson, 2015) for further information on the convergence properties of the partial linearization method.

### 3.3 Link criticality index

This section presents the original UE-based LCI method for link criticality analysis (Almotahari and Yazici, 2019), discusses its properties, identifies two deficiencies of the UE-based LCI, and proposes three modifications to address these deficiencies.

#### 3.3.1 Original UE-based LCI

The LCI method is presented in equations (3.6) - (3.10). It accounts for network connectivity, travel demand, individual travelers' behavior, congestion, and redundancy. It uses link marginal cost (MC) to capture persistent flow assignment despite increasing congestion. If a saturated link is assigned additional flow between iterations  $n$  and  $n + 1$ , the travel time increase can be calculated as a product of link flow increment and MC in

equation (3.7). MCs are normalized by link travel times for comparability. Two weighing coefficients account for links serving alternative routes (3.9) and multiple O-Ds (3.10).

$$LCI_a = \sum_{n=0}^{N-1} \sum_{\forall w} \sum_{\forall r} S_a^n \cdot \delta_{ra}^w \cdot \gamma^w \cdot \mu_r^{w,n}, \quad \forall a \in A \quad (3.6)$$

where  $LCI_a$  is link criticality index for link  $a$ ,  $S_a^n$  is unweighted criticality score for link  $a$  at iteration  $n$ ,  $\gamma^w$  demand specific weight of O-D pairs  $w$  used in  $LCI$ ,  $\mu_r^{w,n}$  is route-specific weight for a route  $r$  of an O-D  $w$  at iteration  $n$ . The unweighted score and the weights can be computed as following:

$$S_a^n = \max([x_a^{n+1} - x_a^n], 1.0) \cdot \frac{mc_a(x_a^n)}{t_a(x_a^n)}, \quad \forall a \in A, \forall n \in N \quad (3.7)$$

$$mc_a(x_a^n) = t_a(x_a^n) + x_a^n t'_a(x_a^n), \quad \forall a \in A \quad (3.8)$$

$$\mu_r^{w,n} = \frac{1/c_r^{w,n}}{\sum_{\forall l} 1/c_l^{w,n}}, \quad \forall r \in \mathcal{R}^w, \forall w \in \mathcal{W}, \forall n \in N \quad (3.9)$$

$$\gamma^w = \gamma^{w,n} = \frac{q^w}{Q}, \quad \forall w \in \mathcal{W}, \forall n \in N \quad (3.10)$$

where  $c_r^{w,n}$  is deterministic travel time on route  $r$  of O-D pair  $w$  at iteration  $n$ ,  $x_a^n$  is flow on link  $a$  at iteration  $n$ ,  $mc_a$  is marginal cost of traveling on link  $a$ ,  $t_a$  is travel time on link  $a$ , and  $t'_a$  is the derivative of link travel time with respect to its flow.

Remark 1: The flow increments in each iteration are not based on behavioral phenomena, but on the objectives of the solution methods. However, it is worth emphasizing that this does not mean that the interim results are irrelevant or meaningless. On the contrary, interim results are arguably still consistent with the behavioral rationale of network users to minimize their travel costs, which allows to assign higher criticality to a link that carries more flow despite increasing saturation, indicating that the link is more congested and more difficult to replace.

Remark 2: Different methods, with different incremental properties, might give different indices. However, this is not a problem, if the indices are consistent and comparable within

each method. The purpose of the indices is to identify critical links and not to compare the methods directly.

#### *Properties of components of LCI*

Figure 3.4 shows the properties of the O-D demand-based and route-based weights of the LCI method.

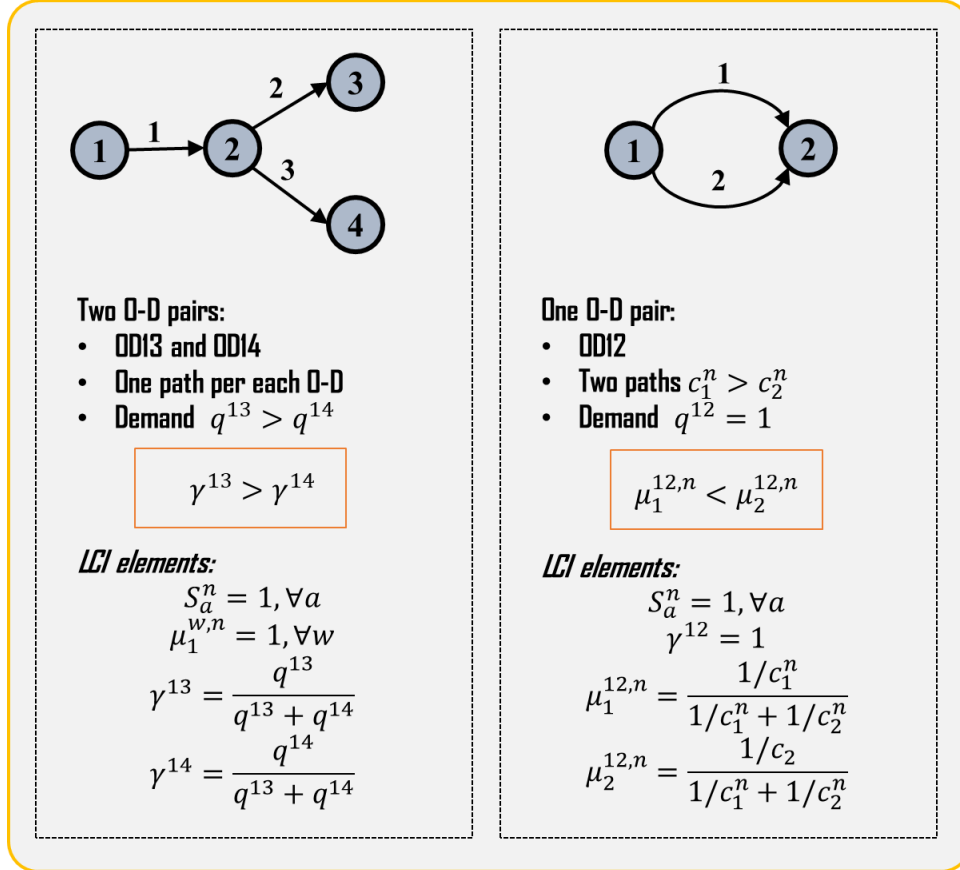


Figure 3.4. Properties of weights for LCI.

As shown in Figure 3.4 (*left*), O-D pairs with higher travel demand have higher O-D weights than O-D pairs with lower travel demand. As shown in Figure 3.4 (*right*), the routes with longer travel times have lower weights than the routes with lower travel times.

#### *Deficiencies of the original UE-based LCI*

Two deficiencies of the original UE-based LCI, which may potentially compromise it, have been identified: (i) *O-D's contribution to LCI when the link has no flow* and (ii) *identical*

links are ranked differently. These issues are explained using the networks in Figure 3.5 and Figure 3.6, respectively.

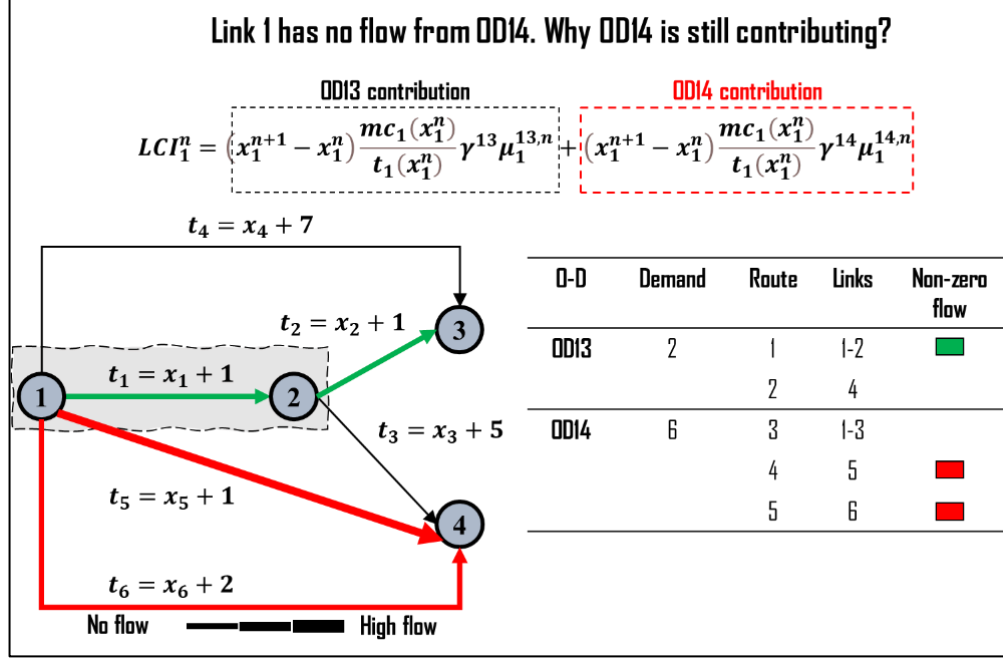


Figure 3.5. A potential limitation of the original UE-based LCI.

**O-D's contribution to LCI when the link has no flow<sup>2</sup>.** The network in Figure 3.5 has six links, two O-D pairs connected with two and three routes, respectively. The network is designed such that the demand of the first O-D (1,3) is served by Route 1 (i.e., Route 2 has zero flow), and the demand of the second O-D (1,4) is served by Route 4 and Route 5 (i.e., Route 3 has zero flow). The LCI value is computed for Link 1. At an iteration  $n$ ,  $LCI_1^n$  is given as a sum of two terms, as shown in Figure 3.5. Each term corresponds to a particular O-D pair. However, the second O-D pair should not contribute to  $LCI_1^n$  because Link 1 has no flow from the second O-D pair. Adding the second term (Figure 3.5) artificially increases

<sup>2</sup> This may be problematic if the route set includes unrealistic alternatives, such as routes with long detours that are unlikely to be used. These unrealistic routes should not contribute to link criticality, but the original LCI cannot capture this, potentially overestimating link criticalities. Conversely, excluding these routes might underestimate link criticality, as any route can contribute to network redundancy. Therefore, both perspectives are valid, and analysts must decide based on the quality of their route sets.

the link's criticality, potentially leading to an overestimation. A formal solution to this example is provided in Section 3.4.1.

**Identical links are ranked differently.** The network in Figure 3.6 has three links, a single O-D pair, and two routes. Link 1 and Link 2 are identical. Link 3 is shared by both routes. The solution process is mimicked, LCI is computed, and the results are summarized in Table 3.2.

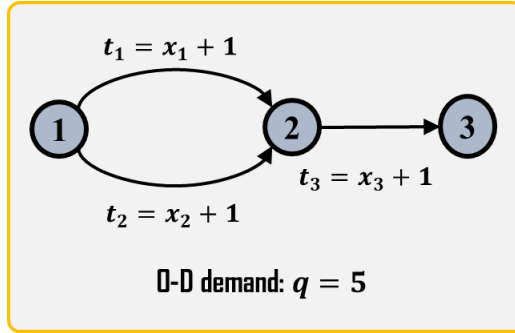


Figure 3.6. A three-link network with two identical parallel links.

As shown in Table 3.2, Link 3 received the highest LCI. This was expected because Link 3 was included in both routes and was assigned flow equal to the full demand. If it were to be disrupted, then the O-D pair would be disconnected. Link 1 and Link 2 were expected to receive equal LCI values because they were identical, but they were assigned different values. Link 1 received a lower LCI value than Link 2.

Table 3.2. Equilibration process and LCI computation.

Link	1				2				3			
	Iteration				Iteration				Iteration			
	1	2	3	LCI	1	2	3	LCI	1	2	3	LCI
Flow	5	3	2.5		0	2	2.5		5	5	5	
Time	6	4	3.5		1	3	3.5		6	6	6	
MC	1.83	1.75	1.71		1	5	6		1.83	1.83	1.83	
$\gamma$	1	1	1		1	1	1		1	1	1	
$\mu$	0.37	0.47	0.5		0.63	0.53	0.5		1	1	1	
Score	-	1.83	1.75		-	2	1.66		-	1.83	1.83	
$LCI^n$	-	0.67	0.83	<b>1.5</b>	-	1.26	0.88	<b>2.14</b>	-	1.83	1.83	<b>3.66</b>

This phenomenon occurred due to the initialization used in the UE framework. In UE, the initial solution and loading procedure is done using AON TA, which assigns the entire travel demand to the shortest route. Based on Table 3.2, since Link 1 is a part of the shortest

route in the first iteration, it received high flow, while Link 2 received no flow. Consequent iterations equalized the flow but taking flow from Link 1 diminished its resulting LCI value and increased the LCI value of Link 2. Moreover, the score of LCI monotonically reduced with each iteration until equilibrium was reached. This suggests that initialization and the first few iterations play an important role in the UE-based LCI calculation.

### 3.3.2 Refined UE-based LCI

This section outlines the refinements made to the original UE-based LCI method to address the issues discussed in Section 3.3.1 and account for the framework extensions discussed in Section 3.2.

To address the first issue (Section 3.3.1), this study proposes to split the score function (3.7) into two parts and substitute link flow increment by route flow increment, as shown in (3.11) - (3.12):

$$LCI_a = \sum_{n=0}^{N-1} \frac{mc_a(x_a^n)}{t_a(x_a^n)} \sum_{\forall w} \gamma^w \cdot z^{w,n} \sum_{\forall r} \mu_r^{w,n} \cdot \delta_{ar}^w, \quad \forall a \in A \quad (3.11)$$

where the score function is split into two parts. The first part remains unchanged while the second part is substituted by a route flow increment  $(f_k^{w,n+1} - f_k^{w,n})$ , i.e.:

$$z^{w,n} = \begin{cases} \sum_{\forall k} (f_k^{w,n+1} - f_k^{w,n}) \delta_{ak}^w, & \text{if } \sum_{\forall k} (f_k^{w,n+1} - f_k^{w,n}) \delta_{ak}^w > 0, \\ 1, & \text{if } \sum_{\forall k} (f_k^{w,n+1} - f_k^{w,n}) \delta_{ak}^w < 0, \\ 0, & \text{if } \nexists f_k^{w,n+1} \neq 0 \text{ and } \nexists f_k^{w,n} \neq 0, \end{cases} \quad \forall w, \forall n \quad (3.12)$$

These changes can be interpreted as follows. The contribution of an O-D pair to the LCI is only considered if there is demand served from that pair. If all O-D pairs that a link serves have non-zero flow passing through that link, the refined UE-based LCI method would be identical to the original UE-based LCI method. This refinement of the functional form allows for a more precise consideration of O-D pairs in the UE-based LCI method. It is worth noting

that this modification may be unnecessary for SUE-based LCI as the SUE model assigns route flows based on positive probabilities and identical routes have equal probabilities.

### 3.3.3 SUE-based LCI

The second issue can be automatically alleviated by adopting an SUE TA model for the LCI method. More importantly, another benefit of using the SUE framework is that it relaxes the assumption of perfect knowledge of travel time, and results in evaluations more consistent with observed travelers' behavior. By extending the framework to SUE, travelers' perception error is incorporated into the model (Sheffi, 1985), and stochastic network loading is performed according to a certain probabilistic route choice model. Theoretically, all routes should have some non-zero flows. Actual route travel times are substituted by perceived route travel time in route-specific weights (3.9), i.e.:

$$\mu_r^{w,n} = \frac{1/C_r^{w,n}}{\sum_{\forall l} 1/C_l^{w,n}}, \quad \forall r \in \mathcal{R}^w, \forall w \in \mathcal{W}, \forall n \in N \quad (3.13)$$

where  $\mu_r^{w,n}$  is route-specific weight for a route  $r$  of an O-D  $w$  at iteration  $n$  and  $C_r^{w,n}$  is the perceived travel time of route  $r$  of O-D  $w$  at iteration  $n$ .

### 3.3.4 SUE-ED-based LCI

Finally, the extension of the SUE framework to SUE-ED enables loosening the assumption of fixed demand and accounting for the potential influence of other travel choices that may affect travelers' behavior, resulting in a more realistic TA model. Demand elasticity results in variable O-D and total network demand. Consequently, the demand-based weight in (3.10) may vary from iteration to iteration.

Incorporating ED into link criticality assessment may be interpreted as adding another conceptual dimension to the metric, namely *trip criticality*. It seems that the core question is *whether the link's criticality should vary under different demand levels or stay constant*. One

of the simplest examples is a trip choice under normal and degraded conditions in a single-link network. In a degraded network, travel demand may reduce due to the decrease in level of service. *Should the criticality of the link reduce with the decrease of travel demand?* To answer this question, travel demand is considered from the perspective of individual trips, which roughly is classified as *mandatory* and *discretionary* (or optional) trips. Demand reduction can be interpreted as cancelation of discretionary trips. The following logic can be used: *“If trips are canceled, then people can ‘survive’ without these trips. If they can survive without these trips, then they may survive without the corresponding connection. If they can survive without this connection, is it really critical?”*. Following this logic, it seems reasonable to reduce the criticality of links if travel demand reduces. As a result, the ED extension may be considered as incorporating the impact of trip criticality into link criticality assessment. The sensitivity analysis conducted on SUE and SUE-ED showed results consistent with this logic.

### 3.4 Numerical experiments

Three experiments were performed in this section. The first issue of the original UE-based LCI was addressed by the refined UE-based LCI in Experiment 1. UE-based LCI and SUE-based LCI were compared, and the second issue was resolved by SUE-based LCI in Experiment 2. SUE-ED-based LCI was also analyzed, and a sensitivity analysis of demand function parameters was conducted on the same network. Two real-size networks were used in Experiment 3 to compare the computation time of LCI for different traffic assignment models. Bridge criticality in the Winnipeg network, Canada, was also assessed and three LCI frameworks were compared with the index from [\(Jansuwan and Chen, 2015\)](#).

In all experiments except Experiment 1 (Section 3.4.1), the travel time of each link is assumed to follow the standard Bureau of Public Road (BPR):



$$t_a(x_a) = t_a^0 \left[ 1 + \alpha \left( \frac{x_a}{O_a} \right)^\beta \right], \quad \forall a \in A \quad (3.14)$$

where  $t_a^0$  is a free-flow travel time on link  $a$ ;  $x_a$  is a flow on link  $a$ ;  $O_a$  is the capacity of link  $a$ ;  $\alpha$  and  $\beta$  are exogenously defined parameters.

Without the loss of generality, in this study, the demand function is modeled using an exponential function of the expected perceived O-D travel cost (EPC), as follows:

$$D^w(u^w) = \bar{q}^w \cdot e^{-\xi u^w}, \quad \forall w \in \mathcal{W} \quad (3.15)$$

where  $\bar{q}^w$  is the maximum (or potential) demand for O-D pair  $w \in \mathcal{W}$ ;  $\xi$  is the scaling parameter, which reflects sensitivity of demand to the travel cost,  $u^w$  is EPC for O-D pair  $w$  computed based on actual travel costs  $c_k^w$   $k \in K^w$  as shown in equation (3.16).

$$EPC_{MNL}^w = -\frac{1}{\theta} \ln \sum_{k \in K^w} e^{-\theta c_k^w}, \quad \forall w \in \mathcal{W} \quad (3.16)$$

To be able to compare the LCI values obtained based on different traffic assignment frameworks, the LCI values are normalized to lie within the range of 0 to 1, i.e.:

$$\widetilde{LCI}_a = \frac{LCI_a}{\sum_{b \in A} LCI_b}, \quad \forall a \in A \quad (3.17)$$

and

$$\sum_{a \in A} \widetilde{LCI}_a = 1 \quad (3.18)$$

### 3.4.1 Experiment 1: Two O-D pair network

The purpose of this section is to compare the original UE-based LCI with the refined UE-based LCI, using the network illustrated in Figure 3.5. To highlight the contrast between the original and refined LCI methods, the results are presented for a single arbitrary iteration  $n$ . The outcomes of this comparison are summarized in Table 3.3.

Table 3.3. An arbitrary iteration of original and refined UE-based LCI methods.

	Components required for computation of LCI	Original LCI	Refined LCI
Target link	Flow on Link 1 (n)	2	
	Cost of Link 1 (n)	3	
	Marginal cost of Link 1 (n)	5	
	Flow on Link 1 (n+1)	2	
OD13	Flow on Route 1 (n)	2	
	Flow on Route 1 (n+1)	2	
	Flow on Route 2 (n)	0	
	Flow on Route 2 (n+1)	0	
	Cost of Route 1 (n)	6	
	Cost of Route 2 (n)	7	
OD14	Flow on Route 3 (n)	0	
	Flow on Route 4 (n)	6	
	Flow on Route 5 (n)	0	
	Cost of Route 3 (n)	8	
	Cost of Route 4 (n)	7	
	Cost of Route 5 (n)	2	
Weights	$\gamma^{OD13}(n)$	0.25	
	$\gamma^{OD14}(n)$	0.75	
	$\mu_1(n)$	0.54	
	$\mu_3(n)$	0.21	
Score of Link 1 (n)		1.67	-
<b>LCI (n)</b>		<b>0.49</b>	<b>0.23</b>

The results presented in Table 3.3 demonstrate that both the original UE-based LCI and the refined UE-based LCI methods require the same initial components for computation. However, the difference lies in the equation used to calculate the LCI value, where the original UE-based LCI method uses (3.6), i.e.:

$$\begin{aligned}
 LCI_1^n &= \max([x_1^{n+1} - x_1^n], 1.0) \frac{mc_1(x_1^n)}{t_1(x_1^n)} [\gamma^{13} \mu_1^{13,n} + \gamma^{14} \mu_1^{14,n}] \\
 &= \max((2 - 2), 1.0) \cdot \frac{5}{3} \cdot [0.25 \cdot 0.54 + 0.75 \cdot 0.21] = 0.49
 \end{aligned}$$

and the refined UE-based LCI method uses (3.11), i.e.:

$$\begin{aligned}
 LCI_1^n &= \frac{mc_1(x_1^n)}{t_1(x_1^n)} [\gamma^{13} z^{13,n} \mu_1^{13,n} + \gamma^{14} z^{14,n} \mu_1^{14,n}] = \frac{5}{3} [0.25 \cdot 1 \cdot 0.54 + 0.75 \cdot 0 \cdot 0.21] \\
 &= 0.23
 \end{aligned}$$

The criticality value calculated by the original UE-based LCI method is more than twice as high as that determined by the refined UE-based LCI method.

It is important to note that this modification is relevant only for the UE-based LCI method, where zero-flow routes may exist. However, for SUE-based LCI or SUE-ED-based

LCI, this modification unnecessary as the SUE models assign route flows based on route choice probabilities, which, theoretically, should not result in zero-flow routes.

### 3.4.2 Experiment 2: Loophole network

This section uses the loophole network to analyze LCI methods based on different TA models. The loophole network is shown in Figure 3.7.

The loophole network has four links and a single O-D pair connected by three routes with equal free-flow travel time. Routes 2 and 3 share Link 2. Moreover, they are identical. The parameters were set as follows:  $\alpha = 0.15, \beta = 4$ .

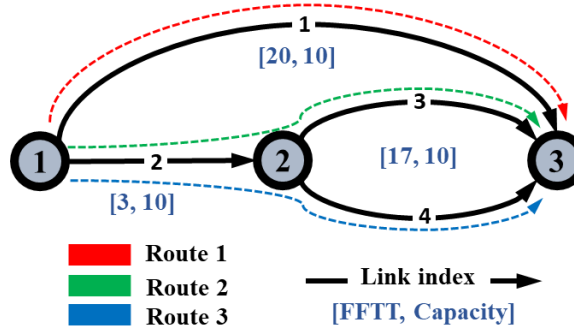


Figure 3.7. Loophole network.

#### 3.4.2.1 UE-based LCI vs. SUE-based LCI

This section compares the original UE-based LCI and SUE-based LCI methods. It sets the travel demand  $q = 20$  and the dispersion parameter  $\theta = 0.5$ . The results are summarized in Table 3.4 and Figure 3.8.

As shown in Table 3.4, Link 2 was assigned the highest criticality value by both UE-based LCI and SUE-based LCI methods. It was followed by Link 1. Link 3 and 4 received the lowest values. This behavior was desired because Link 2 contributes more to route redundancy than any other link. It serves two routes, while the remaining links serve only one route each. If any of these links are disrupted, there would still be two routes available to

connect the given O-D pair. However, if Link 2 is disrupted, there would only be one alternative route available.

Table 3.4. Link criticality values and rankings for the loophole network.

Link	UE-based LCI			SUE-based LCI		
	LCI	Normalized LCI	Rank	LCI	Normalized LCI	Rank
1	1608.95	0.17	2	3.15	0.19	2
2	<b>5050.14</b>	<b>0.53</b>	<b>1</b>	<b>9.25</b>	<b>0.55</b>	<b>1</b>
3	1403.61	0.15	3	2.19	0.13	3
4	1397.46	0.15	4	2.19	0.13	3
Accuracy	1e-5			1e-8		
Iteration count	3885			6		

The reason why Link 2 was assigned a higher criticality value than Link 1 is that all components of the LCI for Link 2 (i.e., link flow, marginal-actual travel cost ratio, and route-based weights) were greater than the corresponding components for Link 1 (Figure 3.8a - Figure 3.8c), which resulted in higher criticality values at each iteration, as shown in (Figure 3.8d).

From Table 3.2, it can also be noticed that the non-normalized values of UE-based LCI and SUE-based LCI differ in three orders of magnitude. It was because a non-normalized LCI depends on the number of iterations and solving the UE problem required a substantially greater number of iterations than solving the SUE problem. For solving the UE and SUE problems, an SRA method and partial linearization method with the SRA step size were used, respectively. Due to the AON network loading procedure, the SRA method was less efficient than the partial linearization algorithm with SRA, which uses a stochastic network loading procedure (3.3).

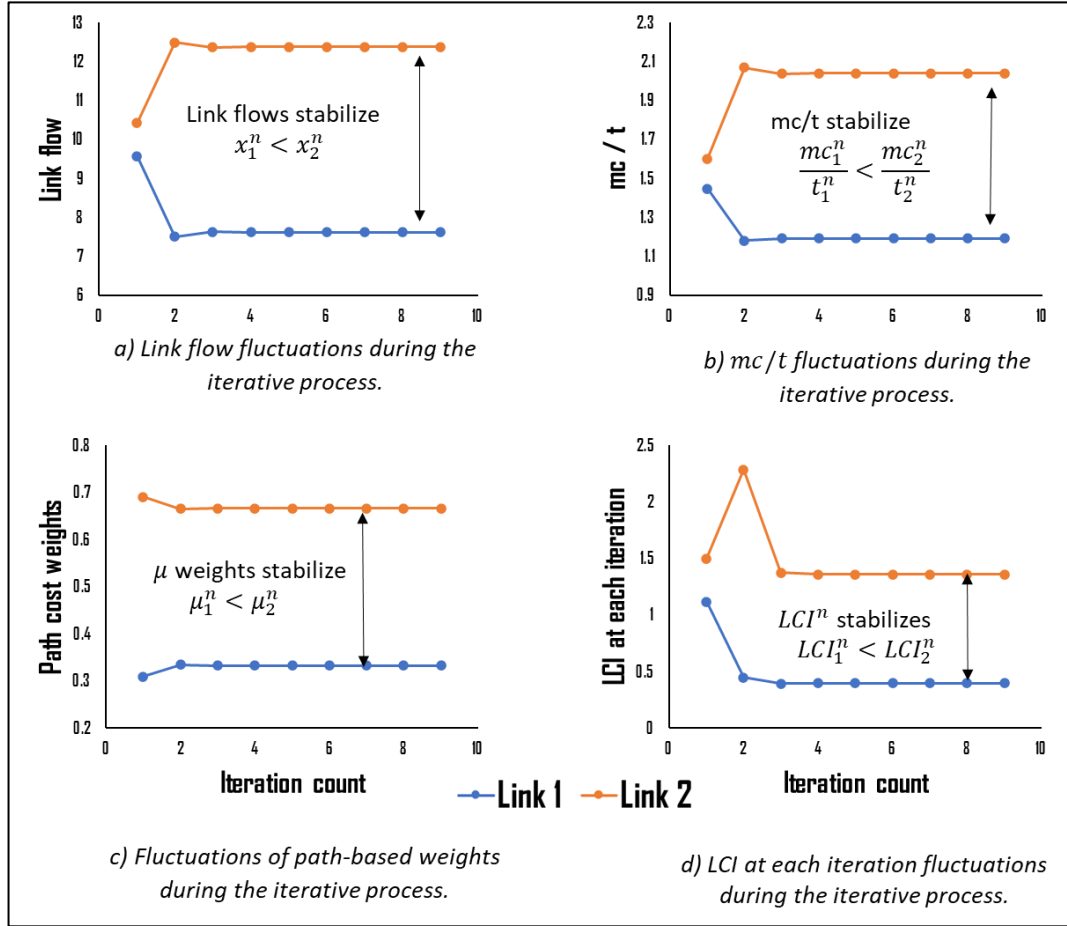


Figure 3.8. Analysis of SUE-based LCI fluctuations at each iteration.

### Sensitivity analysis

A sensitivity analysis was conducted with respect to travel demand and the dispersion parameter. Similarly, the travel demand  $q = 20$  and the dispersion parameter  $\theta = 0.5$ . The results are summarized in Figure 3.9 and Figure 3.10, respectively.

The impact of demand level on the criticality values of identical links was analyzed by examining Link 3 and Link 4. These links were selected to facilitate the study of the issue of initialization.

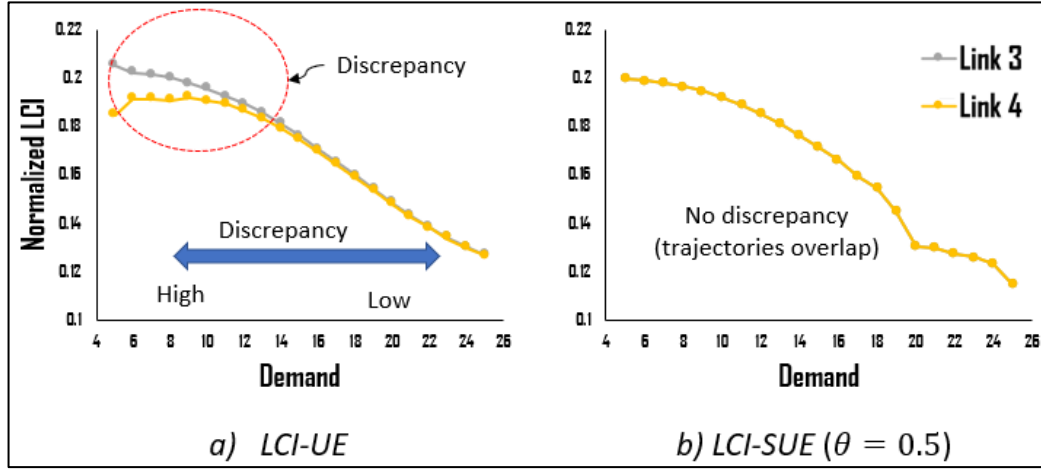


Figure 3.9. Discrepancy of LCI values of two identical links.

Figure 3.9a shows that at low demand values, identical links were assigned different UE-based LCI values, but as demand increased, the differences in criticality values diminished. This can be attributed to three factors. Firstly, the first few iterations have the greatest impact, as demonstrated in Figure 3.8. Secondly, the SRA method requires fewer iterations to converge at lower demand levels than at higher demand levels. Finally, a large number of iterations reduces the impact of the first few iterations because criticality values are summed up at each iteration. Figure 3.9b demonstrates that SUE-based LCI does not suffer from this issue, and identical links receive equal criticality values. This is because the stochastic network loading assigns non-zero flow to all alternatives in the route set, resulting in identical links receiving equal amounts of flow (if not traversed by routes of other O-D pairs). An abrupt bend observed in Figure 3.9b at demand level 20 potentially occurred due to reaching network capacity.

The impact of the dispersion parameter on SUE-based LCI is analyzed. Results in Figure 3.10 revealed that, at low dispersion parameter values, Links 1, 3, and 4 had similar SUE-based LCI values. However, as the dispersion parameter value increased, Link 1 became consistently more critical than Link 3 and 4, indicating that it played a more important role in the network.

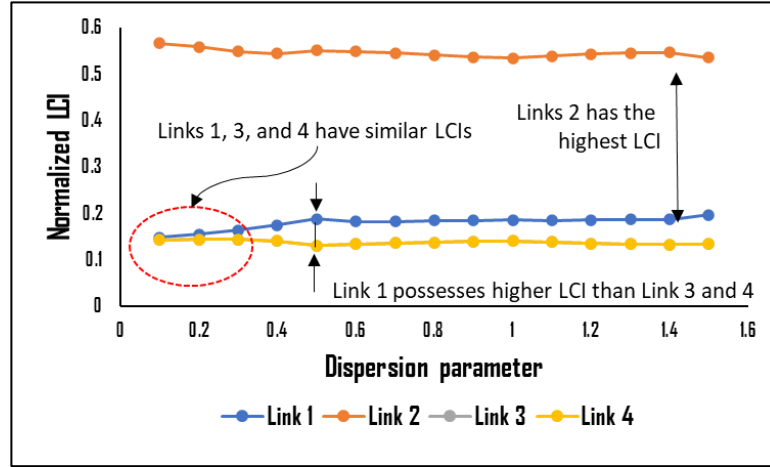


Figure 3.10. Impact of dispersion parameter on SUE-based LCI.

It is well known that when the dispersion parameter has low values, the model is less sensitive to travel time. As the dispersion parameter value increases, the equilibrium solution of a SUE problem becomes more and more sensitive to travel time, hence closer to the UE solution (Sheffi, 1985). At certain iterations, Link 1's lower travel time allowed it to be assigned more flow, thereby increasing its importance over Links 3 and 4. Therefore, the model became sensitive enough to travel time changes, allowing it to differentiate the higher criticality of Link 1 compared to Links 3 and 4 as the dispersion parameter value increased over 0.4.

#### 3.4.2.2 SUE-based LCI vs. SUE-ED-based LCI

This section compares SUE-based LCI and SUE-ED-based LCI. The results are summarized in Table 3.5 and Figure 3.11 – Figure 3.14. The parameters were set as follows:  $q = 20$ ,  $\theta = 0.5$ ,  $\xi = 0.01$ ,  $\bar{q} = 40$ .

From Table 3.5, it is evident that the link rankings have remained unchanged. Link 2 has the highest rank, followed by Link 1, and then by Links 3 and 4 in that order. On the other hand, it should be noted that the SUE-ED-based LCI value of Links 2 is slightly higher, while the SUE-ED-based LCI values for Link 3 and 4 are slightly lower than their corresponding

SUE-based LCI values. Furthermore, the partial linearization algorithm converges in a relatively higher number of iterations in the case of SUE-ED-based LCI than in the case of SUE-based LCI.

Table 3.5. SUE-based LCI and SUE-ED-based LCI values for the loophole network.

Link	SUE-based LCI			SUE-ED-based LCI		
	LCI	Normalized LCI	Rank	LCI	Normalized LCI	Rank
1	3.15	0.19	2	68.81	0.19	2
2	<b>9.25</b>	<b>0.55</b>	<b>1</b>	<b>217.97</b>	<b>0.59</b>	<b>1</b>
3	2.19	0.13	3	41.54	0.11	3
4	2.19	0.13	3	41.54	0.11	3
Accuracy	1e-8			1e-8		
Iteration count	6			81		

The reason why SUE-ED-based LCI value of Link 2 was higher is related to the mechanism of changing demand. In SUE-ED, demand is a function of LOS. Specifically, when LOS is low, then the demand reduces, while when it is high, demand increases. From Figure 3.11, one can see that the network demand fluctuated substantially during the first several iterations before it managed to stabilize.

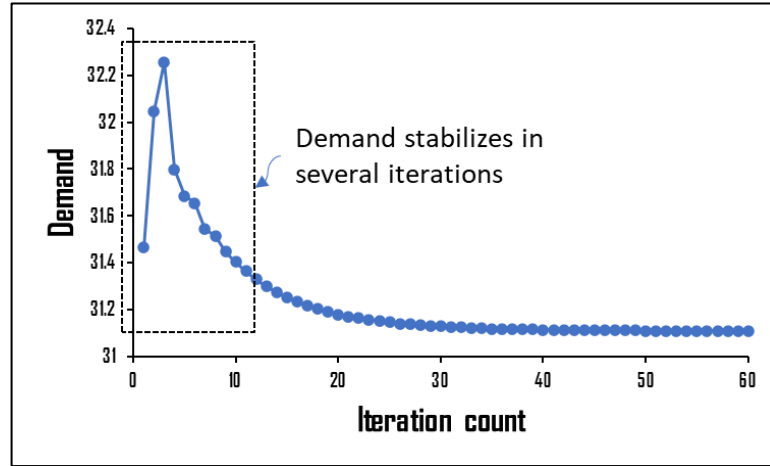


Figure 3.11. Demand changes during the equilibration.

From Figure 3.12, one can see that this affected the flow on Link 2. It also fluctuated considerably during these iterations in the case of SUE-ED, especially during the first two iterations. In contrast, the flow on Link 2 remained relatively stable in the case of SUE, as shown in Figure 3.12.



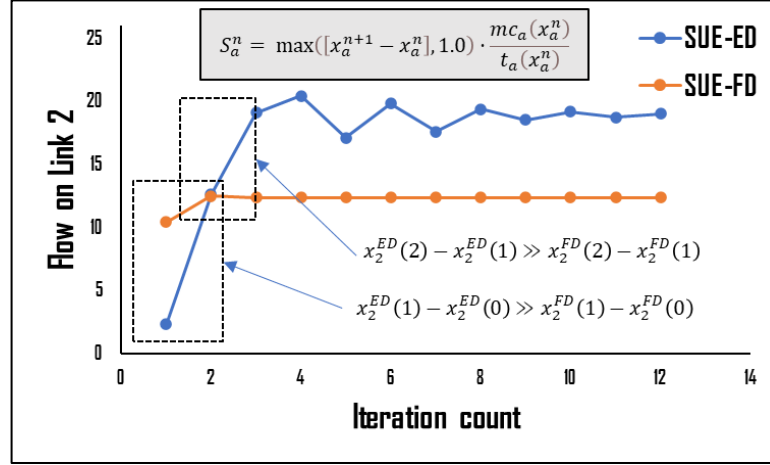


Figure 3.12. Flow fluctuations on Link 2 during the equilibration process.

From Figure 3.13, one can see why SUE-ED-based LCI value of Link 1 did not grow. It happened because the flow on Link 1 was reducing the first few iterations, whereas the flow on Link 2 was increasing.

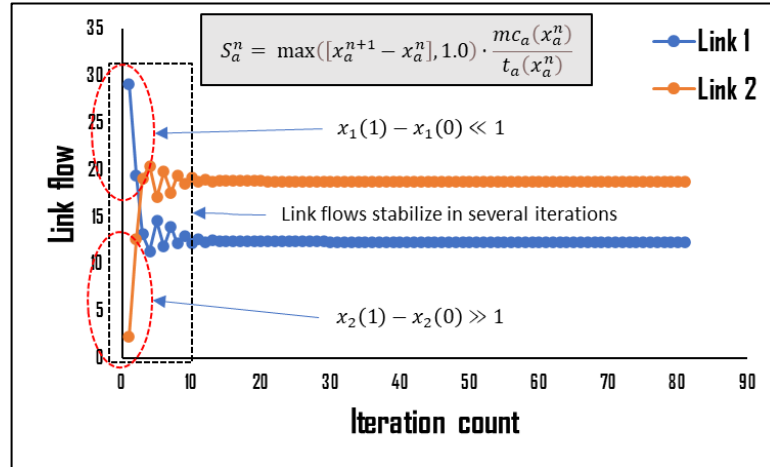


Figure 3.13. Link flow changes during the equilibration process.

The reason why SUE-ED needed more iterations than SUE problem is that ED introduces additional non-linearity in the TA problem, making the problem more complex and challenging to solve. The iterative solution algorithms have to perform additional computations to accommodate this non-linearity, which may take more iterations to converge.

#### *Sensitivity analysis*

The demand function, which is represented by (3.15), has two parameters: the scaling parameter,  $\xi$ , and the maximum potential demand,  $\bar{q}^w$ . The sensitivity analysis for these two parameters is presented in Figure 3.14a for the scaling parameter and Figure 3.14b for the maximum potential demand. The results from Figure 3.14 indicate that these parameters have a limited impact on the SUE-ED-based LCI values.

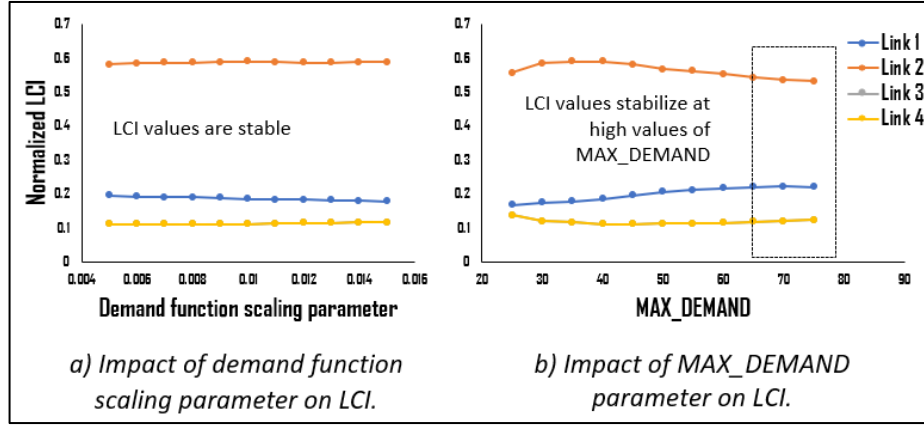


Figure 3.14. Impact of demand function parameters on LCI.

### 3.4.2.3 Discussion on demand elasticity

To support the above discussion, the impact of ED on a full-scan approach (based on the difference of total network travel time) and LCI is analyzed. The experiments were conducted on a simple three-link network as shown in Figure 3.15. The results are summarized in Table 3.6 - Table 3.8.

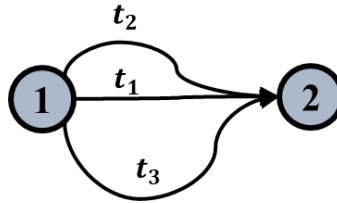


Figure 3.15. Three-link network.

The travel time of each link is computed according to (3.14). All characteristics of the three links were set identical except the free flow travel time. The link free flow travel times were set to obey the following relation:

$$t_1^0 < t_2^0 < t_3^0$$

The demand function is calculated according to (3.15). The SUE and SUE-ED frameworks were selected for the analysis. The solution algorithm described in Section 3.2.5 was utilized. The link criticality of full-scan approach was calculated as follows:

$$Criticality_a = \frac{(T_{ALL LINKS} - T_a)}{T_{ALL LINKS}}, \quad a = \{1,2,3\}$$

where  $Criticality_a$  is the criticality score of link  $a$ ,  $T_{ALL LINKS}$  is the total travel time in the network when all links are intact,  $T_a$  is the total travel time in the network in which link  $a$  is deactivated. To ensure comparability between the full-scan measure and LCI, both are normalized according to equation (3.17).

Table 3.6 provides link criticality values for a full-scan and SUE-based LCI approaches under FD TA.

Table 3.6. Link criticality values for SUE (max demand = 40).

Scenario	Full-scan				Normalized SUE-based LCI
	O-D demand	Total network travel time	Criticality	Normalized Criticality	
Fully functional	11.76	650	-	-	-
Link 1	11.76	3206	3.94	0.47	0.4
Link 2	11.76	2227	2.43	0.29	0.32
Link 3	11.76	2008	2.09	0.25	0.28

As shown in Table 3.6, the total travel time of a fully functioning network is much lower than the total travel time in disrupted networks. It was expected because the travel demand remained fixed regardless of the degradation of the network. Specifically, the removal of Link 1 (i.e., fastest) resulted in the highest discrepancy than removal of Link 2 (i.e., mediocre) or Link 3 (i.e., slowest) as expected. It was reflected in the link criticality scores. The criticality of Link 1 was almost twice as high as the ranks of other two links. The SUE-based LCI followed the same trend but the difference between the criticality scores was lower than for the full-scan method.

Table 3.7 and Table 3.8 provide criticality values of the methods under ED TA under different maximum demand levels, specifically at  $\bar{q} = 2 \cdot q$  and  $\bar{q} = 4 \cdot q$  where  $q = 10$ .

Table 3.7. Link criticality values for SUE-ED (max demand = 20).

Scenario	Full-scan				Normalized SUE-ED-based LCI
	O-D demand	Total network travel time	Criticality	Normalized Criticality	
Fully functional	11.76	650	-	-	-
Link 1	8.41	740	0.14	0.37	0.4
Link 2	9.133	728	0.12	0.32	0.32
Link 3	9.35	723	0.11	0.30	0.28

As shown in Table 3.7, the travel demand reduced when the network was degraded. The degradation was the highest when Link 1 was removed, mediocre when Link 2 was removed, and the lowest when Link 3 was removed. However, due to the decreased demand, the difference in ratings was less pronounced than in FD TA. Compared to the full-scan approach, the SUE-ED-based LCI did not change much. These results are consistent with the given interpretation in the previous section.

As shown in Table 3.8, the travel demand, total network travel time, and hence link criticality values may depend on parameter values of the demand function. These parameter values might be set such that the total travel time of a fully functioning network is worse than the travel time in the degraded network. In this case, link criticality of a full-scan method may have negative values as shown in Table 3.8. In this case these values obtained by the full-scan approach cannot be further used. One can notice that the demand was considerably reduced in these scenarios. This can be interpreted as strong suppression of discretionary trips with each link disruption scenario forced by high sensitivity of demand function to travel cost. Based on the negative results, it seems that the full-scan method used in this section is applicable only in scenarios when the demand function is less sensitive to travel cost. In contrast, the LCI values were consistent with the interpretation given in the previous section and the high sensitivity of demand function to travel cost did not compromise the method.

Table 3.8. Link criticality values for SUE-ED.

Scenario	Full-scan				Normalized SUE-ED-based LCI
	O-D demand	Total network travel time	Criticality	Normalized Criticality	
Fully functional	14.5	<b>1503.0</b>	-	-	-
Link 1	9.78	<b>1101.4</b>	<b>-0.27</b>	-	0.37
Link 2	10.66	<b>1424.4</b>	<b>-0.05</b>	-	0.33
Link 3	10.92	<b>1433.1</b>	<b>-0.05</b>	-	0.3

### 3.4.3 Experiment 3: Real-size networks

The proposed LCI methods were applied to two real-size road networks: the Winnipeg and Chicago Sketch networks. These networks were obtained from an open-source repository. The origins and destinations of the O-D flows were the traffic zones in both networks. Fixed working route sets were used for a fair comparison. The working route set of the Winnipeg network was generated by (Bekhor et al., 2008), and the working route set of the Chicago sketch network was generated by using an open-source software. More details about the test networks are presented in Figure 3.16.

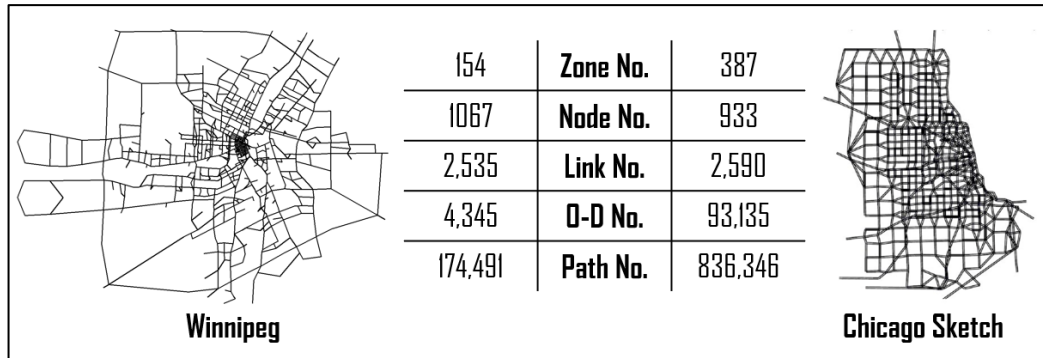


Figure 3.16. Two large-scale test networks and their characteristics.

#### 3.4.3.1 Setting model parameters for real-size networks

This section sets plausible parameter values for route choice and travel demand models.

##### 3.4.3.1.1 Parameter settings for route choice models

This section provides sensitivity analyses on the parameters of the selected route choice models. The results are summarized in Figure 3.17. To set model parameters, we start with

preliminary values and find the equilibrium solution. From this solution, we compute the total coefficient of variation  $\overline{CV}$  and compare it with the target total coefficient of variation  $\overline{CV}_{trg}$  (e.g., 0.1 – moderate level of variation). If  $\overline{CV} < \overline{CV}_{trg}$ , we adjust the parameters and repeat the process until the condition is satisfied.

The total coefficient of variation  $\overline{CV}$  is calculated as follows:

$$\overline{CV} = \frac{\sum_{w \in W} q^w \cdot CV^w}{\sum_{w \in W} q^w} \quad (3.19)$$

where  $CV^w$  is the coefficient of variation for O-D pair  $w$ , calculated as the ratio of standard deviation  $\sigma_\varepsilon$  to mean generalized cost at the equilibrium point  $U^w$ :

$$CV^w = \frac{\sigma_\varepsilon}{U^w}, \quad \forall w \in W \quad (3.20)$$

The standard deviation is derived from the model-specific variance. The mean systematic utility for O-D pair  $w$  is determined as follows:

$$U^w = \frac{\sum_{k \in K^w} f_k^w \cdot c_k^w}{q^w}, \quad \forall w \in W \quad (3.21)$$

Parameter setting was performed for the MNL route choice model across two real-size networks. The MNL model has a single parameter and can be calibrated using the aforementioned procedure without additional assumptions.

Figure 3.17 summarizes the effect of route choice model parameters on the total coefficient of variation for the Winnipeg and Chicago Sketch networks. We set the parameters of the selected route choice models such that the mean coefficient of variation  $\overline{CV}$  remained within the range of 10% to 20%.

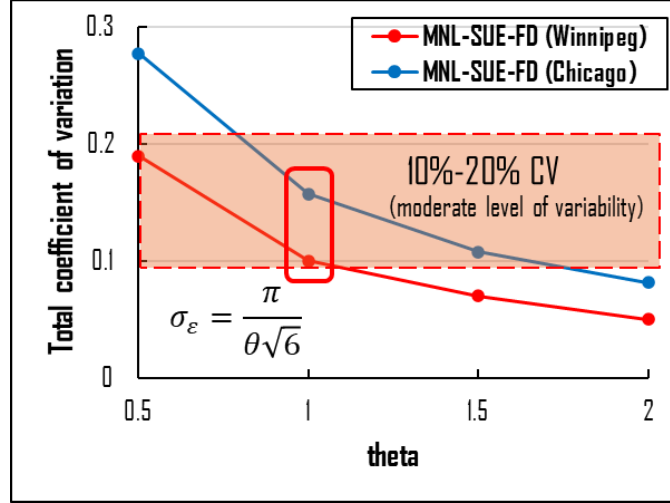
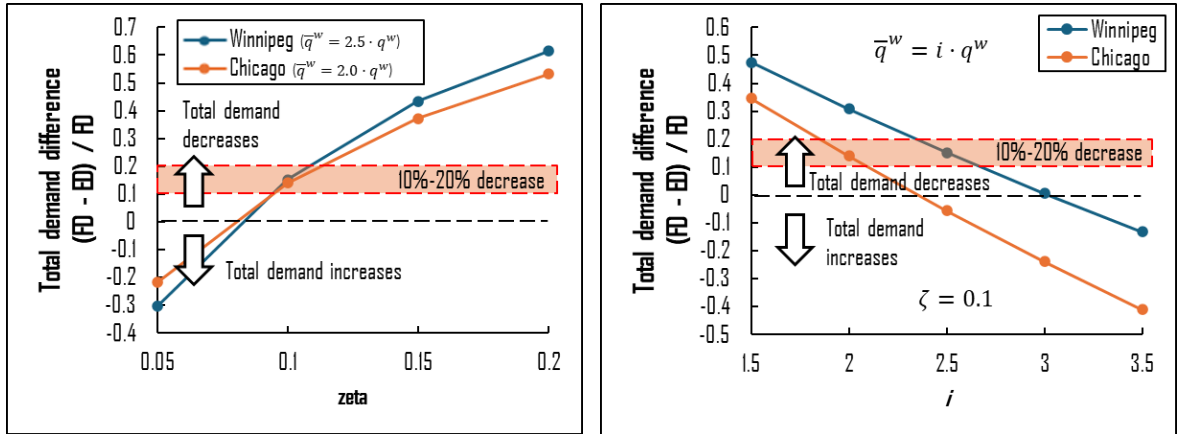


Figure 3.17. Effect of route choice model parameters on the total coefficient of variation for the Winnipeg and Chicago Sketch networks.

### 3.4.3.1.2 Parameter settings for demand function

This section provides sensitivity analyses on parameters of the demand function. The demand function has two parameters: scaling parameter  $\zeta$  and maximum demand  $\bar{q}^w, \forall w \in W$ . The results for two selected real-size networks are summarized in Figure 3.18.



(a) Impact of parameter  $\zeta$  on total travel demand.

(b) Impact of max demand parameter  $\bar{q}^w, \forall w \in W$  on total travel demand.

Figure 3.18. Impact of demand function parameters on total travel demand for two real-size networks.

As shown in Figure 3.18, the parameters of the demand function were adjusted to ensure total travel demand varied between 10% and 20% from the fixed total travel demand. For the

Winnipeg network, we set parameter  $\zeta$  to 0.1 and the maximum demand parameter  $\bar{q}^w$  to  $2.5 \cdot q^w$  for all  $w \in W$ . Similarly, for the Chicago Sketch network, we set  $\zeta$  to 0.1 and  $\bar{q}^w$  to  $2.0 \cdot q^w$  for all  $w \in W$ .

### 3.4.3.2 Computational complexity analysis

In Table 3.9, the computational time of LCI for different traffic assignment models on the two test networks is provided. It reports the average CPU time per iteration for the solution algorithm steps and the computation of LCI scores, which are explicitly separated. The solution algorithm (Section 3.2.5) was terminated either when RMSE=1e-7 or the maximum iteration number was reached (i.e., 500 iterations). The solution algorithm was implemented in Python 3.7.12. The numerical experiments were conducted on a Microsoft Windows 11 operating system with Intel(R) Core (TM) i7-9700 CPU @ 3.00GHz with 24 GB of RAM.

Table 3.9. Convergence characteristics: SUE-based LCI vs. UE-based LCI.

LCI's TA model	Winnipeg					Chicago Sketch				
	Iter. No.	Alg. iter. time (sec)	LCI comp. time (sec)	Total time (min)	Total time with LCI (min)	Iter. No.	Alg. iter. time (sec)	LCI comp. time (sec)	Total time (min)	Total time with LCI (min)
SUE	116	3.68	5.96	7	19	106	9.49	12.59	17	39
SUE-ED	243	3.66	6.09	15	40	208	9.67	12.94	34	78
UE*	500	3.25	6.08	27	78	500	7.74	13.0	65	173
UE-ED*	500	3.32	6.03	28	78	500	7.74	12.8	65	171

\* Reached maximum iteration number

As shown in Table 3.9, the solution algorithm for SUE framework converged in about half the iterations as the SUE-ED framework. This was expected because the ED extension added non-linearity to the objective function, increased the number of decision variables (i.e., one extra demand variable for each O-D pair), and increased the number of constraints. The CPU times for these frameworks were proportional to the iterations. The SUE model took 7 minutes for the Winnipeg network and 17 minutes for the Chicago Sketch network approximately. The SUE-ED model took 15 and 35 minutes, respectively. Computing the LCI method added some extra time, resulting in a total CPU time of 19 minutes for the Winnipeg



network and 39 minutes for the Chicago Sketch network for SUE, and 40 and 78 minutes, respectively, for SUE-ED.

Neither for the UE nor for the UE-ED framework the algorithm converged within 500 iterations for both networks. They reached the maximum number of iterations without satisfying the specified RMSE criterion of  $1e-7$  (although they reached  $RMSE=1e-5$ ). It was expected that the UE-based TA algorithm would require more iterations for convergence because the solution for the UE-based TA was on the boundary of the feasible region (i.e., some constraints were binding – zero-flow routes), which might be more computationally expensive to find. In contrast, the SUE-based TA had an interior point solution (i.e., no binding constraints – no zero-flow routes), which might be less computationally expensive. The total CPU time for computing LCI values was 78 minutes for the Winnipeg network and 171 minutes for the Chicago Sketch network.

It should be noted that a full-scan approach for identifying critical links in the same networks would require substantially more computational time compared to the LCI approach. For example, the Winnipeg network has 2535 links. A full-scan method would need to run  $2^{|A|} - 1$  number of TA procedures, where  $|A|$  is the total number of links. This results in an infeasibly large number of combinations and, hence, computational time.

#### ***3.4.3.3 Criticality of bridges in the city of Winnipeg***

This section evaluated the bridge criticality in Winnipeg, Manitoba, Canada (Figure 3.19). The proposed SUE-based LCI methods were used and compared with the J-C method by (Jansuwan and Chen, 2015). The J-C method was chosen because it was the only known to the authors full-scan method that used SUE TA. Results are summarized in Table 3.11, Figure 3.20, and Table 3.12.

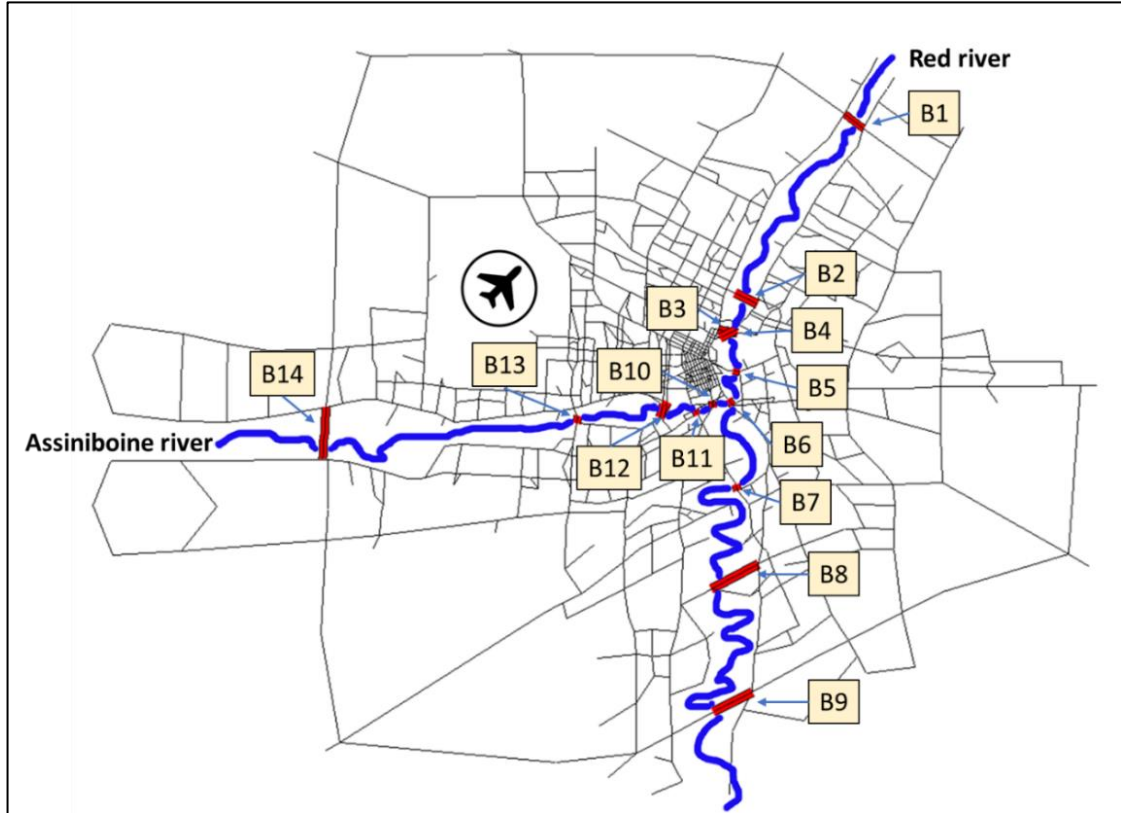


Figure 3.19. The Winnipeg network and selected bridges.

Table 3.10 provides a list of considered bridges for the Winnipeg network.

Table 3.10. List of considered bridges.

Bridge index	Bridge name	Bridge index	Bridge name
B1	North Perimeter	B8	Fort Gary
B2	Kildonan Settlers	B9	South Perimeter
B3	Redwood	B10	Mid Town
B4	Disraeli	B11	Osborne
B5	Provencher	B12	Maryland
B6	Norwood	B13	St. James
B7	St. Vital	B14	West Perimeter

Table 3.11 summarizes the Top-10 critical bridges according to each measure. It is important to note that there is no definitive ground truth for bridge criticality, making it impossible to assert that one measure is superior to another. Therefore, the comparison was based on common sense interpretation. For example, how the measures reflect the network's functional aspects (e.g., providing connection to the airport) and traffic flow characteristics.

Table 3.11. Top-10 LCI critical rank bridges of the Winnipeg network.

Rank	SUE-ED-based LCI		SUE-based LCI		Original UE-based LCI		J-C	
	Bridge	Bound	Bridge	Bound	Bridge	Bound	Bridge	Bound
1	B13	NB	B11	NB	B10	NB	B13	NB
2	B11	NB	B13	NB	B11	NB	B6	WB
3	B5	WB	B10	NB	B4	WB	B5	WB
4	B10	NB	B6	WB	B5	WB	B12	NB
5	B6	WB	B5	WB	B13	NB	B1	WB
6	B4	WB	B4	WB	B6	WB	B4	WB
7	B7	WB	B7	WB	B12	NB	B7	WB
8	B2	WB	B2	WB	B11	SB	B10	NB
9	B11	SB	B11	SB	B3	WB	B14	SB
10	B12	NB	B13	SB	B13	SB	B7	EB

According to Table 3.11, the most important directional routes are northbound Assiniboine River and westbound Red River, as they carry traffic out of Winnipeg City during the PM peak period. SUE-ED-based LCI identified the top three bridges as B13-St. James Bridge (NB), B11-Osborne Bridge (NB), and B5-Provencher Bridge (WB), with St. James Bridge ranked as the most important. Although not the most congested and located outside the city center, it serves as a crucial access point between the airport and residential areas. Any disruption in the NB direction could have an adverse impact on expected travel costs and demands. B11 and B5 are located near the central business district (CBD), which is sensible. SUE-ED-based LCI also included B10-Mid Town (NB) and B6-Norwood (WB) into Top-5 ranked bridges. These bridges are near the center similar to J-C method.

Figure 3.20 shows the Spearman's rank correlation coefficients between the measures.

$$r_{X,Y} = \frac{Cov(R(X), R(Y))}{Var(R(X))Var(R(Y))} \quad (3.22)$$

where  $R(t)$  shows the rank of the observation of  $t$  in  $X$  or  $Y$  data sets. The Spearman's rank correlation takes values in the range from -1 to 1. The positive correlation signifies that the ranks of both the variables are increasing. In contrast, the negative correlation shows that as the rank of one variable increases, the rank of the other decreased. To be consistent with (Almotahari and Yazici, 2019, Almotahari and Yazici, 2021), the strength of the correlation

between two variables is categorized as follows: 0 to 0.19 very weak; 0.2 to 0.39 weak; 0.4 to 0.59 moderate; and 0.6 to 0.79 strong; and 0.8 to 1 very strong.

Table 3.12 lists the criticality values and rankings for all bridges.

Table 3.12. LCI values and ranking of bridges in the Winnipeg network.

Bridge	Bound	SUE-ED-based LCI	Rank	SUE-based LCI	Rank	Original LCI	Rank	J-C	Rank
B1	EB	2.0E-4	27	3.0E-4	27	7.3E-5	25	2.3E-2	22
B1	WB	7.8E-4	13	6.9E-4	14	1.0E-3	11	3.9E-2	5
B2	EB	4.9E-4	18	4.7E-4	20	1.3E-4	22	2.3E-2	18
B2	WB	1.1E-3	8	1.1E-3	8	3.8E-4	14	2.4E-2	17
B3	EB	5.2E-4	17	4.6E-4	22	3.0E-4	15	2.7E-2	11
B3	WB	5.3E-4	16	6.0E-4	17	1.4E-3	9	2.4E-2	16
B4	EB	2.3E-4	26	3.3E-4	26	1.2E-4	23	2.2E-2	24
B4	WB	1.9E-3	6	1.9E-3	6	4.4E-3	3	3.4E-2	6
B5	EB	3.4E-4	21	4.9E-4	19	1.1E-4	24	2.5E-2	14
B5	WB	2.9E-3	3	2.1E-3	5	4.0E-3	4	4.2E-2	3
B6	EB	6.0E-4	15	6.7E-4	15	1.5E-4	19	1.7E-2	28
B6	WB	2.6E-3	5	2.2E-3	4	2.9E-3	6	5.8E-2	2
B7	EB	4.9E-4	19	6.5E-4	16	2.9E-4	17	2.9E-2	10
B7	WB	1.4E-3	7	1.2E-3	7	6.3E-4	12	3.4E-2	7
B8	EB	2.5E-4	25	3.7E-4	25	5.5E-5	26	2.3E-2	21
B8	WB	9.0E-4	11	7.6E-4	13	5.7E-4	13	2.5E-2	15
B9	EB	1.8E-4	28	2.6E-4	28	4.9E-5	27	2.2E-2	25
B9	WB	2.6E-4	24	3.9E-4	24	4.7E-5	28	2.1E-2	26
B10	NB	2.7E-3	4	2.5E-3	3	7.2E-3	1	3.2E-2	8
B10	SB	4.2E-4	20	5.4E-4	18	1.8E-4	18	2.0E-2	27
B11	NB	3.0E-3	2	3.4E-3	1	4.5E-3	2	2.3E-2	19
B11	SB	1.1E-3	9	1.0E-3	9	1.5E-3	8	2.3E-2	20
B12	NB	9.7E-4	10	8.4E-4	11	2.1E-3	7	4.1E-2	4
B12	SB	2.8E-4	23	4.0E-4	23	3.0E-4	16	2.2E-2	23
B13	NB	3.4E-3	1	2.7E-3	2	3.1E-3	5	6.7E-2	1
B13	SB	8.7E-4	12	9.3E-4	10	1.2E-3	10	2.7E-2	12
B14	NB	3.3E-4	22	4.7E-4	21	1.3E-4	21	2.6E-2	13
B14	SB	6.3E-4	14	8.1E-4	12	1.4E-4	20	2.9E-2	9

Figure 3.20 shows that all four measures have positive correlations. The LCI methods are strongly correlated with each other and with the J-C measure. The SUE-ED-based LCI and J-C measures have the highest correlation, which means that the LCI approach gives a similar ranking to the J-C method. However, it should be remembered that there is no definitive ground truth for bridge criticality, making it impossible to assert that one measure is superior to another.

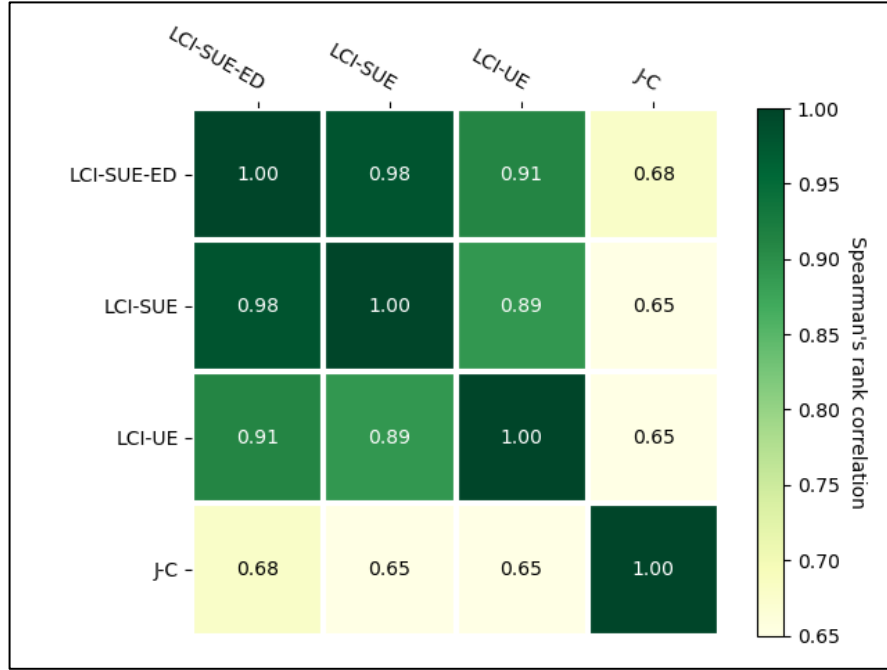


Figure 3.20. Spearman's rank correlation coefficients.

### 3.5 Chapter summary

This chapter adopted the link criticality index (LCI) method, originally based on user equilibrium TA model with fixed demand (UE-FD or UE). It identified common issues of UE-based LCI associated with the all-or-nothing (AON) network loading procedure of the UE TA models. It refined the UE-based LCI method and further advanced the LCI method by integrating the stochastic user equilibrium traffic assignment (TA) model with elastic demand (SUE-ED), which is a more behaviorally plausible TA model than the UE TA. The SUE-ED-based LCI method not only eliminated the identified issues but also relaxed the assumptions that travelers have perfect knowledge of network conditions and fixed demand. The validity of the SUE-ED-based LCI was demonstrated using a large-scale network, with results that were reasonable and consistent with full-scan methodologies.

In summary, this chapter has outlined the base methodology used throughout the thesis, provided a thorough analysis of the selected method's properties, identified the deficiencies of the original method, suggested improvements to eliminate these deficiencies, and

demonstrated the method's applicability to large-scale road networks. However, it did not account for similarity of routes, which is known to persist in networks. Overlooking the route similarity issue may compromise network equilibrium analysis and any subsequent analyses because it affects both individuals' route choice and travel demand. Next chapter addresses this issue by advancing link criticality analysis with a network equilibrium model that is capable of capturing the effects of route similarities on route choice and travel demand.

# CHAPTER 4

## Incorporating route similarity and demand elasticity into link criticality analysis

---

The previous chapter integrated travelers' perception error and demand elasticity into link criticality analysis using a stochastic user equilibrium model with elastic demand (SUE-ED). This chapter further advances link criticality analysis by integrating a cross-nested logit SUE-ED (CNL-SUE-ED) TA model, which flexibly and plausibly captures the impact of route similarity on individual route choices and network flows.

### 4.1 Motivation

Route similarity can affect travelers' route choices, making correlated routes less attractive from a travel cost perspective, altering traffic flow patterns, and consequently affecting the criticality of links for the network's normal operation. Considering route similarity is essential to realistically capture travelers' route choice behavior and avoid systematically erroneous link criticality evaluations. This chapter incorporates the effects of route similarity into the link criticality assessment framework. It aims to answer the following research questions: *(i) Does route similarity affect link criticality? and (ii) if so, in what way?*

Specifically, this study advances the link criticality index (LCI) method, which was originally proposed by [Almotahari and Yazici \(2019\)](#) and later extended in Chapter 3, for link criticality analysis. The LCI method has been chosen for its effectiveness and efficiency. The LCI method is effective, as it accounts for congestion effects and common travelers' behavior

though the use of TA models. It is also efficient because it eliminates the need for network scanning and evaluates the criticality of all links within a single TA procedure. To account for route similarity, the CNL model – an advanced route choice model with a theoretically sound, flexible structure that considers route similarity – and the corresponding SUE TA models with and without ED (Bekhor and Prashker, 1999, Kitthamkesorn et al., 2016, Vovsha, 1997), are integrated into the LCI method. The SUE TA problems are formulated as mathematical programming (MP) problems and solved using a partial linearization method with a self-regulated averaging (SRA) step size (Liu et al., 2009, Ryu et al., 2014, Xu and Chen, 2013). To validate the concept, the resulting LCI method is applied to analyze the criticality of links in large-scale networks.

Therefore, the main contribution of this chapter is an advanced link criticality analysis method that accounts for route similarity, in addition to topology, redundancy, drivers' perception errors, congestion effects, and the elastic nature of urban travel demand. This method promises to provide more behaviorally plausible link criticality evaluations, potentially enabling better decision-making for traffic management and infrastructure investment.

The remainder of this chapter is structured as follows. Section 4.2 discusses how route similarity may affect link criticality analysis. Section 4.3 elaborates on how the route similarity issue has been addressed in this study. Section 4.4 modifies the LCI method to account for the route similarity issue. Section 4.5 explains the numerical experiments and discusses the results. Finally, Section 4.6 offers concluding remarks.

## **4.2 Route similarity and link criticality analysis**

This section discusses the main sources of route similarity and the impact of route similarity on travel demand and link criticality.



## 4.2.1 Sources of route similarity

The severity of route similarity can be attributed to three factors: (i) the number of shared links between routes; (ii) the number of routes sharing the same link; and (iii) the total number of routes considered (Bovy, 2009). Figure 4.1 provides an example of route similarity issue for a selected origin-destination (O-D) pair of a real-size network.

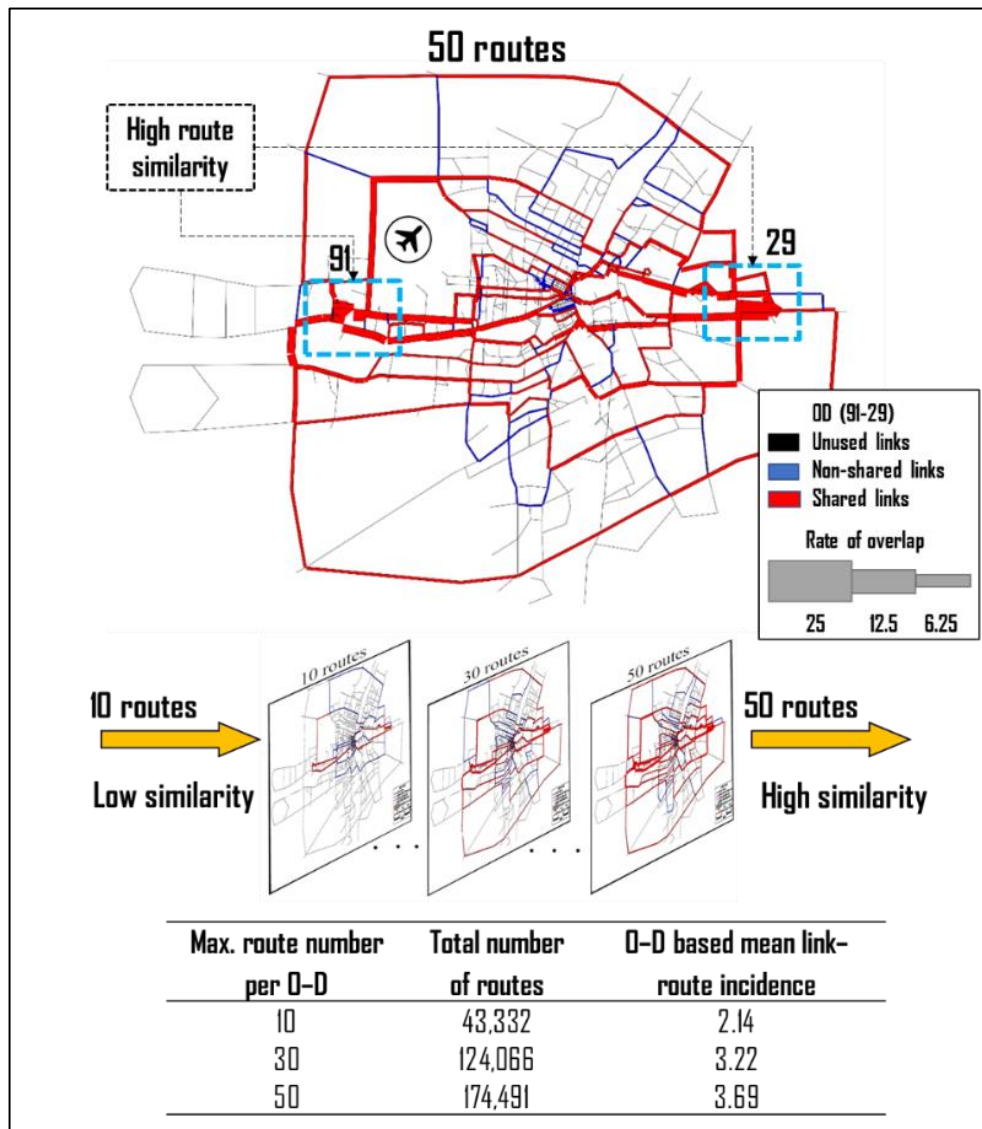


Figure 4.1 Route similarity issue in the Winnipeg network.

As depicted in red in Figure 4.1, route alternatives exhibit a complex correlation structure due to significant topological overlaps. Certain links are utilized by multiple routes, as

indicated by the thick red lines in Figure 4.1. Increase in the route choice set size further amplifies route correlation and, therefore, route similarity. This complexity can substantially impact the estimated network efficiency measures used in link criticality analysis, potentially skewing the results. Therefore, a nuanced approach that accounts for route similarity is required for a more realistic link criticality analysis.

### 4.2.2 Impact of route similarity on travel demand

In TA, understanding the relationship between route similarity and travel demand is crucial. Higher levels of route similarity may result in lower travel demand, whereas lower levels of similarity may boost demand. While adding more routes generally may increase travel demand, it may also introduce new challenges. Shared links often become traffic bottlenecks, leading to congestion that inhibits further growth in demand. This dynamic is illustrated in Figure 4.2.

As shown in Figure 4.2 (top), a network with a single O-D pair is connected by a link with a flow-dependent travel time function  $t(x)$ , where  $x$  represents the link flow, serving a travel demand  $q_1$ . By introducing an intermediate node 3 that can slide between the origin and destination nodes without affecting the overall free-flow travel time (FFTT)  $c$ , route similarity can be controlled (Figure 4.2, middle). Then, when node 3 coincides with node 2, this single-route scenario can be considered an extreme case of full overlap of two routes, making the travel demand  $q_1$  the minimum possible demand. When node 3 coincides with node 1, there are two identical non-overlapping routes, leading to the maximum travel demand  $q_2$ . At any other position of node 3, the travel demand  $q'_2$  is lower than  $q_2$ . Next, adding links from node 3 to node 2 increases the number of similar routes, which can raise travel demand due to the increased capacity of non-shared parts, but the overall demand is constrained by the shared link travel time (Figure 4.2, bottom). This example illustrates that increasing route

similarity can decrease travel demand, and the growth rate of travel demand due to an increasing number of routes may depend on their level of similarity.

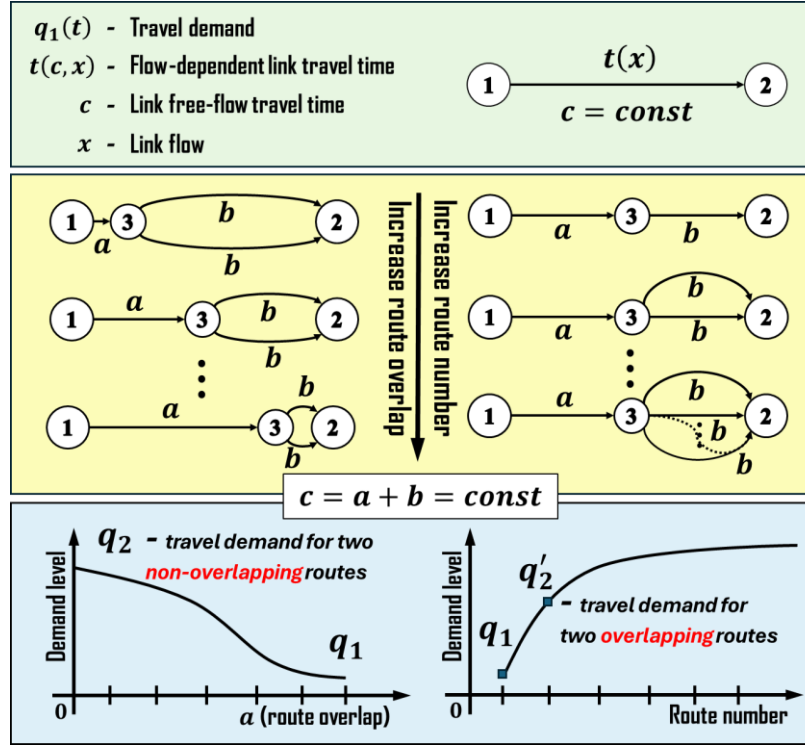


Figure 4.2. Impact of route similarity on travel demand.

### 4.2.3 Impact of route similarity on link criticality

Figure 4.3 provides a visual explanation of the link criticality concept in relation to the route similarity issue.

As shown in Figure 4.3, a link is critical if it is essential for serving travel demand which also implies connectivity. The highest criticality occurs when no other alternatives exist (green box). Increasing the number of alternatives decreases a link's criticality (left yellow box). Splitting a link does not change the criticality of the resulting sub-links (right yellow box). Shared links facilitate redundancy and should have higher criticalities than subsequent links in a route (blue box). However, shared links can cause route similarity issues, leading to overestimated link criticalities due to overestimated route flows. This study incorporates

these features into the LCI method - one of the state-of-the-art methods for link criticality analysis.

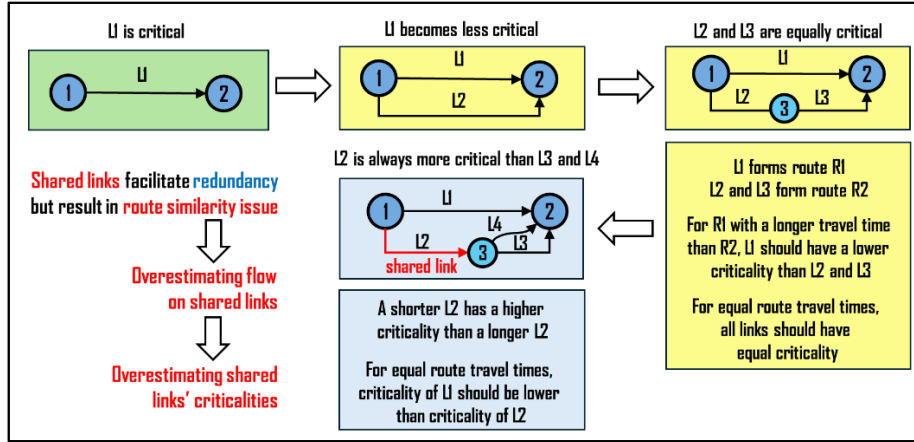


Figure 4.3. Concept of link criticality analysis: Emphasis on route similarity.

### 4.3 Addressing route similarity in SUE

The selected TA models account for travelers' inaccurate perceptions of travel costs, route similarities, and demand elasticity. Considering perception error is important as travelers often misjudge the costs associated with different routes. Addressing route similarity is necessary because routes that share links can affect travelers' choices and the overall traffic flow distribution in networks. Similarly, modeling demand elasticity is important because, as congestion increases, network users may decide to use a different mode of travel, shift the time of travel, or forego some trips altogether. This section elaborates on the selected route choice models, demand function, equivalent MP formulations, and solution algorithm.

#### 4.3.1 Probabilistic route choice model

Probabilistic route choice models are a core of any SUE TA model. These models consider travelers' perception errors in the route choice process by incorporating a random component associated with travel cost into the random utility function. Assuming an additive error term, mathematically it can be represented as follows:

$$C_k^w = c_k^w + \varepsilon_k^w, \quad \forall k \in K^w, \forall w \in \mathcal{W} \quad (4.1)$$

where  $\mathcal{W}$  is set of all O-D pairs,  $K^w$  is a set of routes for O-D pair  $w$ ,  $C_k^w$  is perceived travel time of route  $k$  connecting O-D pair  $w$ ,  $c_k^w$  is the actual (deterministic) travel time, and  $\varepsilon_k^w$  is an error term associated with route  $k$  connecting O-D pair  $w$ . This section discusses two selected route choice models, namely multinomial logit (MNL) and CNL. A toy network in Figure 4.4 is used to illustrate the properties of the selected route choice models.

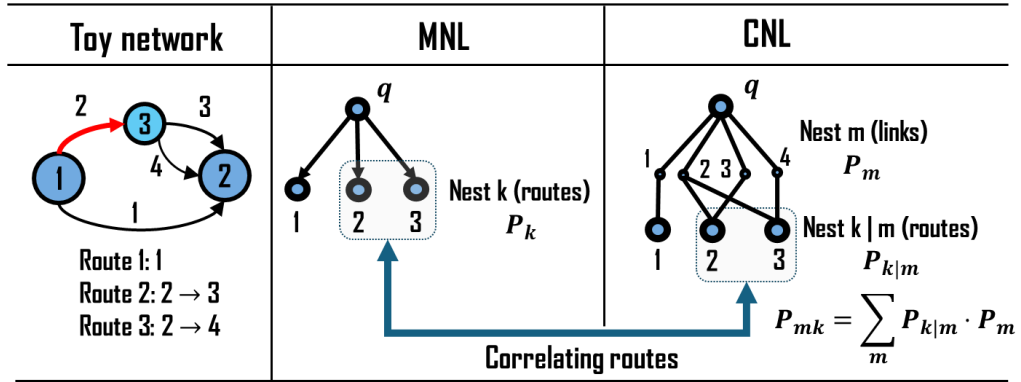


Figure 4.4. MNL and CNL route choice model structures.

MNL (Dial, 1971) is a widely used probabilistic route choice model that assumes that error terms are independently and identically distributed (IID) Gumbel random variables with zero-mean, scaling parameter  $\theta$ , and variance  $Var[\varepsilon_k^w] = \frac{\pi^2}{6\theta^2}, \forall k \in K^w$ . It provides a closed-form probability expression, i.e.:

$$P_k^w = \frac{e^{-\theta c_k^w}}{\sum_{l \in K^w} e^{-\theta c_l^w}}, \quad \forall w \in \mathcal{W}, \forall k \in K^w \quad (4.2)$$

where the dispersion parameter  $\theta$  can be interpreted as drivers' sensitivity to route costs. Higher values of  $\theta$  indicate higher sensitivity (drivers tend to select least-cost routes more), while lower values – lower sensitivity (Damberg et al., 1996).

As shown in Figure 4.4, the MNL model has a simple single-level structure for the choice probability. It is unable to account for similarities among different route alternatives. To

address the limitations of the MNL model, advanced logit-based models were developed. Among them, CNL (Bekhor and Prashker, 1999, Vovsha, 1997) is one of the prominent advanced logit-based models. CNL combines two Gumbel-distributed error components with zero mean, two scaling parameters  $\theta$  (governs route-specific error) and  $\mu$  (governs nest-specific error) with  $\theta \geq \mu$  and  $\mu \in [0,1]$ . The model structure addresses route similarity by permitting routes to belong to multiple nests simultaneously, with each nest represented by a link. The total variance for the CNL model is  $Var = \frac{\pi^2}{6} \left( \frac{1}{\mu^2} + \frac{1}{\theta^2} \right)$ . Lower  $\mu$  results in higher nest variance and stronger correlation within nests, which can be interpreted as travelers perceive routes in the same nest as closer substitutes. Lower  $\mu$  or  $\theta$  increases variance, leading to more uniform choice probabilities. It is important to note that the variance of the CNL model is greater than that of the MNL model for a given value of  $\theta$ . As shown in Figure 4.4, the CNL model uses a two-level hierarchical structure to decompose choice probability into marginal (4.3) and conditional probabilities (4.4). Notably, the model structure accounts for route similarity by allowing links to be shared among multiple routes.

$$P_m^w = \frac{\left[ \sum_{k=1}^{K_m^w} (\alpha_{mk}^w e^{-\theta c_k^w})^{1/\mu} \right]^\mu}{\sum_{b=1}^{M^w} \left[ \sum_{k=1}^{K_b^w} (\alpha_{bk}^w e^{-\theta c_k^w})^{1/\mu} \right]^\mu}, \quad \forall w \in \mathcal{W}, \forall m \in M^w \quad (4.3)$$

$$P_{k|m}^w = \frac{[\alpha_{mk}^w e^{-\theta c_k^w}]^{1/\mu}}{\sum_{l=1}^{K_m^w} [\alpha_{ml}^w e^{-\theta c_l^w}]^{1/\mu}}, \quad \forall w \in \mathcal{W}, \forall m \in M^w, \forall k \in K_m^w \quad (4.4)$$

where  $\alpha_{mk}^w$  is the inclusion coefficient (or degree of membership) of an alternative  $k$  in link nest  $m$  and  $\mu$  is a scaling parameter of the upper choice level.

Using (4.3) and (4.4), joint link nest and route choice probability of the CNL model can be derived as follows:

$$P_{mk}^w = \sum_{m \in M^w} P_m^w \cdot P_{k|m}^w, \quad \forall w \in \mathcal{W}, \forall k \in K_m^w \quad (4.5)$$

The degrees of membership are represented mathematically as:

$$\alpha_{mk}^w = \left( \frac{L_m}{L_k^w} \right)^\gamma \delta_{mk}^w, \quad \forall w \in \mathcal{W}, \forall m \in M^w, \forall k \in K_m^w \quad (4.6)$$

and must satisfy the following normalizing equation for the interpretation and estimation of the parameters:

$$\sum_{m \in M^w} \alpha_{mk}^w = 1, \quad \forall w \in \mathcal{W}, \forall k \in K_m^w \quad (4.7)$$

In particular, the CNL model collapses to the MNL model in two cases: (a) when there is no overlap in the network or (b) when the coefficient of nesting,  $\mu$ , equals 1.

### *Illustrative example<sup>3</sup>*

To show the properties of the MNL and CNL models, the network in Figure 4.5 is considered. Link FFTTs are set to  $x = 8$  and  $b = 20$  where not specified; route choice model's parameters are  $\theta = 1.0, \mu = 0.05$ . Route similarity is varied as shown in Figure 4.6. The results are summarized in Figure 4.7 and Figure 4.8.

---

<sup>3</sup> It is acknowledged that the loophole network may not display all features of CNL due to its simple block-diagonal correlation structure (i.e., CNL collapses into a simple nested logit structure). However, it seems to be sufficient for demonstrating the differences between the selected models.

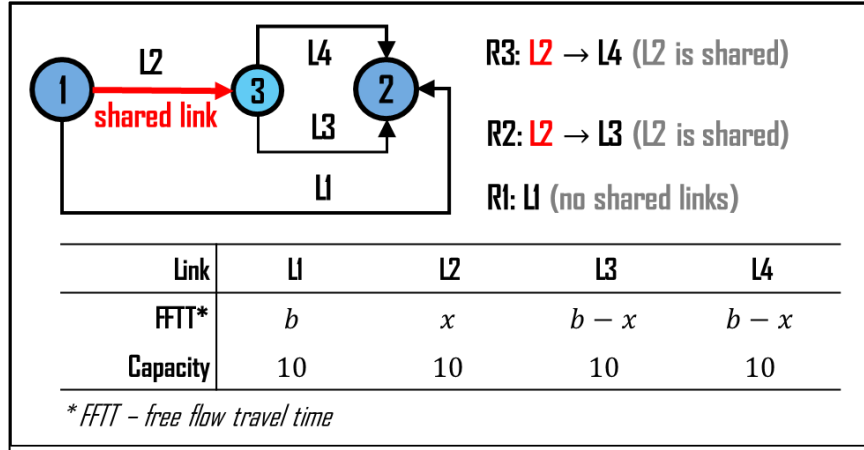


Figure 4.5. Loophole network: Emphasis on shared link.

As discussed in Section 4.1, routes with longer shared links are considered more similar than those with shorter shared links. Additionally, the number of routes sharing the same link affects their attractiveness. Therefore, the models' responses to route similarity are investigated from two sources: the length of shared links (Figure 4.6a) and the number of similar routes (Figure 4.6b).

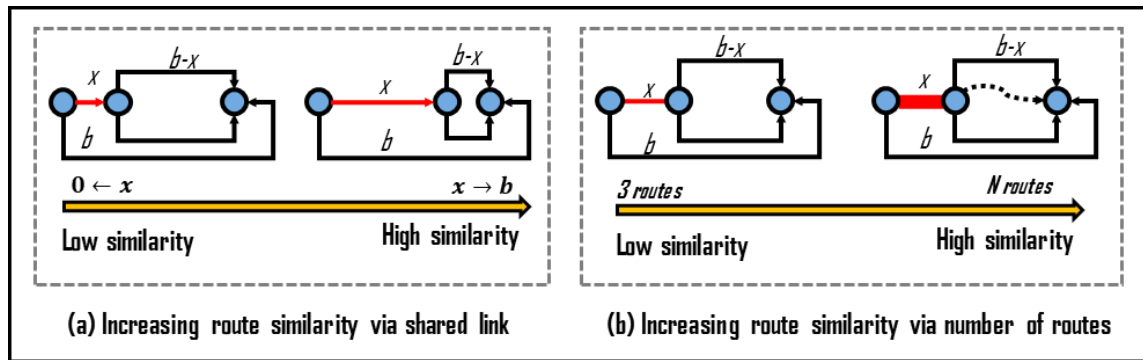
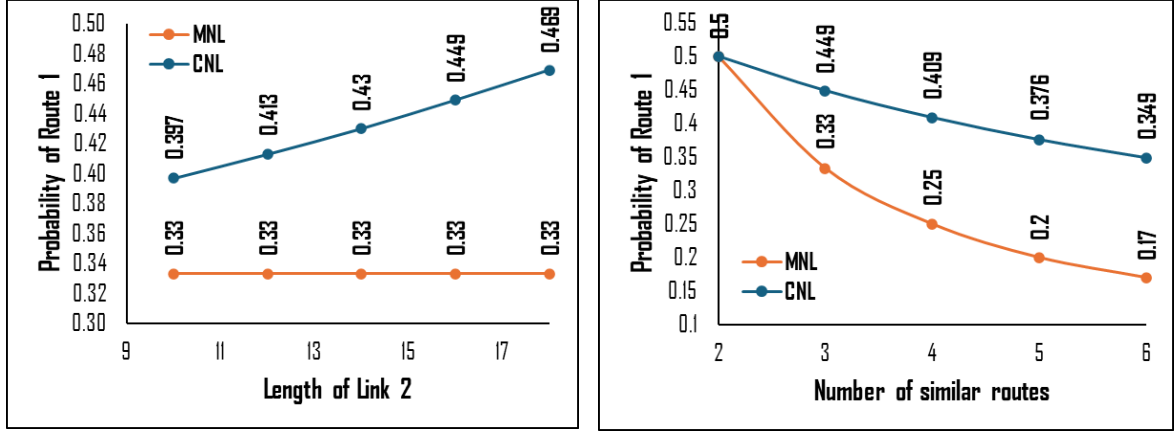


Figure 4.6. Studying effects of route similarity on link criticality analysis.

Figure 4.7 illustrates the impact of route similarity on the selected models. The two models responded differently to route similarity.





(a) Impact of shared link's FTTT on route choice.

(b) Impact of number of similar routes on route choice.

Figure 4.7. Impact of route similarity on route choice.

Specifically, the FTTT of shared links increased the probability of non-overlapping route for CNL but did not affect MNL (Figure 4.7a). Additionally, the probability of non-overlapping route decreased more slowly with an increasing number of overlapping routes for CNL compared to MNL (Figure 4.7b). It shows that the CNL model is sensitive to route similarity and tends to assign relatively higher probabilities to non-overlapping routes, while the MNL model remains unaffected by this factor.

Next, sensitivity analysis is conducted on the scaling parameter  $\mu$  of the CNL model. The results are shown in Figure 4.8.

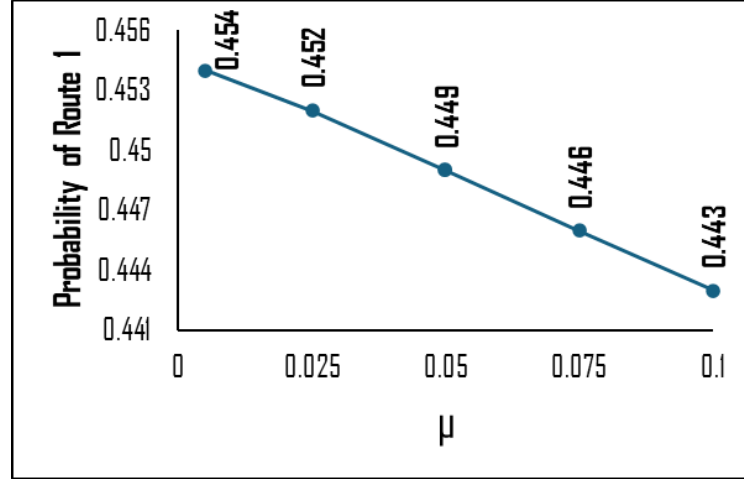


Figure 4.8. Sensitivity analysis for CNL.

As shown in Figure 4.8, with increase of  $\mu$  the probability of choosing R1 decreases. Theoretically, CNL should collapse to MNL when  $\mu = 1$ , meaning that the difference between CNL and MNL disappears. The results in Figure 4.8 are consistent with the theory.

### 4.3.2 Travel demand model

The travel demand is modeled, as detailed in Chapter 3, using an exponential function of the expected perceived cost (EPC) for each O-D pair, as represented in equation (3.4).

### 4.3.3 Equivalent MP formulation

The MP formulation allows analysts to relate it to choice probability based on optimality conditions. It also facilitates solving the problem using convergent optimization algorithms, determining search directions and step sizes, and monitoring convergence. This section provides an equivalent MP formulation for the selected route choice models: multinomial logit stochastic user equilibrium with elastic demand (MNL-SUE-ED) (Yang and Bell, 1998) and cross-nested logit stochastic user equilibrium with elastic demand (CNL-SUE-ED) (Kitthamkesorn et al., 2016). The formulations are summarized in Figure 4.9.

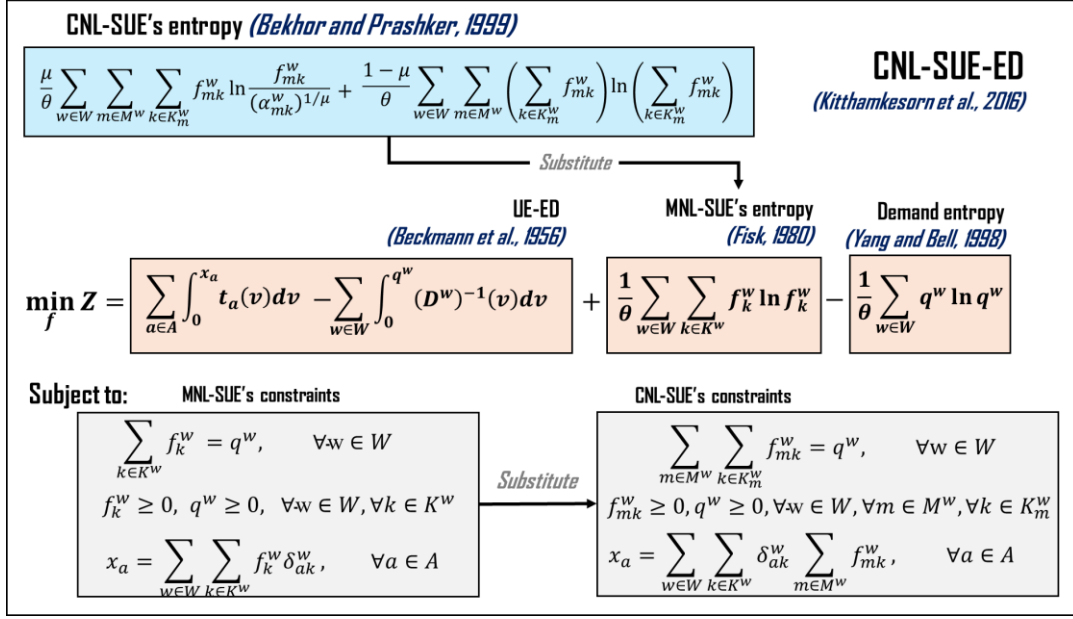


Figure 4.9. MP formulations for MNL-SUE-ED and CNL-SUE-ED models.

As shown in Figure 4.9 [Yang and Bell \(1998\)](#) extended [Fisk \(1980\)](#) MP formulation for the MNL-SUE model to include ED. The decision variables are route flows and travel demand for each O-D pair. The objective function has three components: the Beckmann transformation with ED (including a flow-dependent link cost and an inverse demand function terms), the route flow-based entropy term by [Fisk \(1980\)](#), and the demand entropy term. The ED component,  $D^{-1}(\cdot)$ , represents the cost of an auxiliary link or an additional route for managing elastic demand ([Sheffi, 1985](#)). Constraints include flow conservation, non-negativity, and link-route relation.

In CNL-SUE-ED ([Kitthamkesorn et al., 2016](#)), the route flow decision variables are decomposed to explicitly encode the link nests. Unlike MNL-SUE-ED, the new decision variables relate to both the link and route. This decomposition requires model reformulation, where a route flow entropy term is split into two entropy terms, as shown in Figure 4.9. The rest of the formulation is similar to MNL-SUE-ED.

The uniqueness of the equilibrium solution is guaranteed when the link travel cost functions are separable, strictly convex functions of traffic flow, and the demand function is

monotonically decreasing in the O-D travel cost, bounded from above, and invertible (Sheffi, 1985).

#### 4.3.4 Solution algorithm

This section elaborates on the solution algorithm for solving SUE TA. The partial linearization method with SRA step size was adopted (Ryu et al., 2014, Xu and Chen, 2013). The algorithm is summarized in Figure 4.10.

As shown in Figure 4.10, in each iteration, the algorithm finds a descent search direction and determines the corresponding step-size. The search direction is determined by solving a partially linearized subproblem defined by the linearization of the integral terms of the objective function, which was proven to be a descent and feasible direction (Patriksson, 2015). The travel demand is calculated according to the current route cost pattern in the partially linearized subproblem, similar to that reported by Xu and Chen (2013). The SRA scheme does not need to evaluate the objective function or its derivative (Liu et al., 2009) and has two positive parameters, i.e.,  $\lambda_1 > 1$  and  $\lambda_2 < 1$ , that control the decrease in speed and ensure convergence. For a more comprehensive analysis of the properties of this solution method, readers may refer to Patriksson (2015) and Liu et al. (2009). The relative gap (RGAP) function is used to control the convergence process as shown in Figure 4.10. Once RGAP drops below a specified threshold, the algorithm terminates.

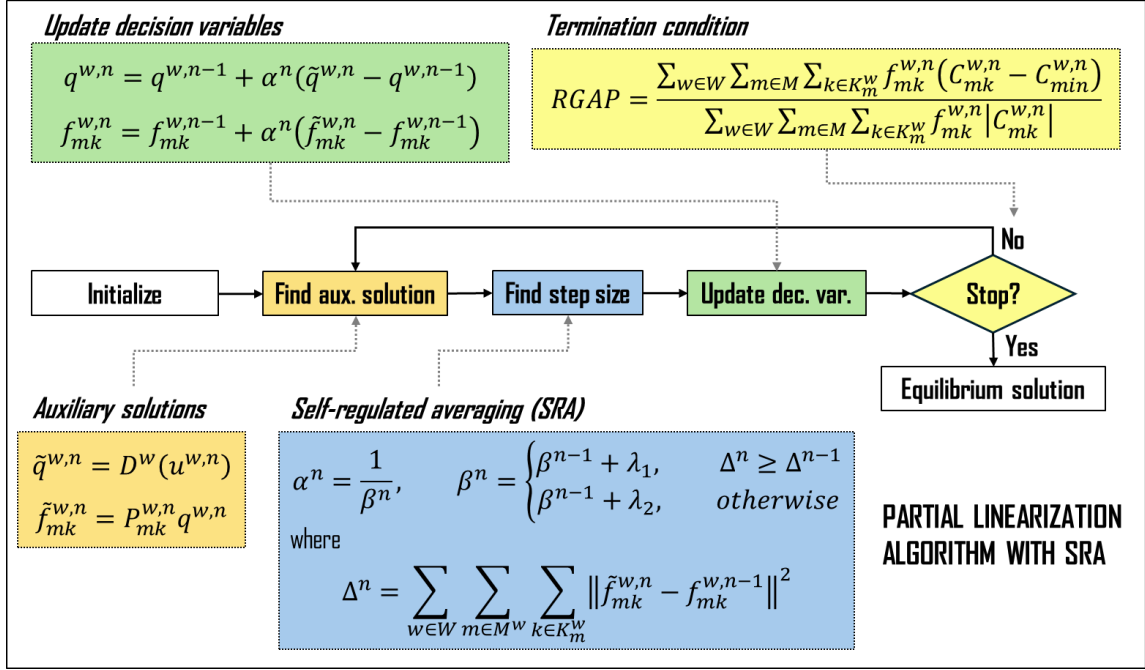


Figure 4.10. Partial linearization algorithm with the SRA step size.

## 4.4 Route similarity in LCI

The criticality of a link is not only a function of its own characteristics but also of its relationship with alternative routes within the network. This section explains the concept of link criticality, elaborates on the selected method for link criticality analysis, and provides an illustrative example.

### 4.4.1 Link criticality index

Not all TA-based link criticality analysis methods can be used in practice due to their computational complexity. This study adopts an efficient method for link criticality analysis - LCI proposed by [Almotahari and Yazici \(2019\)](#) and extended to SUE TA in Chapter 3. The LCI method is presented in Figure 4.11.

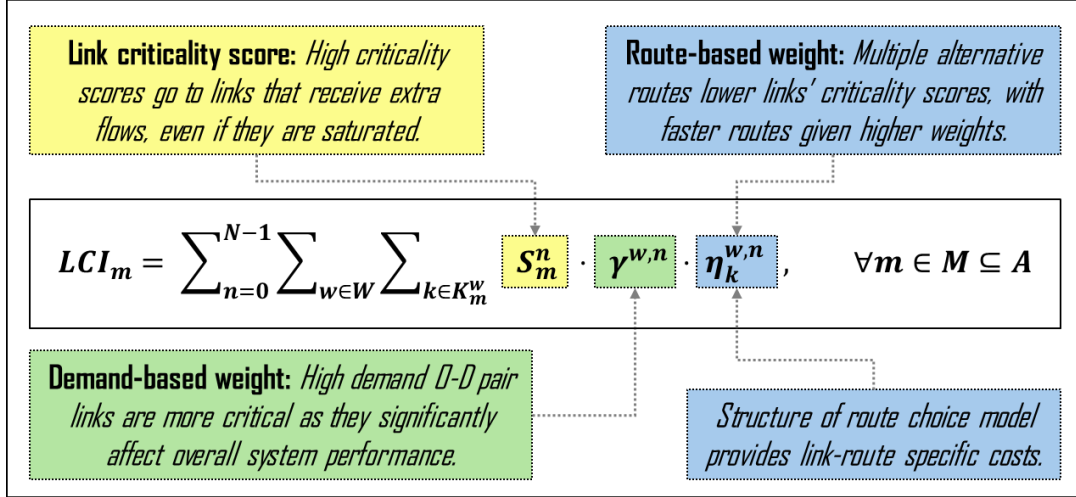


Figure 4.11. Explanation of the link criticality index (LCI) method.

According to [Almotahari and Yazici \(2019\)](#), if a specific link continues to be assigned additional flows despite increasing saturation, it indicates that the link is more critical. The link criticality score  $S_m^n$  is calculated as the product of a link's additional flow at iteration  $n + 1$  and its marginal cost (MC) (4.8).

$$S_m^n = \max([x_m^{n+1} - x_m^n], 1.0) \cdot \frac{mc_m(x_m^n)}{t_m(x_m^n)}, \quad \forall m \in M, \forall n \in N \quad (4.8)$$

where  $x_m^n$  is flow through link  $m$  at iteration  $n$ ,  $mc_m$  is MC on link  $m$ .

MC serves as an indicator of each link's saturation, reflecting the increase in travel time resulting from an additional unit of flow (4.9).

$$mc_m(x_m^n) = t_m(x_m^n) + x_m^n t'_m(x_m^n), \quad \forall m \in M \quad (4.9)$$

where  $t_m$  is travel time on link  $m$ , and  $t'_m$  is the derivative of link travel time with respect to its flow.

Link criticality score is a local measure of criticality and does not explicitly account for a link's role in a network. However, since a link can be part of routes for various O-D pairs, the criticality score should be weighted by both demand-based and route-based factors to incorporate network connectivity information.

The demand-based weights (4.10) are introduced to address the fact that the link criticality score does not fully reflect link's criticality in terms of O-D pairs served. A link that establishes a connection between O-D pairs with a greater demand tends to have a more significant impact on the overall functionality of the system. Additionally, travel demand of each O-D pair can vary from iteration to iteration, hence, the total network travel demand due to demand elasticity.

$$\gamma^{w,n} = \frac{q^{w,n}}{Q^n}, \quad \forall w \in \mathcal{W}, \forall n \in N \quad (4.10)$$

where  $q^{w,n}$  denotes travel demand of O-D pair  $w$  at iteration  $n$  and  $Q^n$  denotes total network travel demand at iteration  $n$ .

The route cost-based weights (4.11) are introduced to address the fact that the link criticality score does not fully reflect link's criticality in terms of route redundancy. The existence of multiple alternative routes not crossing this link should reduce its criticality score. The impact of travelers' perception errors and route similarity should be considered. For this reason, route cost-based weights are modeled to distinguish alternative routes based on perceived travel time. A route with a perceived travel time twice as long as the shortest is given different weight than one slightly longer than the shortest. This ensures that for any O-D pair with multiple routes, the ones perceived to be faster are assigned higher weights.

In CNL, a route  $k \in K^w, w \in W$  may belong to multiple nests in  $M^w$  (see Figure 4.4 for the two-level tree structure). Therefore, a route  $k$  can be represented by multiple perceived route costs  $C_{mk}^w$ , one for each nest  $m \in M^w$ . It is worth emphasizing that each cost includes the actual travel time of route  $k$ . Therefore, it is sufficient to select one cost to represent the perceived travel time on route  $k$ . The max operator is applied to select this cost. It can be interpreted as choosing the worst-case scenario cost.

$$\eta_k^{w,n} = \frac{\max(1/C_{mk}^{w,n}, \forall m \in M^w)}{\sum_{i \in K^w} \max(1/C_{mi}^{w,n}, \forall m \in M^w)}, \quad \forall w \in \mathcal{W}, \forall k \in K^w, \forall n \in N \quad (4.11)$$

where  $C_{mk}^{w,n}$  is perceived travel cost on route  $k$  associated with link nest  $m$  for O-D pair  $w$  at iteration  $n$ . The latter can be derived as a partial derivative of the objective function with respect to the corresponding link nest-route flow:

$$C_{mk}^{w,n} = c_k^{w,n} + \frac{\mu}{\theta} \left[ \ln \left( \frac{f_{mk}^{w,n}}{\alpha_{mk}^w} \right) + 1 \right] + \frac{1-\mu}{\theta} \left[ \ln \left( \sum_{l \in K_m^w} f_{ml}^{w,n} \right) + 1 \right] \quad (4.12)$$

where  $c_k^{w,n}$  denotes the deterministic travel time on route  $k$  connecting O-D pair  $w$  at iteration  $n$ ,  $f_{mk}^{w,n}$  is flow on route  $k$  associated with link nest  $m$  for O-D pair  $w$  at iteration  $n$ , and  $\alpha_{mk}^w$  is the corresponding membership value.

#### 4.4.2 Illustrative example

This section calculates the LCI method for one iteration, focusing on route cost-based weights using the loophole network (Figure 4.5). The route cost-based weights are emphasized because they have been modified more than other components of the LCI method.

The following link travel time function is assumed:

$$t_m(x_m) = x_m$$

With parameter values set to  $\theta = 1.0, \mu = 0.05, x = 10, b = 20, f_{mk}^{w,n} = 1.0 \forall m, \forall k$ , the link-route weights are obtained as shown in Table 4.1.

Table 4.1. Computing route-based weights for LCI.

Route	(m,k)	$t_m(x_m^n)$	$c_k^{w,n}$	$\alpha_{mk}^w$	$C_{mk}^{w,n}$	$\eta_k^{w,n}$
R1	(1,1)	1.0	1.0	1.0	2.35	0.46
R2	(2,2)	2.0	3.0	0.5	4.69	0.27
	(3,2)	1.0		0.5	4.03	
R3	(2,3)	2.0	3.0	0.5	4.69	0.27
	(4,3)	1.0		0.5	4.03	

The LCI values at iteration  $n$  can be found as follows:

$$LCI_1^n = S_1^n \cdot \gamma^{w,n} \cdot \eta_1^{w,n} = S_1^n \cdot \gamma^{w,n} \cdot 0.46$$

$$LCI_2^n = S_2^n \cdot \gamma^{w,n} \cdot (\eta_2^{w,n} + \eta_3^{w,n}) = S_2^n \cdot \gamma^{w,n} \cdot 0.54$$



$$LCI_3^n = S_3^n \cdot \gamma^{w,n} \cdot \eta_2^{w,n} = S_1^n \cdot \gamma^{w,n} \cdot 0.27$$

$$LCI_4^n = S_4^n \cdot \gamma^{w,n} \cdot \eta_3^{w,n} = S_4^n \cdot \gamma^{w,n} \cdot 0.27$$

As observed, although Route 1 had the highest weight, the final weight for Link 2 surpassed that of Link 1 due to the aggregation of route weights. This demonstrates that LCI effectively captured the importance of route cost and redundancy in link criticality assessment. The impact of route similarity is emphasized in the next section.

## 4.5 Numerical experiments

Two sets of experiments were conducted. Using a toy network (Figure 4.5), the properties of the advanced LCI method were investigated. Using real-size networks (Figure 4.16), the applicability of the model to real scenarios were shown.

Without any loss of generality, the link travel time was modeled by the well-known Bureau of Public Roads (BPR) function (3.14).

The EPC value for TA models was computed according to equation (3.16) for MNL-SUE and equation (4.13) for CNL-SUE:

$$EPC_{CNL}^w = -\frac{1}{\theta} \ln \left[ \sum_{m \in M^w} \left( \sum_{k \in K_m^w} (\alpha_{mk}^w \cdot e^{-\theta c_k^w})^{\frac{1}{\mu}} \right)^{\mu} \right], \quad \forall w \in W \quad (4.13)$$

Like in Chapter 3, the LCI values are normalized according to (3.17) - (3.18). The parameters for SRA step size scheme were set at  $\lambda_1 = 1.9$  and  $\lambda_2 = 0.1$ .

### 4.5.1 Experiment 1: A toy network

This section examined the properties of LCI using the toy network in Figure 4.5. The LCI methods based on four TA models were analyzed across different levels of route similarity.

Throughout this section, the following parameter settings were used unless otherwise specified. For the link travel time function, link flow capacity  $Q_a = 10$ ,  $\forall a \in A$ ; link FFTT

$x = 8, b = 20$ ; route choice parameters  $\theta = 1.0, \mu = 0.05$ ; travel demand for SUE with FD  $q = 15$ ; demand function maximum demand parameter  $\bar{q} = 2q$  and demand function scaling parameter  $\zeta = 0.05$ .

#### 4.5.1.1 Computation of LCI

This section calculated the MNL-SUE-based LCI and CNL-SUE-based LCI values for a fixed level of route similarity. The change in components of LCI was studied at iteration level. The results are summarized in Table 4.2 and Figure 4.12.

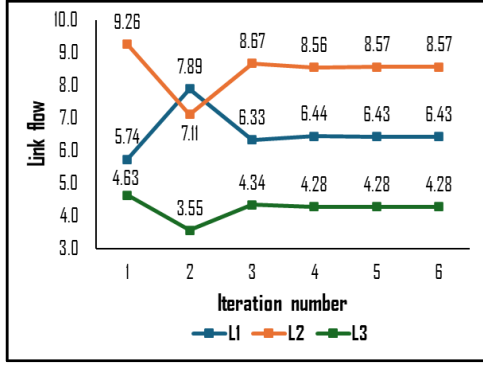
As shown in Table 4.2, the method ranked Link 2 as the highest followed by Link 1, Link 3 and Link 4 for all models. However, the LCI value of Link 2 was almost two times higher than that of Link 1 in the case of MNL-SUE framework, while these values were almost equal in the case of CNL-SUE. For both frameworks, models with ED slightly reduced the gap between the LCI values of Link 1 and Link 2.

Table 4.2. LCI values with and without considering route similarity.

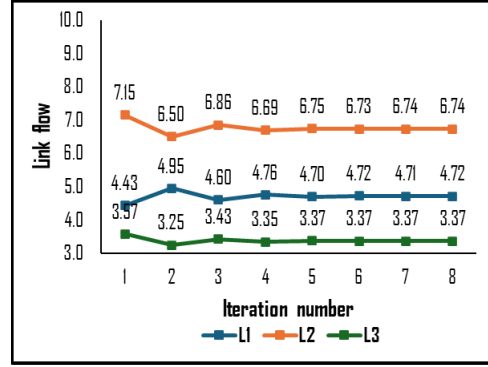
Link	MNL-SUE-based LCI						CNL-SUE-based LCI					
	Fixed demand			Elastic demand			Fixed demand			Elastic demand		
	LCI	$\bar{LCI}$	Rank	LCI	$\bar{LCI}$	Rank	LCI	$\bar{LCI}$	Rank	LCI	$\bar{LCI}$	Rank
1	2.82	0.24	2	2.73	0.19	2	1.95	0.27	2	2.06	0.25	2
2	5.47	0.46	1	6.14	0.43	1	2.11	0.3	1	2.25	0.27	1
3	1.78	0.15	3	2.69	0.19	3	1.53	0.22	3	2.02	0.24	3
4	1.78	0.15	3	2.69	0.19	3	1.53	0.22	3	2.02	0.24	3

In Figure 4.12, the components of the CNL-SUE-based LCI methods are elaborated on to demonstrate how consideration of route similarity issue formed the LCI values.

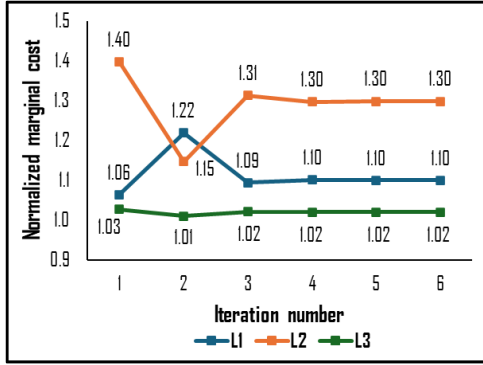
As shown in Figure 4.12, the components of the LCI method fluctuated most during the initial iterations, then gradually converged to specific values. The highest impact on LCI came from fluctuations in link flow and marginal cost. Generally, incorporating ED reduced the fluctuation of component values. These results were consistent with the findings reported in previous studies (Almotahari and Yazici, 2019) and Chapter 3.



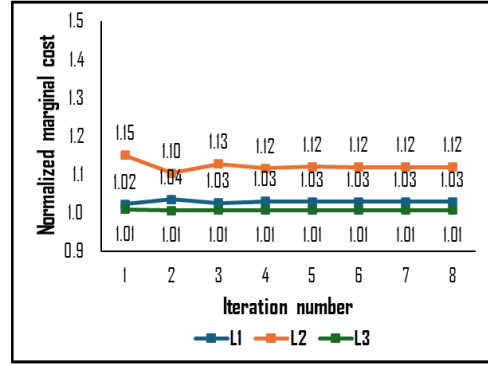
(a) Link flow fluctuations: CNL-SUE.



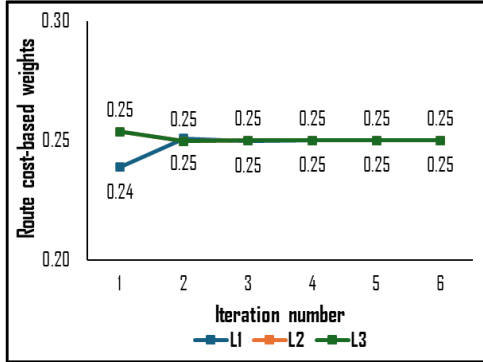
(b) Link flow fluctuations: CNL-SUE-ED.



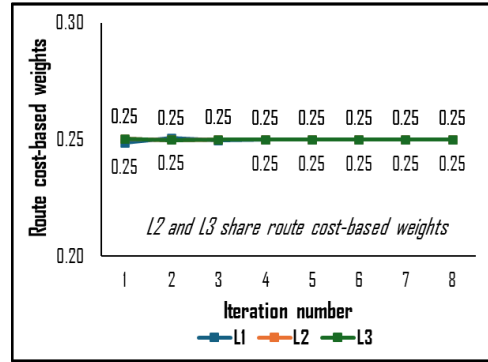
(c) Norm. marginal cost: CNL-SUE.



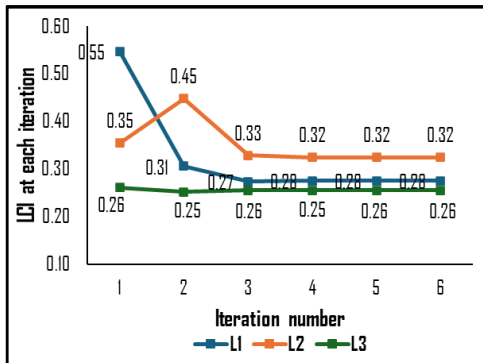
(d) Norm. marginal cost: CNL-SUE-ED.



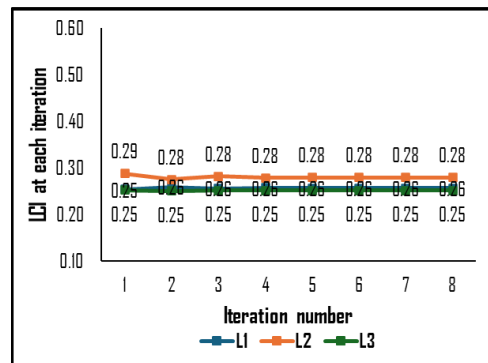
(e) Route-based weight: CNL-SUE.



(f) Route-based weight: CNL-SUE-ED.



(h) CNL-SUE-based LCI.



(j) CNL-SUE-ED-based LCI.

Figure 4.12. Intermediate values of components for two CNL-SUE-based LCI methods.

Following the logic in Figure 4.3, higher criticality rankings were expected for Link 1 and Link 2 than for Link 3 and Link 4. Given identical FFTT for all routes, lower rank for Link 1 than for Link 2 was also expected. As previously stated, not accounting for route similarity led to overestimating the criticality of shared links. To correct this, it was important to explicitly address the issue of route similarity.

#### ***4.5.1.2 Impact of route similarity on LCI***

This section examined the effect of route similarity on LCI by (i) changing the length of a shared link, (ii) changing the number of overlapping routes, and (iii) changing the length of non-overlapping routes. The results are summarized in Figure 4.13 to Figure 4.15.

##### *Changing route similarity via shared link*

In this section, the degree of route similarity in the loophole network was adjusted by changing the shared link's FFTT, as shown in Figure 4.6a. It is important to note that the network was designed so that all routes had equal FFTTs. Since L3 and L4 are identical, L3 was used to represent both links.

Figure 4.13 summarizes the LCI values based on the MNL-SUE and CNL-SUE models in response to these changes.

As shown in Figure 4.13, the LCI value for L2 strongly dominated over those of L1 and L3 in the MNL-SUE framework. At low FFTT values for L2, L1 and L3 had nearly identical LCI values. However, as the FFTT of L2 increased, the LCI value of L1 surpassed that of L3. The gap between the LCI values of L1 and L3 stopped growing after a certain FFTT value. Considering demand elasticity reduced the difference between the LCI values of L1 and L3, making L1 slightly more critical than L3 at higher FFTT values of L2.

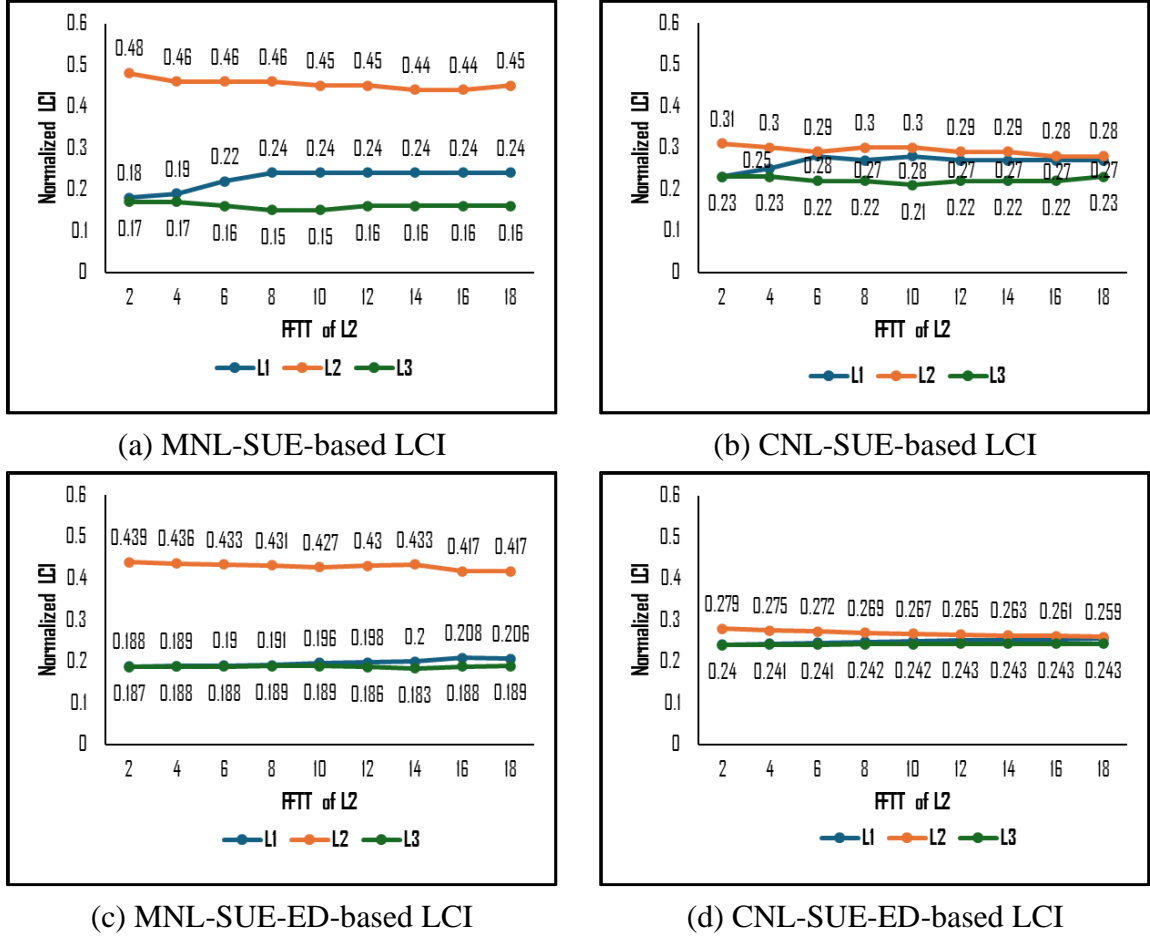
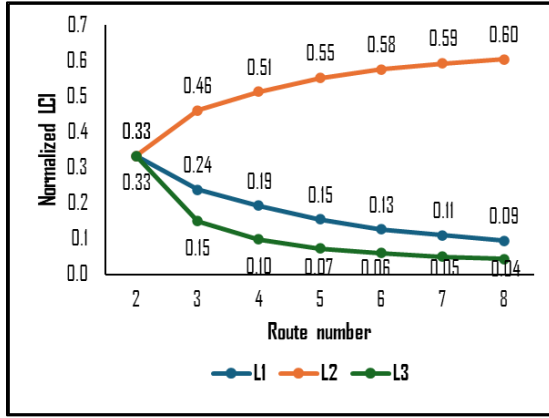


Figure 4.13. Impact of FFTT of shared link on four LCI methods.

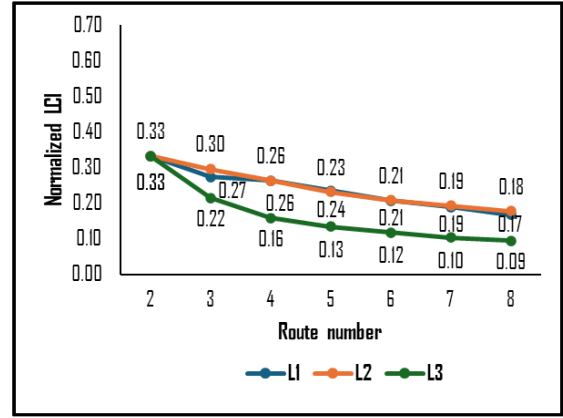
This pattern persisted in the CNL-SUE-based LCI, with the exception that the gap between L1 and L2 narrowed substantially. The LCI values of L1 and L2 were almost identical compared to the values of MNL-SUE-based LCI. Additionally, the difference between the LCI values of L1 and L3 was negligible in the ED case. These results indicate that not accounting for route similarity indeed overestimates the criticality of shared links.

#### *Changing route similarity via number of similar routes*

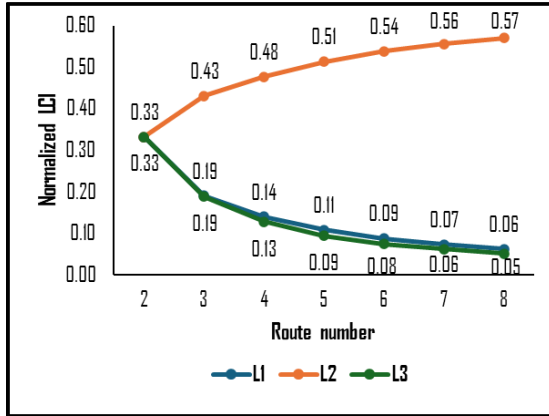
This section adjusted the route similarity in the loophole network by varying the number of overlapping routes, as shown in Figure 4.6b. All routes were designed to have equal FFTTs. Since L3 and L4 were identical, L3 was used to represent both links. Figure 4.14 summarizes the LCI values based on the MNL-SUE and CNL-SUE frameworks for these changes.



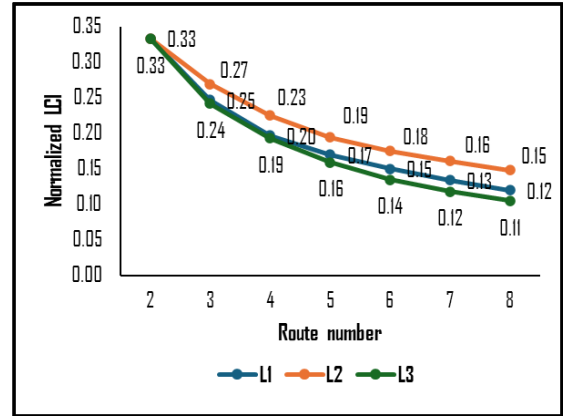
(a) MNL-SUE-based LCI



(b) CNL-SUE-based LCI



(c) MNL-SUE-ED-based LCI



(d) CNL-SUE-ED-based LCI

Figure 4.14. Impact of choice set size on four LCI methods.

As shown in Figure 4.14, the LCI values for L2 exhibited different trends with the increasing number of overlapping routes, depending on the SUE framework used. The LCI values increased under the MNL-SUE framework but decreased under the CNL-SUE framework. For L1 and L3, the LCI values decreased in both frameworks. These results indicate that the criticality of shared links might be overestimated if route similarity is not considered.

#### *Changing attractiveness of similar routes via FFTT of non-overlapping route*

This section investigated the impact of the length of non-overlapping routes on LCI using the loophole network (Figure 4.5). The assumption that all routes have equal FFTTs was

relaxed by varying the FFTT of the non-overlapping route. Figure 4.15 summarizes the LCI values based on the MNL-SUE and CNL-SUE frameworks for these changes.

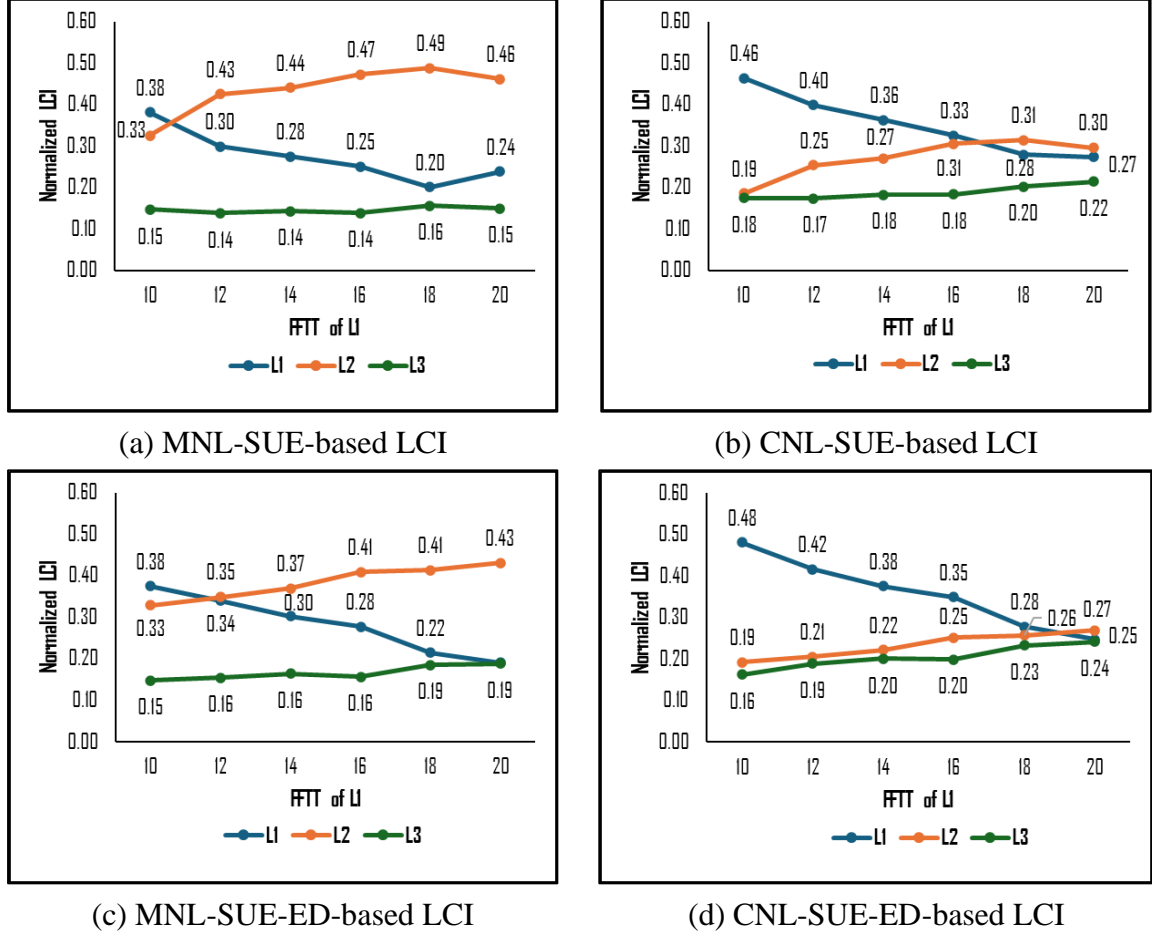


Figure 4.15. Impact of FFTT of non-overlapping route on four LCI methods.

As shown in Figure 4.15, increasing the FFTT of R1 (i.e., L1) decreased its attractiveness. At low FFTT values, L1 was ranked higher than L2, but as FFTT increased, its LCI values decreased, causing the ranks of L1 and L2 to swap. Interestingly, this swap occurred at different FFTT values in different frameworks. In the MNL-SUE framework, the swap happened much earlier than in the CNL-SUE framework. Since the length of route alternatives can vary in real networks, this highlights the importance of considering route similarity for a more realistic assessment of link criticality.

## 4.5.2 Experiment 2: Large-scale networks

In this section, the applicability of the advanced LCI methods to real-size scenario was illustrated. First, parameter settings were discussed. Next, the computational complexity of the method was analyzed. Finally, the method was applied to assess the criticality of bridges in the Winnipeg network.

Two benchmark real-size networks were considered: Winnipeg and Chicago Sketch<sup>4</sup>. Quantitative characteristics of these networks are provided in Figure 4.16. To ensure a fair comparison, fixed working route sets were used. The Winnipeg network's route set was generated by Bekhor et al. (2008), while the Chicago Sketch network's route set was created using a combination of the link elimination method (Azevedo et al., 1993) and the penalty method (De la Barra et al., 1993), which imposed a 5% travel time increase on the shortest route links.



Winnipeg			Chicago Sketch	
	154	Zone No.	387	
	1067	Node No.	933	
	2,535	Link No.	2,590	
	4,345	O-D No.	93,135	
	174,491	Route No.	836,346	
	1,523,688	Nest No.	4,891,295	

Figure 4.16. Two large-scale test networks and their characteristics.

### 4.5.2.1 Setting model parameters for real-size networks

This section sets plausible parameter values for route choice and travel demand models.

<sup>4</sup> The Winnipeg and Chicago Sketch networks were downloaded from <https://github.com/bstabler/TransportationNetworks>



#### 4.5.2.1.1 Parameter settings for route choice models

This section provides sensitivity analyses on the parameters of the selected route choice models. The parameters for the MNL route choice model has been discussed in Section 3.4.3.1.1. To set two parameters for the CNL model, the parameter  $\theta$  (route level parameter) was set using the procedure described in Section 3.4.3.1.1, assuming  $\mu$  (nest level parameter) is given. Subsequently, sensitivity analysis is conducted on  $\mu$ . Figure 4.17 summarizes the effect of route choice model parameters on the total coefficient of variation for the Winnipeg and Chicago Sketch networks. The parameters of the selected route choice models were set such that the mean coefficient of variation  $\overline{CV}$  remained within the range of 10% to 20%.

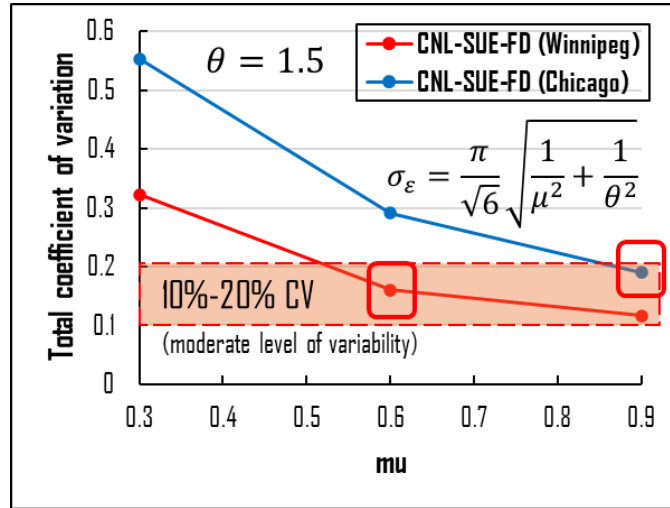


Figure 4.17. Effect of route choice model parameters on the total coefficient of variation for the Winnipeg and Chicago Sketch networks.

#### 4.5.2.1.2 Parameter settings for demand function

The demand function parameters were set in the same way as in Section 3.4.3.1.2. In summary, the parameter settings for the Winnipeg and Chicago Sketch networks are summarized in Table 4.3.

Table 4.3. Parameter settings for the Winnipeg and Chicago Sketch networks.

Model	Parameter	Winnipeg	Chicago Sketch
MNL	$\theta$	1.0	1.0
CNL	$\theta$	1.5	1.5
	$\mu$	0.6	0.9
Demand function (where $w \in W$ )	$\zeta$	0.1	0.1
	$\bar{q}^w$	$2.5 \cdot q^w$	$2.0 \cdot q^w$

#### 4.5.2.2 Computational complexity analysis

This section investigated computational complexity of MNL-SUE-based LCI and CNL-SUE-based LCI methods. The results are summarized in Figure 4.18 and Table 4.4.

To analyze the impact of network size on the computational time, we used two networks with different sizes: the Winnipeg network representing a relatively medium-scale network and the Chicago Sketch representing a large-scale network (Figure 4.16). The solution algorithm was implemented in Python 3.7.12. The numerical experiments were conducted on a Microsoft Windows 11 operating system with Intel(R) Core (TM) i7-9700 CPU @ 3.00GHz with 24 GB of RAM. The model parameters were set according to Table 4.3.

Figure 4.18 shows the convergence curves of the solution algorithm for MNL-SUE and CNL-SUE with both fixed and elastic demand. The LCI calculation took approximately three seconds per iteration for all models on the Winnipeg network and 11 seconds on the Chicago Sketch network. Figure 4.18 demonstrates that the solution algorithm converged in a reasonable time for all four models, highlighting the practical applicability of the LCI method when considering route similarity in real-size networks. With the increase of network size, the computational time increased in general. The algorithm converged substantially faster (more than 10 times) for the MNL-SUE models than for the CNL-SUE models, which was anticipated due to the CNL-SUE models having about five times more decision variables than the MNL-SUE models.

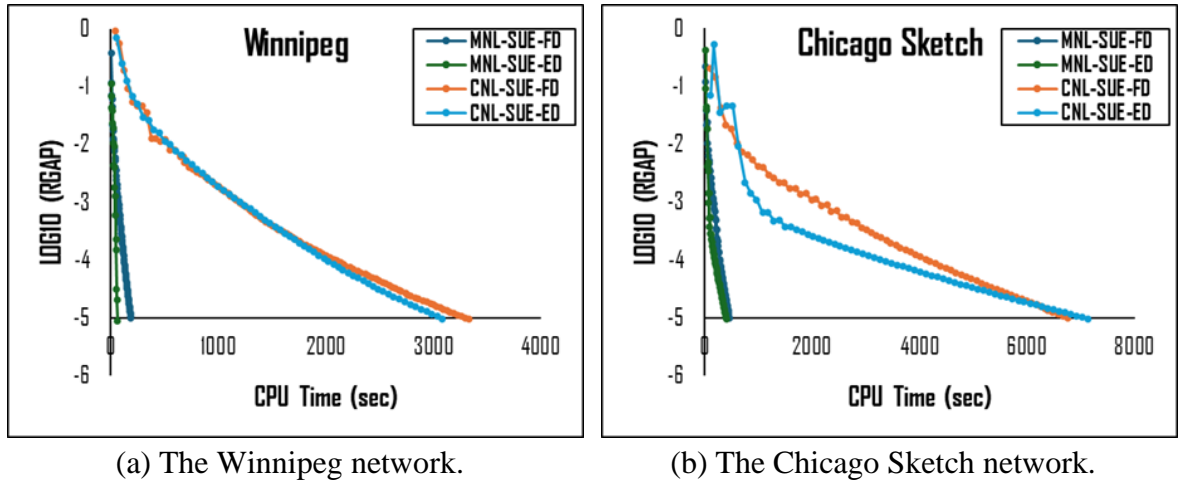


Figure 4.18. Computational time for assessing criticality of all links in the Winnipeg and Chicago Sketch networks.

Table 4.4 elaborates on computational complexity. Specifically, the two SUE-ED models demonstrated a lower total computational time than two SUE-FD in the Winnipeg network, likely due to a high fixed demand level necessitating more iterations for convergence despite its lower computational time per iteration. This is consistent with observations in the paired combinatorial weibit (PCW) SUE model with FD and ED by [Li et al. \(2024\)](#). Conversely, in the Chicago Sketch network, the FD model was computationally faster. This might be due to the ED model's higher number of O-D pairs, which could have increased the computational time needed to handle the additional variables. These contrasting outcomes underscore how computational efficiency may depend on network-specific demand level and problem dimensionality.

Table 4.4. Computational characteristics of four SUE models for two real-sized networks.

LCI's model	Winnipeg				Chicago Sketch			
	Var. No.	Iter. no.	Alg. iter. time (sec)	Total time (min)	Var. No.	Iter. no.	Alg. iter. time (sec)	Total time (min)
MNL-SUE	174,491	122	5	10	836,346	114	13	25
MNL-SUE-ED	178,836	72	5	6	929,481	132	15	33
CNL-SUE	1,698,179	126	75	158	5,727,641	167	172	479
CNL-SUE-ED	1,702,524	103	81	139	5,820,776	172	220	629

### 4.5.2.3 Ranking bridge criticality for Winnipeg network

In this section, the criticality of bridges in the Winnipeg network was assessed. Two rivers separate the network into three areas: Northwest (NW), East (E), and Southwest (SW). These areas are connected by bridges. Fifteen bridges were considered as shown in Figure 4.19. The results are summarized in Table 4.5 and Figure 4.20. For the sake of completeness, the LCI values for all bridges are provided in Table 4.6 and Table 4.7.

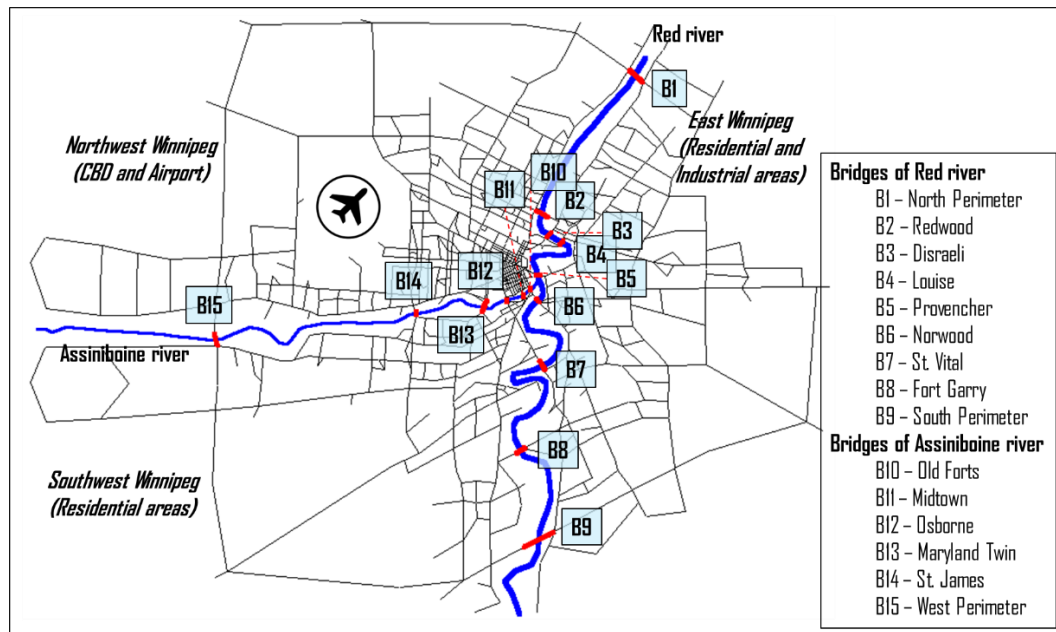


Figure 4.19. The Winnipeg network and selected bridges.

A key challenge in link criticality analysis for transport networks is the absence of ground-truth benchmarks, necessitating comparative analysis across metrics to evaluate ranking consistency. It is important to show that our approach yields rankings that differ meaningfully from conventional metrics in key respects while remaining broadly consistent with established criticality trends. Such comparisons are vital for demonstrating the robustness and reliability of proposed methods. Table 4.5 provides top 5 critical bridges according to four LCI methods. All methods consistently prioritize B12 (Osborne Bridge), B3 (Disraeli Bridge), and B11 (Midtown Bridge)—critical connectors to the central business

district (CBD) – underscoring their functional indispensability. Methodological distinctions emerge between MNL and CNL frameworks: CNL-SUE-FD-based LCI method incorporates B10 (Old Forts Bridge) into its rankings, a bridge absent in MNL-SUE-FD-based LCI method, attributable to the explicit incorporation of route similarity considerations within the CNL model. Similarly, contrasts between FD and ED models are evident: B5 (Provencher Bridge), ranked 4<sup>th</sup> under FD assumptions, is replaced by B6 (Norwood Bridge) in ED-based LCI methods, reflecting demand elasticity’s role in redistributing travel patterns under congestion-induced cost fluctuations. These variations highlight how nuanced modeling assumptions – route similarity in CNL and demand elasticity in ED – refine criticality assessments, offering complementary perspectives on network vulnerability. The findings underscore the necessity of integrating both factors for robust criticality analysis while affirming consensus on primary critical infrastructure. See Table 4.6 and Table 4.7 for the complete LCI values of all bridges for four LCI methods.

Table 4.5. Top 5 critical bridges according to LCI method.

Rank	MNL-SUE-FD	CNL-SUE-FD ( $\mu = 0.6$ )	MNL-SUE-ED	CNL-SUE-ED ( $\mu = 0.6$ )
1	B12	B11	B12	B12
2	B3	B12	B3	B11
3	B11	B3	B11	B3
4	B5	B5	B6	B6
5	B14	B10	B10	B10

The influence of route similarity and demand elasticity on bridge criticality is demonstrated through a sensitivity analysis of parameter  $\mu$ . This analysis compares MNL- and CNL-SUE-based LCI methods. The correlation strength was quantified using Pearson’s formula (4.14).

$$r_{X,Y}^{Pearson} = \frac{Cov(X,Y)}{\sqrt{Var(X)Var(Y)}} \quad (4.14)$$

where  $X$  and  $Y$  are LCI data sets. Correlation strength was categorized as: 0–0.19: Very weak; 0.2–0.39: Weak; 0.4–0.59: Moderate; 0.6–0.79: Strong; and 0.8–1: Very strong. The criticality values for each bridge, considering both directions, were aggregated into a single

measure. Correlations were then computed using absolute normalized LCI values. Results are shown in Figure 4.20.

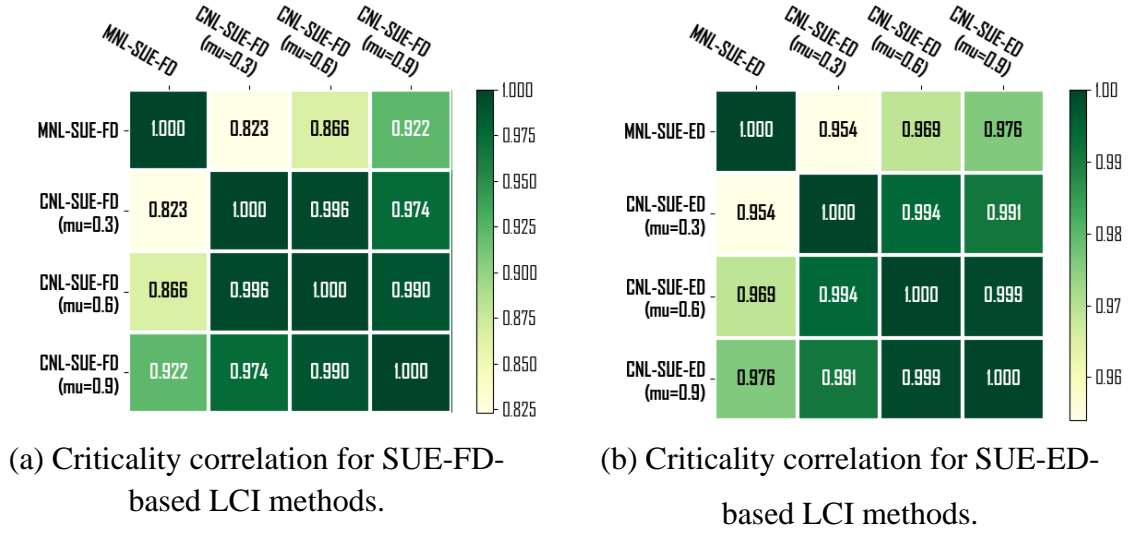


Figure 4.20. Correlation of bridge LCI values and ranks.

All four methods exhibited strong correlations, yet notable trends emerged. As shown in Figure 4.20, the correlation between MNL-SUE-FD and CNL-SUE-FD-based LCIs increased with  $\mu$ , reaching its lowest value at  $\mu = 0.3$  and peaking at  $\mu = 0.9$ . This aligns with the theoretical behavior of CNL-SUE: at low  $\mu$  (e.g.,  $\mu = 0.3$ ), route similarity strongly influences rankings, whereas at high  $\mu$  (e.g.,  $\mu = 0.9$ ), CNL-SUE converges toward MNL-SUE as route similarity effects diminish. A parallel trend occurred for ED models (Figure 4.20), though correlations were considerably higher. The ED model extension nearly eliminated distinctions between methods, likely due to demand reduction under congestion dampening network impacts—a pattern also observed in Section 4.5.1. These findings highlight how integrating route similarity and demand elasticity can refine criticality assessments.

Table 4.6. Bridge LCI based on two SUE models with FD for the Winnipeg network.

Bridge name	Bridge ID	Dir.	MNL-SUE-FD	CNL-SUE-FD ( $\mu = 0.3$ )	CNL-SUE-FD ( $\mu = 0.6$ )	CNL-SUE-FD ( $\mu = 0.9$ )
North Perimeter	B1	EB	6.9E-05	9.5E-05	9.2E-05	9.0E-05
		WB	1.9E-03	9.9E-04	1.1E-03	1.2E-03
Redwood	B2	EB	8.8E-05	2.0E-04	1.9E-04	1.8E-04
		WB	4.4E-04	4.2E-04	4.2E-04	4.3E-04
Disraeli	B3	EB	9.0E-05	1.7E-04	1.5E-04	1.4E-04
		WB	6.9E-03	4.2E-03	4.4E-03	4.7E-03
Louise	B4	EB	1.8E-04	2.2E-04	2.1E-04	2.0E-04
		WB	3.0E-03	1.3E-03	1.3E-03	1.4E-03
Provencher	B5	EB	1.3E-04	1.4E-04	1.4E-04	1.3E-04
		WB	4.9E-03	3.5E-03	3.6E-03	3.7E-03
Norwood	B6	EB	2.1E-04	2.4E-04	2.4E-04	2.4E-04
		WB	1.1E-03	2.6E-03	2.4E-03	1.9E-03
St. Vital	B7	WB	1.5E-03	7.3E-04	8.2E-04	9.1E-04
		EB	3.5E-04	3.2E-04	3.1E-04	3.2E-04
Fort Garry	B8	EB	7.5E-05	8.1E-05	7.2E-05	6.5E-05
		WB	1.5E-03	1.0E-03	1.0E-03	1.1E-03
South Perimeter	B9	EB	5.0E-05	9.8E-05	8.8E-05	8.1E-05
		WB	1.1E-04	1.0E-04	1.0E-04	1.0E-04
Old Forts	B10	NB	1.0E-03	3.1E-03	2.8E-03	2.4E-03
		SB	4.8E-04	4.2E-04	4.4E-04	4.6E-04
Midtown	B11	NB	5.2E-03	5.1E-03	4.9E-03	4.8E-03
		SB	2.5E-04	1.1E-04	1.3E-04	1.7E-04
Osborne	B12	NB	7.0E-03	4.0E-03	4.3E-03	4.9E-03
		SB	3.9E-04	3.9E-04	3.6E-04	3.5E-04
Maryland Twin	B13	NB	2.3E-03	2.1E-03	2.2E-03	2.3E-03
		SB	2.4E-04	3.1E-04	3.0E-04	2.9E-04
St. James	B14	NB	3.1E-03	1.9E-03	1.9E-03	1.9E-03
		SB	1.2E-03	5.8E-04	5.8E-04	6.4E-04
West Perimeter	B15	NB	9.8E-05	9.3E-05	8.4E-05	7.7E-05
		SB	7.0E-04	3.6E-04	4.1E-04	4.7E-04

Table 4.7. Bridge LCI based on two SUE models with ED for the Winnipeg network.

Bridge name	Bridge ID	Direction	MNL-SUE-ED	CNL-SUE-ED ( $\mu = 0.3$ )	CNL-SUE-ED ( $\mu = 0.6$ )	CNL-SUE-ED ( $\mu = 0.9$ )
North Perimeter	B1	EB	3.0E-05	3.1E-05	6.8E-05	4.2E-05
		WB	4.7E-04	2.8E-04	1.1E-03	3.6E-04
Redwood	B2	EB	8.2E-05	7.3E-05	2.1E-04	9.8E-05
		WB	2.5E-04	1.1E-04	7.8E-04	1.7E-04
Disraeli	B3	EB	4.0E-05	5.5E-05	1.7E-04	7.0E-05
		WB	9.5E-03	6.7E-03	5.2E-03	6.9E-03
Louise	B4	EB	4.8E-05	6.1E-05	1.8E-04	6.9E-05
		WB	2.5E-03	1.7E-03	1.4E-03	1.7E-03
Provencher	B5	EB	9.7E-05	6.6E-05	1.5E-04	8.8E-05
		WB	2.1E-03	2.0E-03	5.6E-03	1.9E-03
Norwood	B6	EB	3.2E-04	2.7E-04	2.2E-04	3.2E-04
		WB	4.8E-03	2.3E-03	4.0E-03	3.1E-03
St. Vital	B7	WB	4.1E-03	2.0E-03	5.9E-04	2.7E-03
		EB	2.1E-04	1.1E-04	3.4E-04	1.7E-04
Fort Garry	B8	EB	4.2E-05	4.2E-05	7.4E-05	5.8E-05
		WB	3.7E-04	3.8E-04	9.0E-04	4.5E-04
South Perimeter	B9	EB	2.3E-05	5.0E-05	8.0E-05	6.7E-05
		WB	3.7E-05	4.1E-05	8.2E-05	5.7E-05
Old Forts	B10	NB	4.3E-03	2.1E-03	4.4E-03	3.0E-03
		SB	3.7E-04	4.6E-04	3.4E-04	4.5E-04
Midtown	B11	NB	7.1E-03	5.7E-03	2.1E-03	7.2E-03
		SB	2.1E-04	2.6E-04	1.9E-04	2.4E-04
Osborne	B12	NB	2.6E-02	1.1E-02	6.0E-03	1.5E-02
		SB	2.2E-04	2.0E-04	4.3E-04	1.9E-04
Maryland Twin	B13	NB	1.7E-03	1.1E-03	2.8E-03	1.5E-03
		SB	1.2E-04	1.0E-04	2.9E-04	1.5E-04
St. James	B14	NB	2.6E-03	8.5E-04	4.8E-03	1.3E-03
		SB	1.3E-04	6.5E-05	3.0E-04	1.1E-04
West Perimeter	B15	NB	3.5E-05	3.1E-05	1.0E-04	4.1E-05
		SB	8.5E-05	6.8E-05	6.6E-04	9.3E-05

## 4.6 Chapter summary

This chapter investigated the impact of route similarity on link criticality analysis. It used LCI as a method for the analysis and advanced it by employing a CNL route choice model and a SUE TA model with ED that could account for route similarities. Sensitivity analysis was conducted using a toy network to explore the method's properties, while real-size networks were used to examine computational complexity. The method showed reasonable computational time for large-scale networks, highlighting its potential as a policy tool for informed decision-making. To validate the concept, the advanced LCI method was applied to assess the criticality of links in the Winnipeg network. The results indicate that ignoring route similarity leads to overestimating the criticality of shared links and that incorporating route similarity into LCI may substantially alter the criticality ranking of links assigning shared links lower criticalities.

This chapter concludes Part I of the thesis. Part II focuses on developing a methodology for link criticality analysis that highlights bridges as critical elements of transportation infrastructure, recognizing their greater impact on route choices compared to ordinary road segments.



## **PART II**

# **Advancing link criticality analysis: Bridge-centric transport networks**

---

Part I advanced link criticality analysis using network models that did not distinguish bridges from ordinary road segments. This oversight neglects the essential role bridges may play in bridge-centric transport networks. Bridge-centric transport networks are road networks divided by obstacles such as rivers and valleys, with the divided parts of the networks connected by bridges. The mathematical models for these networks distinguish bridges from ordinary road segments. Part II develops a bridge-centric network equilibrium framework, including a new joint bridge-route choice model, a network equilibrium traffic assignment (TA) model, and a customized route-based solution algorithm. It also integrates this framework into a selected link criticality method and applies it to bridge criticality analysis in a large-scale bridge-centric transport network.

# CHAPTER 5

## Bridges matter: Modeling joint bridge and route choice equilibrium with bridge-centric choice set generation

---

This chapter develops a bridge-centric network equilibrium framework, including a new joint bridge-route choice model, a network equilibrium traffic assignment (TA) model, and a customized route-based solution algorithm, which consists of a bridge-centric choice set generation method and a route equilibration method.

### 5.1 Motivation

The fundamental aim of network equilibrium TA is to obtain traffic flow patterns given the origin-destination (O-D) matrix, network topology, travelers' route choice behavioral assumptions, and flow-dependent travel cost functions (Sheffi, 1985). Network equilibrium TA models typically address all links as homogeneous network components. However, when considering networks divided by natural obstacles and connected by bridges, the route choice behavior can change greatly (Alizadeh et al., 2018, Lee et al., 2017, Manley et al., 2015). Bridges act as traffic bottlenecks that can disproportionately affect travel costs (Alizadeh et al., 2018, Bucskey and Juhász, 2022, Capacci et al., 2022). Given these considerations, it appears reasonable to suggest that bridges, constituting a substantial portion of a route's travel cost and greatly influencing the set of selectable routes, should be viewed as unique network components that influence route choice more than ordinary links. This leads us to the following research questions: *What is the impact of bridges on travelers' behavior?*

*Specifically, how do bridges affect route choice in congested bridge networks? Can these impacts be adequately captured in existing network equilibrium models?*

The real-world evidence supporting the hypothesis that bridge choice is distinct from route choice is provided in [Manley et al. \(2015\)](#), [Habib et al. \(2013\)](#), and [Alizadeh et al. \(2018\)](#). [Manley et al. \(2015\)](#) observed that taxi drivers' route choices in London were influenced by anchor points, including bridges. [Habib et al. \(2013\)](#) and [Alizadeh et al. \(2018\)](#) reported that hierarchical bridge-route choice models could better represent the route choice behavior in Montreal, Canada. Although the existing empirical results have shown several behavioral issues need to (or can) be incorporated to enhance the modeling of bridge and route choice, these issues are based on discrete choice modeling and cannot endogenously consider the congestion effect, which is a critical factor for modeling traffic bottlenecks like bridges.

Bridge-centric transport networks are common in practice. Figure 5.1 provides a well-known real-world network – the Winnipeg network<sup>5</sup>. This network has been used for testing different equilibrium TA models ([Bekhor et al., 2008](#)) and methods for bridge importance assessment ([Jansuwan and Chen, 2015](#)). As shown in Figure 5.1, two rivers separate the network into three regions: Northwest (NW), East (E), and Southwest (SW). These regions are connected via 15 bi-directional bridges. The network contains 4345 O-D pairs, among which about 60% of O-D pairs are mixed-region (i.e., origin and destination zones belong to different regions). Using bridges is unavoidable for these O-D pairs. Additionally, regions are connected by multiple bridges. For example, the NW region is connected to the SW region by six bridges, while NW and E by five bridges. In general, there are a finite number of feasible bridge combinations. However, not all combinations are perceived as equally available in terms of travel cost and distance. On the one hand, since bridges often tend to

---

<sup>5</sup> INRO, 1999. Emme/2 User's Manual: Release 9.2, Montreal.

become traffic bottlenecks and sources of recurrent congestion, travelers try to avoid using them to reduce travel costs. If unavoidable, they attempt to select routes with fewer bridges. On the other hand, to bypass congestion, travelers sometimes opt to take a detour to a bridge that is not too far away. Therefore, it is reasonable to suggest that travelers may separately make the bridge selection in addition to the choice behavior modeled in the traditional route selection problem.

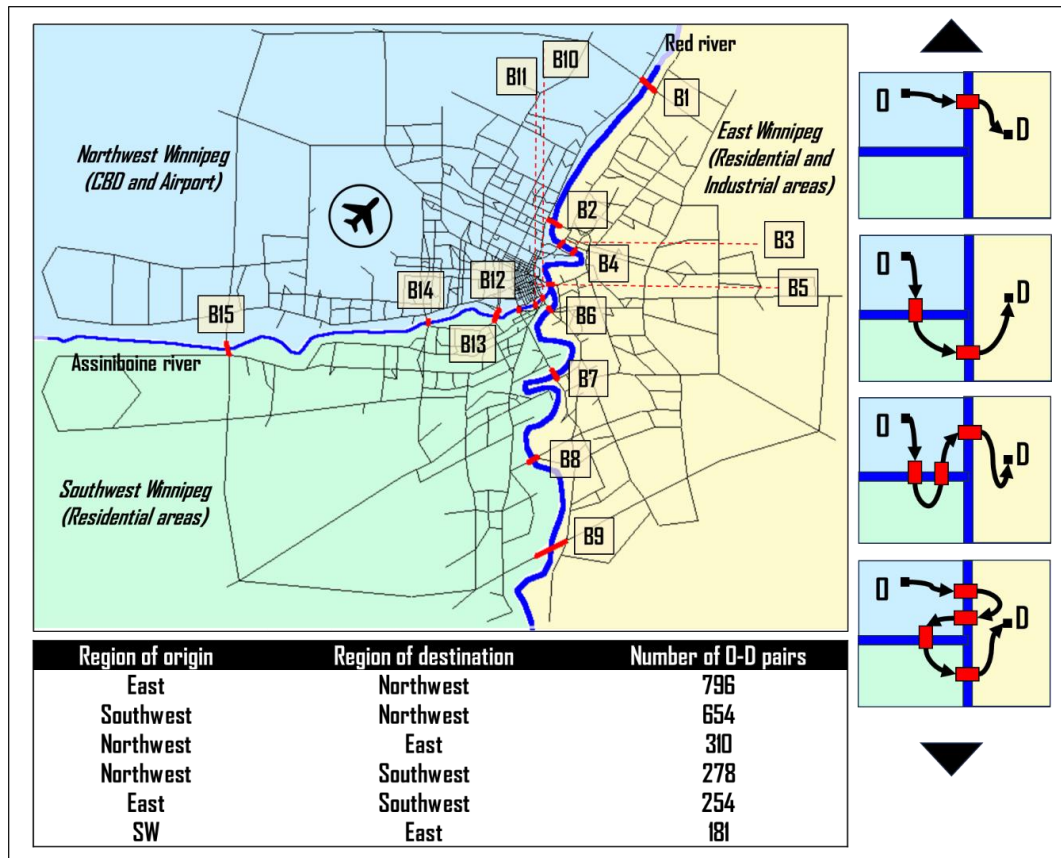


Figure 5.1. Bridge choice alternatives for the Winnipeg network.

To reproduce traffic flow patterns in networks such as the Winnipeg network, it may be necessary to develop a comprehensive equilibrium TA model, and a choice set generation technique consistent with the bridge-centric paradigm. A ‘bridge-centric’ paradigm refers to a methodology that places bridges as the central element in route choice modeling and choice set generation in the networks where bridges are a significant factor. It can be particularly

useful in regions with many waterways or valleys, where bridges are a critical part of the transport infrastructure.

Addressing the joint bridge-route choice problem presents a formidable challenge due to the intricate interdependencies between bridges and routes. The decision-making process is not linear; it requires simultaneous consideration of both elements. Distinguishing between available and unavailable bridges is a complex task, as the viability of a bridge can be contingent upon the costs associated with the routes leading to it. Furthermore, the choice of a route is inherently dependent on the set of bridges perceived to be available, creating a conditional relationship that complicates the planning process. The complexity is further compounded when multiple bridges are involved in routes, leading to a combinatorial explosion in the number of potential bridge choice sets that must be evaluated. Therefore, this problem is especially challenging, and it requires sophisticated analytical tools. This study aims to address these challenges.

The objectives and contributions of this chapter can be summarized as follows:

- ***To develop a hierarchical model for a joint bridge-route choice problem and an equilibrium TA model.*** Without loss of generality, bridge and route choices are modeled in a nested structure. The availability perception concept ([Cascetta and Papola, 2001](#)) is customized to address bridge choice behavior and bridge choice set formation problems. Additionally, the stochastic user equilibrium (SUE) TA model, which is consistent with the joint bridge-route choice model, was developed while considering congestion effects. It was formulated as an equivalent mathematical programming (MP) problem, which guaranteed the existence and uniqueness of solutions.
- ***To propose bridge-centric bridge-route choice set generation.*** A bridge-centric choice set generation strategy that leveraged the inherent properties of both bridges and routes is proposed. Initially, bridge choice alternatives are enumerated and then truncated based

on the perceived availability criterion for each bridge choice alternative. Subsequently, a route choice set is generated conditioned on the bridge choice set, applying a multi-stage column generation algorithm iteratively.

- *To demonstrate model’s properties and its applicability to a real-world setting.* The properties of the developed and existing models using both toy and large-scale networks are compared. It is shown that the method can converge in a reasonable time in a large-scale network scenario.

While prior research acknowledges bridges as critical infrastructure or contextual factors in route choice, our study advances policy relevance by quantifying how travelers perceive bridges as cognitive landmarks—hierarchically shaping their route decisions—and how these perceptions propagate into network-wide traffic patterns under equilibrium. Unlike past studies that focus just on how bridges influence individual route choices, our model connects traveler behavior — like avoiding bridges or choosing routes based on them — to traffic patterns across the entire network with congestion consideration. This can potentially allow policymakers to predict how actions targeting bridges (e.g., tolls, closures, upgrades) shift congestion throughout the system.

The remainder of this chapter is organized as follows. Section 5.2 introduces the concept of bridge availability perception, bridge-route choice model, equivalent MP formulation, and solution algorithm. Sections 5.3 and 5.4 present the numerical results and concluding remarks, respectively.

## **5.2 Modeling joint bridge-route choice equilibrium with bridge-centric choice set generation**

An obstacle such as a river breaks a space into two parts. These parts are connected by bridges. From the behavior point of view, travelers may try to avoid bridges because they are

traffic bottlenecks and often become a source of recurrent congestion. For some O-D pairs, using bridges is unavoidable; for others, using bridges is optional. In the latter case, travelers opt for using bridges if they offer better in terms of distance choice alternatives than other alternatives. Therefore, travelers may prefer not only shortest routes, but also routes without bridges or routes with the least number of bridges.

Adaptation of the implicit availability perception logit (IAPL) model (Cascetta and Papola, 2001) to bridge choice problem is explained in Section 5.2.1. A joint bridge-route choice model is introduced in Section 5.2.2. Section 5.2.3 develops an equilibrium TA model, formulated as an equivalent MP problem.

For a better presentation, the notation used in this study is summarized in Table 5.1.

Table 5.1. Notation.

<i>Sets</i>	
$A$	Set of all links.
$CA$	Set of common links, where $CA \subset A$ .
$BA$	Set of bridge links, where $BA = A \setminus CA$ .
$\mathcal{W}$	Set of all O-D pairs
$C\mathcal{W}$	Set of common O-D pairs that do not need bridges, where $C\mathcal{W} \subset A$ .
$B\mathcal{W}$	Set of O-D pairs that need bridges, where $B\mathcal{W} = \mathcal{W} \setminus C\mathcal{W}$ .
$B$	Set of bridge choice alternatives, where each alternative may include multiple bridges.
$B^w$	Subset of bridge choice alternatives for O-D pair $w$ .
$K^w$	Set of routes between O-D pair $w$ .
$K_b^w$	Set of routes between O-D pair $w$ that passes through bridge choice alternative $b$ .
<i>Inputs and parameters</i>	
$x_a$	Traffic flow on link $a$ .
$ct_a$	Travel time on a common link $a$ .
$bt_a$	Travel time on a bridge link $a$ .
$\delta_{a,k}^w$	Link-route incidence parameter indicating whether link $a$ is on route $k$ between O-D pair $w$ .
$c_k^w$	Generalized travel time of route $k$ between O-D pair $w$ .
$C_k^w$	Travel disutility of route $k$ between O-D pair $w$ .
$\theta$	Scaling parameter at the route choice level.
$\eta$	Scaling parameter at the bridge choice level.
$\bar{\mu}_b$	Expected value of availability perception of bridge nest $b$ .
$P_b^w$	Probability of choosing bridge nest $b$ between O-D pair $w$ .
$P_{k b}^w$	Conditional probability of choosing route $k$ between O-D pair $w$ given bridge nest $b$ .
$P_k^w$	Probability of choosing route $k$ using bridge nest $b$ between O-D pair $w$ .
$q^w$	Travel demand between O-D pair $w$ .
<i>Decision variables</i>	
$f_k^w$	Traffic flow on route $k$ between O-D pair $w$ .
$q_b^w$	Traffic flow through bridge nest $b$ between O-D pair $w$ .

## 5.2.1 Modeling bridge choice alternatives

This section introduces the concept of bridge choice alternative and models their perceived availability for travelers. For convenience, we exclude the superscript notation indicating the O-D pair.

### 5.2.1.1 *Bridge choice alternatives and their viability*

This section introduces the concept of bridge choice alternatives. First, three real-world example networks, where joint bridge-route choice issues may be observed, are discussed to set the context and motivate the modeling decisions. Second, an explicit definition of bridge choice alternatives is provided.

Figure 5.2 depicts a map of Wuhan, China. The city is spanned by the Yangtze River and connected by over a dozen bridges. For some O-D pairs, using these bridges is unavoidable. To be connected, the routes of these O-D pairs must cross at least one bridge. This divides the routes into three segments: origin to bridge, bridge, and bridge to destination. Segment lengths may vary, with bridges potentially near or far from origins and destinations. Depending on the distance of a bridge from the origin or destination, it may be considered viable (black solid line, Figure 5.2) or non-viable (red dashed line, Figure 5.2) for a particular O-D pair. In other words, there might be many feasible bridge alternatives for an O-D pair, but not all may be viable. If a bridge is too far, travelers may not consider it because they may perceive it as unavailable.



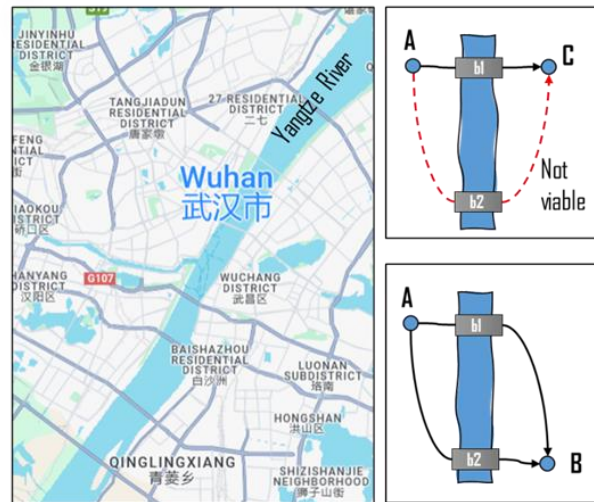
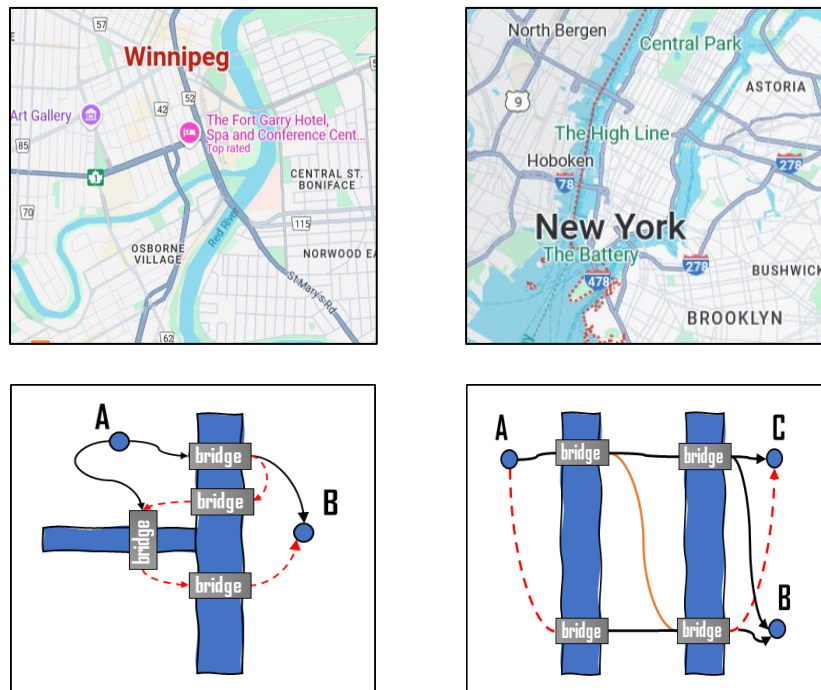


Figure 5.2. Wuhan, China and some most frequent bridge choice alternatives.

Figure 5.3 provides two more real-world examples: Winnipeg, Canada, and New York, US. These cities have more complex combinations of rivers and bridges compared to Wuhan.



a) Two-intersecting-river scenario: Multiple bridges per bridge choice alternative.

b) Two-parallel-river scenario: At least two bridges per bridge choice alternative.

Figure 5.3. Bridge choice alternatives in Winnipeg, Canada, and New York, US.

Winnipeg has two intersecting rivers (Figure 5.3a), while New York has two parallel rivers (Figure 5.3b). In Winnipeg, crossing multiple bridges may offer more efficient connections, especially near the confluence of the rivers. In New York, crossing at least two bridges is unavoidable for trips from opposite sides. This complexity necessitates considering bridge combinations rather than single bridges as potential choice alternatives. In this case, bridges should be considered in strict order because a bridge may require another bridge to be accessible as shown in Figure 5.3b. Bridge sequences result in  $2n + 1$  route segments where  $n$  is the number of bridges in the bridge combination. It necessitates consideration of inter-bridge route segments when evaluating viability of a bridge combination for travelers.

Additionally, if bridges are aimed at facilitating inter-region communication (i.e., between different regions) rather than intra-region (i.e., within a single region), then, due to their limited number, bridges may cause congestion, leading travelers to avoid them unless they offer outstanding travel cost benefits. Therefore, travel demand from intra-region O-D pairs using bridges can be negligibly low.

Based on the discussion above, a bridge choice alternative refers to a specific sequence of bridges that an origin-destination (O-D) pair can use to traverse rivers. This sequence is defined by three main factors: the proximity of the first bridge to the origin, the proximity of the last bridge to the destination, and the distances between bridges in multi-bridge sequences. The viability of a bridge choice alternative depends on the cumulative detour lengths resulting from these spatial relationships and the number of bridges in the sequence. Even if a bridge choice alternative is physically feasible, it may be deemed non-viable if its bridges are too far from the O-D points, if the distances between bridges lead to impractical travel costs, or if the bridge sequence is too long.

Next section models viability of bridge choice alternatives through availability perception concept.

### 5.2.1.2 Availability perception attribute<sup>6</sup>

This section models viability of bridge choice alternatives by means of the concept of availability perception (Cascetta and Papola, 2001). Viable alternatives are close to both origin and destination (black solid line, Figure 5.2), while non-viable ones are far from both (red dashed line, Figure 5.2). If no other alternatives exist, a bridge choice alternative is viable even if the distance is long. In other words, alternatives are non-viable if there are less distant options exist.

Conceptually, travelers' perception of the availability of a bridge choice alternative is influenced by travel distance and the number of bridges in its sequence. Longer distances increase travel costs, making bridge choice alternatives with distant bridges less appealing. Additionally, longer sequences of bridges increase route complexity. In summary, long route segments and bridge sequences with high number of bridges should be penalized. This implies that bridge choice alternatives closer to the origin and destination, with shorter route segments and fewer bridges, are perceived as more available.

To achieve this, the availability perception attribute is calculated in three steps. Firstly, route segments are categorized into two types: *bridge segments* and *non-bridge segments*. For convenience, the lengths of route segments in each category are categorized so that each category can be represented by a scalar. The former type (i.e., *bridge segments*) is labeled as  $i = 1$ , and the latter type is labeled as  $i = 2$ . The aggregated length of route segment of type  $i$  for bridge choice alternative  $b$ , denoted as  $rs_{ib}$ , is calculated as follows:

$$rs_{ib} = \begin{cases} l_b, & \text{if } i = 1 \\ \frac{1}{|b| + 1} (L_{\bar{k}b} - l_b), & \text{if } i = 2 \end{cases} \quad (5.1)$$

---

<sup>6</sup> The proposed attribute has been designed by connecting and extrapolating theoretical insights on route choice set formation and route choice (Cascetta and Papola, 2001; Prashker and Bekhor, 2004; Bovy, 2009) as well as empirical insights on bridge and route choice (Habib et al., 2013; Manley et al., 2015; Alizadeh et al., 2018).

where  $L_{\bar{k}b}$  is the FFTT of the shortest route  $\bar{k}$  for bridge choice alternative  $b$ ,  $l_b$  is the sum of FFTT of bridges in  $b$ , and  $|b|$  is the number of bridges in bridge choice alternative  $b$ . Essentially,  $rs_{1b}$  equals the total FFTT of all bridges, and  $rs_{2b}$  equals the average FFTT of all non-bridge route segments of the shortest route  $\bar{k}$ .

Secondly, the representative length of route segments for bridge choice alternative  $b$  is determined as follows:

$$L_b = \max\{rs_{1b}, rs_{2b}\} \cdot (|b| + 1)^\alpha, \quad \forall b \in B \quad (5.2)$$

where  $B$  is set of all bridge choice alternatives for an O-D pair and  $\alpha \geq 0$  is a parameter to calibrate. Essentially,  $\alpha$  controls the sensitivity of the attribute to the number of bridges in a bridge choice alternative. A high  $\alpha$  results in a high sensitivity to long bridge sequences, and a low  $\alpha$  results in lower sensitivity. At its extreme,  $\alpha = 0$ , the bridge sequence length is not penalized.

Finally, to ensure that the availability perception attribute  $Y_b$  spans from  $-\infty$  to  $+\infty$ , we centered it with respect to its mean:

$$Y_b = L_b - \bar{L}, \quad \forall b \in B \quad (5.3)$$

where  $\bar{L}$  is the mean of  $L_b$  for all bridge choice alternatives  $b$  of an O-D pair.

Next, we discuss availability perception function ([Cascetta and Papola, 2001](#)).

### 5.2.1.3 Availability perception value

Availability perception value for bridge choice alternative  $b$  is denoted as  $\mu_b$ . Availability perception value can be interpreted as a probability of bridge choice alternative  $b$  being perceived as available. Its feasible region is an interval from 0 to 1, where the values close to zero (i.e.,  $\mu_b \rightarrow 0$ ) can be interpreted as alternative  $b$  being fully unavailable and the values close to one (i.e.,  $\mu_b \rightarrow 1$ ) as fully available. The natural logarithm over availability perception value (i.e.,  $\ln \mu_b$ ) may range from 0 to  $-\infty$ . If a bridge choice alternative  $b$  is

perceived as fully available (i.e.,  $\mu_b \rightarrow 1$ ) then its natural logarithm tends to zero,  $\ln \mu_b \rightarrow 0$ . In other cases, it is a negative non-zero value.

The term  $\ln \mu_b$  is interpreted as availability perception function. It shows that alternative  $b$  is theoretically available but not completely perceived as such. Because the true value of the availability and perception level  $\mu_b$  is unknown to the analyst, it is modeled as a random variable with expected value  $\bar{\mu}_b$ . If  $\mu_b$  is a random variable, so is  $\ln \mu_b$ . A random variable can be expressed as the sum of its mean value and a random residual:

$$\ln \mu_b = E[\ln \mu_b] + \xi_b, \quad \forall b \in B \quad (5.4)$$

To make the model operational, the term  $E[\ln \mu_b]$  is expressed in terms of  $\bar{\mu}_b$  by means of second-order Taylor's series expansion around the point  $\bar{\mu}_b$ :

$$\ln \mu_b = \ln \bar{\mu}_b + \frac{1}{\bar{\mu}_b} (\mu_b - \bar{\mu}_b) - \frac{1}{2[\bar{\mu}_b]^2} (\mu_b - \bar{\mu}_b)^2 + o(3) \quad (5.5)$$

and consequently:

$$\begin{aligned} E[\ln \mu_b] &\cong E[\ln \bar{\mu}_b] + E\left[\frac{1}{\bar{\mu}_b} (\mu_b - \bar{\mu}_b)\right] - E\left[\frac{1}{2[\bar{\mu}_b]^2} (\mu_b - \bar{\mu}_b)^2\right] \\ &= \ln \bar{\mu}_b - \frac{1}{2[\bar{\mu}_b]^2} Var(\mu_b) \end{aligned} \quad (5.6)$$

In general,  $Var(\mu_b)$  is unknown but can be substituted by its upper bound given by the variance of a Bernoulli variable with the same mean  $\bar{\mu}_b$ :

$$Var(\mu_b) \leq \bar{\mu}_b [1 - \bar{\mu}_b] \quad (5.7)$$

This gives us the following expression:

$$E[\ln \mu_b] \cong \ln \bar{\mu}_b - \frac{1 - \bar{\mu}_b}{2\bar{\mu}_b}, \quad \forall b \in B \quad (5.8)$$

The expected availability perception  $\bar{\mu}_b$  is specified using a binomial logit model, following the methodologies like in [Swait and Ben-Akiva \(1987\)](#) and [Ben-Akiva and Boccara \(1995\)](#):

$$\bar{\mu}_b = \frac{1}{1 + e^{\beta Y_b}}, \quad \forall b \in B \quad (5.9)$$

where  $Y_b$  is availability perception attribute of bridge choice alternative  $b$  and  $\beta$  is a corresponding scaling parameter.

In this study, the availability perception value serves two distinct objectives. Firstly, it is used for truncation of unreasonably distant bridge choice alternatives. Secondly, it is used for modeling intermediate degrees of availability of bridge choice alternatives that tackles the potential issue of bridge choice set misspecification.

#### ***5.2.1.4 Illustrative example for calculating availability perception***

This section illustrates how to calculate availability perception using six routes (Figure 5.4). Each route has its own composition of bridges, which form bridge choice alternative (i.e., there are six bridge choice alternatives). For simplicity, it is assumed that all short non-bridge route segments were length 2, all long non-bridge route segments were length 5, and all bridge segments of length 1. According to the mechanics described in Section 5.2.1.1 and Section 5.2.1.2, the highest availability perception value is assigned to bridge choice alternative  $b_1$  because it has the shortest route segments and the least number of bridges among six alternatives. Then,  $b_2, b_3, b_4$  are assigned lower values to because the first two have longer route segments than  $b_1$ ,  $b_4$  has two bridges while  $b_1$  had one. For the same reasons, low availability perception is assigned to  $b_5$  and  $b_6$ .



For the results summarized in Table 5.2, the scaling parameter  $\beta$  was set to 0.05. In Figure 5.5, the impact of the scaling parameter  $\beta$  on the availability perception of bridge choice alternatives  $b_1$  and  $b_6$  is analyzed.

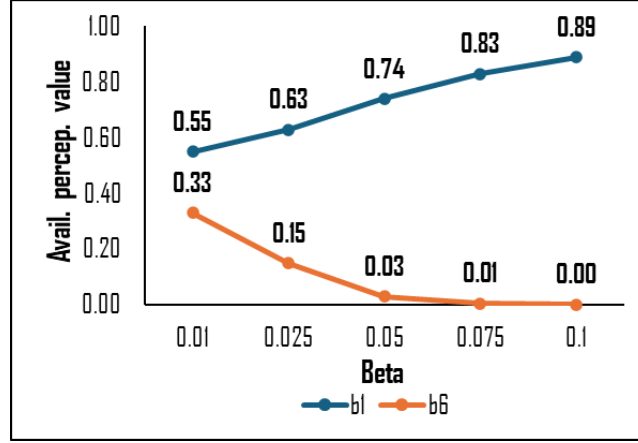


Figure 5.5. Impact of  $\beta$  on availability perception value of bridge choice alternatives.

This parameter controls the gap between the availability perception value of different alternatives. High values increase the gap between them, while the low values decrease. In other words, higher values of  $\beta$  increase the model's sensitivity to differences in perceived availability, while lower values decrease this sensitivity. In practice, the parameters  $\alpha$  and  $\beta$  must be estimated using real data to ensure accurate representation.

### 5.2.2 Bridge-route choice model with availability perception of bridges

Multiple empirical studies reported hierarchical relationships between bridge and route choices. This implies that routes are chosen conditional on bridge choices. This section develops a nested model for a joint bridge-route choice problem. The developed model combines the IAPL model, which handles the perception of available bridge choice alternatives along with the choice itself, for bridge choice, and the MNL model for route choice (IAPL-MNL). In IAPL-MNL, each route belongs to a single nest because bridge



choice alternatives are represented by specific bridge sequences. These sequences must be followed in order, as changing the order can make the bridge choice infeasible (e.g., no connection to the second bridge if the first is missing). The model's closed-form probability expression ensures analytical tractability.

The IAPL-MNL model is based on random utility theory. It assumes that travelers assign a certain perceived utility to each alternative based on its measurable characteristics and choose alternatives such that their perceived utility is maximized. The model is represented by choice probabilities. The general probability for this hierarchical model can be written as follows:

$$P_{k,b} = \Pr(U_b \geq U_h \wedge U_k \geq U_j, \forall h \neq b, \forall j \neq k, \forall b, h \in B, \forall k \in K_b, \forall j \in K_h), \quad \forall b \in B, \forall k \in K_b \quad (5.10)$$

where  $U_b$  is a random utility function of bridge choice alternative  $b$  and  $U_k$  is random utility function of route  $k$ .

The model components – random utility functions and corresponding probability expressions – and an illustrative example are provided below. For convenience, the superscript notation indicating the O-D pair is removed.

### ***5.2.2.1 Specification of utility function with availability perception of bridges***

This section presents the utility function with intermediate degrees of availability perception of bridges.

The utility function of bridge nest  $b$  can be expressed as a sum of systematic utility and an error term  $\varepsilon_b$  associated with nest  $b$ :

$$U_{k,b} = V_{k,b} + \varepsilon_b, \quad \forall b \in B \quad (5.11)$$

where error term  $\varepsilon_b$  can be represented as a sum of  $\delta_b$  with  $\tau_{k|b}$ :

$$\varepsilon_b = \delta_b + \tau_{k|b}, \quad \forall b \in B, \forall k \in K_b \quad (5.12)$$

Error term  $\tau_{k|b}$  is a zero-mean independently and identically distributed (IID) Gumbel random variable with scaling parameter  $\theta$ , i.e.:

$$E[\tau_{k|b}] = 0, \quad Var[\tau_{k|b}] = \frac{\pi^2}{6\theta^2}, \quad \forall b \in B, \forall k \in K_b \quad (5.13)$$

The distribution of error term  $\delta_b$  is picked up such that  $\varepsilon_b$  is also a zero-mean IID Gumbel random variable with the scaling parameter  $\eta \leq \theta$ .

The utility function for route  $k$  can be expressed as follows:

$$U_k = V_k + \tau_{k|b}, \quad \forall b \in B, \forall k \in K_b \quad (5.14)$$

where  $V_k$  is systematic utility of route  $k$  (elementary alternative). The systematic utility  $V_{k,b}$  of bridge nest  $b$  is represented as a function of expected value of maximum perceived utility of its elementary alternatives and availability perception component:

$$V_{k,b} = E \left[ \max_{k \in K_b} \{V_k + \tau_{k|b}\} \right] - \ln \mu_b, \quad \forall b \in B \quad (5.15)$$

where  $\mu_b$  is availability perception value for bridge nest  $b$ ; and  $\tau_{k|b}$  is random error term associated with route  $k$  in bridge nest  $b$ . It is important to note that the systematic utility of route  $k$  and its trip time  $c_k$  have the following relationship:

$$V_k = -\theta c_k, \quad \forall b \in B, \forall k \in K_b \quad (5.16)$$

Due to the assumption on the distribution of  $\tau_{k|b}$ , the systematic utility of bridge nest can be expressed as follows:

$$V_{k,b} = -\frac{1}{\theta} \ln \sum_{k \in K_b} e^{-\theta c_k} - \ln \mu_b, \quad \forall b \in B \quad (5.17)$$

#### 5.2.2.2 Joint probabilistic bridge-route choice model

The joint bridge-route choice probability can be stated as a multiplication of the route choice probability conditional on bridge nest and the marginal probability of bridge nest, i.e.:

$$P_{k,b} = P_{k|b} \cdot P_b, \quad \forall b \in B, \forall k \in K_b \quad (5.18)$$

where the conditional probability of selecting route  $k$  in nest  $b$  is modeled by MNL:

$$P_{k|b} = \frac{e^{-\theta c_k}}{\sum_{j \in K_b} e^{-\theta c_j}}, \quad \forall b \in B, \forall k \in K_b \quad (5.19)$$

and the marginal probability of bridge nest  $b$  is modeled by IAPL:

$$P_b = \frac{\left[ \sum_{k \in K_b} e^{-\theta \left( c_k - \left( \ln \bar{\mu}_b - \frac{1 - \bar{\mu}_b}{2 \bar{\mu}_b} \right) \right)} \right]^{\frac{\eta}{\theta}}}{\sum_{h \in B} \left[ \sum_{k \in K_h} e^{-\theta \left( c_k - \left( \ln \bar{\mu}_h - \frac{1 - \bar{\mu}_h}{2 \bar{\mu}_h} \right) \right)} \right]^{\frac{\eta}{\theta}}}, \quad \forall b \in B \quad (5.20)$$

where  $K_b$  is set of routes that passes through bridge nest  $b$ ;  $\theta$  and  $\eta$  are scaling parameters at the route choice and bridge choice levels, respectively; and  $c_k$  is deterministic travel time for route  $k$ .

Next, an illustrative example is conducted to highlight the properties of the IAPL-MNL model.

### 5.2.2.3 Illustration of model's features

A simple example can effectively communicate the underlying mechanics of complex ideas. A toy network (Figure 5.6) is used to demonstrate the properties of the IAPL-MNL model, compared to the MNL and nested logit (NL) models. The results are schematically summarized in Figure 5.7 and Figure 5.8.

MNL is used for modeling route choice. It includes a scaling parameter,  $\theta$ , controlling sensitivity to travel costs. The NL model, with an additional scaling parameter,  $\eta$ , captures the hierarchical relationship between bridge choices and routes, emphasizing correlation among routes. The NL model collapses to MNL when  $\eta = 1$ . The IAPL-MNL model advances the NL model by accounting for the perception of availability of bridge choice

alternatives and collapses to NL when  $\bar{\mu}_b = 1$  for all bridge choice alternatives. Thus, the IAPL-MNL model is the most general model among the three.

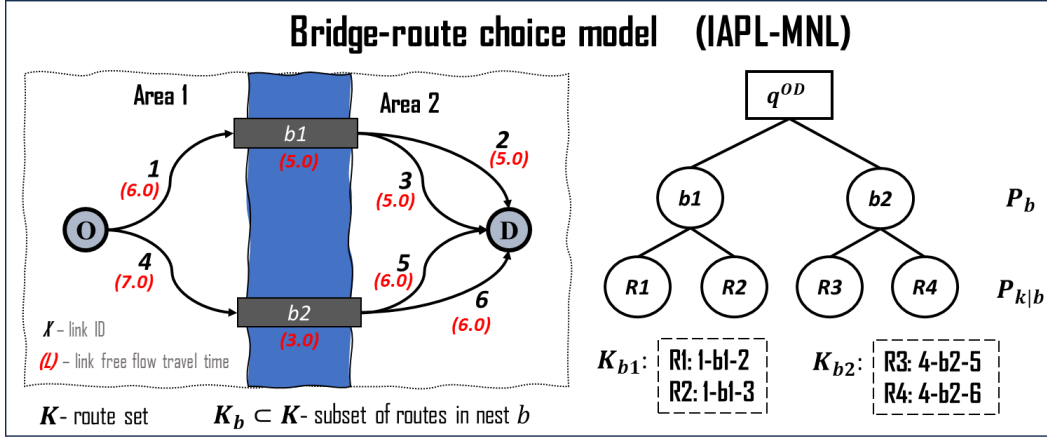


Figure 5.6. Toy network and its bridge-route choice model.

The following parameter settings were used where it was not specified. The scaling parameter  $\theta$  was set at 1.0,  $\eta$  was set at 0.5, and  $\beta$  was set at 1.0. FFTT on Link 1 is initially set to 4 and then gradually increased to 10 in one-unit increments. Changes in FFTT on Link 1 result in increased FFTTs on routes R1 and R2, as both routes traverse this link. The FFTTs on R3 and R4 remain unaffected. Since R1 is identical to R2 and R3 is identical to R4, these pairs are denoted as R1 and R3, respectively.

Figure 5.7 depicts the variation in availability perception values of bridge choice alternatives relative to the FFTT of Link 1.

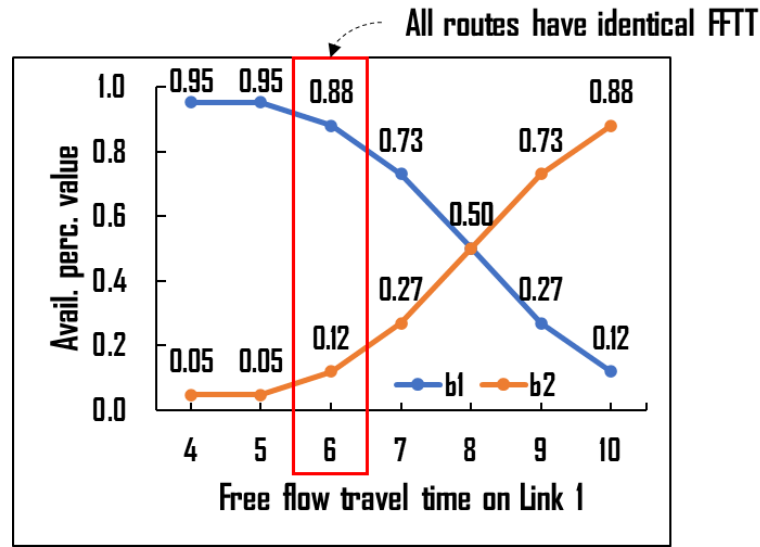


Figure 5.7. Impact of Link 1's FFTT on availability perception of bridge choice alternatives.

As shown in Figure 5.7, as FFTT on Link 1 (hence, on route R1) increases, the availability perception of bridge *b1* decreases. Conversely, the availability perception of bridge *b2* increases as the FFTT of route R1 increases. At the point where R1 and R3 had identical FFTT, the availability perception value for the *b1* - bridge choice alternative of R1 - was about 7 times higher than the corresponding value of *b2*. From this, we can observe that the perception of availability is negatively correlated with a route's FFTT. In other words, bridge choice alternatives that are spanned by shortest routes with higher FFTTs would have a lower perception of availability compared to alternatives spanned by shortest routes with lower FFTTs.

In Figure 5.8, the impact of FFTT of R1 on its choice probabilities is shown. The IAPL-MNL, NL, and MNL models are compared. As shown in Figure 5.8, as FFTT increases R1's probability decreases for all three models. Due to the hierarchical structure and the perceived availability component, the IAPL-MNL model substantially deviates from the other two models. Predominantly, it tends to assign higher probabilities to route R1 due to the perceived availability component of its corresponding bridge choice alternative. From this example, one

can clearly see that the proposed joint bridge-route choice model can capture the impact of bridge choice on route choice.

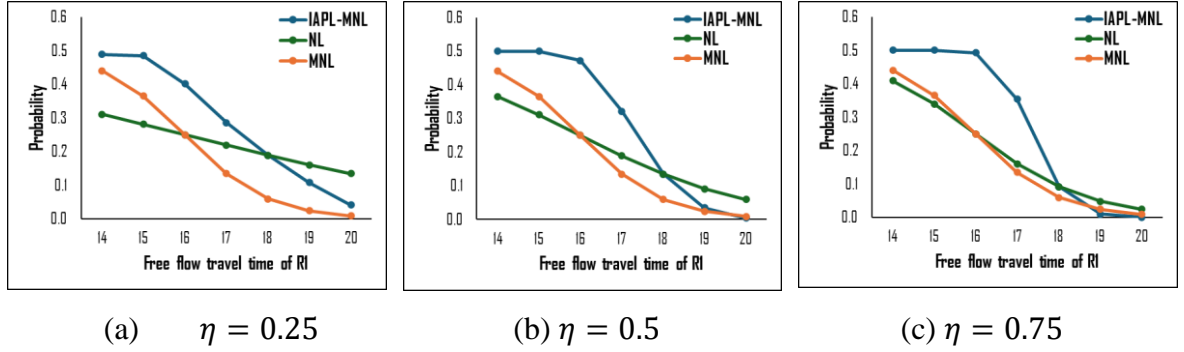


Figure 5.8. Impacts of FFTT and parameter  $\eta$  on choice probability for Route 1.

**Remark:** The study assumes that single-region O-D pairs may use bridges if the routes crossing them are cost-optimal. However, it does not explicitly model bridge choice for these pairs, assuming negligible bridge usage due to the availability of lower-cost, bridge-free alternatives. This assumption is based on rational cost minimization and network topology, where bridge-free routes serve local traffic efficiently, while routes with bridges prioritize mixed-region O-D pairs. This approach maintains the model's computational efficiency, focusing on bridge-route choices for mixed-region O-D pairs. Future research could relax this assumption.

### 5.2.3 Equivalent MP formulation

For consistent prediction of traffic flow patterns in urban road networks it is important to incorporate congestion effects into the model. Congestion rises with the increase of traffic flow forcing travelers to consider alternative bridges and routes that are believed to have lower travel costs. While there are numerous other ways to measure congestion, travel time is one of the most straightforward indicators of how it impacts travelers. This study expresses congestion using flow-dependent link travel time functions. It is assumed that travelers

continue to shift their routes until a stochastic user equilibrium is reached, at which point no one believes they can improve their travel time any further (Daganzo and Sheffi, 1977).

In this section, an equivalent MP formulation for the proposed IAPL-MNL bridge-route choice model is provided. The proposed equilibrium model will be referred to as IAPL-MNL SUE.

Mathematically, the SUE conditions are expressed in (5.21):

$$f_k^w = q^w \cdot P_{k,b}^w(f_k^w), \quad \forall w \in \mathcal{W}, \forall b \in B^w, \forall k \in K_b^w, \quad (5.21)$$

where  $\mathcal{W}$  is set of all O-D pairs,  $K_b^w$  is set of routes between O-D pair  $w$ ,  $q^w$  is travel demand between O-D pair  $w$ ,  $f_k^w$  is traffic flow on route  $k$  between O-D pair  $w$ ,  $P_{k,b}^w$  is probability of choosing route  $k$  using bridge choice alternative  $b$  between O-D pair  $w$ . For O-D pairs that do not require bridges  $P_{k,b}^w = P_k^w$ . The probability expression for the IAPL-MNL bridge-route choice model is given in (5.18).

To be consistent with the utility maximization behavior underlying the hierarchical choice structure (Ben-Akiva and Lerman, 1985b), the dispersion (scaling) parameters at different choice levels satisfy the condition that  $\theta > \eta$ . To facilitate the formulation of the developed equilibrium model with multiple choice levels, the dispersion parameters are rescaled as  $\theta_r = \theta$ ,  $\frac{1}{\theta_b} = \frac{1}{\eta} - \frac{1}{\theta}$ .

The resulting SUE model is formulated as an equivalent MP problem:

$$\begin{aligned} \min_f Z = & \sum_{a \in CA} \int_0^{x_a} c t_a(v) dv + \sum_{a \in BA} \int_0^{x_a} b t_a(v) dv + \frac{1}{\theta_r} \sum_{w \in CW} \sum_{k \in K^w} f_k^w \ln f_k^w \\ & + \frac{1}{\theta_r} \sum_{w \in BW} \sum_{b \in B^w} \sum_{k \in K_b^w} f_k^w \ln f_k^w + \frac{1}{\theta_b} \sum_{w \in BW} \sum_{b \in B^w} q_b^w \ln(q_b^w) \\ & - \sum_{w \in BW} \sum_{b \in B^w} q_b^w \left( \ln \bar{\mu}_b - \frac{1 - \bar{\mu}_b}{2 \bar{\mu}_b} \right) \end{aligned} \quad (5.22)$$

s.t.

$$\sum_{k \in K^w} f_k^w = q^w, \quad \forall w \in \mathcal{CW} \quad (5.23)$$

$$\sum_{k \in K_b^w} f_k^w = q_b^w, \quad \forall w \in B\mathcal{W}, b \in B^w \quad (5.24)$$

$$\sum_{b \in B^w} q_b^w = q^w, \quad \forall w \in B\mathcal{W} \quad (5.25)$$

$$f_k^w \geq 0, \quad \forall w \in \mathcal{W}, k \in K^w \quad (5.26)$$

$$q_b^w \geq 0, \quad \forall w \in B\mathcal{W}, b \in B^w \quad (5.27)$$

$$x_a = \sum_{w \in \mathcal{W}} \sum_{k \in K^w} f_k^w \delta_{a,k}^w, \quad \forall a \quad (5.28)$$

where  $\mathcal{CA}$  is set of common links,  $\mathcal{BA}$  is set of bridge links,  $\mathcal{CW}$  is set of common O-D pairs that do not need bridges,  $B\mathcal{W}$  is a set of O-D pairs that need bridges,  $B^w$  is subset of bridges for O-D pair  $w$ ,  $\delta_{a,k}^w$  is a route-link incidence indicator,  $x_a$  is traffic flow on link  $a$ ,  $ct_a(\cdot)$  is travel time on common link  $a$ ,  $bt_a(\cdot)$  is travel time on bridge link  $a$ ,  $q_b^w$  is traffic flow passing through bridge nest  $b$  between O-D pair  $w$ ,  $q^w$  is travel demand between O-D pair  $w$ ,  $\bar{\mu}_b$  is expected value of availability perception of bridge choice alternative  $b$ , respectively.

The formulation in (5.22) - (5.28) possesses the following features. Firstly, it is a convex problem with a non-linear objective function (5.22) and linear constraints (5.23) - (5.28). Assuming that link travel time functions are strongly increasing functions of traffic flow, existence and uniqueness of the solution can be ensured (see Prop. 1 and Prop. 2). Secondly, travel time on common links and bridge links can be expressed by dissimilar functions. Thirdly, the model can distinguish O-D pairs that must use bridges and those that can avoid them while accommodating both. The bridge choice applies only to O-D pairs that must use bridges, while the route choice covers both types of O-D pairs.

**Proposition 1.** *The MP formulation given in Eq. (5.22) - (5.28) has the solution of the IAPL-MNL model.*



**Proof.** To demonstrate the equivalence of the formulation to bridge-route choice model, the Lagrangian is created, partial derivatives are calculated and equated to zero. The corresponding probability expressions (5.19) - (5.20) are obtained by elementary arithmetic operations. The formal proof of equivalence is provided in Section 5.2.3.1.

**Proposition 2.** *The solution of IAPL-MNL-SUE is unique.*

**Proof.** It is sufficient to prove that the objective function in (5.22) is strictly convex in the vicinity of route flow and that the feasible region is convex. The convexity of the feasible region is assured by the linear equality constraints in (5.23) - (5.25). The non-negative and definitional constraints in (5.26) - (5.27) do not alter this characteristic. The formal proof of uniqueness is provided in Section 5.2.3.2.

### 5.2.3.1 Proof of equivalence

In this section, the equivalence of the MP formulation to the bridge-route choice model with bridge availability perception is proved.

The Lagrangian of model (5.22) - (5.28) is:

$$\begin{aligned}
 L = Z + \sum_{w \in \mathcal{W}} u_1^w \cdot \left( q^w - \sum_{k \in K^w} f_k^w \right) + \sum_{w \in R} \sum_{b \in B^w} u_2^w \cdot \left( q_b^w - \sum_{k \in K_b^w} f_k^w \right) \\
 + \sum_{w \in R} u_3^w \left( q^w - \sum_{b \in B^w} q_b^w \right)
 \end{aligned} \tag{5.29}$$

After the  $L$  function is formed, the partial re waere equated to zero and multiplied by  $\theta$ , the following expression is obtained:

$$\begin{aligned}
 \theta c_k^w + \ln f_k^w - \theta \left( \ln \bar{\mu}_b - \frac{1 - \bar{\mu}_b}{2\bar{\mu}_b} \right) + \left( \frac{\theta}{\eta} - 1 \right) \ln q_b^w - \theta \left( u_3^w - \frac{1}{\eta} \right) = 0, \quad \forall w \in B\mathcal{W}, b \in B^w, k \\
 \in K_b^w
 \end{aligned} \tag{5.30}$$

The following expression is obtained after some elementary arithmetic manipulations:

$$f_k^w (q_b^w)^{\frac{\theta}{\eta} - 1} = e^{-\theta \left( c_k^w - \left( \ln \bar{\mu}_b - \frac{1 - \bar{\mu}_b}{2\bar{\mu}_b} \right) \right)} e^{\theta \left( u_3^w - \frac{1}{\eta} \right)}, \quad \forall w \in B\mathcal{W}, b \in B^w, k \in K_b^w \tag{5.31}$$

Summing the above expression by route  $k$  result in the following expression:

$$(q_b^w)^{\frac{\theta}{\eta}} = e^{\theta(u^w - \frac{1}{\eta})} \sum_{k \in K_b^w} e^{-\theta(c_k^w - (\ln \bar{\mu}_b - \frac{1 - \bar{\mu}_b}{2\bar{\mu}_b}))}, \quad \forall w \in B\mathcal{W}, b \in B^w \quad (5.32)$$

By elevating both sides by  $\frac{\eta}{\theta}$ , the following expression is obtained:

$$q_b^w = e^{\eta(u^w - \frac{1}{\eta})} \left[ \sum_{k \in K_b^w} e^{-\theta(c_k^w - (\ln \bar{\mu}_b - \frac{1 - \bar{\mu}_b}{2\bar{\mu}_b}))} \right]^{\frac{\eta}{\theta}}, \quad \forall w \in B\mathcal{W}, b \in B^w \quad (5.33)$$

The corresponding marginal probability is obtained as follows:

$$P_b^w = \frac{\sum_{k \in K_b^w} f_k^w}{\sum_{h \in B} \sum_{k \in K_h^w} f_k^w} = \frac{\left[ \sum_{k \in K_b^w} e^{-\theta(c_k^w - (\ln \bar{\mu}_b - \frac{1 - \bar{\mu}_b}{2\bar{\mu}_b}))} \right]^{\frac{\eta}{\theta}}}{\sum_{h \in B} \left[ \sum_{k \in K_h^w} e^{-\theta(c_k^w - (\ln \bar{\mu}_h - \frac{1 - \bar{\mu}_h}{2\bar{\mu}_h}))} \right]^{\frac{\eta}{\theta}}}, \quad \forall w \in B\mathcal{W}, b \in B^w \quad (5.34)$$

The conditional probability is obtained by dividing (5.31) by (5.32):

$$P_{k|b}^w = \frac{f_k^w}{\sum_{j \in K_b^w} f_j^w} = \frac{e^{-\theta(c_k^w - (\ln \bar{\mu}_b - \frac{1 - \bar{\mu}_b}{2\bar{\mu}_b}))}}{\sum_{l \in K_b^w} e^{-\theta(c_l^w - (\ln \bar{\mu}_b - \frac{1 - \bar{\mu}_b}{2\bar{\mu}_b}))}} = \frac{e^{-\theta c_k^w}}{\sum_{l \in K_b^w} e^{-\theta c_l^w}}, \quad (5.35)$$

$\forall w \in B\mathcal{W}, b \in B^w, k \in K_b^w$

This concludes the proof of the equivalence for the O-D pairs that require bridges.

Similarly, the equivalence for the O-D pairs that do not require bridges is shown. The partial derivatives with respect to  $f_k^w$  are found and equated to zero, and multiplying by  $\theta$ , the following expression is derived:

$$\theta c_k^w + \ln f_k^w + 1 - u_1^w = 0, \quad \forall w \in C\mathcal{W}, k \in K^w \quad (5.36)$$

The following expression is acquired after some elementary arithmetic manipulations:

$$f_k^w = e^{-\theta c_k^w} e^{u_1^w - 1}, \quad \forall w \in C\mathcal{W}, k \in K^w \quad (5.37)$$

The expression for  $k \in K^w$  in equation (5.37) is summed up as follows:

$$\sum_{k \in K^w} f_k^w = e^{u_1^w - 1} \sum_{k \in K^w} e^{-\theta c_k^w}, \quad \forall w \in C\mathcal{W} \quad (5.38)$$

The probability can be obtained as follows:

$$P_k^w = \frac{f_k^w}{\sum_{j \in K^w} f_j^w} = \frac{e^{u_1^w-1} e^{-\theta c_k^w}}{e^{u_1^w-1} \sum_{l \in K^w} e^{-\theta c_l^w}} = \frac{e^{-\theta c_k^w}}{\sum_{l \in K^w} e^{-\theta c_l^w}}, \quad \forall w \in \mathcal{CW}, k \in K^w \quad (5.39)$$

This concludes the proof of the equivalence for the O-D pairs that do not require bridges.

### 5.2.3.2 Proof of uniqueness

In this section, the uniqueness of the solution of the MP formulation is proved.

Given the convex feasible region constructed by the sets of linear constraints, the proof of the solution uniqueness is equivalent to proving the strict convexity of the objective function (5.22). The Hessian matrix with respect to  $f_k^w$ ,  $\forall w \in B\mathcal{W}, k \in K_b^w$ :

$$\frac{\partial^2 Z}{\partial f_l^w \partial f_k^w} = \begin{cases} \frac{\partial c_k^w(f_k^w)}{\partial f_k^w} + \frac{1}{\theta} \cdot \frac{1}{f_k^w} > 0 & k = l \\ 0 & k \neq l \end{cases} \quad (5.40)$$

With the increasing travel time function with respect to traffic flow, the above expression implies the positive definite matrix.

$$\frac{\partial^2 Z}{\partial q_h^w \partial q_b^w} = \begin{cases} \left( \frac{1}{\eta} - \frac{1}{\theta} \right) \cdot \left( \frac{1}{\sum_{j \in K_b^w} f_j^w} \right) > 0 & h = b \text{ and } \theta \geq \eta \\ 0 & h \neq b \text{ and } \theta \geq \eta \end{cases} \quad (5.41)$$

In the hierarchical choice structure, the dispersion parameter at the upper level should be smaller than the dispersion parameter at the lower level, which requires the dispersion parameter for conditional bridge choice smaller than that for route choice. Therefore, the Hessian matrix w.r.t.  $q_b^w$ ,  $\forall w \in B\mathcal{W}, b \in B^w$  is positive definite.

The Hessian matrix with respect to  $f_k^w$ ,  $\forall w \in \mathcal{CW}, k \in K^w$ :

$$\frac{\partial^2 Z}{\partial f_l^w \partial f_k^w} = \begin{cases} \frac{\partial c_k^w(f_k^w)}{\partial f_k^w} + \frac{1}{\theta} \cdot \frac{1}{f_k^w} > 0 & k = l \\ 0 & k \neq l \end{cases} \quad (5.42)$$

In summary, the proposed equilibrium model has a unique solution for both the bridge flow and route flow. This completes the proof.

## 5.2.4 Solution algorithm

Solving the proposed model necessitates (i) a technique for distinguishing between O-D pairs for which the use of bridges is inevitable (bridge O-D pairs), and O-D pairs for which the use of bridges is optional (non-bridge O-D pairs), (ii) a method to generate bridge and route choice sets, and (iii) an iterative algorithm to equilibrate network traffic flows. This section elaborates on these components. The flowchart of the solution algorithm is shown in Figure 5.9.

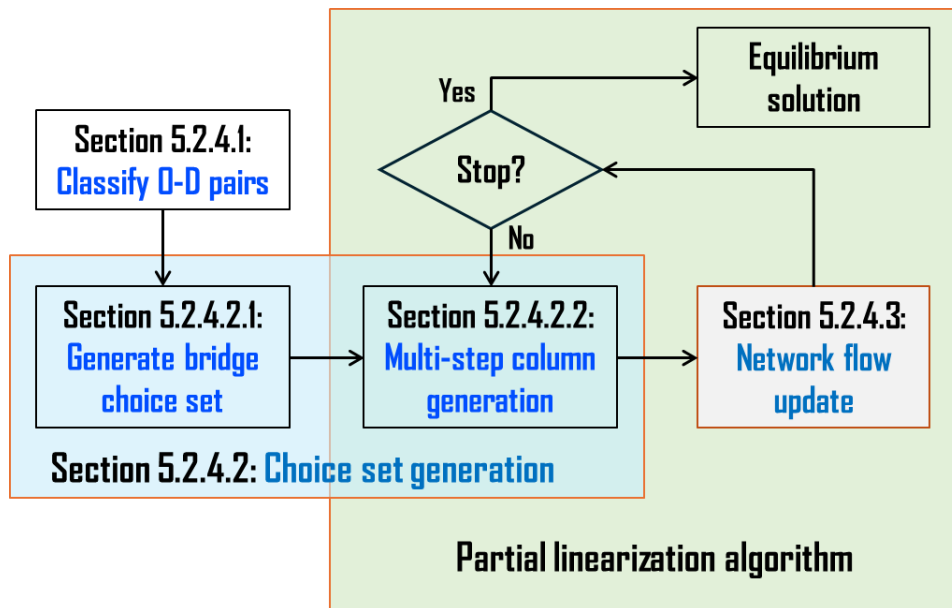


Figure 5.9. Flowchart for solution algorithm.

As shown in Figure 5.9, the algorithm begins with dividing the O-D pairs into bridge and non-bridge O-D pairs. In Section 5.2.4.1, a technique for automatically classifying O-D pairs is proposed. Next, the algorithm generates a bridge choice set for O-D pairs that must use bridges. In Section 5.2.4.2.1, a strategy for generating O-D-specific bridge choice alternatives is proposed. The algorithm then enters its iterative phase, which combines a route-generation scheme with a network flow update method. In Section 5.2.4.2.2, a multi-step column generation algorithm that ensures that generated routes pass through specified bridge choice alternatives is presented. For O-D pairs that do not need bridges, a conventional column

generation algorithm is used (Damberg et al., 1996) at this stage. Without loss of generality, a route-based partial linearization method is adapted for network flow updates in Section 5.2.4.3.

#### 5.2.4.1 Automatic identification of bridge O-D pairs

In road networks segmented by rivers, the use of bridges is unavoidable for some O-D pairs, while for others, it is optional. Why is this distinction important? It's because the bridge choice problem is modelled exclusively for bridge O-D pairs – O-D pairs that cannot avoid using bridges.

This section describes a method for automatically detecting O-D pairs of the former type.

Figure 5.10 schematically depicts the key idea of this technique.

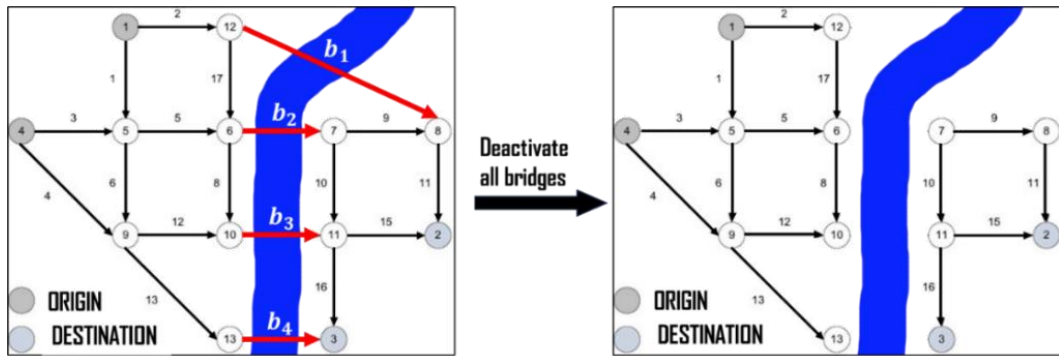


Figure 5.10. Method for automatically identifying bridge O-D pairs.

As shown in Figure 5.10, the method involves temporarily deactivating all bridges and determining whether O-D pairs remain connected. An O-D pair is disconnected if no route can be found from the origin to the corresponding destination. If an O-D pair becomes disconnected, it indicates the need to use a bridge. Importantly, this approach objectively and systematically categorizes O-D pairs into two groups without requiring additional manual effort during network changes, regardless of network size or bridge count.

#### ***5.2.4.2 Bridge-centric choice set generation***

The formation of bridge and route choice sets in travelers' minds may be inseparable and unconscious. Integrated approaches (route-first/bridge-second) could be favorable if not for the practical challenges they face, such as the inability to enumerate routes and the existence of implausible but feasible routes in transport networks. Disjoint methods offer a plausible trade-off between realistic processes and practical implementation. They can effectively leverage the features of both bridges and routes, mitigating the issues associated with integrated approaches.

The disjoint choice set generation for a joint bridge-route choice problem essentially involves two parts: the generation of bridge choice sets and the generation of route choice sets. Bridge choice alternatives can be enumerated, and unreasonable options excluded based on their availability perception values, whereas route choice alternatives, having no specific location and being stretched throughout the network, cannot be enumerated and sieved in a similar manner. Therefore, generating route choice set requires specific heuristics to form a choice set explicitly ([Bekhor et al., 2008](#)) or an iterative technique for implicit selection ([Damberg et al., 1996](#)).

A disjoint bridge-centric strategy that makes effective use of the properties of bridges and routes is proposed. For each bridge O-D pair, feasible bridge choice alternatives are enumerated explicitly and sieved based on their availability perception values. Routes are generated implicitly for each bridge choice alternative of each O-D pair using a column generation technique embedded into iterations of a partial linearization algorithm ([Patriksson, 2015](#)). For bridge O-D pairs, a multi-step column generation is employed to enforce the routes to pass through a specified set of bridge choice alternatives, while for non-bridge O-D pairs, a traditional column generation technique is used.

#### 5.2.4.2.1 Bridge choice set generation

This section details the proposed bridge choice set generation algorithm. It begins with a description of the travelers' behavior that the model aims to replicate, followed by an introduction to the algorithm.

Figure 5.11 presents three different O-D pairs that share a common feature: their origins and destinations belong to the same regions, NW and E, respectively. It is reasonable to assume that these O-D pairs may share a common set of bridge choice alternatives. However, these bridge choice alternatives may vary in how they are perceived by the travelers of different O-D pairs. Some bridge choice alternatives that are attractive for one O-D pair may not be as appealing for another O-D pair within the same group. Therefore, while O-D pairs in the same group may have a generic bridge choice set, each O-D pair may have its own specific consideration set.

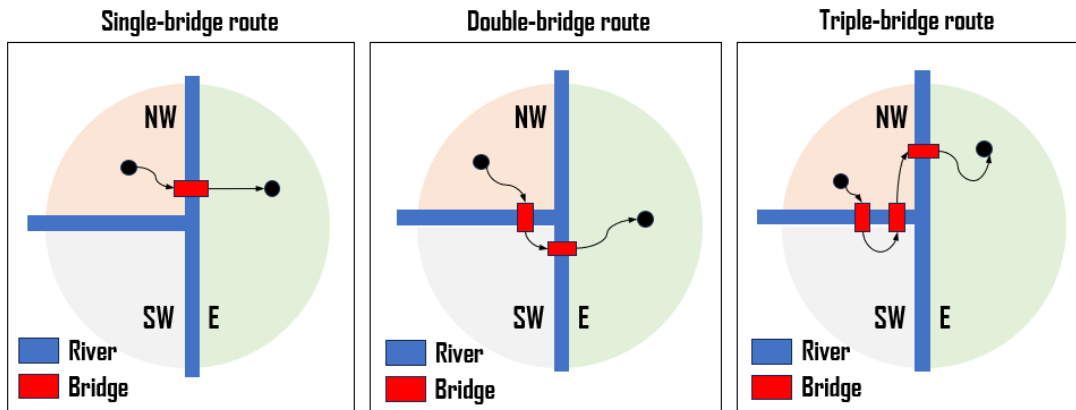


Figure 5.11. Three scenarios of routes with bridges for the Winnipeg network.

These behavioral considerations are incorporated into the developed bridge choice set generation algorithm. The steps of the algorithm are depicted in Figure 5.12. It is worth emphasizing that this algorithm is executed once prior to solving the bridge-route choice problem.

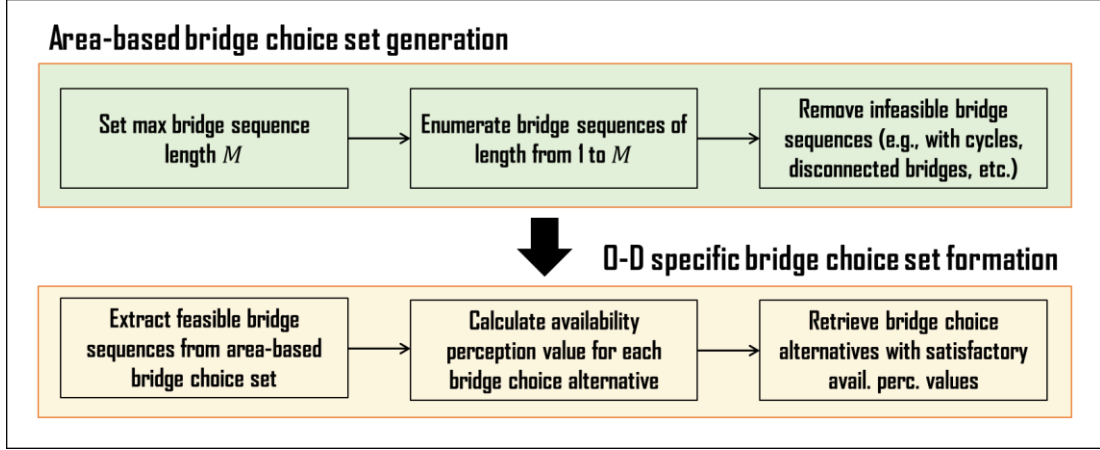


Figure 5.12. Flowchart for the bridge choice set generation.

As shown in Figure 5.12, first, a generic region-based bridge choice set of bridge choice alternatives is generated using pure combinatorial methods (i.e., the shortest path algorithm is not required at this stage). The number of bridge sequence variations can be found as follows:

$$Bridge\ seq.\ \# = \sum_{i=1}^M \frac{|BA|!}{(|BA| - i)!} \quad (5.43)$$

where  $|BA|$  is the total number of bridges in network and  $M$  is the maximum number of bridges in bridge sequences.

Then, the set of bridge choice alternatives obtained by (5.43) includes both feasible and infeasible bridge sequences. Infeasible bridge sequences are removed. The problem's inherent directionality allows us to do it easily. For example, the origin of an O-D pair and the head of the first bridge must be in the same region; similarly, the tail of the first bridge and the head of the second bridge must also be within the same region, and so on. We contend that the set of feasible bridge sequences remains manageable, even for large networks, as previously discussed. At this step, the region-based bridge choice set is not specific to O-D pairs.

Next, O-D specific bridge choice sets are formed. They can be extracted from the region-based bridge choice set. The main consideration here is that some feasible bridge choice



alternatives may be practically implausible for some O-D pairs. For example, a bridge may be too distant from origin and/or destination nodes, making it an unreasonable option for travelers. This issue can be addressed by truncating O-D specific bridge choice sets based on the availability perception values of bridge choice alternatives. The availability perception attribute is designed to penalize both alternatives with distant bridges and long bridge sequences (see Section 5.2.1). This results in a plausible set of bridge choice alternatives.

#### ***5.2.4.2.2 Route choice set generation***

Routes are implicitly generated for each bridge nest of each O-D pair by employing a column generation technique within the iterations of a partial linearization algorithm. Column generation for the route choice problem relies on identifying the shortest route from the origin to the destination. For non-bridge O-D pairs, a standard one-step column generation process was employed. Conversely, for bridge O-D pairs, the process was transformed into a multi-step column generation to guarantee that the routes cross a predetermined set of bridge choice alternatives. This section focuses on multi-step column generation. A special case of a multi-step column generation procedure – a two-step column generation – is schematically illustrated in Figure 5.13.

In Figure 5.13, a column generation technique consistent with the hierarchical structure of the model necessitates the use of a two-step shortest route algorithm. A shortest route going through a particular bridge is a special case of shortest route algorithm. The approach involves decomposing the problem into two subproblems: 1) finding the shortest route from origin to the bridge start node (green) and 2) determining the shortest route from the bridge end to the destination (yellow). Once these steps are completed, the two route segments are concatenated. Essentially, this process is equivalent to executing a shortest route algorithm twice. Dijkstra's shortest route algorithm is a suitable choice for this purpose, with a time

complexity of  $O(m + n \log n)$ , where  $m$  represents the number of links in the graph, and  $n$  denotes the number of nodes.

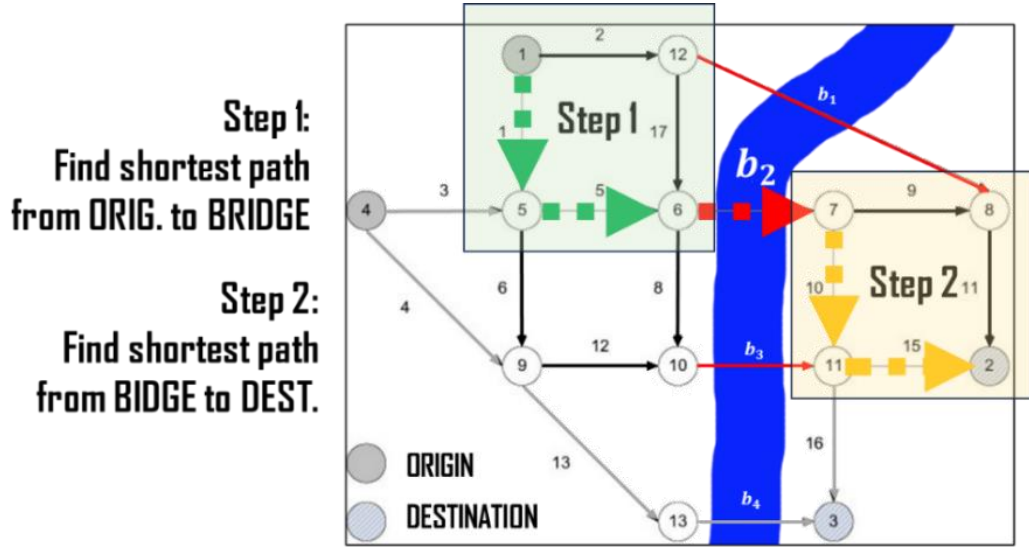


Figure 5.13. Illustration of two-step shortest route algorithm.

For bridge choice alternatives that involve sequences of multiple bridges, the algorithm is generalized to a multi-step column generation approach. In this scenario, the process begins by finding the shortest route from the origin to the start node of the first bridge in the sequence. Subsequently, the shortest route is determined from the end node of the first bridge to the start node of the subsequent bridge. This procedure is repeated for each bridge in the sequence. Finally, the shortest route from the end node of the last bridge to the destination node is established. This necessitates running the two-step column generation algorithm as many times as there are bridges in the sequence.

#### 5.2.4.3 Network flow update

The solution algorithm combines a route-generation scheme with a network flow update method. A route-based partial linearization is adapted for network flow updates. This section elaborates on the partial linearization method and its components such as search direction, step size, and a measure for termination condition.

The partial linearization method is one of the types of descent direction methods used for continuous optimization problems. It iteratively determines a search direction and step size until convergence is reached (Patriksson, 2015).

To obtain the search direction, a partially linearized subproblem is solved using a first-order approximation of the first two terms (i.e., Beckmann transformation terms) of the objective function. All other terms except the last one are entropy terms and should be retained to ensure compliance with logit-based stochastic equilibrium conditions for both route and bridge choices. By retaining the entropy terms, the subproblem's first-order conditions naturally yield closed-form logit probabilities for both route and bridge choices. The last term is already linear in  $q_b^w$ , so no need to linearize it.

To obtain an appropriate step size, a self-regulated averaging (SRA) scheme proposed by (Liu et al., 2009) is used. This scheme allows determining a step size without the need to evaluate the objective function. Because the objective function is relatively complex, it may reduce considerable computational efforts spent on objective function evaluation. SRA uses the residual error  $\beta$  and step size in the current iteration to determine the next step size and guarantees convergence with either  $\lambda_1 > 1$  or  $0 < \lambda_2 < 1$  controlling the decreasing speed. Refer to (Patriksson, 2015) for further information on the convergence properties of the partial linearization method.

Relative gap (RGAP) function (5.44) is employed to control the convergence process. Once RGAP drops below a specified threshold, the algorithm terminates.

$$RGAP = 1 - \frac{\sum_{w \in W} q^w C_{min}^w}{\sum_{w \in W} \sum_{k \in K^w} f_k^w \cdot C_k^w} \quad (5.44)$$

where  $C_k^w$  is the perceived cost of route  $k$  between O-D pair  $w$  and  $C_{min}^w$  is the minimum perceived cost between O-D pair  $w$ . The key idea of RGAP is as follows. The relative gap between the shortest route in terms of perceived travel cost and all other routes is expected to

shrink with each iteration, and, at equilibrium, it is expected to approach zero. This is due to the assumption that all active routes of an O-D pair should have equal perceived travel time at equilibrium (Sheffi, 1985). Considering that route costs cannot be a positive value to have a physical interpretation, the feasible range of values for the relative gap lies between 0 and 1, i.e.,  $RGAP \in [0, 1]$ .

## 5.3 Numerical experiments

In this section, experiments were conducted on two networks. Using a toy network (Figure 5.6) the properties of the proposed IAPL-MNL-SUE model were investigated. Using the real-size network (Figure 5.1), the applicability of the model was shown in a real case study.

Both common link and bridge link travel times are modelled as a well-known Bureau of Public Road (BPR) function, as shown in equation (3.14).

### 5.3.1 Experiment 1: A toy network

In this section, the properties of the IAPL-MNL-SUE model were analyzed using the toy network in Figure 5.6. Specifically, the effects of congestion on equilibrium solutions were investigated and how demand level may affect the traffic flow pattern was studied.

#### 5.3.1.1 *Equilibrium solution*

In this section, the effect of congestion on traffic flow prediction was investigated. The results are summarized in Table 5.3 and Table 5.4.

The parameters were set as follows. The demand level was set at 20, the availability attribute scaling parameter  $\beta$  was set at 1.0, the scaling parameters  $\theta$  and  $\eta$  were set at 1.0 and 0.5, respectively. The average availability perception values of bridges were set according to Section 5.2.2.3. Link free flow travel times were set according to Figure 5.6 for all links

except Link 2, for which it was set at 7. This change made R1 non-identical to R2. Link capacity was set at 10 for all links. For fairness of comparison of route flows, routes were enumerated. All routes except R1 had a free flow travel time of 16. For R1, it was 18.

As shown in Table 5.3, the IAPL-MNL-SUE model assigns higher flows to the routes R1 and R2 – routes of bridge choice alternative *b1* – than the other two models. It attributed to the higher perceived availability value of *b1* than of *b2*. It is consistent with the results in previous sections.

Table 5.3. Route flows for three SUE models.

Routes	IAPL-MNL-SUE	NL-SUE	MNL-SUE
R1	1.86	1.47	1.45
R2	8.80	7.99	7.93
R3	4.67	5.27	5.31
R4	4.67	5.27	5.31

This indicates that the proposed SUE model is indeed capable of accounting for the impact of bridges on route choice in a congested network.

Table 5.4 shows how each term (e.g., travel cost integrals, entropy terms, bridge choice set formation errors), contributes to the overall objective function value.

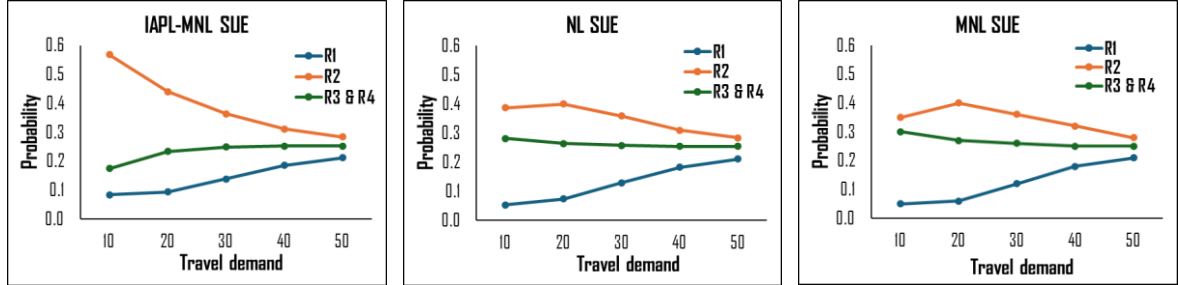
Table 5.4. Objective function values for three SUE models.

Objective function	IAPL-MNL-SUE	NL-SUE	MNL-SUE
Bec. trans.	331.27	329.97	329.96
Route flow entropy	34.68	34.69	34.7
Bridge flow entropy	46.1	46.08	-
Bridge avail.	30.18	-	-
Total obj.	442.23	410.75	364.66

Examining Table 5.4, it is observed that the objective function of the IAPL-MNL SUE model has a larger value than that of the NL SUE and MNL SUE models. This is because the IAPL-MNL SUE model incorporates additional considerations related to route correlation due to bridges. Specifically, the objective function of the IAPL-MNL SUE model includes a bridge availability perception term, which still influences bridge flow and route flow-related entropy terms.

### 5.3.1.2 Impact of demand level on route choice probabilities

In this section, the impact of demand level on equilibrium was investigated by gradually increasing demand level. The results are summarized in Figure 5.14 and Table 5.5.



(a) IAPL-MNL SUE model.

(b) NL SUE model.

(c) MNL SUE model.

Figure 5.14. Impact of demand level on route choice probabilities.

In Figure 5.14, we observe a distinct difference between the IAPL-MNL SUE, NL SUE, and MNL SUE models, particularly at lower demand levels. The NL SUE and MNL SUE tended to assign higher probability values to R3 and R4 than the IAPL-MNL SUE model. At low demand levels, the IAPL-MNL SUE model assigned almost two times higher probabilities to R1 and R2 than the other two models. This was attributed to the higher perceived availability of  $b1$ , which the latter two routes cross. The probabilities of R3 and R4 were identical to each other for all models. This was expected because they shared the same features and belonged to the same bridge choice alternative  $b2$ . Similarly, the probability of R1 was lower than the probability of R2 for all scenarios due to R1 having a higher FFTT than R2. We can also see that the difference in bridge choice probabilities between different bridge choice alternatives was evident at low demand levels. As demand increased, this difference gradually diminished. This behavior aligns with the SUE framework, which predicts that all SUE models tend to converge toward deterministic user equilibrium as congestion levels rise due to increased demand. Table 5.5 supplements Figure 5.14 by providing predicted route choice probabilities.

Table 5.5. Equilibrium probabilities for different demand levels.

$q$	Average v/c ratio	IAPL-MNL-SUE				NL-SUE				MNL-SUE			
		R1	R2	R3	R4	R1	R2	R3	R4	R1	R2	R3	R4
10	0.5	0.11	0.70	0.10	0.10	0.05	0.39	0.28	0.28	0.05	0.35	0.30	0.30
20	1	0.12	0.47	0.20	0.20	0.07	0.40	0.26	0.26	0.06	0.40	0.27	0.27
30	1.5	0.15	0.37	0.24	0.24	0.13	0.36	0.26	0.26	0.12	0.36	0.26	0.26
40	2	0.19	0.31	0.25	0.25	0.18	0.31	0.25	0.25	0.18	0.32	0.25	0.25
50	2.5	0.21	0.28	0.25	0.25	0.21	0.28	0.25	0.25	0.21	0.28	0.25	0.25

Results presented in Figure 5.14 and Table 5.5 show that the proposed network equilibrium TA model based on the IAPL-MNL bridge-route choice model could successfully capture the hierarchical relationship between bridge and route choices, account for congestion effects, and difference between availability perception of bridge choice alternatives.

### 5.3.2 Experiment 2: A large-scale network

This section adopts the Winnipeg network as a case study to demonstrate the applicability of the proposed model and choice set generation technique in a real network. The network is shown in Figure 5.1. Two rivers separate the space into three regions: Northwest (NW), East (E), and Southwest (SW). These regions are connected via 15 bi-directional bridges. The network consists of 154 zones, 1067 nodes, 2535 links, and 4345 O-D pairs. The network topology, link characteristics, and O-D demands can be found in Emme/2 software.

#### 5.3.2.1 Bridge choice set generation

In this section, O-D pairs were split into two groups, and region-based and O-D specific bridge choice sets were generated as described in Section 5.2.4.1. The results are summarized in Table 5.6, Table 5.7, Figure 5.15, and Figure 5.16.

Table 5.6 presents statistics for the number of mixed-region O-D pairs (where the origin and destination are in different regions). As shown in Table 5.6, there are a total of 2473 mixed-region O-D pairs, constituting approximately 57% of all O-D pairs. This observation underscores the potential importance of accounting for bridge impact when making route choices for this network. From visual investigation of the network, all mixed-region O-D pairs

could be connected by single bridges. Nonetheless, longer bridge sequences were checked as well because they might be used to bypass congestion in the center business district (CBD). With the increase of the maximum length of bridge sequences, the number of bridge sequence variations increase according to (5.43). For example, for  $M = 3$ , enumeration of region-based bridge sequences produced 25260 variations, among which 22626 were infeasible and only 2634 feasible. Because bridge choice was modeled only for mixed-region O-D pairs, the final number of feasible bridge sequences was reduced to 1790. Therefore, the number of feasible bridge sequences remained relatively manageable.

Table 5.6. Region-based distribution of O-D pairs and corresponding bridge sequences.

Region of origin	Region of destination	Number of O-D pairs	Number of feasible bridge sequences		
			M=1	M=2	M=3
E	NW	796	4	34	254
SW	NW	654	6	22	334
NW	E	310	5	29	303
NW	SW	278	6	30	342
E	SW	254	5	29	303
SW	E	181	4	34	254
<b>Total</b>		2473	30	178	1790

The distribution of bridge choice alternatives with respect to their availability perception values is provided in Table 5.7 and Figure 5.15.

Table 5.7. Number of region-based bridge sequences and O-D specific bridge choice alternatives.

Bridge sequence maximum allowed length M	Region-based bridge sequences #	O-D specific feasible bridge choice alternative #	
		Before truncation	After truncation
1	30	12,320	11,336
2	178	72,302	52,654
3	1790	731,941	483,176

Table 5.7 provides the total number of region-based bridge sequences and O-D specific bridge choice alternatives for different values of maximum allowed bridge sequence length. Based on Table 5.6, the total number of O-D specific bridge choice alternatives could be calculated by summing up the multiplication of number of O-D pairs and the corresponding number of feasible region-based bridge sequences. For example,  $M = 2$  resulted in 72,302 bridge choice alternatives. As shown in Figure 5.15, about a third of all bridge choice alternatives had the availability perception value lower than 0.1 (for  $\alpha = 2$  and  $\beta = 0.1$ ).



Therefore, they could be truncated with a little effect on the equilibrium traffic flow pattern and a significant impact on computational time.

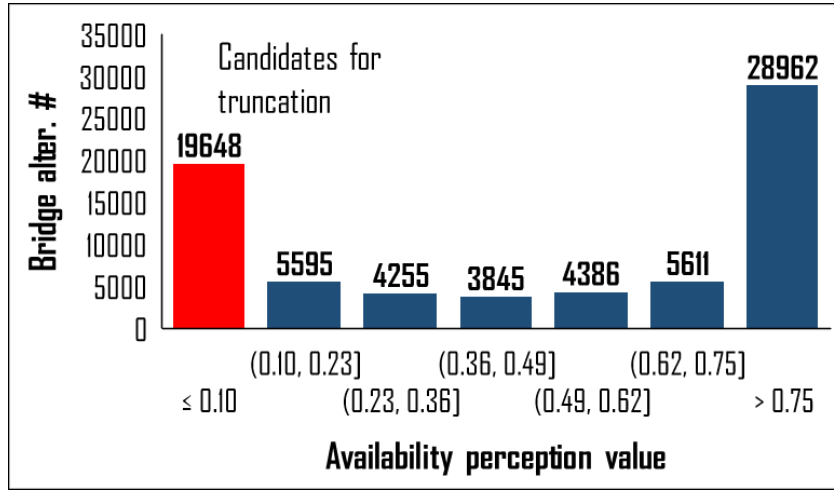


Figure 5.15. Availability perception values for bridge choice alternatives at  $M = 2$ .

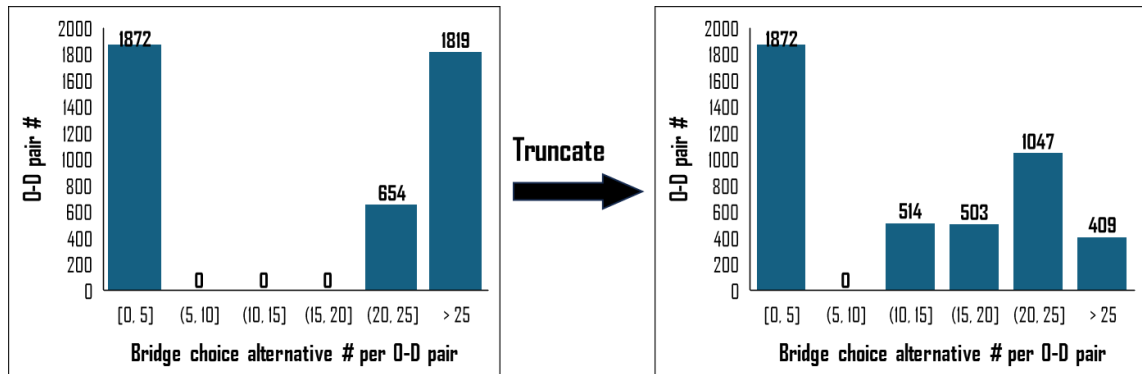


Figure 5.16. Number of bridge choice alternatives before and after truncation.

Figure 5.16 shows the distribution of O-D pairs before and after bridge choice alternative truncation for  $M = 2$ . There were 1872 single-region O-D pairs. Since bridge choice was not modelled for these O-D pairs, they had no bridge choice alternatives. The remaining O-D pairs had bridge choice alternatives. Before truncation, almost the same number of mixed-region O-D pairs had more than 25 bridge choice alternatives. After truncation, the number of alternatives was reduced by a third, and the distribution of the number of bridge choice alternatives among mixed-region O-D pairs became more uniform. Reducing the number of

bridge choice alternatives also decreased computational time, as fewer computations needed to be performed.

### Sensitivity analysis

This section conducts a sensitivity analysis for parameters  $\alpha$  and  $\beta$ , which influence the availability perception score.

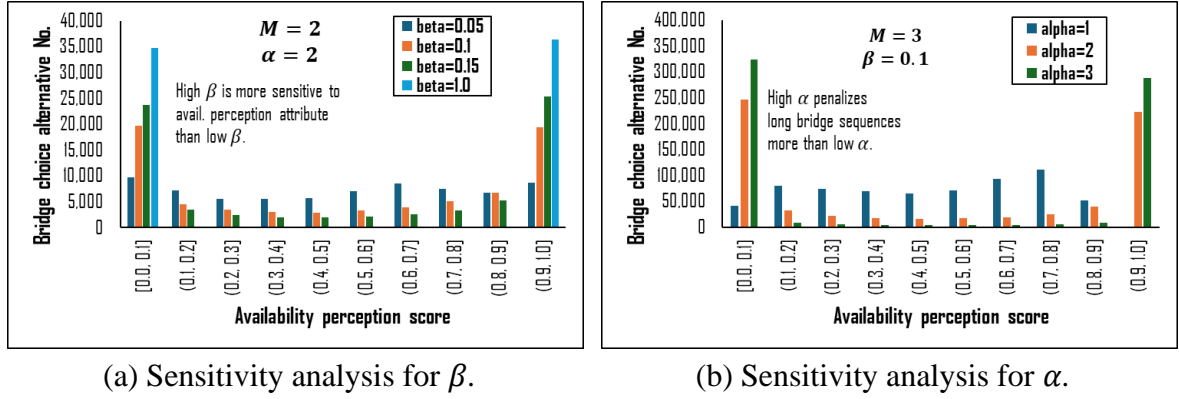


Figure 5.17. Sensitivity analysis on the parameters of the availability perception value.

Parameter  $\beta$  controls sensitivity to the availability perception attribute  $Y_b$  (5.3), with higher values increasing sensitivity and lower values decreasing it (Figure 5.17a). Parameter  $\alpha$  affects sensitivity to long bridge sequences, with higher values penalizing alternatives with longer sequences. To illustrate the impact of  $\alpha$ , the distribution of bridge choice alternatives with  $M = 3$  is presented (Figure 5.17b). Increasing  $\alpha$  and  $\beta$  resulted in a greater number of bridge choice alternatives with extreme availability perception values, both low and high. This is because  $Y_b$  is centered around its mean, calculated among bridge alternatives of the same O-D pair. This makes  $Y_b$  range from  $-\infty$  to  $+\infty$ . Without centering,  $Y_b$  would not have negative values, which are crucial for calculating the availability perception score.

#### 5.3.2.2 Setting model parameters

This section provides sensitivity analyses on the parameters of the selected choice models. The results are summarized in Figure 5.18.

To set model parameters, the total coefficient of variation analysis has been used as described in Section 3.4.3.1.1. To set parameters for the IAPL-MNL model, we find  $\theta$  (route level parameter) using the above procedure, assuming  $\eta$  (nest level parameter) is given. Subsequently, sensitivity analysis is conducted on  $\eta$ .

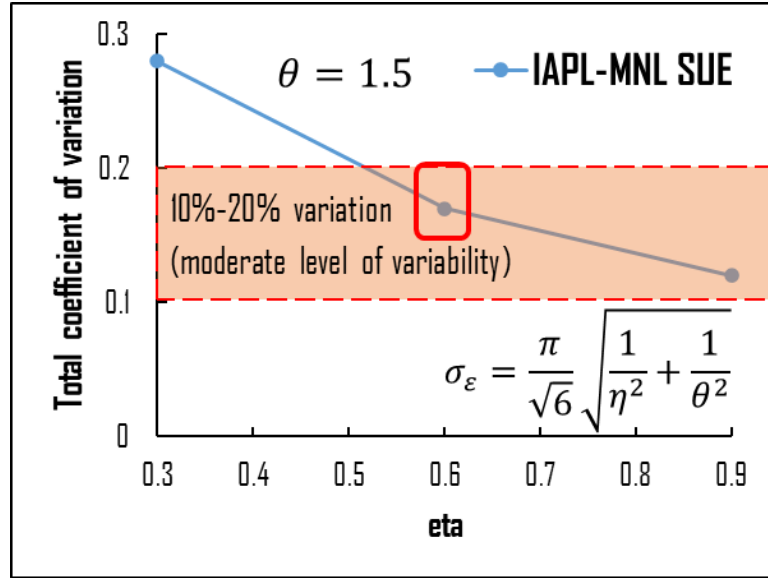


Figure 5.18. Effect of the selected choice model parameters on the total coefficient of variation for the Winnipeg network.

As shown in Figure 5.18, the parameters of the selected choice models were set such that the mean coefficient of variation  $\overline{CV}$  remained within the range of 10% to 20%.

### 5.3.2.3 Computational complexity analysis

This section investigates convergence characteristics of the solution algorithm. The algorithm was executed for the MNL-SUE and IAPL-MNL-SUE models only.

The stopping value of the relative gap was set at  $10^{-5}$ . For MNL-SUE, the parameter  $\theta$  was set at 1.0. For IAPL-MNL-SUE, the parameters  $\theta$  and  $\eta$  were set at 1.5 and 0.6, respectively. Parameters  $\alpha$  and  $\beta$  were set at 2 and 0.1. The numerical experiments were conducted on a MS Windows 11 operating system with Intel(R) Core (TM) i7-9700 CPU @ 3.00GHz with 24 GB of RAM. The results are shown in Figure 5.19 and Table 5.8.

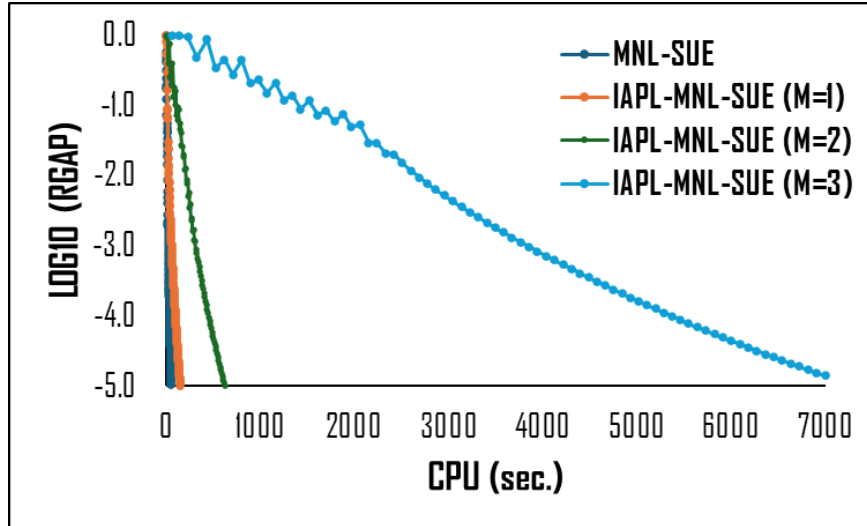


Figure 5.19. Convergence characteristics of the solution algorithm.

Figure 5.19 illustrates the convergence time of the solution algorithm for both the MNL-SUE model and the IAPL-MNL-SUE model. Table 5.8 further elaborates on it. The IAPL-MNL-SUE model was tested under different values of  $M$ . As shown in Figure 5.19, the computational complexity increased with  $M$ . Nonetheless, the algorithm managed to converge in reasonable times for all three cases. As expected, the MNL-SUE had the lowest computational time because it was the simplest among the two. In the IAPL-MNL-SUE model case, the computational time showed to be highly dependent on the parameter  $M$  – the maximum allowed bridge number in a bridge sequence. Higher values required more computational time for the algorithm to converge than the lower ones. The reason was that higher  $M$  values resulted in higher number of region-based bridge sequence variations, which increased the number of O-D specific bridge choice alternatives as shown in Table 5.8.

Based on Table 5.8, the IAPL-MNL-SUE model converged in fewer iterations than the MNL-SUE model. Moreover, with the increase of  $M$ , the number of iterations reduced. This was attributed to the higher number of variations of bridge sequence in the choice set. However, the computation time increased proportionally to the increased number of

alternatives. Therefore, assuming that greater a number of variations provide more realistic combinations of bridges, tradeoff has to be found between realism and computational time.

Table 5.8. Convergence characteristics: MNL-SUE vs. IAPL-MNL-SUE.

Model	Iteration #	Total CPU time (in sec.)	Bridge choice set generation time (in sec.)	Aver. CPU time per iter. (in sec.)	Total route #
MNL-SUE	105	57.1	-	0.6	15,312
IAPL-MNL-SUE (M=1)	101	150.6	1.3	1.5	51,482
IAPL-MNL-SUE (M=2)	76	631.8	2.8	8.3	247,530
IAPL-MNL-SUE (M=3)	82	7354.9	34.4	89.7	2,358,473

It was observed that with the increase of  $M$ , the number of iterations reduced for the IAPL-MNL-SUE model. This was attributed to the higher number of variations of bridge sequence in the choice set. However, the computation time increased proportionally to the dimensionality of the problem.

#### 5.3.2.4 Flow allocation comparison

In this section, the difference between the traffic flow patterns obtained from the IAPL-MNL-SUE and MNL-SUE models were investigated. The results are summarized in Figure 5.20 and Figure 5.21 for  $M = 2$ .

Direct comparison of route flows infeasible due to different choice sets from the models. Instead, absolute and relative differences were analyzed, with aggregated link flow differences measured using RMSE (5.45).

$$RMSE = \sqrt{\frac{1}{|A|} \sum_{a \in X} (x_a^{IAPL} - x_a^{MNL})^2} \quad (5.45)$$

where  $X \subseteq A$  denotes the set of investigated links, which is a subset of the whole link set  $A$ ;  $x_a^{IAPL}$  and  $x_a^{MNL}$  are flow on link  $a$  for the IAPL-MNL-SUE and MNL-SUE models, respectively. The relative link flow difference was calculated according to (5.46).

$$Relative\ Diff\ (\%) = \frac{|x_a^{IAPL} - x_a^{MNL}|}{0.5 (x_a^{IAPL} + x_a^{MNL})} \times 100\ \% \quad (5.46)$$

Figure 5.20 illustrates link absolute flow differences in GIS map. The size of the blue circles indicates how much the link flows of the two models deviate from each other. For clarity, flow differences in both directions were summed for each link.

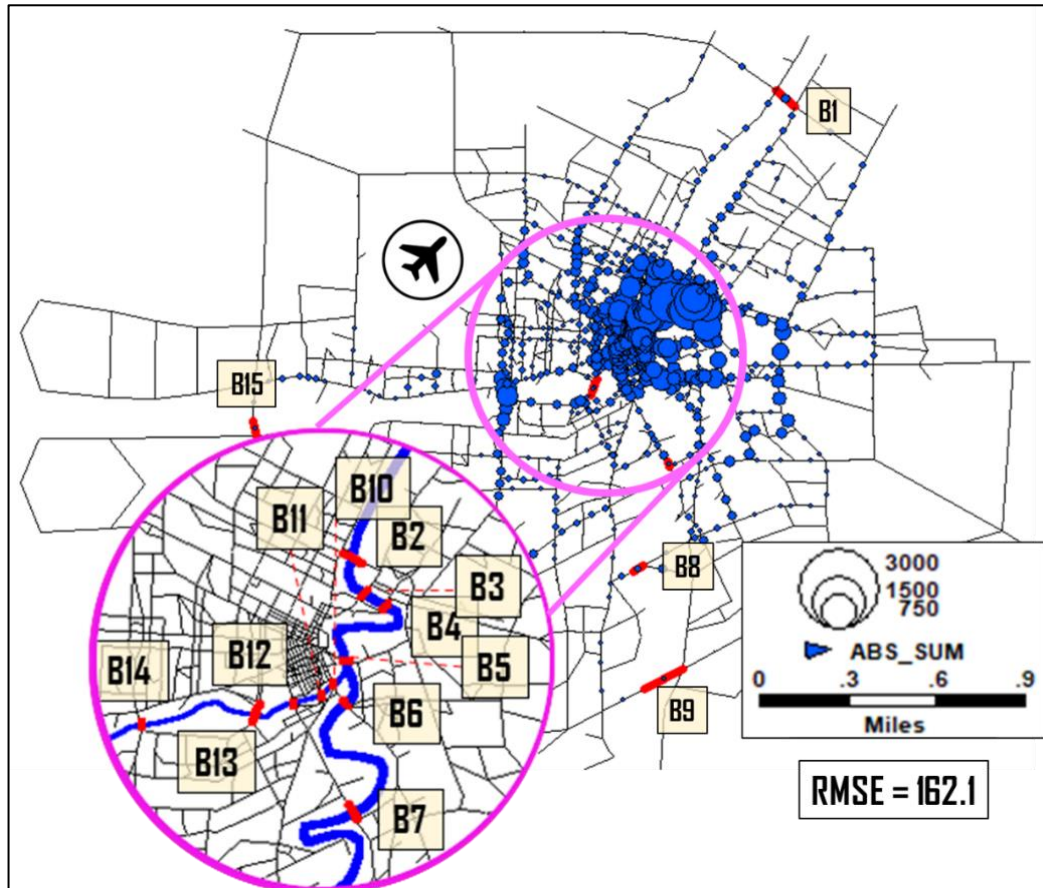
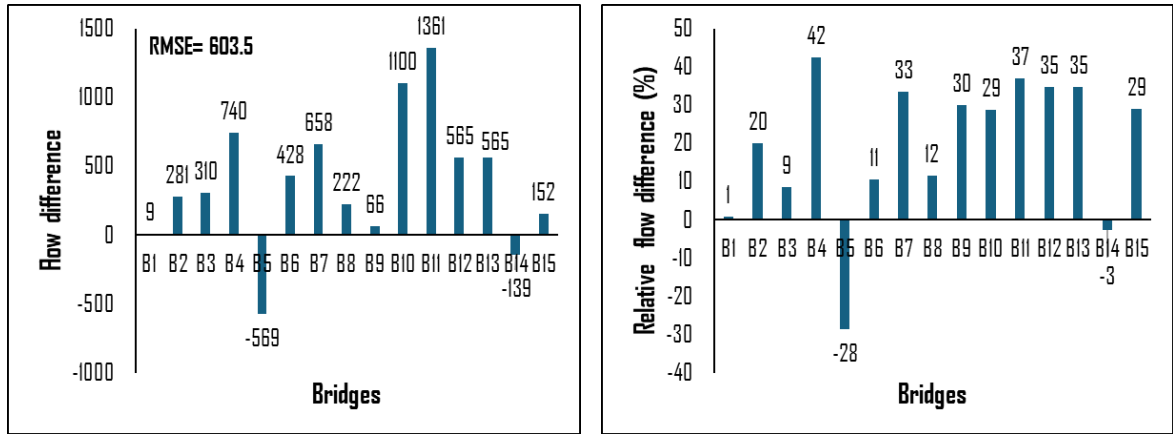


Figure 5.20. The Winnipeg network: Link flow difference visualized on GIS map.

Figure 5.20 illustrates that larger differences were observed in links near the CBD. Notably, flow discrepancies between the two models were pronounced for bridges near the CBD, gradually diminishing with distance from the CBD. Figure 5.21 further elaborates on the link flow differences at  $M = 2$ .



(a) Absolute differences of bridge flows. (b) Relative differences of bridge flows.

Figure 5.21. Equilibrium link flow differences for IAPL-MNL and MNL-SUE models.

Figure 5.21 demonstrates that the MNL-SUE model substantially underestimated bridge flows for all bridges except B5 and B14, with the most pronounced underestimations observed for B4 and B11. Conversely, it overestimated flows for B5 and B14. These discrepancies suggest that incorporating the hierarchical relationship between bridge and route choices, along with the availability perception of bridge choice alternatives, as done by the developed IAPL-MNL-SUE model, may be crucial for achieving plausible equilibrium traffic assignment.

### 5.3.3 Discussion on practical implications

While prior research acknowledges bridges as critical infrastructure or contextual factors in route choice, our study advances policy relevance by quantifying how travelers perceive bridges as cognitive landmarks—hierarchically shaping their route decisions—and how these perceptions propagate into network-wide traffic patterns under equilibrium. Unlike past studies that focus narrowly on how bridges influence individual route choices, our model connects traveler behavior — like avoiding bridges or choosing routes based on them — to traffic patterns across the entire network. This can potentially allow policymakers to predict

how actions targeting bridges (e.g., tolls, closures, upgrades) shift congestion throughout the system.

## **5.4 Chapter summary**

This chapter developed a new joint bridge-route choice model, incorporating an implicit availability/perception logit model for bridge choice and a multinomial logit model for route choice (IAPL-MNL). The hierarchical structure of this joint model reflects the complex decision-making processes in urban mobility, where bridges often serve as critical points, particularly in bridge-centric transport networks. The availability perception characteristics capture the viability of bridge choice alternatives. Additionally, it developed a corresponding network equilibrium TA model (IAPL-MNL-SUE) and a customized route-based solution algorithm with bridge-centric choice set generation. These models and the solution algorithm acknowledge bridges as pivotal elements within transportation networks and align well with strategic transport policy objectives, which might prioritize the management of bridge congestion.

Next chapter applies the developed bridge-centric network equilibrium framework to bridge criticality analysis.



## CHAPTER 6

# Proactive disruption mitigation: Bridge criticality analysis with a bridge-centric traffic assignment framework

---

The previous chapter developed a bridge-centric network equilibrium traffic assignment (TA) framework that effectively captured the impact of bridges on individual route choices and network flows. In this chapter, the developed bridge-centric TA framework is integrated into a selected link criticality analysis method. The properties of the method are demonstrated, and it is then applied to analyze bridge criticality in a large-scale bridge-centric transport network.

### 6.1 Motivation

Bridges are critical components of bridge-centric transport networks (i.e., networks spanned by natural barriers and connected by bridges). They play a vital role in connecting parts of the network divided by obstacles such as rivers, making them essential for reaching certain destinations. However, they are also costly to design, construct, and maintain ([Argyroudis et al., 2019](#), [Bocchini and Frangopol, 2011](#), [Kurth et al., 2020](#)). Bridges are elevated from the ground. They consist of three main components: foundation (includes piles, caps, and bents), substructure (includes abutments, piers, and pier caps), and superstructure (includes girders, bearings, trusses, decks, barriers, and arches) ([Hancilar et al., 2013](#), [Singh et al., 2002](#)). Thus, bridges are more important and vulnerable than ordinary road segments ([Capacci et al., 2022](#)).

Disruption of bridges may result in high socio-economic losses. Structural complexity makes bridges more vulnerable to hazards than ordinary roads. For example, earthquakes can dislocate permanently abutment walls or cause bridge deck to pound against abutment walls (Fakharifar et al., 2015); floods can induce scours undermining piers and abutments (Tubaldi et al., 2022); and hydraulic forces from high water levels and strong currents can potentially lead to settlement or tilting (Sullivan et al., 2024). The structural complexity also leads to considerably more time and cost required for repairing bridges than repairing road segments. Additionally, bridge collapses can have far more severe consequences than road segment failures. For example, a failure of a single bridge can hinder movement of people and goods in a region for months or years beyond lives lost and the costs of replacement (Adam et al., 2024). All these factors can result in substantial socio-economic losses (Zhang et al., 2023).

Because of high and long-term potential socio-economic losses that bridge disruption can cause, assessing the criticality of bridges in the road networks divided by natural obstacles is of paramount importance for prioritizing disaster mitigation efforts. However, the essential functional importance of bridges, including their impacts on individual route choices and network flows, and their structural vulnerability have not been sufficiently emphasized in existing link criticality analysis methods. Traditional TA models used in link criticality analysis tend to treat all network links as uniformly important, making no distinction between bridges and ordinary road segments (Alizadeh et al., 2018, Habib et al., 2013, Manley et al., 2015). On the other hand, although road link failures often allow for quicker recovery compared to bridges, due to less complex repairs (Singh et al., 2002) and the availability of alternative routes (Tubaldi et al., 2022), some road links can still remain more critical functionally than some bridges. Their failure can disrupt network operations to an extent that exceeds the potential impact of certain bridge collapses (Kurth et al., 2020). These suggest that proactive disruption mitigation may require an approach that would be able to

endogenously find a trade-off between acknowledging potential high negative consequences of bridge collapses and respecting functional importance of ordinary road links for normal operation of bridge-centric transport networks.

This chapter advances the link criticality index (LCI) method introduced in Chapter 3 by integrating the bridge-centric TA framework from Chapter 5 and incorporating structural vulnerability considerations. This approach recognizes the higher structural vulnerability of bridges and their greater impact on the route choice process compared to ordinary road segments when assessing link criticality. In contrast to previous chapters where bridge criticalities were discussed in isolation from other network links, this chapter compares the criticalities of bridges with those of other network links.

The structure of this chapter is as follows: Section 6.2 presents the bridge-centric link criticality analysis method. Section 6.3 details the experimental design and discusses the results. Section 6.4 offers concluding remarks.

## **6.2 Bridge-centric link criticality analysis methodology**

This section provides a brief introduction to the bridge-centric TA framework developed in Chapter 5 and elaborates on the advancements of the LCI method introduced in this chapter.

### **6.2.1 Bridge-centric network equilibrium framework**

This chapter adopts a bridge-centric TA framework developed in Chapter 5. The bridge-centric TA framework includes an intricate mathematical network model, a new joint bridge-route choice model, a corresponding TA model, and a customized route-based solution algorithm.

### *Bridge-centric transport network model*

Road network models used in conventional TA models do not distinguish between bridge links and common road segment links. They treat all network links uniformly. The bridge-centric transport network model makes this distinction, emphasizing bridges as critical infrastructure elements as shown in Figure 6.1. The bridge-centric transport network model can be considered as a generalization of conventional road network models.

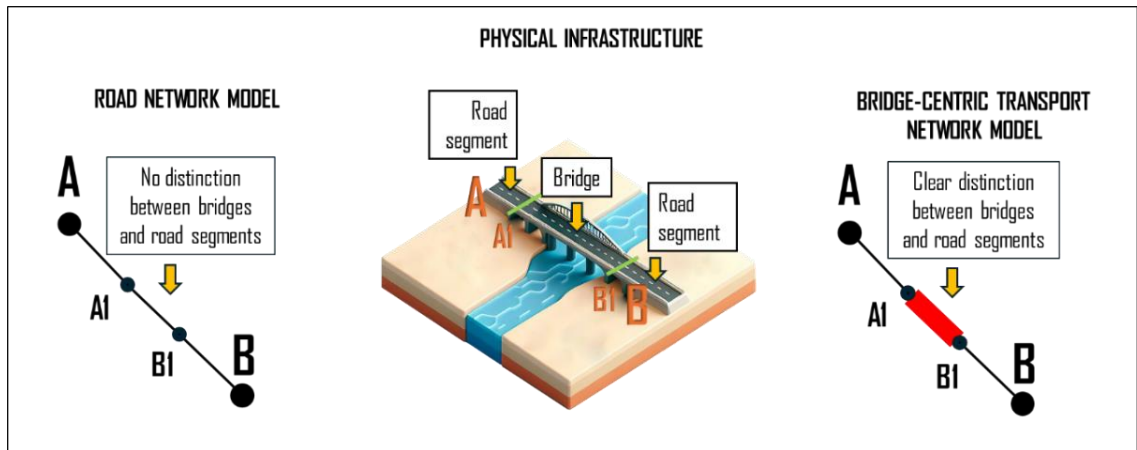


Figure 6.1. Network models: Road network vs. bridge-centric transport network.

### *Joint bridge-route choice model*

Multiple empirical studies have reported hierarchical relationships between bridge and route choices, implying that routes are chosen conditional on bridge choices (Alizadeh et al., 2018). The joint bridge-route choice model adopted in this study is a nested model, incorporating the implicit availability perception logit (IAPL) model for managing the availability perception of bridge choice alternatives and the bridge choice itself, along with the MNL model for route choice (IAPL-MNL). In the IAPL-MNL model, bridge choice alternatives are O-D specific and may include more than one bridge represented by bridge sequences, i.e., the specific order that bridges are used. Different orders of the same combination of bridges are represented by different bridge sequences, as changing the order can make the bridge choice alternative infeasible (e.g., no connection to the second bridge if

the first is missing). At the marginal choice level, each bridge choice alternative forms a bridge nest; at the conditional choice level, each route belongs to a single bridge nest. It is worth emphasizing that this model has a closed-form probability expression, which ensures analytical tractability.

The joint bridge-route choice probability  $P_k$  can be stated as a multiplication of the route choice probability conditional  $P_{k|b}$  on bridge nest and the marginal probability of bridge nest  $P_b$  as follows:

$$P_k = P_{k|b} \cdot P_b, \quad \forall b \in B, \forall k \in K_b \quad (6.1)$$

where the conditional probability of selecting route  $k$  in nest  $b$  is modeled by MNL:

$$P_{k|b} = \frac{e^{-\theta c_k}}{\sum_{j \in K_b} e^{-\theta c_j}}, \quad \forall b \in B, \forall k \in K_b \quad (6.2)$$

and the marginal probability of bridge nest  $b$  is modeled by IAPL:

$$P_b = \frac{\left[ \sum_{k \in K_b} e^{-\theta \left( c_k - \left( \ln \bar{\mu}_b - \frac{1 - \bar{\mu}_b}{2 \bar{\mu}_b} \right) \right)} \right]^{\frac{\eta}{\theta}}}{\sum_{h \in B} \left[ \sum_{k \in K_h} e^{-\theta \left( c_k - \left( \ln \bar{\mu}_h - \frac{1 - \bar{\mu}_h}{2 \bar{\mu}_h} \right) \right)} \right]^{\frac{\eta}{\theta}}}, \quad \forall b \in B \quad (6.3)$$

where  $B$  is a set of bridge nests;  $K_b$  is set of routes that passes through bridge nest  $b$ ;  $\theta$  and  $\eta$  are scaling parameters at the route choice and bridge choice levels, respectively;  $c_k$  is deterministic travel time for route  $k$ ; and  $\bar{\mu}_b$  is expected value of availability perception of bridge choice alternative  $b$  specified as a binomial logit model:

$$\bar{\mu}_b = \frac{1}{1 + e^{\beta Y_b}}, \quad \forall b \in B \quad (6.4)$$

where  $Y_b$  is availability perception attribute of bridge choice alternative  $b$  and  $\beta$  is a corresponding scaling parameter. The availability perception value serves two objectives: truncating unreasonably distant bridge choice alternatives and modeling intermediate

availability degrees to address potential bridge choice set misspecification. For more information on the availability perception value, an interested reader may refer to Chapter 5.

#### *Equivalent mathematical programming (MP) formulation*

This section presents an equivalent MP formulation for the joint bridge-route choice IAPL-MNL model. The adopted TA model is referred to as IAPL-MNL-SUE.

Mathematically, the SUE conditions are expressed in (6.5):

$$f_k^w = q^w \cdot P_k^w(f_k^w), \quad \forall w \in W, \forall b \in B^w, \forall k \in K_b^w, \quad (6.5)$$

where  $W$  is set of all O-D pairs,  $K_b^w$  is set of routes between O-D pair  $w$ ,  $q^w$  is travel demand between O-D pair  $w$ ,  $f_k^w$  is traffic flow on route  $k$  between O-D pair  $w$ ,  $P_k^w$  is probability of choosing route  $k$  using bridge choice alternative  $b$  between O-D pair  $w$ . The probability expression for the IAPL-MNL bridge-route choice model is given in (6.1).

To be consistent with the utility maximization behavior underlying the hierarchical choice structure (Ben-Akiva and Lerman, 1985a), the dispersion (scale) parameters at different choice levels must satisfy the condition that  $\theta > \eta$ . To facilitate the formulation of the developed equilibrium model with multiple choice levels, the dispersion parameters are re-expressed as  $\theta_r = \theta$ ,  $\frac{1}{\theta_b} = \frac{1}{\eta} - \frac{1}{\theta}$ . Owing to the above condition on dispersion parameters,

$$\theta_r, \theta_b > 0.$$

The resulting SUE model is formulated as an equivalent MP problem:

$$\begin{aligned} \min_f Z = & \sum_{a \in A_C} \int_0^{x_a} ct_a(v)dv + \sum_{a \in A_B} \int_0^{x_a} bt_a(v)dv + \frac{1}{\theta_r} \sum_{w \in W_C} \sum_{k \in K^w} f_k^w \ln f_k^w \\ & + \frac{1}{\theta_r} \sum_{w \in W_B} \sum_{b \in B^w} \sum_{k \in K_b^w} f_k^w \ln f_k^w + \frac{1}{\theta_b} \sum_{w \in W_B} \sum_{b \in B^w} q_b^w \ln(q_b^w) \\ & - \sum_{w \in W_B} \sum_{b \in B^w} q_b^w \left( \ln \bar{\mu}_b - \frac{1 - \bar{\mu}_b}{2\bar{\mu}_b} \right) \end{aligned} \quad (6.6)$$

subject to

$$\sum_{k \in K^w} f_k^w = q^w, \quad \forall w \in W_C \quad (6.7)$$

$$\sum_{k \in K_b^w} f_k^w = q_b^w, \quad \forall w \in W_B, b \in B^w \quad (6.8)$$

$$\sum_{b \in B^w} q_b^w = q^w, \quad \forall w \in W_B \quad (6.9)$$

$$f_k^w \geq 0, \quad \forall w \in W, k \in K^w \quad (6.10)$$

$$q_b^w \geq 0, \quad \forall w \in W_B, b \in B^w \quad (6.11)$$

$$x_a = \sum_{w \in W} \sum_{k \in K^w} f_k^w \delta_{a,k}^w, \quad \forall a \quad (6.12)$$

where  $A_C$  is set of common links,  $A_B$  is set of bridge links,  $W_C$  is set of common O-D pairs that do not need bridges,  $W_B$  is a set of O-D pairs that need bridges,  $B^w$  is subset of bridges for O-D pair  $w$ ,  $\delta_{a,k}^w$  is a route-link incidence indicator,  $x_a$  is traffic flow on link  $a$ ,  $ct_a(\cdot)$  is travel time on common link  $a$ ,  $bt_a(\cdot)$  is travel time on bridge link  $a$ ,  $q_b^w$  is traffic flow passing through bridge nest  $b$  between O-D pair  $w$ ,  $q^w$  is travel demand between O-D pair  $w$ , respectively.

This study customizes a route-based partial linearization algorithm for bridge-centric TA model. First, the bridge choice set is explicitly generated prior to the iterative network equilibration process. Then, within the iterative equilibration process, the route choice set is implicitly generated based on the bridge choice set using a multi-step column generation algorithm, ensuring routes pass through specified bridges. Network flows are updated using a route-based partial linearization algorithm as explained in [Patriksson \(1994\)](#).

### 6.2.2 Bridge-centric link criticality index

Earlier LCI methods could not plausibly capture the criticality of bridges for two main reasons. First, they rely on conventional TA models that overlook the hierarchical relationship between bridges and routes. Second, they fail to account for bridges' higher structural vulnerabilities compared to ordinary road segments. This omission can lead to equal criticality

values being assigned to both types of links representing bridges and ordinary road segments, as shown in Figure 6.2.

Figure 6.2 provides an illustrative example with a single-route network where all links appear equally critical if no distinction is made between links representing bridges and ordinary road segments. However, as previously noted, bridge links often hold greater criticality due to their structural complexity, high reconstruction costs, and extended repair timelines.

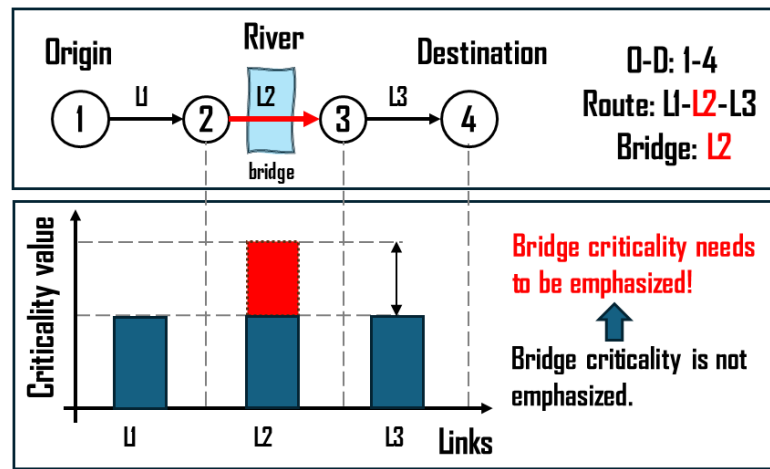


Figure 6.2. Rationale for incorporating structural vulnerability weights into LCI.

This chapter advances the LCI method by integrating the IAPL-MNL-SUE TA model and a structural vulnerability coefficient,  $\varphi_a$ , for each link  $a \in A$ . This integration enables the efficient identification of links that are both functionally critical and structurally vulnerable. The method introduced in this section is termed the bridge-centric LCI method. The bridge-centric LCI method is schematically shown in Figure 6.3.



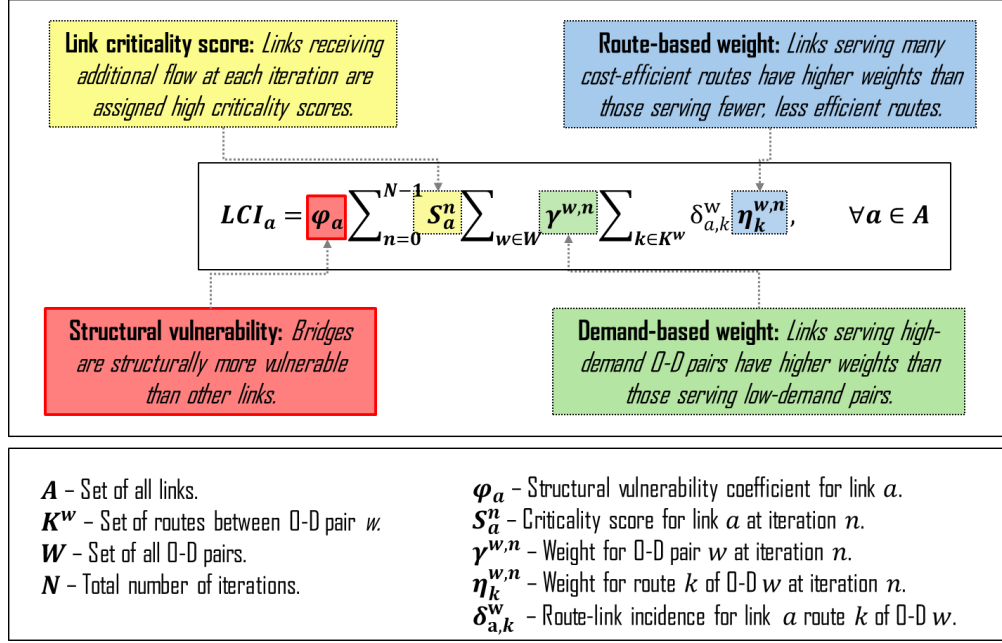


Figure 6.3. Bridge-centric link criticality index.

Typically, vulnerability coefficients  $\varphi_a, \forall a$  are derived from fragility curves (Argyroudis et al., 2019), which estimate the likelihood of infrastructure failure under various hazard intensities. To plausibly capture the higher structural vulnerability of bridges compared to ordinary road segments, without aiming to replicate reality precisely, we manually assign higher structural vulnerability coefficients to bridge links. These coefficients range from 0 (least vulnerable) to 1 (most vulnerable). Additionally, sensitivity analysis on this coefficient is conducted in numerical experiments to evaluate its impact on the results. For a more accurate representation, fragility curves should be calibrated using real-world data.

The link criticality score  $S_a^n$  is calculated as the product of a link's additional flow at iteration  $n + 1$  and its marginal cost (MC):

$$S_a^n = \max([x_a^{n+1} - x_a^n], 1.0) \cdot \frac{mc_a(x_a^n)}{t_a(x_a^n)}, \quad \forall a \in A, \forall n \in N \quad (6.13)$$

where  $x_a^n$  is flow through link  $a$  at iteration  $n$ ,  $mc_a$  is MC on link  $a$ . The latter is calculated as follows:

$$mc_a(x_a^n) = t_a(x_a^n) + x_a^n t'_a(x_a^n), \quad \forall a \in A \quad (6.14)$$

where  $t_a$  is travel time on link  $a$ , and  $t'_a$  is the derivative of link travel time with respect to its flow.

Link criticality score is a local metric that overlooks a link's network role. Weighing it by demand-based (6.15) and route-based (6.16) factors can incorporate network connectivity information effectively.

$$\gamma^w = \frac{q^w}{Q}, \quad \forall w \in W \quad (6.15)$$

where  $q^w$  denotes travel demand of O-D pair  $w$  and  $Q$  denotes total network travel demand.

$$\eta_k^{w,n} = \frac{1/C_k^{w,n}}{\sum_{i \in K^w} 1/C_i^{w,n}}, \quad \forall w \in W, \forall k \in K^w, \forall n \in N \quad (6.16)$$

where  $C_k^{w,n}$  is perceived travel cost on route  $k$  for O-D pair  $w$  at iteration  $n$ .

### 6.3 Numerical experiments

This section conducts three experiments, in which the properties of the bridge-centric LCI method were analyzed showing its practical feasibility for bridge criticality assessment as shown in Table 6.1.

Table 6.1. Analyzing feature impacts on bridge criticality across experiments.

Features	Experiment 1: Toy network	Experiment 2: Nguyen-Dupuis	Experiment 3: Winnipeg
1 Joint bridge-route choice	✓	✓	✓
2 Congestion effects	✓	✓	✓
3 Multiple O-D pairs		✓	✓
4 Network structure		✓	✓
5 Choice set		✓	✓
6 Non-uniform travel demand		✓	✓
7 Bridge choice alternatives with multiple bridges			✓
8 Structural vulnerability coefficient			✓

Throughout this section, the following parameter settings for joint bridge-route choice model were used unless otherwise specified: the availability attribute scaling parameter  $\beta$  was

set at 0.3, the structural vulnerability coefficient was set to 1, the scaling parameters  $\theta$  and  $\eta$  were set at 1.0 and 0.5, respectively.

In this chapter, availability perception is defined at a disaggregated level for bridge choice alternatives, which may include multiple bridges. To apply this concept to individual bridges, the availability perception values are aggregated as follows:

$$\hat{\mu}_a = \sum_{b \in B} \bar{\mu}_b, \quad \forall a \in A_B \quad (6.17)$$

where  $A_B$  is set of all bridges,  $B$  is set of all bridge choice alternatives,  $\hat{\mu}_a$  is availability perception of bridge  $a$ , and  $\bar{\mu}_b$  is expected availability perception of bridge choice alternative  $b$ .

To facilitate the comparison of LCI values derived from different TA models, these values were normalized to fall within the range of 0 to 1, i.e.:

$$\widetilde{LCI}_a = \frac{LCI_a}{\sum_{i \in A} LCI_i}, \quad \forall a \in A \quad (6.18)$$

and

$$\sum_{a \in A} \widetilde{LCI}_a = 1.0 \quad (6.19)$$

### 6.3.1 Experiment 1: A toy bridge-centric transport network

This section analyses the properties of the bridge-centric LCI method using the toy network in Figure 6.4. It investigates the impact of joint bridge-route choice TA model on link criticality values. Sensitivity analysis is then conducted for the key parameters of the underlying bridge-centric TA model.

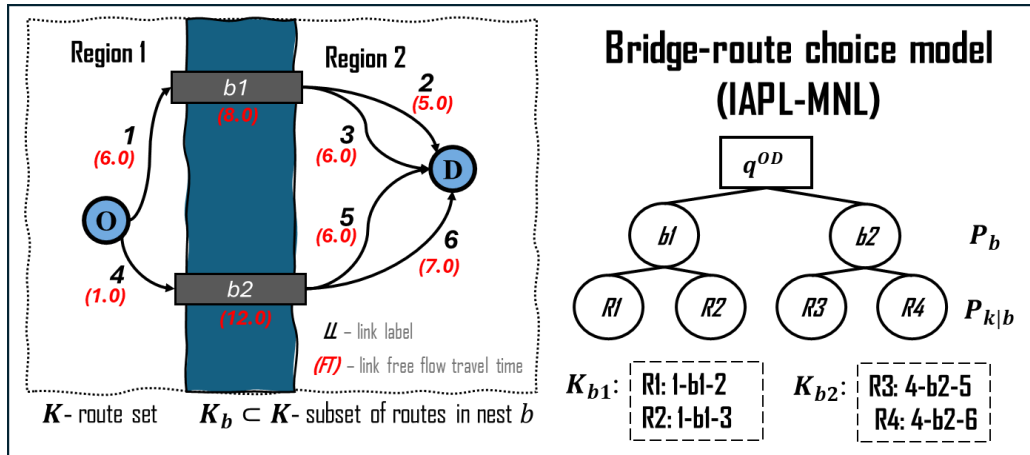


Figure 6.4. A toy network and structure of the corresponding joint bridge-route choice model.

As shown in Figure 6.4, the network is divided by a river into two regions, connected by two bridges. It consists of eight links and a single O-D pair with four routes. Routes  $R1$  and  $R2$  use bridge  $b1$ , while routes  $R3$  and  $R4$  use bridge  $b2$ . It can be interpreted as travelers choosing among four routes conditioned on two bridges. Link free-flow travel times (FFTT) are provided in Figure 6.4. Routes  $R1$  and  $R3$  have the shortest FFTT values of 19. Routes  $R2$  and  $R4$  have FFTT values of 20. The O-D demand is set at 30.

The network is designed so that Link 1, Link 2,  $b1$ , and  $b2$  are expected to have higher criticality values than the other links in the network due to their critical role in connecting the O-D pair. Moreover, Link 1 and bridge  $b1$ , shared by  $R1$  and  $R2$ , are expected to have identical criticality values because they are adjacent to each other and equally important for the connection, as are Link 4 and bridge  $b2$ , shared by  $R3$  and  $R4$ . Depending on the selected TA model, either Link 1 and  $b1$  or Link 4 and  $b2$  can be ranked higher.

The impact of TA models on link criticality values is explored in the subsection below.

### 6.3.1.1 Impact of TA model on bridge criticality

This subsection evaluates and compares the MNL-SUE LCI proposed in Chapter 3 and the bridge-centric LCI method proposed in the current chapter. The results are summarized in Table 6.2, Figure 6.5, and Figure 6.6.

Table 6.2 provides link criticality values and corresponding criticality ranks for the LCI methods based on the selected models.

Table 6.2. Criticality values for MNL-SUE and bridge-centric LCI.

Link label	MNL-SUE LCI			Bridge-centric LCI		
	LCI	Norm. LCI	Criticality rank	LCI	Norm. LCI	Criticality rank
<b>b1</b>	<b>152.77</b>	<b>0.203</b>	<b>2</b>	<b>156.31</b>	<b>0.227</b>	<b>1</b>
<b>b2</b>	<b>157.08</b>	<b>0.208</b>	<b>1</b>	<b>128.12</b>	<b>0.186</b>	<b>2</b>
1	152.77	0.203	2	156.31	0.227	1
2	39.52	0.052	3	42.06	0.061	3
3	27.75	0.037	6	21.64	0.031	5
4	157.08	0.208	1	128.12	0.186	2
5	38.22	0.051	4	35.47	0.052	4
6	28.84	0.038	5	19.43	0.028	6

As shown in Table 6.2, the choice of TA model can, indeed, affect link criticality ranks. The MNL-SUE LCI method ranked Link 1 and *b1* lower than Link 4 and *b2*, whereas the bridge-centric LCI method ranked Link 1 and *b1* higher than Link 4 and *b2*. One feasible explanation is that, unlike the MNL-SUE model, the IAPL-MNL-SUE model considers bridge availability perception, influencing joint bridge-route choice probabilities. With availability perception values of 0.92 for *b1* and 0.08 for *b2*, it is reasonable that the bridge (*b1*) that was perceived more available and the upstream link (Link 1) received a higher criticality value.

Figure 6.5 complements Table 6.2 by displaying normalized link criticality values in descending order for the two LCI methods, visually highlighting the magnitude of criticality values across different ranks within each method and between the methods.

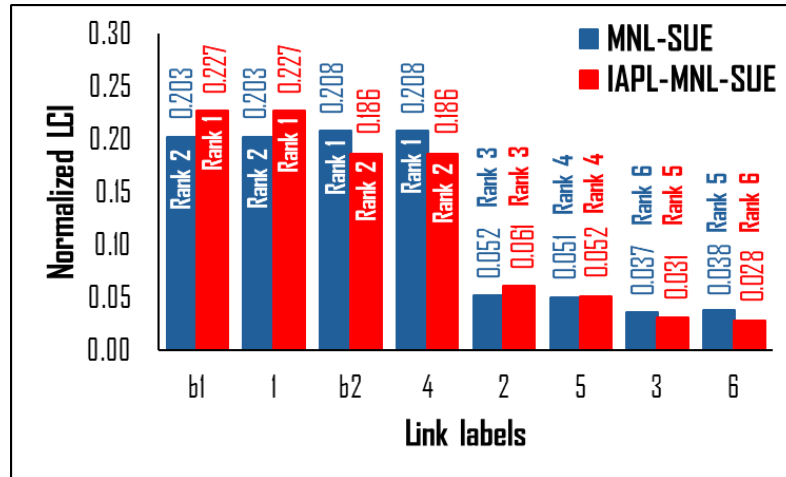
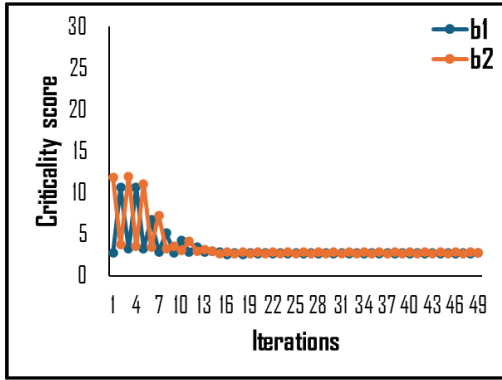


Figure 6.5. Sorted criticality values for MNL-SUE LCI and bridge-centric LCI methods.

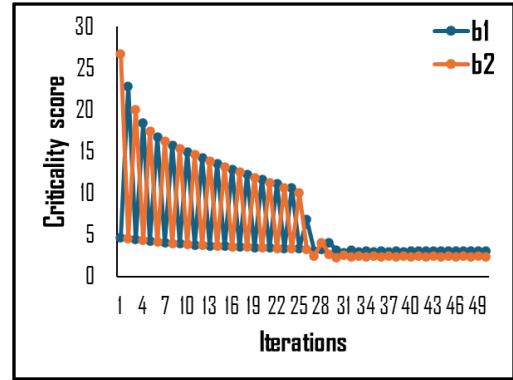
Figure 6.5 shows that Link 1, Link 4, *b1*, and *b2* had substantially higher LCI values than other links as expected. Notably, the magnitude difference between rank 1 and rank 2 links was almost 10 times greater for the bridge-centric LCI method (i.e.,  $0.227 - 0.186 = 0.041$ ) compared to the MNL-SUE LCI method (i.e.,  $0.208 - 0.203 = 0.005$ ). The significant difference in availability perception values for the two bridges (0.92 for *b1* and 0.08 for *b2*) could also cause the large criticality magnitude difference between rank 1 and rank 2 links.

Figure 6.6 elaborates on the criticality values of bridges, breaking them down by components and first 49 iterations. It facilitates the explanation why the bridge-centric LCI method ranked Link 1 and *b1* higher than Link 4 and *b2*, while the MNL-SUE LCI method did the opposite.

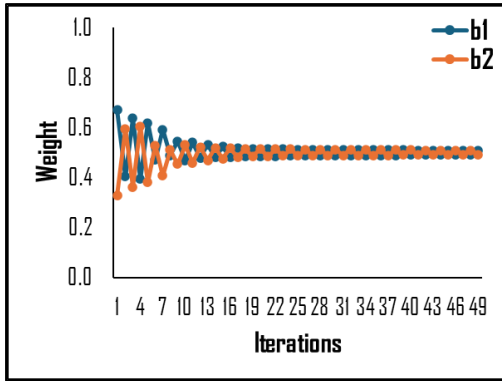
Figure 6.6 shows that the LCI methods oscillate, with greater oscillation in the IAPL-MNL-SUE-based method than in the MNL-SUE-based method. These oscillations damped with iterations. It seems that the MNL-SUE-based method ranked *b2* higher than *b1* due to slightly higher criticality scores (Figure 6.6a). However, the magnitudes of the final LCI values of these bridges were visually similar (Figure 6.6e). Conversely, the bridge-centric method ranked *b1* higher than *b2* due to dominant weights (Figure 6.6d), resulting in noticeably different final criticality values (Figure 6.6f).



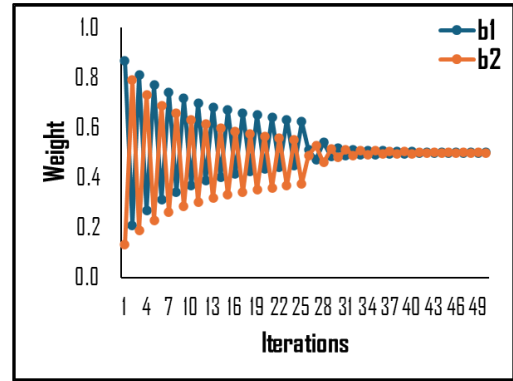
(a) Criticality scores: MNL-SUE.



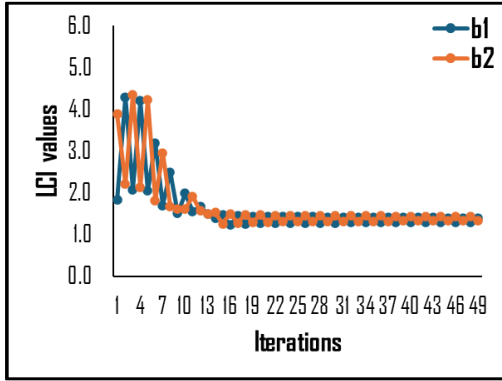
(b) Criticality scores: IAPL-MNL-SUE.



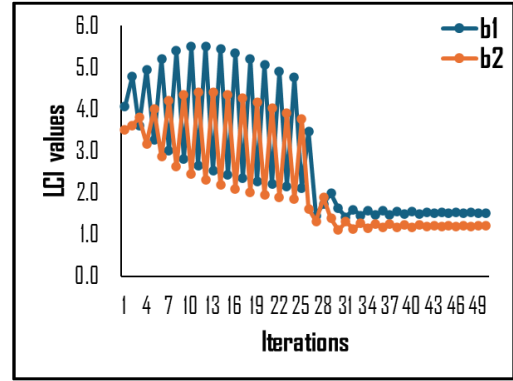
(c) Combined weight: MNL-SUE.



(d) Combined weight: IAPL-MNL-SUE.



(e) LCI values: MNL-SUE.



(f) LCI values: IAPL-MNL-SUE.

Figure 6.6. Decomposition of two LCI methods by components and iteration.

This subsection compared the link criticality values of the MNL-SUE LCI and bridge-centric LCI methods. The results suggest that the criticality of links in routes crossing bridges perceived as more available can be significantly underestimated, while the criticality of links in routes crossing bridges perceived as less available can be substantially overestimated. The

next section performs sensitivity analysis for the key parameters of the bridge-centric TA model and analyzes how these parameters impact the corresponding LCI method.

### 6.3.1.2 Sensitivity analysis

This subsection conducts sensitivity analysis for the key parameters of the adopted bridge-centric TA model and investigates their impact on the corresponding LCI method. The results are summarized in Figure 6.7 - Figure 6.9.

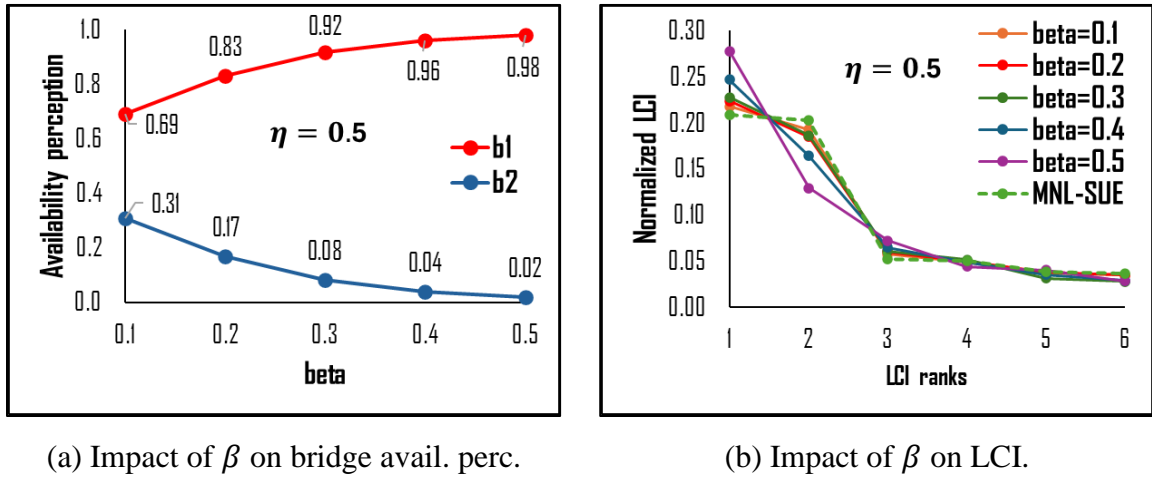


Figure 6.7. Sensitivity analysis for parameter  $\beta$  of the IAPL-MNL-SUE model.

Parameter  $\beta$  scales the availability perception attribute, influencing travelers' sensitivity to perceived availability of bridge choice alternatives. Figure 6.7a shows that increasing  $\beta$  raised the availability perception of bridge  $b1$  and lowers it for bridge  $b2$ . Adjusting  $\beta$  modifies these perceptions. Figure 6.7b demonstrates that at low  $\beta$  levels, bridge-centric LCI values were close to the MNL-SUE-based values but diverge as  $\beta$  increased. This indicates that the bridge-centric LCI method offers greater flexibility in controlling link criticality values by adjusting  $\beta$ .

Figure 6.8 shows that the bridge nest level scaling parameter  $\eta$  has a minimal effect on criticality measures compared to the parameter  $\beta$ , as LCI ranks exhibit negligible variation across different  $\eta$  values.



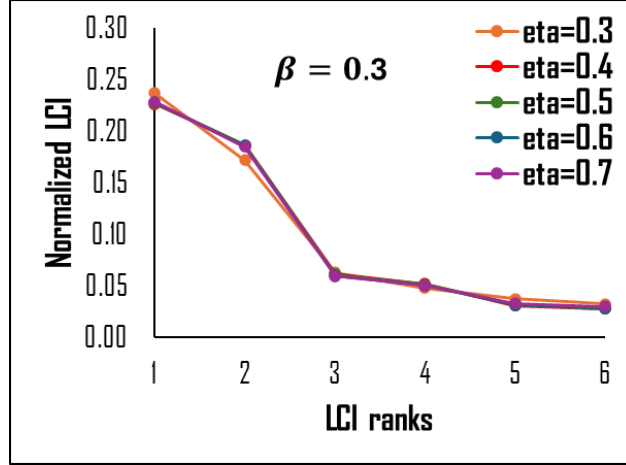


Figure 6.8. Impact of the parameter eta of the bridge-centric TA model on LCI values.

Figure 6.9 indicates that the difference between criticality values of the bridge-centric LCI and MNL-SUE LCI methods vanishes at high demand levels.

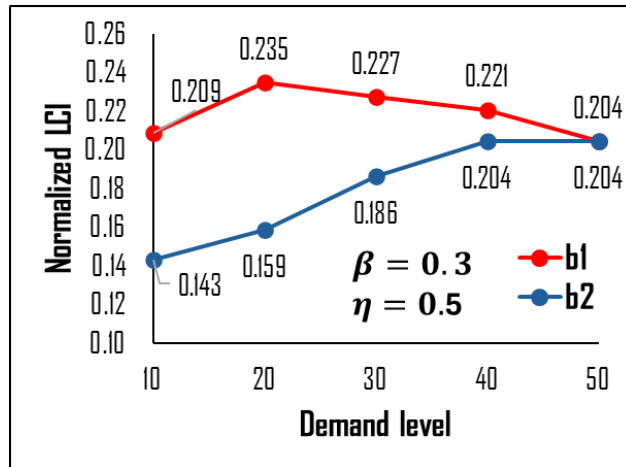


Figure 6.9. Impact of demand level on criticality of bridges.

This section investigated the properties of the bridge-centric LCI method and compared it to the MNL-SUE LCI method using a simple network. The next section applies the developed method to a relatively more complex network with multiple O-D pairs.

### 6.3.2 Experiment 2: The Nguyen-Dupius network

The previous section showed that bridges perceived as more available tended to receive higher criticality scores than those perceived as less available. This section further

investigates the properties of the bridge-centric LCI method. It demonstrates that not only availability perception but also network structure, choice set, and O-D interactions can substantially influence overall link criticalities.

This section adapts the Nguyen-Dupuis network (Figure 6.10). The network comprises 13 nodes, including four zones, and 19 links. It includes four O-D pairs, each with a travel demand of 200. These O-D pairs are connected by a total of 25 routes. The network is divided by a river, with three bridges providing connectivity. For all O-D pairs except (1, 2), routes have no other option but to cross one of the bridges. Figure 6.10 presents the network topology and link characteristics.

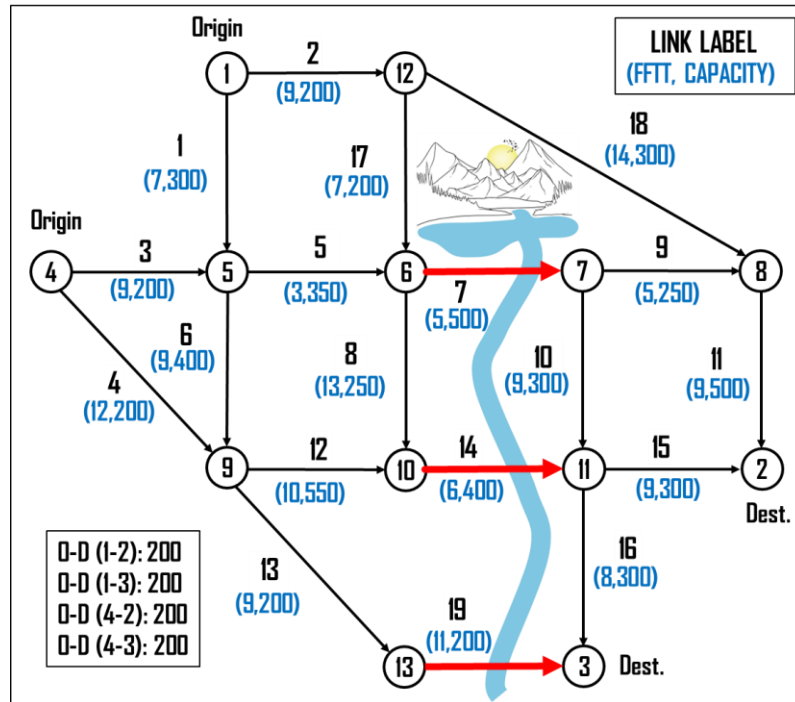


Figure 6.10. The Nguyen-Dupuis bridge-centric transport network.

### 6.3.2.1 Impact of network structure on bridge criticality

This subsection examines the impact of network structure on bridge criticalities, assuming uniform travel demand for all O-D pairs and enumerated bridge and route choices

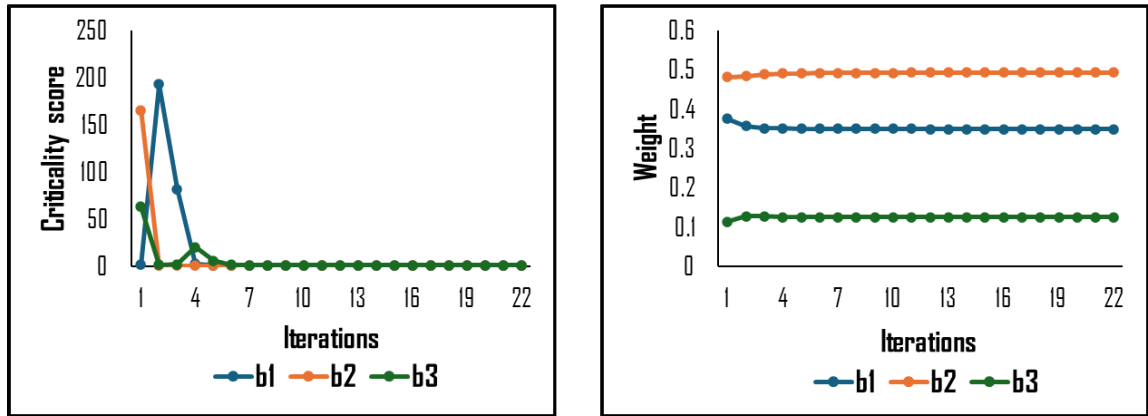
(see Table 6.10). The results are summarized in Table 6.3 and Figure 6.11. The LCI values for all links can be found in Table 6.11 and Table 6.12.

For each bridge, Table 6.3 provides the route numbers for each bridge, their availability perceptions, LCI values, and overall rankings.

Table 6.3. Characteristics of bridges in the Nguyen-Dupius network.

Bridge	Link ID	Route number	Avail. perc.	LCI	Norm. LCI	Overall rank
<i>b1</i>	7	9	1.56	114.45	0.120	2
<i>b2</i>	14	12	1.07	96.74	0.102	3
<i>b3</i>	19	3	1.36	16.26	0.017	16

As shown in Table 6.3, bridge *b2* with a lower availability perception value was assigned with a higher criticality ranking than bridge *b3* with a higher availability perception value. Figure 6.11 presents the criticality scores and their corresponding weights for bridges across the first 22 iterations.



(a) Criticality scores for bridges.

(b) Weights for bridges.

Figure 6.11. Bridge criticality scores and weights for the Nguyen-Dupius network.

As shown in Figure 6.11, bridges *b1* and *b2* had higher criticality scores and weights than bridge *b3*. At first few iterations, bridge *b1* had the highest scores, with *b2* surpassing *b3*. By iteration 5, the algorithm started approaching equilibrium, equalizing the scores (Figure 6.11a). Weights in Figure 6.11b represent the aggregated O-D demand- and route-based weights. Due to uniform O-D demands, the O-D demand-based weights were the same for all links. Therefore, the aggregated weights varied due to the number of routes and their costs.

Bridge *b2*, crossed by 12 routes, had the highest weights, while *b3*, crossed by three routes, had the lowest. These weights, combined with criticality scores, produced the LCI values in Table 6.3.

The bridge-centric LCI method ranks *b2* higher than *b3*, despite *b2* having a lower availability perception value than *b3*, suggesting that higher availability perception values do not always result in higher bridge criticality rankings. A bridge can be ranked high due to its role in facilitating redundancy. Within a single network, it is possible that bridges serving O-D pairs in sparse regions, where redundancy tends to be lower, are ranked lower than those in dense regions, where redundancy is typically higher.

This subsection demonstrated that network structure can influence bridge criticalities, assuming uniform O-D demand and an enumerated choice set. The next subsection investigates how relaxing the enumerated choice set affects bridge criticalities.

#### ***6.3.2.2 Impact of choice set on bridge criticality***

In large-scale networks, it is impractical to enumerate all routes. Instead, analysts create subsets of feasible routes either before or during TA process using various techniques. These subsets can differ in size and composition. This subsection employs a bridge-centric method for generating route choice sets and examines its effect on the criticality of bridges. A uniform travel demand for all O-D pairs is assumed. The results are summarized in Table 6.4 and Figure 6.12. LCI values for all links can be found in Table 6.11 and Table 6.12.

Table 6.4 provides bridge criticalities using the bridge-centric LCI method with both enumerated and implicitly generated route choice sets.

As shown in Table 6.4, the number of routes using bridge *b2* halved from 12 to 6, causing its overall rank to fall from 3rd to 9th. Meanwhile, bridge *b3*'s rank improved by one position, likely due to absorbing some of the flow from bridge *b2*.

Table 6.4. Bridge criticalities: Enumerated vs. implicit choice sets.

Bridge label	Link label	Aggregated avail. perc.	Enumerated choice set			Bridge-centric choice set generation		
			Norm. LCI	Route No.	Rank	Norm. LCI	Route No.	Rank
<i>b1</i>	7	1.56	0.120	9	2	0.133	6	2
<i>b2</i>	14	1.07	0.102	12	3	0.050	6	9
<i>b3</i>	19	1.36	0.017	3	16	0.018	3	15

Figure 6.12 demonstrates the aggregated LCI weights for bridges over the first 22 iterations in two scenarios.

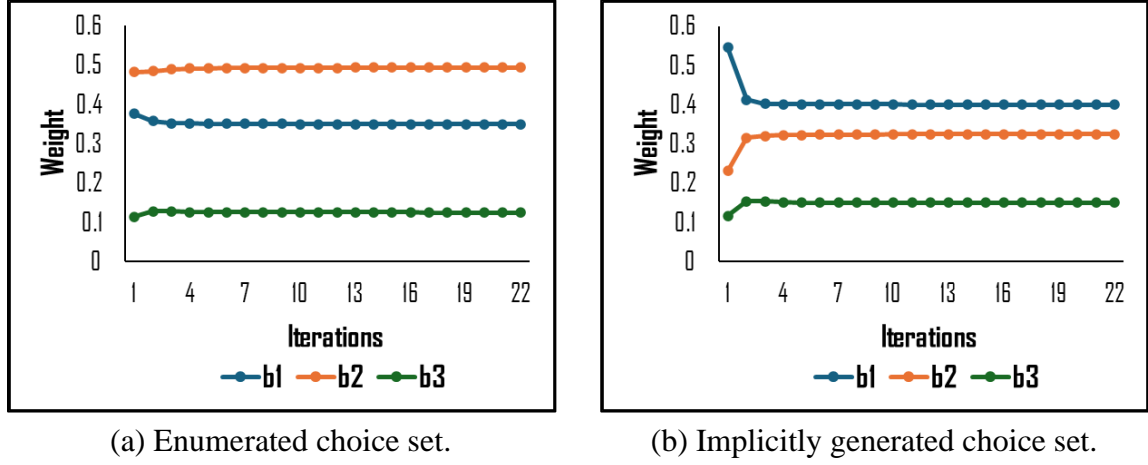


Figure 6.12. Weights for bridges: Enumerated choice set vs. generated choice set.

As shown in Figure 6.12, the aggregated weights for bridge *b2* were the highest in the enumerated route set scenario, but they dropped below the aggregated weights for bridge *b1*. This demonstrates that the method of generating route choices (explicitly or implicitly) can affect the ranking of link criticality. Bridges with a greater number of routes can be assessed as more critical than bridges with a lower number of routes.

This subsection investigated how choice sets can affect bridge criticalities under the assumption of uniform O-D demands. Next subsection relaxes this assumption.

### 6.3.2.3 Impact of non-uniform O-D travel demands on bridge criticality

Previous subsections assumed that all four O-D pairs had the same travel demand levels. However, this assumption does not hold true in practice. Often, O-D pairs in real networks have different travel demands. This subsection investigates how varying travel demands can affect bridge criticalities by increasing the travel demand for the O-D pair (4, 3) from 200 to

400. The results are summarized in Table 6.5 and Figure 6.13. LCI values for all links can be found in Table 6.12.

Table 6.5 provides bridge criticalities using the bridge-centric LCI method with both enumerated and implicitly generated route choice sets for non-uniform O-D demands scenario.

Table 6.5. Bridge criticalities: Non-uniform travel demand.

Bridge label	Link label	Aggregated avail. perc.	Enumerated choice set			Bridge-centric choice set generation		
			Norm. LCI	Route No.	Rank	Norm. LCI	Route No.	Rank
<i>b1</i>	7	1.56	0.058	9	<b>6</b>	0.060	6	<b>5</b>
<i>b2</i>	14	1.07	0.061	12	<b>5</b>	0.046	8	<b>7</b>
<i>b3</i>	19	1.36	0.047	3	<b>8</b>	0.053	3	<b>6</b>

As shown in Table 6.5, the rank of bridge *b2* became higher than the rank of *b1* for the problem with the enumerated choice set. For the problem with the bridge-centric choice set generation, bridge *b1* was ranked the highest, whereas *b3* was ranked higher than *b2*. Figure 6.13 demonstrates the LCI values for bridges over the first 20 iterations for the enumerated and implicitly generated choice sets.

As shown in Figure 6.13a, bridge *b2* received sufficiently high LCI value at first iteration to dominate over the LCI value of bridge *b1*, although the gap between the two was relatively small, for the enumerated choice set scenario. This was due to the redundancy of routes crossing bridge *b2*. However, with implicit choice set generation, bridge *b2*'s initial advantage was eliminated, significantly reducing its LCI value and resulting in its lowest rank (Figure 6.13b). Additionally, the overall rank of bridge *b3* increased, as it connected to node 3, a destination with increased demand. Therefore, non-uniform O-D demands can affect link criticalities.

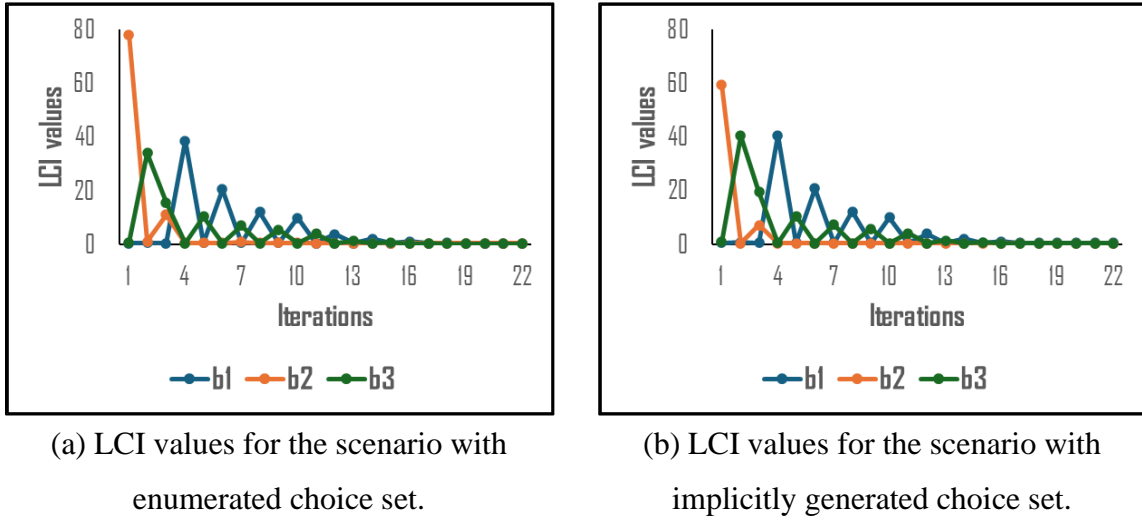


Figure 6.13. LCI values for non-uniform demand: Enumerated vs. generated choice sets.

This section applied the bridge-centric LCI method to a relatively simple network where each bridge choice alternative consisted of a single bridge and demonstrated that, although bridges perceived as more available can be assigned higher criticality values than those perceived as less available, higher availability perception does not always result in higher ranks due to the impacts of network structure, choice set, and non-uniform O-D travel demands. The next section applies the same method to a real-size network, where each bridge choice alternative may consist of a sequence of bridges rather than just a single bridge.

### 6.3.3 Experiment 3: Large-scale bridge-centric transport network

This section analyzes the Winnipeg network - a real-world bridge-centric transport network. The section employs the bridge-centric LCI method and includes a network description, a sensitivity analysis of bridge sequence length, an assessment of computational complexity, and a discussion of the results.

### 6.3.3.1 Descriptive analysis of the Winnipeg network

This subsection analyzes characteristics of the Winnipeg network for a better interpretation of the bridge criticality assessment results. Figure 6.14 depicts the Winnipeg network.

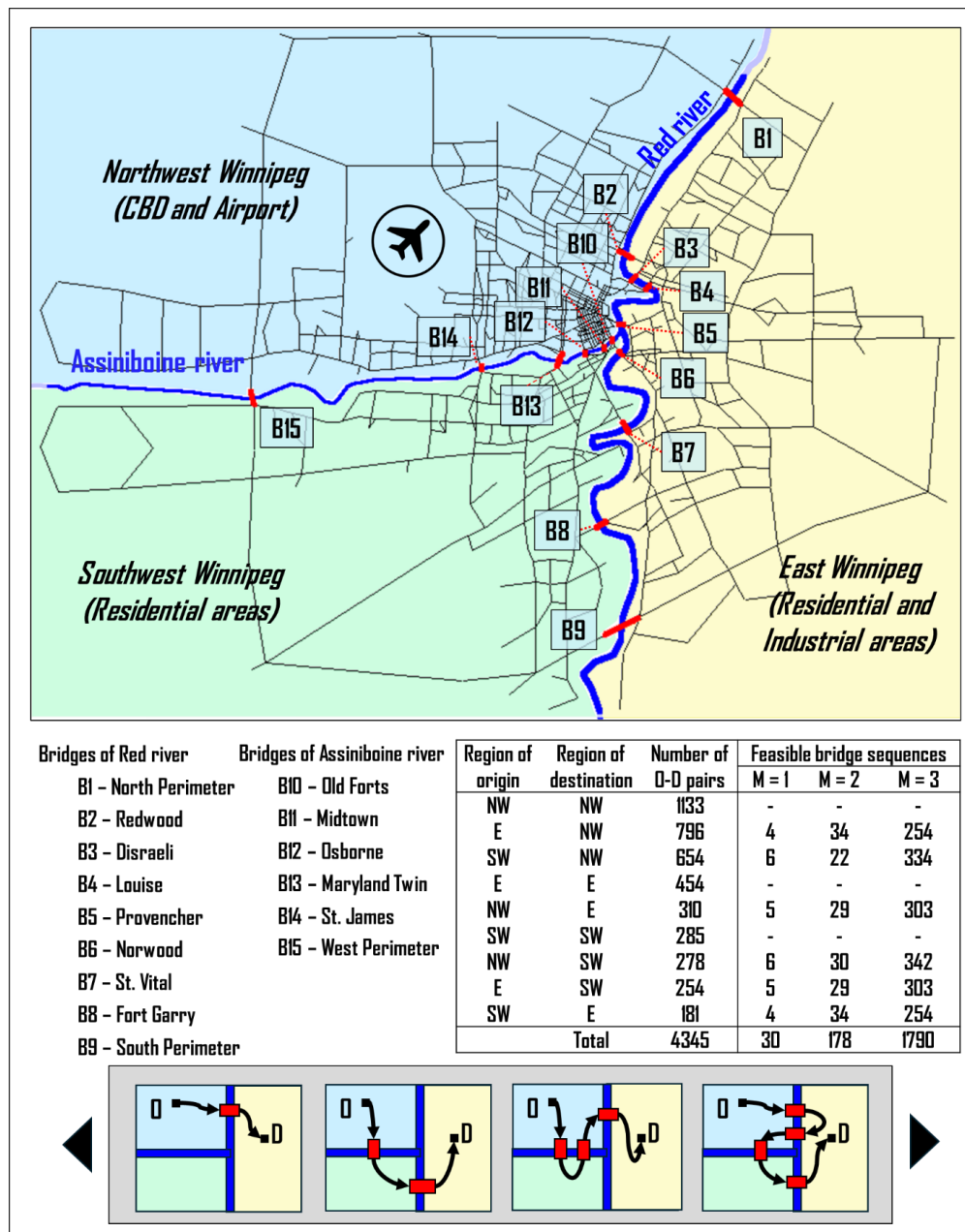


Figure 6.14. The Winnipeg network: Emphasis on bridges.

The Winnipeg network is divided by two rivers into three regions: Northwest (NW), East (E), and Southwest (SW). These regions are connected by 15 bi-directional bridges. The



network comprises 154 zones, 1067 nodes, 2535 links, and 4345 origin-destination (O-D) pairs, with 2473 being mixed-region pairs and the rest single-region pairs. For their trips, travelers of mixed-region O-D pairs consider various bridge options, including single bridges or sequences of multiple bridges. Since bridge choice is not modeled for single-region O-D pairs, their feasible bridge options are not specified in Figure 6.14. However, routes for these O-D pairs can still include bridge crossings. Detailed network topology, link characteristics, and O-D demands are available in the Emme/2 software.

Figure 6.15 provides a visual representation of land use in the Winnipeg network, showing where the main trip production and attraction zones are located.

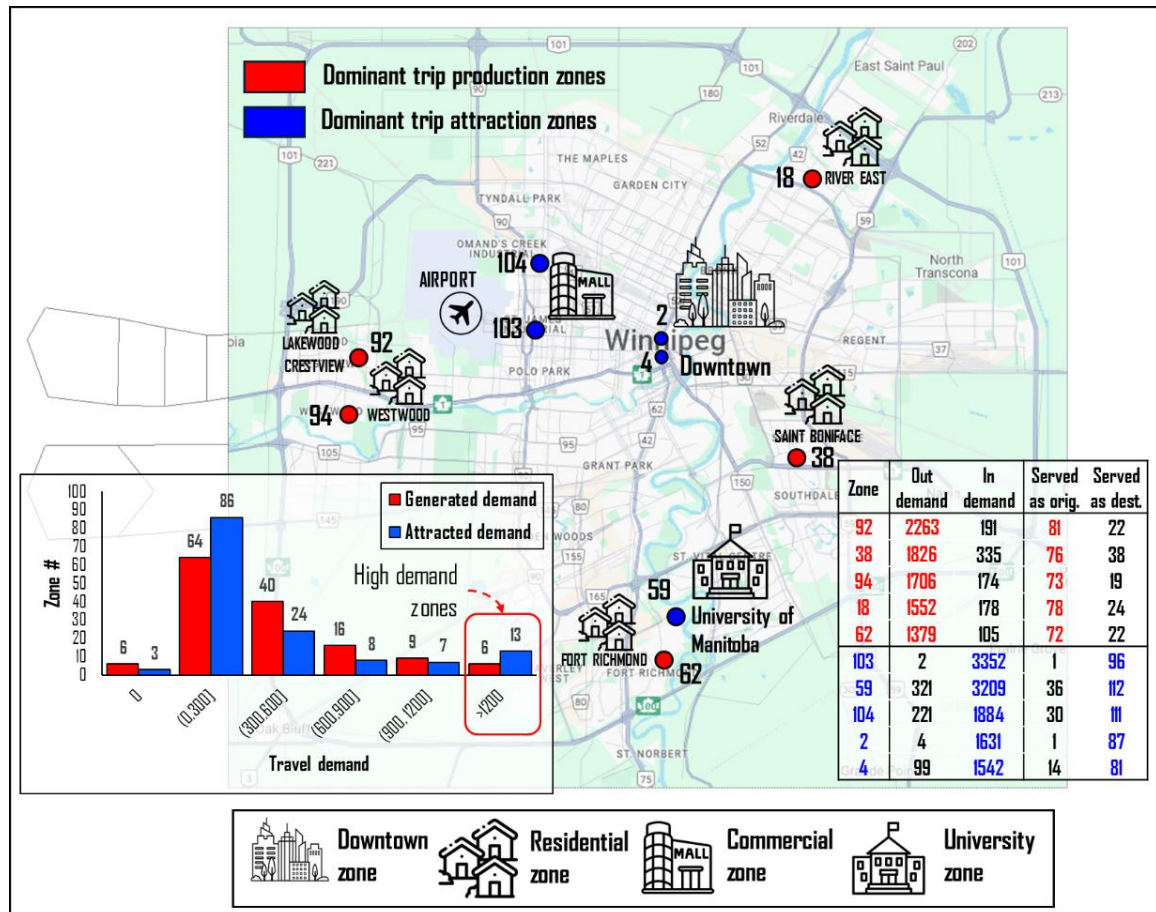


Figure 6.15. Schematic representation of land use in the Winnipeg network.

As shown in Figure 6.15, the NW region included high trip production and attraction zones which encompassed residential, business, and airport areas. Notably, the E and SW



are predominantly single-region. The network topology is sparse near regions with high-demand O-D pairs. Therefore, considering the network's complexity, the distribution of travel demands, and the sparse topology near high-demand areas, it is reasonable to expect that bridges may not be ranked as the most critical elements in the network. The next subsection will perform bridge criticality analysis using the bridge-centric LCI method.

### 6.3.3.2 Model parameter settings

To set model parameters, the total coefficient of variation analysis has been used as described in Chapter 3 and Chapter 5. The parameters of the selected choice models were set such that the mean coefficient of variation  $\overline{CV}$  remained within the range of 10% to 20%. For MNL-SUE, the parameter  $\theta$  was set at 1.0. For IAPL-MNL-SUE, the parameters  $\theta$  and  $\eta$  were set at 1.5 and 0.6, respectively. Parameters  $\alpha$  and  $\beta$  were set at 2 and 0.1.

### 6.3.3.3 Bridge criticality analysis for the Winnipeg network

Table 6.6 shows the Top 5 critical bridges. For simplicity of interpretation, the maximum number of bridges per bridge nest  $M$  was set to 1 for the bridge-centric LCI method and, for the MNL-SUE LCI, it is unrestricted.

Table 6.6. Top 5 critical bridges for the Winnipeg network ( $M=1$ ).

Bridge rank	MNL-SUE LCI					Bridge-centric LCI ( $M=1$ )					
	Bridge	Dir.	Route No.	Norm. LCI	Overall rank	Bridge	Dir.	Avail. perc.	Route No.	Norm. LCI	Overall rank
1	B3	WB	1204	6.3E-3	32	B3	WB	524.43	6900	2.3E-2	1
2	B11	NB	847	5.9E-3	38	B4	WB	484.64	6536	1.7E-2	4
3	B12	NB	693	5.6E-3	40	B11	NB	399.83	6559	5.6E-3	37
4	B5	WB	809	3.3E-3	67	B10	NB	360.65	5917	4.3E-3	53
5	B14	NB	1092	3.3E-3	68	B2	WB	470.82	4309	4.2E-3	56

Table 6.6 shows that bridge rankings differ between the two LCI methods. The bridge-centric LCI method generally assigns higher overall ranks to the top critical bridges compared to the MNL-SUE LCI method. For instance, bridge B3 (WB) is ranked 32nd by the MNL-SUE LCI method but 1st by the bridge-centric LCI method. This indicates that the MNL-SUE LCI method may not be able to sufficiently emphasize the criticality of bridges.

This subsection used the bridge-centric LCI method to assess bridge criticalities in Winnipeg network. The results were consistent with the discussion in the previous two sections. The results suggest that the MNL-SUE LCI method may underestimate bridge criticality. This analysis assumed only bridge choice alternatives of length one for mixed-region O-D pairs, which might be unrealistic. Next subsection relaxes this assumption.

#### 6.3.3.4 Impact of maximum bridge sequence length on bridge criticality

Setting  $M$  to 1 restricts routes to a single bridge crossing. However, cost-effective routes may cross multiple bridges, such as trips from the E region to the NW region using bridges B6 and B10 (see Figure 6.14). It is reasonable to expect routes that use both bridges simultaneously. Therefore, it seems that a higher  $M$  value may provide behaviorally more plausible route choice set than lower a  $M$  value. This subsection performs sensitivity analysis for the maximum number of bridges per bridge choice alternative of mixed-region O-D pairs. The results are summarized in Table 6.7 and Figure 6.17. Table 6.13 lists the information on all bridges.

Table 6.7 lists the top 5 critical bridges for three parameter  $M$  settings. The bridge-centric LCI method with  $M = 2$  and  $M = 3$  ranked bridges B10 and B12 as more critical than B3 and B4, as higher  $M$  values allow the inclusion of routes that combine multiple bridges. The observed shift in rankings reflects the impact of considering such bridge combinations when  $M > 1$ .

Table 6.7. Top 5 critical bridges for three  $M$  settings.

Bridge rank	M = 1				M = 2				M = 3			
	Bridge	Dir.	Norm. LCI	Overall rank	Bridge	Dir.	Norm. LCI	Overall rank	Bridge	Dir.	Norm. LCI	Overall rank
1	B3	WB	2.3E-2	1	B10	NB	1.4E-2	5	B10	NB	1.4E-2	4
2	B4	WB	1.7E-2	4	B12	NB	8.6E-3	15	B12	NB	1.3E-2	6
3	B11	NB	5.6E-3	37	B3	WB	7.4E-3	26	B11	NB	1.1E-2	8
4	B10	NB	4.3E-3	53	B6	WB	6.4E-3	38	B3	WB	8.7E-3	13
5	B2	WB	4.2E-3	56	B11	NB	3.5E-3	65	B10	SB	6.3E-3	33

Figure 6.17 shows the Spearman correlation between the bridge overall criticality ranks obtained by means of the bridge-centric LCI methods for three parameter  $M$  settings as well as the MNL-SUE LCI method.

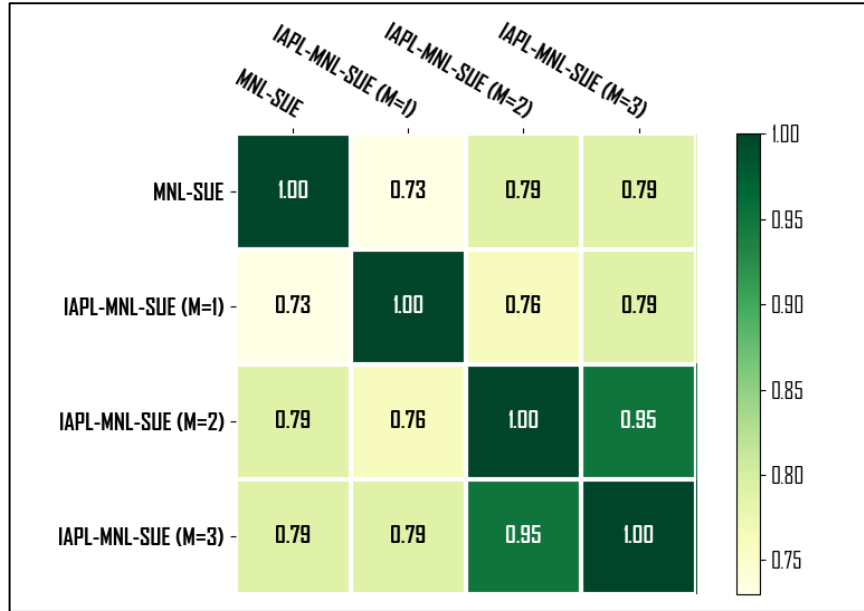


Figure 6.17. Spearman correlation of bridge criticality ranks across four LCI methods.

The results indicate that the bridge-centric LCI methods with  $M = 2$  and  $M = 3$  had correlation close to one. The correlation among other methods was considerably lower. This is likely due to greater overlap in choice alternatives at higher  $M$  values. The bridge choice set for  $M = 1$  was a subset of that for  $M = 2$ , which in turn was a subset of  $M = 3$ . This led to smaller traffic flow fluctuations during the iterative solution algorithm compared to  $M = 1$ .

This subsection conducted a sensitivity analysis for parameter  $M$ , suggesting that a higher  $M$  value may provide a more realistic route choice set. However, higher  $M$  values also increase the method's computational complexity, necessitating a tradeoff. The next subsection analyzes this computational complexity.

### 6.3.3.5 Computational complexity analysis

This subsection investigates the computational complexity of the bridge-centric LCI method. The results are summarized in Table 6.8. The numerical experiments were conducted on MS Windows 11 operating system with Intel(R) Core (TM) i7-9700 CPU@3.00GHz with 24 GB of RAM.

Table 6.8 lists the characteristics of the MNL-SUE LCI method and the bridge-centric LCI method across three values of  $M$ . Table 6.8 shows that the MNL-SUE LCI method had the lowest computational complexity, while the bridge-centric LCI method with  $M = 3$  had the highest, with a CPU time difference of over 100 times. The bridge-centric LCI method with  $M = 1$  and  $M = 2$  required about three and ten times more CPU time, respectively, than the MNL-SUE LCI method. Most computational time was spent solving the underlying TA problem, though LCI computation time also increased with the number of routes considered. Therefore, parameter  $M$  can be used for controlling computational time of the bridge-centric LCI link criticality assessment.

Table 6.8. Computation efforts of the LCI methods (CPU time in sec.).

LCI's model	Iter. No.	Bridge nest No.	Total route No.	Aver. iter. CPU time	Aver. LCI iter. CPU time	Total LCI CPU time	Total CPU time
MNL SUE	99	-	15,312	0.6	0.04	4.2	58.1
IAPL-MNL SUE (M=1)	101	11,336	51,482	1.5	0.2	16.3	166.9
IAPL-MNL SUE (M=2)	76	52,654	247,530	8.3	1.1	81.2	713.0
IAPL-MNL SUE (M=3)	82	483,176	2,358,473	89.7	11.28	924.6	8279.5

CPU time in sec.

### 6.3.3.6 Impact of structural vulnerability coefficients on bridge criticality<sup>7</sup>

For this study, the structural vulnerability of bridges is set at 1, while the structural vulnerability of links representing ordinary road segments (hereafter referred to as ordinary links) is set at a lower value. This reflects the fact that bridges are generally more structurally

<sup>7</sup> In practice, the structural vulnerability coefficients of links is evaluated using fragility curves calibrated with historical data from past disruptive events. However, collecting data and calibrating fragility curves are beyond the scope of this study.

vulnerable than ordinary road segments. Since the actual structural vulnerability coefficients are unknown, a sensitivity analysis is conducted to show how the criticality of bridges changes in response to variations in the structural vulnerability coefficients of ordinary links. The results are summarized in Table 6.9.

Table 6.9. Impact of structural vulnerability coefficients on bridge criticality rankings.

Bridge name	Bridge ID	Dir.	Overall Rank ( $M=2$ )				
			$\varphi_a = 1.0$	$\varphi_a = 0.75$	$\varphi_a = 0.5$	$\varphi_a = 0.25$	$\varphi_a = 0.1$
North Perimeter	B1	EB	1331	1282	1220	1070	870
		WB	517	440	352	230	135
Redwood	B2	EB	584	525	425	285	172
		WB	121	96	65	30	10
Disraeli	B3	EB	415	354	279	194	96
		WB	26	11	7	3	3
Louise	B4	EB	420	356	280	196	97
		WB	117	89	60	24	9
Provencher	B5	EB	558	490	394	263	153
		WB	212	189	138	75	27
Norwood	B6	EB	291	245	198	122	57
		WB	38	19	9	4	4
St. Vital	B7	WB	94	67	47	13	6
		EB	190	154	109	59	17
Fort Garry	B8	EB	435	371	290	201	105
		WB	242	207	163	95	43
South Perimeter	B9	EB	1016	944	859	739	525
		WB	928	862	794	646	423
Old Forts	B10	NB	5	3	1	1	1
		SB	189	151	108	58	16
Midtown	B11	NB	65	51	33	9	5
		SB	236	199	159	91	40
Osborne	B12	NB	15	8	5	2	2
		SB	428	363	285	199	102
Maryland Twin	B13	NB	148	117	81	45	12
		SB	805	750	654	487	290
St. James	B14	NB	294	251	200	128	58
		SB	259	215	180	104	49
West Perimeter	B15	NB	905	846	778	613	398
		SB	869	821	749	576	369

As shown in Table 6.9, the criticality ranks of bridges increase with the decrease of the structural vulnerability of ordinary links. It is expected that at certain points all bridges would be assessed more critical than ordinary links.

This section analyzed the bridge-centric LCI method with structural vulnerability coefficients, demonstrating its practical feasibility for bridge criticality analysis in a real-world transport network. The method efficiently evaluated the criticality of all used links, allowing for comparisons between bridges and ordinary links. It also enabled systematic and interpretable adjustments to bridge criticality, providing a useful tool for highway and bridge management agencies to prioritize resources.

### 6.3.3.7 Reliability implications

Figure 6.18 highlights the 100 most critical links based on the IAPL-MNL-SUE-based LCI method. As shown in Figure 6.18, the top 100 links include not only links representing bridges but also links representing ordinary roadway segments. These links connect major trip production zones (e.g., 92 and 94) to high trip attraction zones near the airport (e.g., 103) and in the CBD. Additionally, some critical links connect the E region to the NW region and the SW region to the NW region, which is consistent with the mixed-region O-D pair distribution shown in Figure 6.14.

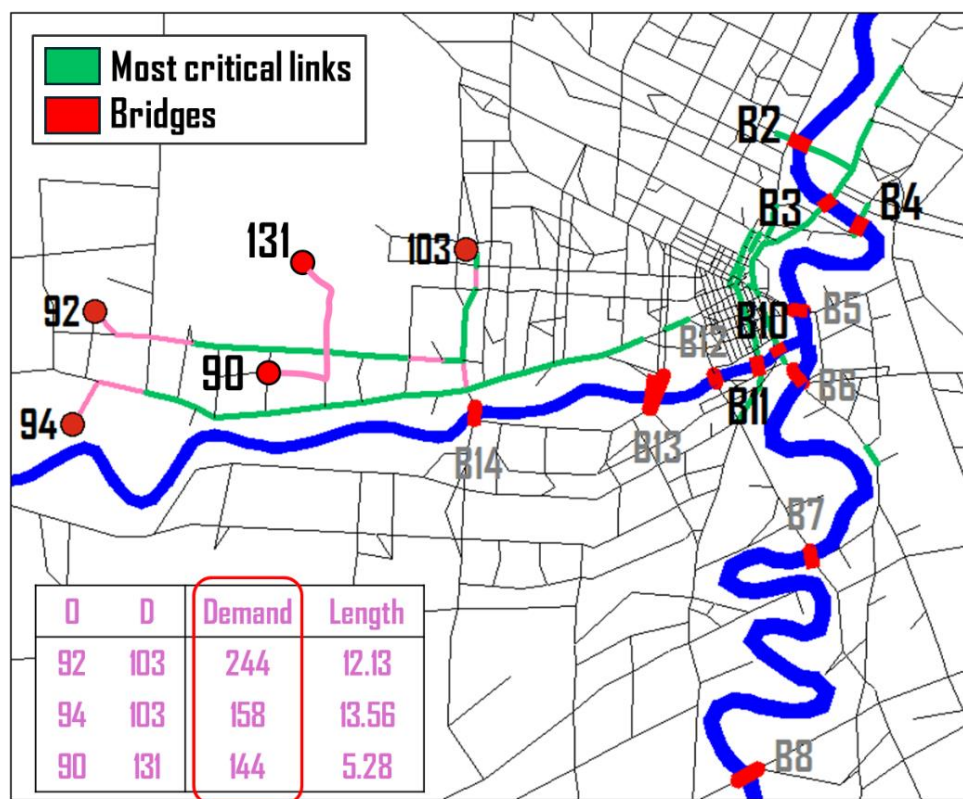


Figure 6.18. Top 100 critical links according to IAPL-MNL-SUE-based LCI.

Not all bridges are included in the top 100 most critical links. The labels of critical bridges are shown in black, while the labels of less critical ones are displayed in gray, as illustrated in Figure 6.18. Structural vulnerability coefficients offer a means to control criticality values, as detailed in Section 3.3.6. For instance, reducing the coefficient for ordinary links can ensure



all bridges become the most critical below a specific threshold. In practice, these coefficients should be calibrated using real-world data tailored to each facility type. Moreover, available data can enable differentiation among bridge types by assigning distinct vulnerability coefficients to each type.

In summary, while bridges are undeniably structurally more vulnerable, the analysis demonstrates that regular links also play a vital role and may be more critical for normal network operation than some bridges. Therefore, it is essential to assess criticality of both for a balanced and effective approach to infrastructure maintenance planning. This suggests that if planning agencies or transport departments prioritize bridges exclusively and neglect regular links, it could lead to issues.

This section conducted an arguably comprehensive analysis of the properties of the bridge-centric LCI method and applied it to a real-world transport network showing its practical feasibility for bridge criticality assessment.

### 6.3.4 Supplementary material

Table 6.10. Specification of the bridge and route choice sets (the Nguyen-Dupuis network).

O-D pair	Usage of bridges	Bridge nest	Bridge sequence	Route	Route links	FFTT
(1, 2)	Optional	-	[7]	R1	[1, 5, 7, 9, 11]	29
				R2	[1, 5, 7, 10, 15]	33
				R3	[2, 17, 7, 9, 11]	35
				R4	[2, 17, 7, 10, 15]	39
			[14]	R5	[1, 6, 12, 14, 15]	41
				R6	[2, 17, 8, 14, 15]	44
				R7	[1, 5, 8, 14, 15]	38
			-	R8	[2, 18, 11]	32
(1, 3)	Unavoidable	BN1	[7]	R9	[1, 5, 7, 10, 16]	32
		BN2	[14]	R10	[2, 17, 7, 10, 16]	38
				R11	[1, 5, 8, 14, 16]	37
				R12	[1, 6, 12, 14, 16]	40
		BN3	[19]	R13	[2, 17, 8, 14, 16]	43
				R14	[1, 6, 13, 19]	36
(4, 2)	Unavoidable	BN4	[7]	R15	[3, 5, 7, 9, 11]	31
		BN5	[14]	R16	[3, 5, 7, 10, 15]	35
				R17	[3, 5, 8, 14, 15]	40
				R18	[3, 6, 12, 14, 15]	43
				R19	[4, 12, 14, 15]	37
(4, 3)	Unavoidable	BN6	[7]	R20	[3, 5, 7, 10, 16]	34
		BN7	[14]	R21	[3, 5, 8, 14, 16]	39
				R22	[3, 6, 12, 14, 16]	42
				R23	[4, 12, 14, 16]	36
		BN8	[19]	R24	[3, 6, 13, 19]	38
				R25	[4, 13, 19]	32

Table 6.11. Link attributes for the Nguyen-Dupuis network with uniform O-D travel demands.

Link label	Enumerated choice set				Bridge-centric choice set generation			
	Route number	LCI	Norm. LCI	Rank	Route number	LCI	Norm. LCI	Rank
1	8	62.511	0.066	6	4	62.903	0.063	4
2	6	54.856	0.058	7	3	62.698	0.063	5
3	8	76.291	0.080	4	6	71.846	0.072	3
4	3	29.423	0.031	11	3	54.227	0.054	7
5	10	189.714	0.200	1	8	245.574	0.246	1
6	6	18.573	0.020	14	2	4.959	0.005	18
7	9	114.450	0.120	2	6	132.928	0.133	2
8	6	9.247	0.010	17	4	7.851	0.008	17
9	3	31.476	0.033	10	2	53.597	0.054	8
10	6	27.880	0.029	12	4	24.101	0.024	14
11	4	24.662	0.026	13	3	56.045	0.056	6
12	6	47.828	0.050	8	2	25.272	0.025	13
13	3	16.263	0.017	16	3	18.017	0.018	15
14	12	96.740	0.102	3	6	49.764	0.050	9
15	9	65.770	0.069	5	3	31.406	0.031	11
16	9	44.318	0.047	9	7	40.390	0.040	10
17	5	18.260	0.019	15	2	11.728	0.012	16
18	1	6.280	0.007	18	1	26.142	0.026	12
19	3	16.263	0.017	16	3	18.017	0.018	15

Table 6.12. Link attributes for the Nguyen-Dupuis network with non-uniform O-D travel demands..

Link label	Enumerated choice set				Bridge-centric choice set generation			
	Route number	LCI	Norm. LCI	Rank	Route number	LCI	Norm. LCI	Rank
1	8	86.936	0.036	9	4	83.812	0.036	9
2	6	67.476	0.028	12	3	72.670	0.031	10
3	8	472.563	0.193	1	8	427.444	0.182	1
4	3	171.707	0.070	4	3	178.972	0.076	4
5	10	313.772	0.128	3	8	330.222	0.141	2
6	6	62.343	0.025	13	4	52.087	0.022	13
7	9	142.890	0.058	6	6	141.117	0.060	5
8	6	34.661	0.014	14	4	22.771	0.010	17
9	3	28.501	0.012	17	2	45.714	0.019	14
10	6	117.668	0.048	7	4	98.650	0.042	8
11	4	29.275	0.012	16	3	60.513	0.026	12
12	6	81.977	0.033	10	4	71.303	0.030	11
13	3	115.080	0.047	8	3	123.349	0.053	6
14	12	148.254	0.061	5	8	108.075	0.046	7
15	9	75.064	0.031	11	4	43.211	0.018	15
16	9	345.037	0.141	2	8	317.308	0.135	3
17	5	32.731	0.013	15	2	18.102	0.008	18
18	1	7.759	0.003	18	1	29.783	0.013	16
19	3	115.080	0.047	8	3	123.349	0.053	6

Table 6.13. Criticality values and ranks for bridge-centric LCI with different parameter settings (the Winnipeg network).

Bridge name	Bridge ID	Dir.	$M=1$		$M=2$		$M=3$	
			Value	Overall Rank	Value	Overall Rank	Value	Overall Rank
North Perimeter	B1	EB	2.5E-5	1205	5.1E-6	1593	4.1E-5	1022
		WB	9.5E-4	203	1.8E-4	599	9.0E-4	224
Redwood	B2	EB	1.4E-3	167	1.9E-4	586	7.8E-4	258
		WB	4.8E-3	50	2.0E-3	118	4.3E-3	55
Disraeli	B3	EB	3.5E-3	78	3.1E-4	447	6.9E-4	280
		WB	2.1E-2	1	7.1E-3	30	8.2E-3	19
Louise	B4	EB	1.5E-3	150	2.6E-4	489	4.4E-4	365
		WB	1.9E-2	2	2.0E-3	120	4.1E-3	62
Provencher	B5	EB	1.6E-4	639	1.5E-4	648	1.7E-4	645
		WB	1.1E-3	186	8.7E-4	226	6.3E-4	294
Norwood	B6	EB	1.1E-4	731	5.3E-4	305	1.1E-3	198
		WB	2.6E-3	101	7.3E-3	28	5.1E-3	47
St. Vital	B7	WB	7.9E-4	232	2.7E-3	89	2.9E-3	87
		EB	7.2E-5	907	1.1E-3	200	1.4E-3	174
Fort Garry	B8	EB	2.3E-5	1223	2.8E-4	468	2.5E-4	542
		WB	1.6E-4	640	6.9E-4	257	8.5E-4	238
South Perimeter	B9	EB	1.1E-5	1468	2.4E-5	1152	5.7E-5	931
		WB	1.4E-5	1392	3.3E-5	1053	7.6E-5	866
Old Forts	B10	NB	5.3E-3	43	1.6E-2	5	1.9E-2	1
		SB	2.2E-4	538	1.7E-3	135	8.4E-3	18
Midtown	B11	NB	5.2E-3	45	3.8E-3	65	1.4E-2	7
		SB	1.1E-4	733	8.3E-4	228	1.8E-3	133
Osborne	B12	NB	8.3E-4	225	9.4E-3	12	1.5E-2	6
		SB	6.6E-5	932	3.4E-4	423	1.2E-3	188
Maryland Twin	B13	NB	3.7E-4	418	1.5E-3	162	4.1E-3	63
		SB	2.9E-5	1149	6.6E-5	889	1.2E-4	753
St. James	B14	NB	5.7E-4	320	5.2E-4	311	1.8E-3	138
		SB	2.4E-4	529	5.6E-4	292	1.1E-3	202
West Perimeter	B15	NB	2.3E-5	1222	3.3E-5	1047	4.4E-5	995
		SB	2.6E-5	1199	3.6E-5	1020	7.0E-5	889

## 6.4 Chapter summary

This chapter addressed the problem of bridge criticality analysis by recognizing the unique functional importance of bridges in route choice and their inherent high structural vulnerability. The link criticality index (LCI) was enhanced by integrating a joint bridge-route choice stochastic user equilibrium model, which uses an implicit availability/perception logit (IAPL) model for bridge choice and a multinomial logit (MNL) model for route choice (bridge-centric LCI). The IAPL model considered the perceived availability of bridges in travelers' decision-making, both in bridge choice set formation and behavior. This joint model provided a more behaviorally plausible representation of travelers' route choices while assessing bridge criticalities. Structural vulnerability coefficients were added to the LCI method to emphasize bridge vulnerability. The results show that ignoring bridge choice and its hierarchical relationship with route choices can lead to underestimating bridge criticality and overestimating other network links' criticality. Ordinary roadway segments, though structurally less vulnerable, can also be critical for normal network operation. Therefore, bridge criticality should be assessed jointly with ordinary roadway segments. The proposed method effectively highlights the functional importance and high structural vulnerability of bridges, as well as the criticality of ordinary roadway segments, making it a valuable tool for transportation network reliability assessment.

# CHAPTER 7

## Conclusions

---

### 7.1 Summary of research contributions

This research has addressed link criticality analysis problem with a focus on network equilibrium traffic assignment (TA)-based methods, which are important for disaster management applications where common travelers' behavior and congestion effects cannot be neglected. Because these methods have relied on traffic flow patterns and travel costs induced by TA models, plausibly modelling travel choices has been of paramount importance for a representative link criticality evaluation.

In the first part, this thesis has advanced link criticality analysis for large-scale road networks by integrating nuanced traffic assignment (TA) models that account for travelers' imperfect perception of network conditions, their responses to congestion, and route similarity issues. Specifically, Chapter 3 has laid the foundation for the thesis. First, it introduced the selected method for link criticality analysis and meticulously investigated its properties. Second, it advanced the selected method by incorporating two stochastic user equilibrium (SUE) TA models: SUE with fixed demand (SUE) and SUE with elastic demand (SUE-ED). The original method was based on the user equilibrium (UE) model with fixed demand. UE is known to be restrictive because it assumes that travelers have perfect knowledge of network conditions and that they do not change their travel plans, which is inconsistent with actual traveler behavior and can generate non-representative traffic flow patterns. The adopted models have relaxed these assumptions. The results demonstrated that the UE-based method

overestimated the criticality of links on least-cost routes, while the SUE-based methods minimized this overestimation.

Chapter 4 has acknowledged that route correlation is common in road networks and that it can raise the issue of route similarity. This issue can greatly affect travelers' route choices and overall travel demand, altering traffic flows, travel costs, and, consequently, link criticality values. This chapter has incorporated the SUE-ED TA model based on the cross-nested logit (CNL) route choice model, which effectively captures the influence of route similarity on both individual route choices and aggregate travel demand. The results have indicated that ignoring route similarity leads to overestimating the criticality of shared links, while incorporating route similarity considerations can notably alter the criticality ranking of links.

In the second part, emphasizing the crucial role of bridges in the route choice process, this thesis has developed a bridge-centric framework. This framework includes a joint bridge-route choice model, a network equilibrium model, and a customized route-based algorithm, and has been integrated into the selected link criticality analysis method. The models and methods developed in this part of the thesis are applicable to bridge-centric transport networks—road networks separated by obstacles such as valleys or rivers, and connected by bridges. Specifically, Chapter 5 has developed an advanced individual travel choice model for the joint bridge-route choice problem, a corresponding network equilibrium model, and a solution algorithm that effectively leverages the features of both bridges and routes. The results of these experiments have demonstrated that network equilibrium models can produce substantially different traffic flow patterns, depending on whether they account for the importance of bridges in route choice.

Chapter 6 has applied the developed bridge-centric methodology in Chapter 5 to bridge criticality analysis in large-scale bridge-centric transport networks. The results have shown

markedly different traffic flow patterns and link criticality values for the proposed method compared to a model that did not consider bridge choice. These findings suggest that link criticality analysis methods based on models that do not consider bridge choice may greatly underestimate the importance of bridges.

## **7.2 Limitations and future research directions**

This research has three primary limitations. First, the traffic assignment (TA) models and methodologies for evaluating link criticality lack validation against real-world datasets. Their development is grounded in theoretical frameworks and empirical observations from prior literature, with sensitivity analyses of key parameters serving as a compensatory mechanism for the absence of empirical validation. Second, the assessment of link criticality is conducted independently of specific disruptive scenarios, emphasizing the generalized functional role of network links rather than their vulnerability to particular event-driven disruptions. This limits the applicability of findings to context-agnostic resilience planning. Third, the conceptualization of “bridges” is narrowly defined as physical infrastructure components, excluding non-physical or abstract interpretations of connectivity that may hold relevance in broader network resilience discourse.

Building on the limitations identified, four key directions emerge for advancing this research. First, empirical validation of the proposed TA and link criticality assessment methods using real-world datasets is essential to bridge the gap between theoretical frameworks and practical applicability. Such validation would require systematic data collection, network calibration, and parameter estimation, as the current reliance on sensitivity analyses and literature-derived insights remains insufficient for operational deployment. Second, extending the link criticality analysis to scenario-specific disruptions—such as floods or earthquakes—could enhance its utility for mitigating long-term

infrastructure risks. This would entail integrating probabilistic models of disruption frequency, magnitude, and cascading consequences into the assessment framework. Third, broadening the conceptualization of “bridges” from purely physical infrastructure elements to functional interconnections between regions or cities could expand the methodological scope, enabling applications beyond traditional infrastructure resilience. Finally, methodological innovations—such as refining network equilibrium models to better capture traveler behavior dynamics or developing novel criticality metrics—could address existing gaps in behavioral realism and analytical rigor, strengthening the theoretical foundations of link criticality analysis.



## REFERENCES

- Adam, J. M., Makoond, N., Riveiro, B. & Buitrago, M. 2024. Risks of bridge collapses are real and set to rise - here's why. *Nature (London)*, 629, 1001-1003.
- Alizadeh, H., Farooq, B., Morency, C. & Saunier, N. 2018. On the role of bridges as anchor points in route choice modeling. *Transportation*, 45, 1181-1206.
- Almotahari, A. & Yazici, A. 2019. A link criticality index embedded in the convex combinations solution of user equilibrium traffic assignment. *Transportation Research Part A: Policy and Practice*, 126, 67-82.
- Almotahari, A. & Yazici, A. 2021. A computationally efficient metric for identification of critical links in large transportation networks. *Reliability Engineering & System Safety*, 209, 107458.
- Argyroudis, S. A., Mitoulis, S. A., Winter, M. G. & Kaynia, A. M. 2019. Fragility of transport assets exposed to multiple hazards: State-of-the-art review toward infrastructural resilience. *Reliability Engineering & System Safety*, 191, 106567.
- Azevedo, J., Santos Costa, M. E. O., Silvestre Madeira, J. J. E. R. & Vieira Martins, E. Q. 1993. An algorithm for the ranking of shortest paths. *European Journal of Operational Research*, 69, 97-106.
- Beckmann, M. J., McGuire, C. B. & Winsten, C. B. 1956. *Studies in the Economics of Transportation*, Santa Monica, CA, RAND Corporation.
- Bekhor, S. & Prashker, J. N. 1999. Formulations of extended logit stochastic user equilibrium assignments. *14th International Symposium on Transportation and Traffic Theory*. Jerusalem, Israel
- Bekhor, S. & Prashker, J. N. 2001. Stochastic user equilibrium formulation for generalized nested logit model. *Transportation Research Record*, 1752, 84-90.
- Bekhor, S., Toledo, T. & Prashker, J. N. 2008. Effects of choice set size and route choice models on path-based traffic assignment. *Transportmetrica*, 4, 117-133.
- Ben-Akiva, M. & Bierlaire, M. 1999. Discrete choice methods and their applications to short term travel decisions. In: HALL, R. W. (ed.) *Handbook of Transportation Science*. Boston, MA: Springer US.
- Ben-Akiva, M. & Boccara, B. 1995. Discrete choice models with latent choice sets. *International Journal of Research in Marketing*, 12, 9-24.
- Ben-Akiva, M. E. & Lerman, S. R. 1985a. *Discrete choice analysis : Theory and application to travel demand*, Cambridge, Mass, MIT Press.
- Ben-Akiva, M. E. & Lerman, S. R. 1985b. *Discrete choice analysis: Theory and application to travel demand*, MIT press.
- Berdica, K. 2002. An introduction to road vulnerability: What has been done is done and should be done. *Transport Policy*, 9, 117-127.
- Bliemer, M. & Bovy, P. 2008. Impact of route choice set on route choice probabilities. *Transportation Research Record*, 2076, 10-19.
- Bocchini, P. & Frangopol, D. M. 2011. A probabilistic computational framework for bridge network optimal maintenance scheduling. *Reliability Engineering & System Safety*, 96, 332-349.
- Bovy, P. H. L. 2009. On modelling route choice sets in transportation networks: A synthesis. *Transport Reviews*, 29, 43-68.

- Bucsky, P. & Juhász, M. 2022. Long-term evidence on induced traffic: A case study on the relationship between road traffic and capacity of Budapest bridges. *Transportation Research Part A: Policy and Practice*, 157, 244-257.
- Cantarella, G. E., Carotenì, A. & de Luca, S. 2015. Stochastic equilibrium assignment with variable demand: Theoretical and implementation issues. *European Journal of Operational Research*, 241, 330-347.
- Capacci, L., Biondini, F. & Frangopol, D. M. 2022. Resilience of aging structures and infrastructure systems with emphasis on seismic resilience of bridges and road networks: Review. *Resilient Cities and Structures*, 1, 23-41.
- Cascetta, E., Nuzzolo, A., Russo, F. & Vitetta, A. 1996. A modified logit route choice model overcoming path overlapping problems. Specification and some calibration results for interurban networks. *The 13th International Symposium on Transportation and Traffic Theory*. Lyon, France.
- Cascetta, E. & Papola, A. 2001. Random utility models with implicit availability/perception of choice alternatives for the simulation of travel demand. *Transportation Research Part C: Emerging Technologies*, 9, 249-263.
- Chen, A., Pravinongvuth, S., Xu, X., Ryu, S. & Chootinan, P. 2012a. Examining the scaling effect and overlapping problem in logit-based stochastic user equilibrium models. *Transportation Research Part A: Policy and Practice*, 46, 1343-1358.
- Chen, A., Ryu, S., Xu, X. & Choi, K. 2014. Computation and application of the paired combinatorial logit stochastic user equilibrium problem. *Computers & Operations Research*, 43, 68-77.
- Chen, A., Xu, X., Ryu, S. & Zhou, Z. 2013. A self-adaptive Armijo stepsize strategy with application to traffic assignment models and algorithms. *Transportmetrica*, 9, 695-712.
- Chen, B. Y., Lam, W. H. K., Sumalee, A., Li, Q. & Li, Z.-C. 2012b. Vulnerability analysis for large-scale and congested road networks with demand uncertainty. *Transportation Research Part A: Policy and Practice*, 46, 501-516.
- Chu, C. 1989. A paired combinatorial logit model for travel demand analysis. *The 5th World Conference on Transportation Research*.
- Corley, H. W. & Sha, D. Y. 1982. Most vital links and nodes in weighted networks. *Operations Research Letters*, 1, 157-160.
- Council, C. C. 2011. Cumbria floods November 2009: Preliminary Assessment Report.
- Daganzo, F. C. & Sheffi, Y. 1977. On stochastic models of traffic assignment. *Transportation Science*, 11, 253-274.
- Damberg, O., Lundgren, J. T. & Patriksson, M. 1996. An algorithm for the stochastic user equilibrium problem. *Transportation Research Part B: Methodological*, 30, 115-131.
- De la Barra, T., Perez, B. & Anez, J. 1993. Multidimensional path search and assignment. *PTRC 21st Summer Annual Meeting*. University of Manchester, United Kingdom.
- Dial, R. B. 1971. Probabilistic assignment: A multipath traffic assignment model which obviates path enumeration. *Transportation Research*, 5, 83-111.
- Du, M., Tan, H. & Chen, A. 2021. A faster path-based algorithm with Barzilai-Borwein step size for solving stochastic traffic equilibrium models. *European Journal of Operational Research*, 290, 982-999.
- Du, Y., Wang, H., Gao, Q., Pan, N., Zhao, C. & Liu, C. 2022. Resilience concepts in integrated urban transport: A comprehensive review on multi-mode framework. *Smart and Resilient Transportation*, 4, 105-133.
- Fakharifar, M., Chen, G., Dalvand, A. & Shamsabadi, A. 2015. Collapse vulnerability and fragility analysis of substandard RC bridges rehabilitated with different repair jackets

- under post-mainshock cascading events. *International Journal of Concrete Structures and Materials*, 9, 345-367.
- Faturechi, R. & Miller-Hooks, E. 2015. Measuring the performance of transportation infrastructure systems in disasters: A comprehensive review. *Journal of Infrastructure Systems*, 21.
- Fisk, C. 1980. Some developments in equilibrium traffic assignment. *Transportation Research Part B: Methodological*, 14, 243-255.
- Frank, M. & Wolfe, P. 1956. An algorithm for quadratic programming. *Naval Research Logistics Quarterly*, 3, 95-110.
- Fulkerson, D. R. & Harding, G. C. 1977. Maximizing the minimum source-sink path subject to a budget constraint. *Mathematical Programming*, 13, 116-118.
- Gauthier, P., Furno, A. & El Faouzi, N.-E. 2018. Road network resilience: How to identify critical links subject to day-to-day disruptions. *Transportation Research Record*, 2672, 54-65.
- Gu, Y., Fu, X., Liu, Z., Xu, X. & Chen, A. 2020. Performance of transportation network under perturbations: Reliability, vulnerability, and resilience. *Transportation Research Part E: Logistics and Transportation Review*, 133, 101809.
- Habib, K. N., Morency, C., Trépanier, M. & Salem, S. 2013. Application of an independent availability logit model (IAL) for route choice modelling: Considering bridge choice as a key determinant of selected routes for commuting in Montreal. *Journal of Choice Modelling*, 9, 14-26.
- Hancilar, U., Taucer, F., Tsionis, G. & Khazai, B. 2013. Guidelines for typology definition of European physical assets for earthquake risk assessment. Publications Office.
- Holme, P., Kim, B. J., Yoon, C. N. & Han, S. K. 2002. Attack vulnerability of complex networks. *Physical Review E: Statistical Physics, Plasmas, Fluids, and Related Interdisciplinary Topics*, 65, 056109.
- Jansuwan, S. & Chen, A. 2015. Considering perception errors in network efficiency measure: An application to bridge importance ranking in degradable transportation networks. *Transportmetrica*, 11, 793-818.
- Jenelius, E. 2009. Network structure and travel patterns: Explaining the geographical disparities of road network vulnerability. *Journal of Transport Geography*, 17, 234-244.
- Jenelius, E., Petersen, T. & Mattsson, L.-G. 2006. Importance and exposure in road network vulnerability analysis. *Transportation Research Part A: Policy and Practice*, 40, 537-560.
- Jung, S., Lee, S., Kwon, O. & Kim, B. 2020. Grid-based traffic vulnerability analysis by using betweenness centrality. *Journal of the Korean Physical Society*, 77, 538-544.
- Kazagli, E., Bierlaire, M. & Flötteröd, G. 2016. Revisiting the route choice problem: A modeling framework based on mental representations. *Journal of Choice Modelling*, 19, 1-23.
- Kitthamkesorn, S., Chen, A., Xu, X. & Ryu, S. 2016. Modeling mode and route similarities in network equilibrium problem with go-green modes. *Networks and Spatial Economics*, 16, 33-60.
- Knoop, V. L., Snelder, M., van Zuylen, H. J. & Hoogendoorn, S. P. 2012. Link-level vulnerability indicators for real-world networks. *Transportation Research Part A: Policy and Practice*, 46, 843-854.
- Kurth, M., Kozłowski, W., Ganin, A., Mersky, A., Leung, B., Dykes, J., Kitsak, M. & Linkov, I. 2020. Lack of resilience in transportation networks: Economic implications. *Transportation Research Part D: Transport and Environment*, 86, 102419.

- Larsson, T. & Patriksson, M. 1992. Simplicial decomposition with disaggregated representation for the traffic assignment problem. *Transportation Science*, 26, 4-17.
- Latora, V. & Marchiori, M. 2001. Efficient behavior of small-world networks. *Physical Review Letters*, 87, 198701.
- Leblanc, L. J. 1975. An algorithm for the discrete network design problem. *Transportation Science*, 9, 183-199.
- Lee, M., Barbosa, H., Youn, H., Holme, P. & Ghoshal, G. 2017. Morphology of travel routes and the organization of cities. *Nature Communications*, 8, 2229.
- Li, G., Chen, A., Ryu, S., Kitthamkesorn, S. & Xu, X. 2024. Modeling elasticity, similarity, stochasticity, and congestion in a network equilibrium framework using a paired combinatorial weibit choice model. *Transportation Research Part B: Methodological*, 179, 102870.
- Liu, H. X., He, X. & He, B. 2009. Method of successive weighted averages (MSWA) and self-regulated averaging schemes for solving stochastic user equilibrium problem. *Networks and Spatial Economics*, 9, 485-503.
- Liu, Z., Chen, H., Liu, E. & Hu, W. 2022. Exploring the resilience assessment framework of urban road network for sustainable cities. *Physica A: Statistical Mechanics and its Applications*, 586, 126465.
- Liu, Z., Chen, Z., He, Y. & Song, Z. 2021. Network user equilibrium problems with infrastructure-enabled autonomy. *Transportation Research Part B: Methodological*, 154, 207-241.
- Mahajan, K. & Kim, A. M. 2020. Vulnerability assessment of Alberta's provincial highway network. *Transportation Research Interdisciplinary Perspectives*, 6, 100171.
- Manley, E. J., Addison, J. D. & Cheng, T. 2015. Shortest path or anchor-based route choice: A large-scale empirical analysis of minicab routing in London. *Journal of Transport Geography*, 43, 123-139.
- Meyer, M. D. 2016. *Transportation planning handbook*, Hoboken, New Jersey, Wiley.
- MunichRe 2013. Floods dominate natural catastrophe statistics in first half of 2013.
- Nagurney, A. & Qiang, Q. 2007. A transportation network efficiency measure that captures flows, behavior, and costs with applications to network component importance identification and vulnerability. *The POMS 18th Annual Conference*. Dallas, Texas, U.S.A.
- Ohi, S. J. & Kim, A. M. 2021. Identifying critical corridors during an area-wide disruption by evaluating network bottleneck capacity. *International Journal of Disaster Risk Reduction*, 64, 102487.
- Patriksson, M. 1994. *The Traffic Assignment Problem - Models and Methods*, VSP International Science.
- Patriksson, M. 2015. *The traffic assignment problem: Models and methods*.
- Peng, Y., Xu, M., Li, G. & Chen, A. 2024. Sequencing post-disruption concurrent restoration via a network flow approach. *Transportation Research Part D: Transport and Environment*, 133, 104234.
- Prashker, J. N. & Bekhor, S. 2004. Route choice models used in the stochastic user equilibrium problem: A review. *Transport Reviews*, 24, 437-463.
- Prato, C. G. 2009. Route choice modeling: Past, present and future research directions. *Journal of Choice Modelling*, 2, 65-100.
- Pravinongvuth, S. & Chen, A. 2005. Adaptation of the paired combinatorial logit model to the route choice problem. *Transportmetrica*, 1, 223-240.
- Rymsza, J. 2021. Causes of the collapse of the Polcevera viaduct in Genoa, Italy. *Applied Sciences* [Online], 11.

- Ryu, S., Chen, A., Xu, X. & Choi, K. 2014. Modeling demand elasticity and route overlapping in stochastic user equilibrium through paired combinatorial logit model. *Transportation Research Record*, 2429, 8-19.
- Scott, D. M., Novak, D. C., Aultman-Hall, L. & Guo, F. 2006. Network robustness index: A new method for identifying critical links and evaluating the performance of transportation networks. *Journal of Transport Geography*, 14, 215-227.
- Serdar, M. Z., Koç, M. & Al-Ghamdi, S. G. 2022. Urban transportation networks resilience: Indicators, disturbances, and assessment methods. *Sustainable Cities and Society*, 76, 103452.
- Shapouri, M., Fuller, J. D., Wolshon, B. & Herrera, N. 2023. Disruptions in megaregional network evacuations: Identifying and assessing critical links. *Transportation Research Record*, 2677, 669-682.
- Sheffi, Y. 1985. *Urban transportation networks: Equilibrium analysis with mathematical programming methods*, Englewood Cliffs, N.J., Prentice-Hall.
- Singh, M. P., Khaleghi, B., Saraf, V. K., Jain, S. K., Norris, G., Goel, R. & Murty, C. V. R. 2002. Roads and Bridges. *Earthquake Spectra*, 18, 363-379.
- Sugiura, S. & Kurauchi, F. 2023. Isolation vulnerability analysis in road network: Edge connectivity and critical link sets. *Transportation Research Part D: Transport and Environment*, 119, 103768.
- Sullivan, J. L., Novak, D. C., Aultman-Hall, L. & Scott, D. M. 2010. Identifying critical road segments and measuring system-wide robustness in transportation networks with isolating links: A link-based capacity-reduction approach. *Transportation Research Part A: Policy and Practice*, 44, 323-336.
- Sullivan, J. L., Sentoff, K., Segale, J., Marshall, N. L., Fitzgerald, E. & Schiff, R. 2024. A new risk-based measure of link criticality for flood risk planning. *Transportation*, 51, 2051-2071.
- Swait, J. & Ben-Akiva, M. 1987. Incorporating random constraints in discrete models of choice set generation. *Transportation Research Part B: Methodological*, 21, 91-102.
- Tubaldi, E., White, C. J., Patelli, E., Mitoulis, S. A., de Almeida, G., Brown, J., Cranston, M., Hardman, M., Koursari, E., Lamb, R., McDonald, H., Mathews, R., Newell, R., Pizarro, A., Roca, M. & Zonta, D. 2022. Invited perspectives: Challenges and future directions in improving bridge flood resilience. *Natural Hazards and Earth System Sciences*, 22, 795-812.
- Twumasi-Boakye, R. & Sobanjo, O. J. 2018. Resilience of regional transportation networks subjected to hazard-induced bridge damages. *Journal of Transportation Engineering Part A: Systems*, 144, 04018062.
- Vovsha, P. 1997. Application of cross-nested logit model to mode choice in Tel Aviv, Israel, metropolitan area. *Transportation Research Record*, 1607, 6-15.
- Wardrop, J. G. 1952. Road paper. Some theoretical aspects of road traffic research. *Proceedings of the Institution of Civil Engineers*, 1, 325-362.
- Wen, C.-H. & Koppelman, F. S. 2001. The generalized nested logit model. *Transportation Research Part B: Methodological*, 35, 627-641.
- Xu, X. & Chen, A. 2013. C-logit stochastic user equilibrium model with elastic demand. *Transportation Planning and Technology*, 36, 463-478.
- Xu, Z. & Chopra, S. S. 2023. Interconnectedness enhances network resilience of multimodal public transportation systems for safe-to-fail urban mobility. *Nature Communications*, 14, 4291.
- Yang, H. & Bell, M. G. 1998. Models and algorithms for road network design: A review and some new developments. *Transport Reviews*, 18, 257-278.

- Zhang, T., Niu, C., Nair, D. J., Robson, E. N. & Dixit, V. 2023. Transportation resilience optimization from an economic perspective at the pre-event stage. *Sustainability Analytics and Modeling*, 3, 100027.
- Zhou, Y., Wang, J. & Yang, H. 2019. Resilience of transportation systems: Concepts and comprehensive review. *IEEE Transactions on Intelligent Transportation Systems*, 20, 4262-4276.
- Zhou, Z., Chen, A. & Bekhor, S. 2012. C-logit stochastic user equilibrium model: Formulations and solution algorithm. *Transportmetrica*, 8, 17-41.